N°d'ordre NNT : **2018LYSEI002**

THESE de DOCTORAT DE L'UNIVERSITE DE LYON

opérée au sein de
l'Institut national des sciences appliquées de Lyon

Ecole Doctorale N°ED162
(Ecole Doctorale MEGA de Lyon
Mécanique – Energétique – Génie Civil – Acoustiquee)

Spécialité: Génie Mécanique

Soutenue publiquement le 24/01/2018, par :

Rabii MLIKA

Nitsche method for frictional contact and self-contact: mathematical and numerical study

---

Devant le jury composé de :

Nom, prénom	grade/qualité	établissement/entreprise	
LE TALLEC, Patrick	Professeur	Ecole Polytechnique	Rapporteur
DE LORENZIS, Laura	Professeur	University of Brunswick	Rapportrice
FERNANDEZ, Miguel Angel	Dir. de recherche	Inria de Paris	Examinateur
HAURET Patrice	Ing. R&D, HDR	Michelin	Examinateur
RENARD Yves	Professeur	INSA-Lyon	Directeur de thèse
CHOULY Franz	MCF., HDR	UBFC	Co-directeur de thèse
DELDON, Jean-François	Ingénieur R&D	Michelin	Invité

Département FEDORA – INSA Lyon - Ecoles Doctorales – Quinquennal 2016-2020

SIGLE	ÉCOLE DOCTORALE	NOM ET COORDONNEES DU RESPONSABLE
CHIMIE	**CHIMIE DE LYON** **http://www.edchimie-lyon.fr** Sec. : Renée EL MELHEM Bât. Blaise PASCAL, 3e étage **secretariat@edchimie-lyon.fr** INSA : R. GOURDON	M. Stéphane DANIELE Institut de recherches sur la catalyse et l'environnement de Lyon IRCELYON-UMR 5256 Équipe CDFA 2 Avenue Albert EINSTEIN 69 626 Villeurbanne CEDEX **directeur@edchimie-lyon.fr**
E.E.A.	**ÉLECTRONIQUE, ÉLECTROTECHNIQUE, AUTOMATIQUE** **http://edeea.ec-lyon.fr** Sec. : M.C. HAVGOUDOUKIAN **ecole-doctorale.eea@ec-lyon.fr**	M. Gérard SCORLETTI École Centrale de Lyon 36 Avenue Guy DE COLLONGUE 69 134 Écully Tél : 04.72.18.60.97 Fax 04.78.43.37.17 **gerard.scorletti@ec-lyon.fr**
E2M2	**ÉVOLUTION, ÉCOSYSTÈME, MICROBIOLOGIE, MODÉLISATION** **http://e2m2.universite-lyon.fr** Sec. : Sylvie ROBERJOT Bât. Atrium, UCB Lyon 1 Tél : 04.72.44.83.62 INSA : H. CHARLES **secretariat.e2m2@univ-lyon1.fr**	M. Fabrice CORDEY CNRS UMR 5276 Lab. de géologie de Lyon Université Claude Bernard Lyon 1 Bât. Géode 2 Rue Raphaël DUBOIS 69 622 Villeurbanne CEDEX Tél : 06.07.53.89.13 **cordey@univ-lyon1.fr**
EDISS	**INTERDISCIPLINAIRE SCIENCES-SANTÉ** **http://www.ediss-lyon.fr** Sec. : Sylvie ROBERJOT Bât. Atrium, UCB Lyon 1 Tél : 04.72.44.83.62 INSA : M. LAGARDE **secretariat.ediss@univ-lyon1.fr**	Mme Emmanuelle CANET-SOULAS INSERM U1060, CarMeN lab, Univ. Lyon 1 Bâtiment IMBL 11 Avenue Jean CAPELLE INSA de Lyon 69 621 Villeurbanne Tél : 04.72.68.49.09 Fax : 04.72.68.49.16 **emmanuelle.canet@univ-lyon1.fr**
INFOMATHS	**INFORMATIQUE ET MATHÉMATIQUES** **http://edinfomaths.universite-lyon.fr** Sec. : Renée EL MELHEM Bât. Blaise PASCAL, 3e étage Tél : 04.72.43.80.46 Fax : 04.72.43.16.87 **infomaths@univ-lyon1.fr**	M. Luca ZAMBONI Bât. Braconnier 43 Boulevard du 11 novembre 1918 69 622 Villeurbanne CEDEX Tél : 04.26.23.45.52 **zamboni@maths.univ-lyon1.fr**
Matériaux	**MATÉRIAUX DE LYON** **http://ed34.universite-lyon.fr** Sec. : Marion COMBE Tél : 04.72.43.71.70 Fax : 04.72.43.87.12 Bât. Direction **ed.materiaux@insa-lyon.fr**	M. Jean-Yves BUFFIÈRE INSA de Lyon MATEIS - Bât. Saint-Exupéry 7 Avenue Jean CAPELLE 69 621 Villeurbanne CEDEX Tél : 04.72.43.71.70 Fax : 04.72.43.85.28 **jean-yves.buffiere@insa-lyon.fr**
MEGA	**MÉCANIQUE, ÉNERGÉTIQUE, GÉNIE CIVIL, ACOUSTIQUE** **http://edmega.universite-lyon.fr** Sec. : Marion COMBE Tél : 04.72.43.71.70 Fax : 04.72.43.87.12 Bât. Direction **mega@insa-lyon.fr**	M. Philippe BOISSE INSA de Lyon Laboratoire LAMCOS Bâtiment Jacquard 25 bis Avenue Jean CAPELLE 69 621 Villeurbanne CEDEX Tél : 04.72.43.71.70 Fax : 04.72.43.72.37 **philippe.boisse@insa-lyon.fr**
ScSo	**ScSo*** **http://ed483.univ-lyon2.fr** Sec. : Viviane POLSINELLI Brigitte DUBOIS INSA : J.Y. TOUSSAINT Tél : 04.78.69.72.76 **viviane.polsinelli@univ-lyon2.fr**	M. Christian MONTES Université Lyon 2 86 Rue Pasteur 69 365 Lyon CEDEX 07 **christian.montes@univ-lyon2.fr**

*ScSo : Histoire, Géographie, Aménagement, Urbanisme, Archéologie, Science politique, Sociologie, Anthropologie

To my beloved parents Fatiha & Saleh.
To my sweetheart Nahed.
To my dear sisters and brother Rahma, Rimel and Raafet.

Abstract

In this thesis, we present and study a new formulation of frictional contact between two elastic bodies based on Nitsche's method. This method aims to treat the interface conditions in a weak sense, thanks to a consistent additional term stabilized with the parameter γ. At first, we introduce the study carried out in the small strain framwork for an unbiased version of the method. The non-distinction between a master surface and a slave one will allow the method to be more generic and directly applicable to the self-contact problem. The restrictive framework of small strain allowed us to obtain theoretical results on the consistency and convergence of the method. Then, we present the extension of the Nitsche method to the large strain case more relevant for industrial applications and situations of self-contact. This Nitsche's method is formulated for an hyper-elastic material and declines in the two versions: biased and unbiased. We describe a class of methods through a generalisation parameter θ . Particular variants have different properties from a numerical point of view, in terms of accuracy and robustness. To prove the accuracy of the method for large deformations, we provide several academic and industrial tests. We also study the influence of numerical quadrature on the accuarcy and convergence of the method. This study covers a comparison of several integration rules proposed in the literature for other integral methods.

Key words — frictional contact for small and large strain, Nitsche's method, unbiased methods, numerical quadrature for contact.

Résumé

Dans cette thèse, nous présentons et étudions une nouvelle formulation du problème de contact frottant entre deux corps élastiques se basant sur la méthode de Nitsche. Dans cette méthode les conditions de contact sont imposées faiblement, grâce à un terme additionnel consistant et stabilisé par un paramètre γ. En premier lieu, nous introduisons, l'étude effectuée en petites déformations pour une version non biaisée de la méthode. La non-distinction entre une surface maître et une surface esclave permettera à la méthode d'être plus générique et applicable directement au problème d'auto-contact. Le cadre restrictif des petites déformations nous permet d'obtenir des résultats théoriques sur la stabilité et la convergence de la méthode. Ces résultats sont complétés par une validation numérique. Ensuite, nous introduisons l'extension de la méthode de Nitsche au cadre des grandes déformations qui est d'avantage pertinent pour les applications industrielles et les situations d'auto-contact. La méthode de Nitsche est formulée pour un matériau hyperélastique avec frottement de Coulomb et se décline en deux versions : biaisée ou non. La formulation est généralisée à travers un paramètre θ pour couvrir toute une famille de méthodes. Chaque variante particulière a des propriétés différentes du point de vue théorique et numérique, en termes de précision et de robustesse. La méthode est testée et validée à travers plusieurs cas tests académiques et industriels. Nous effectuons aussi une étude de l'influence de l'intégration numérique sur la précision et la convergence de la méthode. Cette étude couvre une comparaison entre plusieurs schémas d'integration proposés dans la littérature pour d'autres méthodes intégrales.

Mots clés — contact frottant en petites et grandes déformations, méthode de Nitsche, formulation non biaisée, intégration numérique.

Acknowledgements

This work could not be achieved without the wise guidance of my scientific adviser Pr. Yves Renard. I would like to express my sincere gratitude to him for his continuous guidance and encouragement throughout these three years of thesis. I highly appreciate his deep knowledge and precious support on research as well as on my career.
I am, as well, thankful to my co-adviser Franz Chouly, for his contributions of time and ideas to make my Ph.D. experience far more fruitful. His unconditioned support and valuable contributions were very important to achieve this work.

Afterwards, I want to thank Pr. Laura De Loranzis and Pr. Patrick Le Tallec for accepting to be reporters of this thesis and for their precious time that they have dedicated to help me improving this work. I would like to thank, also, Mr. Miguel Angel Fernandez and Mr. Patrice Hauret for accepting to be part of my jury.

My sincere thanks also goes to MFP Michelin for giving me the opportunity and financial support to carry out this work under the best conditions, especially Jean-François Deldon, for welcoming me in Clermont-Ferrand and supervising my works there. His pieces of advice were very useful to carry out the numerical part of this thesis. I thank, as well, all the other members of the computational mechanics team of Michelin for their heartwarming welcome, especially the team's head Mr. Ramzy Boussetta. Great appreciation goes, also, to Mr Makrem Arfaoui for making possible this collaboration with Michelin.

I warmly thank all my colleagues and friends in the ICJ Mathematics pole LAMCoS laboratory, notably Rafik Ben Hassine and Mathieu Fabre for their collaboration and for facilitating my integration within a friendly atmosphere.
Finally, I would like to thank my family, my beloved Nahed and all my friends for their tremendous and unconditioned support and encouragement.

Contents

List of Figures

List of Tables

Glossary of acronyms and symbols

The following acronyms are used in this thesis.

Acronyms

FEM	Finite Element Method
NTS	Node-to-Segment
STS	Segment-to-Segment
X-FEM	Extended finte element method
IBVP	Initial Boundary Value Problem
KKT conditions	Karush-Kuhn-Tucker conditions
PVW	Principle of Virtual Work
CIFRE	"Convention Industrielle de Formation par la Recherche"
INSA	"Institut National des Sciences Appliquées"

The following mathematical symbols are used in this thesis.

General notation

For an arbitrary field, we note:

- a A scalar field
- $\mathbf{a}$ A vectorial field
- $\underline{\underline{\mathbf{a}}}$ A second order tensor
- $\underline{\underline{\underline{\underline{\mathbf{a}}}}}$ A fourth order tensor

Greek symbols

Ω^i	The domain in $\mathbb{R}^d$ occupied by the reference configuration of the body (i)
Ω	$= \Omega^1 \cup \Omega^2$
$\partial\Omega^i$	The boundary of the body (i)
Γ_c^i	The reference contact surface
Γ_c	$=\Gamma_c^1 \cup \Gamma_c^2$
$(\Gamma_c^i)^t$	The deformed contact surface
Γ_c^t	$=(\Gamma_c^1)^t \cup (\Gamma_c^2)^t$
Γ_D^i	The reference Dirichlet surface (where the displacement $\mathbf{u}^i$ is imposed)
$(\Gamma_D^i)^t$	The deformed Dirichlet surface.
Γ_N^i	The reference Neumann surface (where the traction $\mathbf{t}^i$ is imposed)
$(\Gamma_N^i)^t$	The deformed Neumann surface.
$\boldsymbol{\varphi^i}$	The motion transformation of Ω^i
$\boldsymbol{\varphi}$	The motion transformation of Ω
Π^i	A one to one application mapping the two contact surfaces.
σ_n	Normal stress for small strain
$\boldsymbol{\sigma}_t$	Tangential stress for small strain
$\hat{\boldsymbol{\sigma}}_{\boldsymbol{N}}$	The contact stress on the reference configuration for large strain
$\hat{\sigma}_n$	Normal stress for large strain
$\hat{\boldsymbol{\sigma}}$	Tangential stress for large strain
$\boldsymbol{\lambda}$	Lagrange multiplier
θ	A generalization parameter ($\in \mathbb{R}$)
γ	Positive real function on Γ_C^i (Nitsche's or augmentation parameter)
γ_0	A positive given constant
ν	An arbitrary positive real
ϵ_n	Normal penalization
ϵ_t	Tangential penalization

Latin symbols

i	The bodies indexation $= 1, 2$
d	The dimension of the problem
$\mathbf{x}$	A point of the deformed slave contact surface
$\mathbf{y}$	The point corresponding to $\mathbf{x}$ in the deformed master contact surface
$\mathbf{X}$	A point of the reference slave contact surface
$\mathbf{Y}$	The point corresponding to $\mathbf{X}$ in the reference master contact surface
$\mathbf{u}^i$	The displacement field of the domain Ω^i
$\mathbf{u}$	The displacement field of the system
u_n/u_n^i	The normal displacement field
$\mathbf{u}_t/\mathbf{u}_t^i$	The tangential displacement field
$\mathbf{v}^i/\delta\mathbf{u}^i$	An arbitrary displacement field of the domain Ω^i
$\mathbf{v}/\delta\mathbf{u}$	An arbitrary displacement field of the system
$\mathbf{t}^i$	The traction field of the boundary Γ_N^i
$\mathbf{f}^i$	The body force of the body i
$\mathbf{n}^i$	The outward unit normal vector on Γ_C^i (or$(\Gamma_C^i)^t$) for the latge strain
$\mathbf{N}^i$	The outward unit normal vector on Γ_C^i on the reference configuration
$\tilde{\mathbf{n}}^i$	A unit vector defined on Γ_C^i
$\mathbf{v}$	Velocity
$g(\mathbf{u})$	The normal gap (for large strain)
$[\![u]\!]_n^i$	The relative normal displacement (normal gap/jump) for small strain on Γ_c^i
$[\![\mathbf{u}]\!]_t^i$	The relative tangential displacement (tangential jump) for small strain on Γ_c^i
g_n	Initial normal gap
$[\![\mathbf{u}]\!]$	Jump operator along an interface
$\langle\boldsymbol{\sigma}\rangle$	Average operator along an interface
s^i	Tresca friction threshold
$\mathscr{F}$	Coulomb friction coefficient
h	The mesh size
$\mathcal{J}$	The system's energy
$\mathcal{J}_c$	The contact's energy
G	The virtual work
$W(\underline{\underline{\mathbf{E}}})$	The energy potentiel of an hyper-elastic law
$\mathscr{L}$	Lagrangian functional
$\mathbf{V}^i$	Hilbert space $\mathbf{V}_0^i = \left\{\mathbf{v}^i = 0 \in \mathbf{V}^i : \quad \mathbf{v}^i = 0 \text{ on } \Gamma_D^i\right\}$
$\mathbf{V}$	Hilbert space $\mathbf{V}_0 = (\mathbf{V}_0^1 \times \mathbf{V}_0^2)$
$\mathbf{K}$	Convex cone of admissible displacements
$\mathbf{V}_h^i$	A family of finite dimensional vector spaces of $\mathbf{V}_0^i$ indexed by h
$\mathbf{V}_h$	$(\mathbf{V}_{0h}^1 \times \mathbf{V}_{0h}^2)$
S	A closed convex set

Operators

$det(\cdot)$	The determinant of a matrix
$\otimes$	The tensor product
:	The double contraction
$\cdot$	The scalar product
$\|\cdot\|$	Euclidean norm
$\|\cdot\|_0$	L^2-norm
$\|\cdot\|_{H^1}$	H^1-norm
$\|\cdot\|$	Absolute value
∇	The gradient operator in the deformed configuration
$\nabla_{\mathbf{X}}$	The gradient operator in the reference configuratio
$\dot{A}$	Time derivative of A
$\mathcal{D}A(\mathbf{u})[\delta\mathbf{u}]$	The directional derivative of A with respect to the displacement, in direction $\delta\mathbf{u}$
$H(\cdot)$	The Heaviside function
$[\cdot]_{\mathbb{R}^-}$	The rojection onto $\mathbb{R}^-$ of a real
$[\cdot]_\tau / \boldsymbol{P}_{B(\tau)}(\cdot)$	The projection onto the closed ball centered at the origin and of radius τ
$\underline{\underline{\mathbf{T_n}}}$	The projection on the tangent plane corresponding to normal vector $\mathbf{n}$
$\boldsymbol{\mathcal{P}}_{B(\mathbf{n},\tau)}(\cdot)$	$= \boldsymbol{P}_{B(\tau)} \circ \underline{\underline{\mathbf{T}_n}}$
$a(\cdot,\cdot)/A_{\theta\gamma}(\cdot,\cdot)$	Bilinear form
$L(\cdot)/\mathrm{P}^{\mathbf{n}}_{\theta,\gamma}(\cdot)$	Linear form
$\mathbf{P}^{\mathbf{t}}_{\theta,\gamma}(\cdot)$	Linear operator
$\mathbf{B}\cdot$	Trace-like linear operator
$\langle\cdot,\cdot\rangle_\Gamma$	A duality product
$\boldsymbol{\mathcal{C}}_{\gamma,\mathscr{F}}(\cdot,\cdot,\cdot,\cdot)$	A non smooth operator

Tensors

$\underline{\underline{\mathbf{I}}}$	The identity tensor of size $d \times d$
$\underline{\underline{\mathbf{F}}}$	The deformation gradient
$\underline{\underline{\mathbf{C}}}$	Cauchy-Green tensor
$\underline{\underline{\mathbf{E}}}$	Green-Lagrange tensor
$\underline{\underline{\boldsymbol{\sigma}}}$	The Cauchy stress tensor
$\underline{\underline{\hat{\boldsymbol{\sigma}}}}$	The first Piola-Kirchhoff stress tensor
$\underline{\underline{\mathbf{S}}}$	The second Piola-Kirchhoff stress tensor
$\underline{\underline{\boldsymbol{\mathcal{C}}}}/\underline{\underline{\mathbf{A}}}$	The fourth order symmetric elasticity tensor
$\underline{\underline{\boldsymbol{\varepsilon}}}$	The strain tensor field

Présentation de la thèse

Contents

Introduction

Le présent travail est une étude mathématique et numérique d'une nouvelle méthode éléments finis permettant l'approximation numérique du contact et du frottement. Le phénomène de contact entre corps déformables et ses effets associés, tel que le frottement, l'usure ou l'adhésion, génèrent des complexités significatives dans la modélisation numérique et la simulation en mécanique des solides. Ceci est principalement dû à la non-linéarité de ce type de condition aux limites et à la non-régularité des principes physiques simulés. Plusieurs difficultés s'opposent à la mise en place d'un outil de simulation général pour la mécanique de contact, en prenant en compte ses deux aspects les plus importants: la robustesse et l'approximation précise et efficace des déplacements et des contraintes.

Cette étude, réalisée en partenariat avec la Manufacture Française des Pneumatiques Michelin sous forme d'un contrat CIFRE entre l'INSA de Lyon, l'entreprise et moi-même, est motivée par la présence et l'influence éminentes des phénomènes de contact et d'auto-contact dans la simulation des pneumatiques.

Dans cette thèse, nous présentons une nouvelle formulation de contact frottant entre deux corps élastiques basée sur la méthode de Nitsche. La méthode de Nitsche est une méthode consistante et primale pour traiter le contact. Son aspect intégral lui permet d'être très adaptée au contact de corps déformables avec des maillages non-conformes.
La motivation principale de ce travail est le besoin d'une méthode d'approximation simple et efficace pour l'auto-contact. Pour répondre à cette exigence, nous proposons une méthode non biaisée dans laquelle nous ne faisons pas la distinction entre une surface maître et une surface esclave et nous imposons la non-pénétration et les conditions de frottement sur les deux. La méthode de Nitsche est adaptée au formalisme non biaisé puisque la méthode permet d'imposer faiblement les conditions de contact sur les deux surfaces en vis-à-vis. La méthode doit d'abord être formulée et testée en petites déformations dans

le cadre de l'élasticité linéaire. Ce cadre restrictif nous permet d'obtenir des résultats théoriques sur la stabilité et la convergence de la méthode.
Elle doit, ensuite, être étendue au cadre des grandes transformations élastiques, d'avantage pertinent pour les applications et les situations d'auto-contact.
Comme dans [CHR15c], nous décrivons une famille de méthodes (symétrique, non-symétrique, anti-symétrique) à l'aide d'un paramètre θ, chaque variante particulière ayant des propriétés différentes du point de vue numérique, en termes de précision et de robustesse. La méthode sera testée sur une palette de cas de tests académiques et industiels pour les petites et grandes déformations afin de s'assurer de sa performance.

Ce chapitre, ayant pour objectif de présenter ce travail de thèse et résumer le prérent manuscrit, est organisé comme suit: La première partie 0.1 résume les travaux effectués pendant la thèse et l'essentiel des résultats. La deuxième partie 0.2 est un bref sommaire de ce manuscrit et de son organisation.

0.1 Résumé des travaux

Nous donnerons, d'abord, les notions et les concepts de base de la mécanique de contact et introduirons la méthode de Nitsche pour traiter les différents types de conditions aux limites. Puis, nous formulerons cette méthode pour le problème de contact de deux corps élastiques:

0.1.1 Méthode non biaisée de Nitsche pour le contact et le frottement de Tresca dans le cadre des petites déformations

Nous considérons deux corps Ω^i pouvant entrer en contact via leurs surfaces Γ_C^i. Afin d'obtenir une formulation non biaisée du problème de contact nous prescrivons les conditions de contact déduites du problème de Signorini et les conditions de frottement de Tresca sur les deux surfaces Γ_C^i d'une manière symétrique et nous allons intégrer sur chacune d'elles. La dérivation d'une méthode de type Nitsche provient d'une reformulation des conditions de contact sous forme d'une seule équation (voir par exemple [CH13] et [CHR15c]). De même, une simple adaptation au frottement de Tresca est proposée dans [Cho14]. Si on note $\sigma_n^i(\mathbf{u}^i)$ la contrainte normale sur le bord de contact du corps (i) et $[\![u]\!]_n^i$ le saut normal de déplacement entre les deux surfaces calculé sur le bord Γ_C^i, on démontre que les conditions de contact et de frottement inscrites sur les deux surfaces de contact sont équivalentes aux deux équations (1) et (2).

$$\sigma_n^i(\mathbf{u}^i) = [\sigma_n^i(\mathbf{u}^i) - \gamma^i [\![u]\!]_n^i]_{\mathbb{R}_-}, \tag{1}$$

où, γ^i est réel positif (on l'appellera paramètre de Nitsche) et $[a]_{\mathbb{R}_-}$ indique la partie négative d'un réel $a \in \mathbb{R}$.
De même, dans [Cho14], en notant $\boldsymbol{\sigma}_t(\mathbf{u}^i)$ la contrainte tangentielle et $[\![\mathbf{u}]\!]_t^i$ le saut tangentiel de deplacement sur le bord de contact, la condition de frottement de Tresca est

équivalente à l'équation:

$$\boldsymbol{\sigma}_t(\mathbf{u}^i) = [\boldsymbol{\sigma}_t(\mathbf{u}^i) - \gamma^i [\![\mathbf{u}]\!]^i_t]_{s^i}, \tag{2}$$

où s^i est le seuil de frottement de Tresca. Pour tout $\alpha \in \mathbb{R}^+$, la notation $[\cdot]_\alpha$ fait référence à la projection orthogonale sur la boule fermée $\mathcal{B}(0,\alpha) \subset \mathbb{R}^{d-1}$, centrée à l'origine et de rayon α. L'utilisation de la méthode de Nitsche nous permet de diviser l'effort de contact équitablement sur les deux surfaces de contact en utilisant la loi d'action-réaction. Ensuite, nous utilisons la formule de Green et toutes les équations d'équilibre et les conditions aux limites pour avoir la formulation éléments finis non biaisée (3) dans laquelle le contact et le frottement sont imposés faiblement sur les deux surfaces de contact Γ^i_C d'une manière symétrique.

$$\left\{\begin{array}{l} \text{Trouver } \mathbf{u}^h \in \mathbf{V}^h \text{ tel que,} \\ \\ A^{1,2}_{\theta\gamma}(\mathbf{u}^h, \mathbf{v}^h) + \dfrac{1}{2}\displaystyle\sum_{i=1}^{2} \int_{\Gamma^i_C} \frac{1}{\gamma^i} \Big[P^i_{n,1\gamma^i}(\mathbf{u}^h)\Big]_{\mathbb{R}^-} P^i_{n,\theta\gamma^i}(\mathbf{v}^h)\, \mathrm{d}\Gamma \\ + \dfrac{1}{2}\displaystyle\sum_{i=1}^{2} \int_{\Gamma^i_C} \frac{1}{\gamma^i} \Big[\mathbf{P}^i_{t,1\gamma^i}(\mathbf{u}^h)\Big]_{s^i} \cdot \mathbf{P}^i_{t,\theta\gamma^i}(\mathbf{v}^h)\, \mathrm{d}\Gamma = L(\mathbf{v}^h), \quad \forall \mathbf{v}^h \in \mathbf{V}^h, \end{array}\right. \tag{3}$$

avec:

$$P^i_{n,\theta\gamma^i}(\mathbf{v}) = \theta\sigma^i_n(\mathbf{v}^i) - \gamma^i [\![v]\!]^i_n \ , \quad \text{et} \qquad \mathbf{P}^i_{t,\theta\gamma^i}(\mathbf{v}) = \theta\boldsymbol{\sigma}^i_t(\mathbf{v}^i) - \gamma^i [\![\mathbf{v}]\!]^i_t \ ,$$

et

$$A^{1,2}_{\theta\gamma}(\mathbf{u},\mathbf{v}) = \sum_{i=1}^{2} \left(\int_{\Omega^i} \sigma(\mathbf{u}^i) : \boldsymbol{\varepsilon}(\mathbf{v}^i)\, d\Omega - \frac{1}{2}\int_{\Gamma^i_C} \frac{\theta}{\gamma^i} \boldsymbol{\sigma}^i(\mathbf{u}^i)\mathbf{n}^i \cdot \boldsymbol{\sigma}^i(\mathbf{v}^i)\mathbf{n}^i\, \mathrm{d}\Gamma \right).$$

Le paramètre θ permet de retrouver des variantes qui possèdent des propriétés théoriques et numériques différentes (voir [CHR15c]). Par exemple, quand $\theta = 1$ la méthode est symétrique. Pour $\theta = 0$ la méthode est assez simple, mais elle n'est pas symétrique. Et quand $\theta = -1$, on obtient une méthode plus robuste qui converge indépendamment du paramètre de Nitsche γ^i.

Pour prouver l'efficacité de la méthode, nous avons effectué son analyse mathématique. Nous montrons, dans un premier temps, l'équivalence formelle entre les formulations forte et variationnelle pour le problème continu. Étant donné que la construction de la méthode consiste en particulier à séparer les conditions de contact en deux parties, cette étape est nécessaire pour assurer la cohérence de la formulation. Nous montrons également la consistance, qui provient de la consistance de la méthode de Nitsche, et l'existence et l'unicité d'une solution et la convergence optimale de la méthode pour la norme H^1 pour γ^i suffisamment grand. Si $\theta = -1$, aucune condition sur γ^i n'est requise pour assurer l'existence et l'unicité d'une solution et la convergence optimale.

Pour tester la méthode, une validation numérique a été faite à travers le test de Hertz en deux et trois dimensions. Les tests comportent une étude de convergence pour

les différentes valeurs du paramètre de généralisation θ et du paramètre de Nitsche γ^i. À titre d'exemple, nous présentons dans la Figure.1 la courbe de convergence pour la méthode avec $\theta = 0$ et $\gamma_0 = 100E$, tel que

$$\gamma^i_{|K^i \cap \Gamma^i_C} = \frac{\gamma_0}{h_{K^i}}.$$

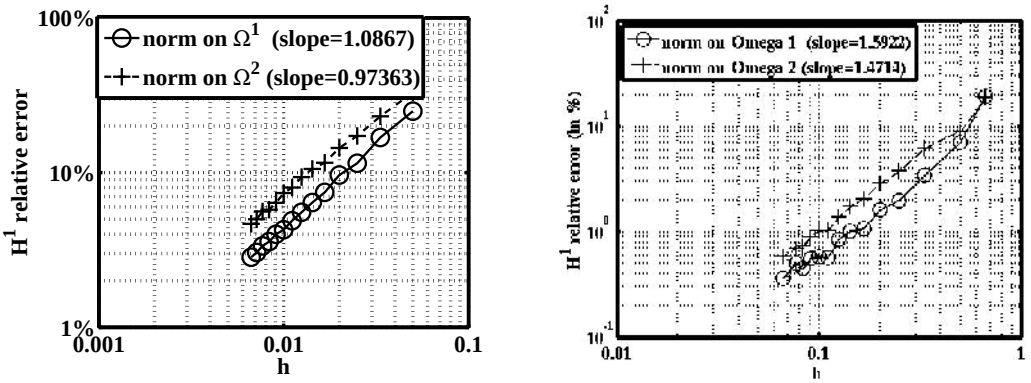

(a) (b)

Figure 1: Courbe de convergence en 2D pour la méthode $\theta = 0$ et la norme H^1 de l' erreur relative, avec $\gamma_0 = 100E$ et des élément finis de Lagrange P_1 (a) et P_2 (b).

Comme prévu par l'analyse mathématique la convergence est obtenue avec des taux optimaux.
L'environnement libre GetFEM ++ [1] a été utilisé pour effectuer les tests. Tous les détails de la construction et des analyses de la méthode ainsi que les résultats numériques sont donnés au chapitre 3 du manuscript et aussi publiés dans l'article [CMR16].

0.1.2 Méthode de Nitsche en grandes déformations

Soit $\Omega \subset \mathbb{R}^d$ un ensemble ouvert borné qui présente la configuration de référence. Le domaine Ω représente, cette fois, tout les corps susceptibles d'entrer en contact (un seul pour l'auto-contact) et Γ_c est l'union de toutes les surfaces de contact dans la configuration de référence.
La configuration déformée Ω^t est définie à travers la transformation $\boldsymbol{\varphi}$ qui relie tout point $\mathbf{X}$ de la configuration de référence au point $\mathbf{x} \in \Omega^t$. On définit ainsi le déplacement $\mathbf{u}$ par rapport à la configuration de référence par: $\mathbf{u}(\mathbf{X}) = \boldsymbol{\varphi}(\mathbf{X}) - \mathbf{X}$.
Pour étendre notre méthode au frottement de Coulomb, on considère un processus quasi-statique et le cas statique sera traité comme un cas particulier.
Étant donné que le choix d'une loi de comportement n'est pas central dans l'approximation proposée du contact, nous allons considérer une énergie potentielle globale $\mathcal{J}(\mathbf{u})$ dépendante d'un potentiel hyper-élastique $W(\mathbf{F})$. Notons, par ailleurs, le premier tenseur de Piola-

[1] http://getfem.org

Kirchhoff

$$\hat{\underline{\underline{\boldsymbol{\sigma}}}} = \frac{\partial W}{\partial \underline{\underline{\mathbf{F}}}}(\underline{\underline{\mathbf{F}}}),$$

qui sert à définir la contrainte de contact: $\hat{\boldsymbol{\sigma}}_{\boldsymbol{N}} = \hat{\underline{\underline{\boldsymbol{\sigma}}}}(\mathbf{u})\mathbf{N}_x$ en $\partial\Omega$. En définissant une fonction de correspondance qui relie un point $\mathbf{x}$ d'une surface de contact à son projeté $\mathbf{y} \in \Gamma_C^t$, on peut définir la fonction de gap $\mathrm{g}(\mathbf{u})$. Cette fonction va dépendre du choix du mapping et ainsi ce choix influence naturellement notre méthode. Dans le chapitre 4 deux stratégies de mapping sont introduites: la projection et le lancé de rayon puis une comparaison entre les deux est donnée.
Dans ce formalisme les conditions de contact sont:

$$\begin{aligned} g(\mathbf{u}) &\geq 0 && && (4a)\\ \hat{\sigma}_n(\mathbf{u}) &\leq 0 && \text{sur } \Gamma_c. && (4b)\\ \hat{\sigma}_n(\mathbf{u})g(\mathbf{u}) &= 0 && && (4c) \end{aligned}$$

Et celle de frottement de Coulomb sont:

$$\begin{cases} \|\hat{\sigma}_t(\mathbf{u})\| \leq -\mathscr{F}\hat{\sigma}_n(\mathbf{u}) & \text{si } \mathbf{v} = 0,\\ \hat{\sigma}_t(\mathbf{u}) = \mathscr{F}\hat{\sigma}_n(\mathbf{u})\dfrac{\mathbf{v}}{\|\mathbf{v}\|} & \text{sinon,} \end{cases} \tag{5}$$

où $\mathscr{F}$ est le coefficient de frottement de Coulomb et $\mathbf{v}$ une vitesse définie de façon objective (voir section 2.1.2.2 du chapitre 2) Comme en petites déformations, les conditions de contact et de frottement (4) et (5) sont équivalentes à l'équation (6) qui intègre les conditions de contact dans sa composante normale et les conditions de frottement dans la composante tangentielle :

$$\boldsymbol{\mathcal{C}}_{\gamma,\mathscr{F}}(\hat{\boldsymbol{\sigma}}_{\boldsymbol{N}}, g, \mathbf{v}, \mathbf{n}_x) = \hat{\boldsymbol{\sigma}}_{\boldsymbol{N}}, \tag{6}$$

où $\boldsymbol{\mathcal{C}}_{\gamma,\mathscr{F}}$ est un opérateur non linéaire défini par :

$$\boldsymbol{\mathcal{C}}_{\gamma,\mathscr{F}}(\boldsymbol{\sigma}, g, \mathbf{v}, \mathbf{n}) = -[\boldsymbol{\sigma}\cdot\mathbf{n} + \gamma\, g]_{\mathbb{R}^-}\,\mathbf{n} + \boldsymbol{\mathcal{P}}_{B(\mathbf{n},\mathscr{F}\,[\boldsymbol{\sigma}\cdot\mathbf{n}+\gamma\, g]_{\mathbb{R}^-})}(\boldsymbol{\sigma} - \gamma\,\mathbf{v}).$$

$\boldsymbol{\mathcal{P}}_{B(\mathbf{n},\tau)}$ est la composition d'une projection sur le plan tangent correspondant à la normale $\mathbf{n}$ et la projection sur la boule de rayon τ.

En considérant l'équilibre et le principe d'action réaction en $\mathbf{x}$ et $\mathbf{y}$, on obtient le problème variationnel suivant:

$$\begin{cases} \mathcal{D}\mathcal{J}(\mathbf{u})[\delta\mathbf{u}] - \dfrac{1}{2}\displaystyle\int_{\Gamma_c} \frac{\theta}{\gamma}\hat{\boldsymbol{\sigma}}_{\boldsymbol{N}}(\mathbf{u})\cdot\mathcal{D}\hat{\boldsymbol{\sigma}}_{\boldsymbol{N}}(\mathbf{u})[\delta\mathbf{u}]\; d\Gamma \\ +\dfrac{1}{2}\displaystyle\int_{\Gamma_c} \frac{1}{\gamma}\mathcal{C}_{\gamma,\mathscr{F}}(\hat{\boldsymbol{\sigma}}_{\boldsymbol{N}}, g, \mathbf{v}, \mathbf{n}_x)\cdot\mathcal{D}\Big(\theta\hat{\boldsymbol{\sigma}}_{\boldsymbol{N}} + \gamma(\mathbf{u}(\mathbf{Y}) - \mathbf{u}(\mathbf{X}))\Big)[\delta\mathbf{u}]\; d\Gamma \;= 0 \quad \forall\,\delta\mathbf{u} \in \mathbf{V}\,, \end{cases} \tag{7}$$

Le paramètre θ est un réel qui, comme en petites déformation, sert à généraliser la méthode.

Ce problème correspond à une méthode non biaisée où on intègre sur toutes les surfaces de contact Γ_c.
Une formulation plus complète de la méthode ainsi qu'une preuve qu'elle dérive d'un potentiel d'énergie dans sa version symétrique ($\theta = 1$) sont données dans le chapitre 4.

Remarque 0.1.1. *L'avantage essentiel de la méthode proposée est qu'elle est consistante sans ajout de variables supplémentaires. Mais l'inconvénient le plus important de cette méthode est l'utilisation de la loi de comportement ainsi que de sa dérivée. Le problème tangent fait alors intervenir la dérivée seconde de la loi de comportement (dérivée troisième du potentiel), via le terme* $\mathcal{D}^2\hat{\boldsymbol{\sigma}}_{\boldsymbol{N}}(\mathbf{u})[\delta\mathbf{u}, \Delta\mathbf{u}]$. *Ce terme peut être difficile à expliciter pour des lois de comportement complexes. Il n'apparaît cependant plus lorsque* $\theta = 0$, *ce qui rend cette variante plus attractive du point de vue de l'implémentation.*

La méthode proposée a été implémentée sous GetFEM++ et testée à travers quelques tests classiques. Les différents tests et les résultats sont détaillés au chapitre 4 ainsi que dans l'aricle [MRC17].

Contact de Hertz

Parmi ces tests, le test de contact de Hertz permet de vérifier la capacité de la méthode à approximer un profil de pression de contact connu avec un nombre limité de points d'intégration. Comme en petites déformations la convergence de la méthode est influencée par la valeur du paramètre de Nitsche γ et cette influence dépend de la valeur de θ (voir [CHR15c,CMR16]). On teste alors la méthode pour différentes valeurs de γ et θ pour vérifier son comportement et sa robustesse. La table 1 résume les résultats de convergence pour un matériau de Saint-venant Kirchhoff et 3 points d'intégration par élément. Il est remarquable que la version $\theta = -1$ soit plus robuste et converge avec toutes les valeurs de γ. Cette propriété démontrée théoriquement dans le cadre des petites déformations est alors vérifiée numériquement pour les grandes déformations. La version symétrique $\theta = 1$ est la plus sensible et ne converge que pour γ élevé. En comparant $\theta = 0$ à $\theta = 1$, on remarque que la version simple ($\theta = 0$) est plus robuste par rapport à γ même si on perd également la convergence quand γ est faible. Les mêmes observations sont déduites avec ou sans frottement. Nous mentionnons, aussi, que quand γ est très élevé la convergence est plus difficile à obtenir, surtout avec frottement. Cela est dû au fait que, quand γ est élevé, le problème devient raide et mal conditionné.

Tubes croisés

Le dernier exemple numérique présenté est le test des tubes croisés. Dans cet exemple, nous simulons le contact entre deux cylindres élastiques creux croisés. Étant donné que le déplacement imposé est grand, les déformations des tubes sont très importantes et on observe une configuration d'auto-contact dans le tube le moins rigide. Ce test nous permet donc de valider notre modèle pour le cas d'auto-contact.

Sans frottement				Coefficient de frottement= 0.3			
Valeur de θ	Paramètre de Nitsche γ_0	Iterations de Newton	Erreure moyenne de pression(en %)	Valeur de θ	Paramètre de Nitsche γ_0	Iterations de Newton	Erreure moyenne de pression(en %)
0	$\frac{E}{100}$	7.24	17	0	$\frac{E}{100}$	8.5	14.4
	E	3.5	2.4		E	4.6	2.4
	$100 \cdot E$	4.6	2.7		$100 \cdot E$	20.7	6.8
-1	$\frac{E}{100}$	4.8	3.7	-1	$\frac{E}{100}$	5.3	3.3
	E	4.3	3.0		E	4.3	3.1
	$100 \cdot E$	4.6	4.1		$100 \cdot E$	9.2	4
1	$\frac{E}{100}$	14.8	54.8	1	$\frac{E}{100}$	29.8	59
	E	26.8	52.2		E	30	64
	$100 \cdot E$	4	4.2		$100 \cdot E$	11.2	4.1

Table 1: Erreur moyenne de pression de contact et nombre moyen d'iterations de Newton sur les 10 étapes de chargement

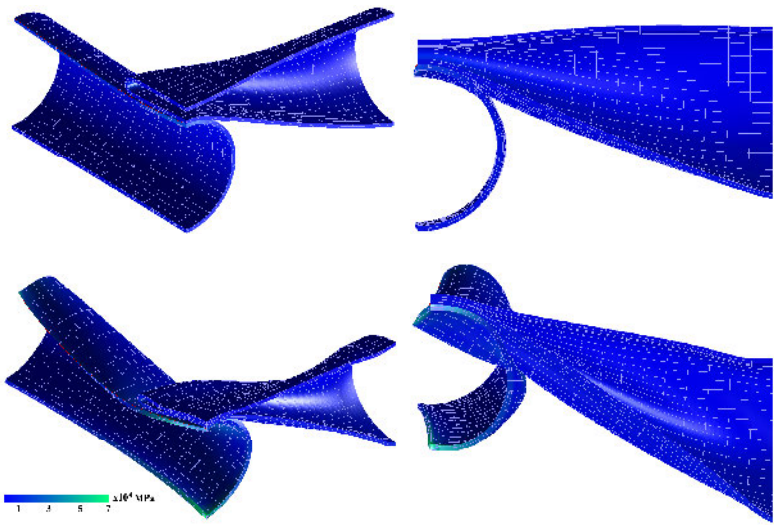

Figure 2: Déformation et pression de Von-Mises des deux tubes sans frottement et pour un déplacement de 20, 30 et 40 mm avec $\gamma = E$ et $\theta = 0$

0.1.3 Influence de l'erreur d'intégration pour le problème de contact

Le calcul précis et efficace des intégrales prescrites dans les formulations de contact (3) ou (7) est l'un des principaux défis des algorithmes de contact intégral. Ceci est dû au fait que le problème de contact fait intervenir, en général, des surfaces non coincidantes et des maillages non conformes, où nous intégrons des fonctions non-régulières qui ne peuvent pas être évaluées exactement en utilisant des quadratures de Gauss standard. Cette non-régularité a pour origine les termes par morceaux provenant des produits de grandeurs définies sur les deux surfaces et aussi l'opération de projection présentant le basculement entre les états contact/non contact et glissement/adhérence. L'intégration de telles fonctions à travers des schémas de quadrature numérique classiques génère généralement des oscillations de la solution sur l'interface de contact et empêche la méthode de passer les "patch tests".

Cette problématique est abordée au chapitre 5. Pour dépasser ces difficultés, nous avons testé quelques stratégies d'integration et comparé leurs efficacité avec une formulation de Nitsche.

L'erreur d'intégration est générée par deux type de discontinuité:

- Des discontinuités dites "faibles": Elles sont présentes à l'intérieur de la surface de contact. Ces irrégularités sont la conséquence de la discrétisation non conforme de la surface de contact et elles se manifestent sous la forme d'une intégrande continue, mais polynomiale par morceaux au sein d'un élément esclave.
- Des discontinuités "fortes": Elles sont observées au bord de la surface de contact. Celle ci sont, généralement plus singulières puisqu'elles sont causées par un changement non-continu (un saut) d'état entre contact/non-contact, ou adhérence/glissement.

Pour pouvoir intégrer des fonctions avec de telles irrégularités, plusieurs techniques d'intégration numérique ont été testées:

"L' intégration par élément"

Dans ce cas, nous n'effectuons pas de découpage de la méthode d'intégration. Le schéma d'intégration utilisé est celui de la surface esclave, tout en augmentant le nombre de point de Gauss pour améliorer la précision. Cette stratégie, utilisée par exemple dans [FW05, FW06], est la plus simple mais elle génère une erreur d'integration significative même avec un grand nombre de point de Gauss.

"L'intégration par segment"

Pour gérer ces problèmes d'intégration, beaucoup de méthodes segment-à-segment utilisent un algorithme de segmentation du schéma d'intégration. Nous appellerons cette technique "l'intégration par segment". L' idée générale a été décrite pour les méthodes classiques

de contact segment-segment dans [SWT85, ZW98]. Puis, la technique a été appliquée aux formulations "mortar" du contact dans [ML00a, PL03]. Pour éviter toutes les discontinuités dans l'intégration de la méthode (3), l'intégration par segment propose de couper chaque élément esclave en fonction des maîtres correspondants. Un segment d'intégration (polygone) est ainsi construit par le chevauchement d'un élément maître et d'un élément esclave. La caractéristique principale de ces segments est que la fonction intégrée est régulière et polynomiale sur chaque segment.
L'approximation avec l'intégration basée sur le segment est exacte à la précision machine près pour le Patch test. (voir voir Tableau 2 et Section 5.1.3 du Chapitre 5).
Cependant en observant le temps de calcul, la segmentation augmente considérablement le coût de calcul. Sachant que, dans le cas des grandes déformations, cette segmentation doit être effectuée pour chaque itération de Newton sur toute la surface de contact et que l'opération est beaucoup plus difficile dans ce cas avec une géométrie 3D car l'emplacement des points d'intégration n'est pas fixe, nous pourrions conclure que l'utilisation de l'intégration par segments entraîne des efforts considérables pour la mise en œuvre et le calcul.

La "segmentation des bords"

Pour réduire le coût de calcul de l'intégration par segment, [FPW15] a proposé, pour la méthode "mortar", une combinaison des deux méthodes d'intégration pour trouver un équilibre entre la simplicité de la première et l'exactitude de la deuxième. En notant que les fortes discontinuités provoquent plus d'erreur de quadrature que les faibles, il s'agit de couper le schéma d'intégration seulement lorsqu'une forte discontinuité se manifeste. Cette technique a été appelée "segmentation des bords" puisqu'on ne découpe que les éléments du bord de la surface de contact.
En d'autres termes, le schéma d'intégration par segments sera utilisé pour les éléments esclaves problématiques ayant de fortes discontinuités (bords libres, par exemple) et pour les éléments esclaves non critiques à l'intérieur de la zone de contact, l'intégration par éléments sera utilisée.

Ainsi, la segmentation des bords améliore la précision de l'approximation avec un coût de calcul beaucoup plus faible; mais l'erreur causée par les faibles discontinuités est toujours présente et nous ne réussissons toujours pas à passer le patch test.

L'intégration non-symétrique

Cette stratégie d'intégration a été introduite et testée pour la méthode "mortar" dans [CLM97, MRW02]. En constatant que réduire l'erreur d'approximation nécessite une formule en quadrature basée sur le côté esclave et que l'erreur de consistance est plutôt réduite par une intégration du côté maître, les auteurs proposent de combiner les deux règles d'intégration. En adaptant le concept à la méthode de Nitsche, la formulation

obtenue est:

$$\left\{\begin{array}{l} \mathcal{D}\mathcal{J}(\mathbf{u}^h)[\delta\mathbf{u}^h] - \dfrac{1}{2}\displaystyle\int_{\Gamma_c} \frac{\theta}{\gamma}\hat{\boldsymbol{\sigma}}_{\boldsymbol{N}}{}^h \cdot \mathcal{D}\hat{\boldsymbol{\sigma}}_{\boldsymbol{N}}{}^h[\delta\mathbf{u}^h]\; d\Gamma + \dfrac{1}{2}\displaystyle\int_{\Gamma_c} \frac{\theta}{\gamma}\boldsymbol{\mathcal{C}}_{\gamma,\mathscr{F}}(\hat{\boldsymbol{\sigma}}_{\boldsymbol{N}}{}^h, g, \mathbf{v}^h, \mathbf{n}_x) \cdot \mathcal{D}\hat{\boldsymbol{\sigma}}_{\boldsymbol{N}}{}^h[\delta\mathbf{u}^h] \\ + \dfrac{1}{2}\displaystyle\int_{\Gamma_c} \Big(\boldsymbol{\mathcal{C}}_{\gamma,\mathscr{F}}(\hat{\boldsymbol{\sigma}}_{\boldsymbol{N}}{}^h, g, \mathbf{v}^h, \mathbf{n}_x) - \boldsymbol{\mathcal{C}}_{\gamma,\mathscr{F}}(\hat{\boldsymbol{\sigma}}_{\boldsymbol{N}}{}^h(\mathbf{Y}), g(\mathbf{Y}), \mathbf{v}^h(\mathbf{Y}), \mathbf{n}_y)\Big) \cdot [\delta\mathbf{u}^h(\mathbf{X})]\; d\Gamma = 0 \\ \qquad\qquad \forall\, \delta\mathbf{u}^h \in \mathbf{V}_h. \end{array}\right. \tag{8}$$

Pour comparer ces différentes stratégies, nous avons effectué au chapitre 5 plusieurs tests. Nous rapportons, à titre d'exemple, dans le Tableau 2 le maximum d'erreur de pression et de gap obtenus avec les différents schémas, pour le patch test de Taylor avec bords de contact coincidants.

Nbre de pts de Gauss/face (méthode d'integration)	3 maillage conforme	3 (par segment)	3 (par élément)	45 (par élément)	3 (non-symmetrique)
Max erreur relative de pression	$2.48 \cdot 10^{-12}$	$2.9 \cdot 10^{-12}$	$3.4 \cdot 10^{-3}$	$1.51 \cdot 10^{-4}$	$7.26 \cdot 10^{-11}$
Max gap(mm)	$2.61 \cdot 10^{-18}$	$3.22 \cdot 10^{-17}$	$2.1 \cdot 10^{-7}$	$1.2 \cdot 10^{-9}$	$3.21 \cdot 10^{-16}$
Temps de calcul (ms)	76.4	281	79.5	273	77.4

Table 2: Maximum d'erreur relative de pression et de gap et temps de calcul avec les differents schémas d'intégration pour le patch test.

La "segmentation des bords" a été testée avec d'autres testes comportants des bords non-conformes (voir chapitre 5).

D'après les tests effectués, l'intégration non symétrique semble être une bonne solution pour réduire l'erreur d'intégration à l'intérieur de la surface de contact, mais au bords de la surface il est nécessaire de découper le schéma d'intégration et dans ce cas la segmentation des bords est la stratégie adaptée.

0.2 Structure du rapport

Cette thèse présente la modélisation mathématique et numérique et l'analyse de la méthode de type de Nitsche pour le contact et le frottement. Elle constitue une présentation générale de tous les aspects de la méthode de Nitsche et fournit l'analyse théorique et numérique effectuée tout au long des études doctorales. Ce manuscript de thèse de doctorat est organisé comme suit:

Le **Chapitre 1** est un chapitre introductif où nous presentons le contexte scientifique et industiel de la thèse et résumons les objectifs et les réalisations du travail.

Le **Chapitre 2** est un rappel préliminaire des problèmes de contact et de frottement pour les petites et grandes déformations. En outre, la deuxième section de ce chapitre donne un aperçu sur la méthode de Nitsche. Nous présentons dans cette partie du rapport la conception de la méthode pour traiter les conditions aux limites, en particulier le contact

et le frottement.
Dans le **Chapitre 3**, nous construisons une formulation non biaisée du contact entre deux corps élastiques avec un frottement de Tresca. La formulation décrit toute une classe de méthodes à travers un paramètre de généralisation θ.
Le **Chapitre 4** étend la méthode de Nitsche au cadre des grandes déformations avec un formalisme non biaisé permettant de traiter plus simplement le cas d'auto-contact et de contact multi-corps. En plus du contact, le frottement de Coulomb est pris en compte. Le cadre envisagé est celui d' un matériau hyper-élastique. Dans la dernière section du chapitre, nous fournissons une validation numérique de la méthode.
Le dernier **Chapitre 5** constitue une étude de l'influence de l'erreur d'intégration sur l'approximation du contact. Cette étude est réalisée pour la méthode de Nitsche et elle examine l'efficacité de la segmentation du schéma d'intégration et des différentes alternatives à cette opération coûteuse. Dans ce chapitre, nous évaluons les performances pour le patch test et l'impact sur l'ordre de convergence des différents schémas d'intégration.
Le manuscrit est cloturé par un chapitre de conclusion.

Chapter 1

Introduction

Contents

The work presented in this thesis consists in a mathematical and numerical modelization and analysis of a new finite element method allowing the simulation of contact and friction.
Contact interaction of deformable bodies and its associated effects, as frictional sliding, originate significant complexities in the numerical modeling and simulation of solid mechanics. This is chiefly due to the non-linearity of this type of boundary conditions and the lack of smoothness of the simulated physical principles. Several challenges face the construction of a truly general simulation tool for computational contact mechanics, with the three most important aspects in the constraint enforcement: robustness, accuracy and efficiency.

This study, carried out in partnership with the Manufacture Française des Pneumatiques Michelin, is motivated by the outstanding presence and influence of frictional contact and self-contact phenomena in the tire simulation. The tire is a quite complex and highly challenging structure for mechanical modeling and numerical simulation, since it couples different types of non-linearities and undergoes very large deformations and high pressures. Thus, the improvement of contact models to get further robust and accurate simulation with a lower cost is always a challenging task.
In this context, this work is fulfilled in the framework of a partnership in the form of a CIFRE contract between INSA of Lyon, the company Michelin and myself. This partnership aims to offer a complete study of a new integral formulation of contact ensuring an accurate and robust approximation of the frictional contact problem.
This introductive chapter is organized as follows: The first section 1.1 gives an overview of the industrial context of the problem and highlights the different motivations and specifications of the work. The Section 1.2, describes the general scientific environment of the thesis with a literature review of computational contact and the Nitsche's method proposed in the current work . We give, then, in section 1.3 an overview of the thesis underlining its main achievements and contributions. Finally, Section 1.4 is dedicated to a brief outline of this manuscript and its organization.

1.1 Industrial context and objectives

As part of its R&D and innovation effort, Michelin adopts numerical modeling and simulation as one of the main tools to ensure the safety and integrity of its various tire models and to improve its production process. Users of this tool are therefore faced to more and more complex modeling which involves a large number of degrees of freedom and all types of non-linearities.
The tire is one of nonlinear industrial structures, locally incompressible (rubber), highly heterogeneous (steel/rubber) and non isotropic operating in large strain. In addition, self-contact situations within the lamellae and increasing stress especially when braking could, further, complicate the simulation. But, nowadays, computational mechanics have reached an advanced level of description allowing a relatively accurate approximation of tire features and production process. The finite element method (FEM), which is the standard approach in this numerical field, represents an efficient simulation tool for this structural analysis.
When rolling or in the manufacturing stage, the tire is subjected to several contact configurations with road, sidewalk board, the mold or even itself. Thus, the models of contact with friction are often present in the tire simulation. The complexity of tire mechanics makes primordial the robustness and precision of this used models. Research needs in the field of computational contact mechanics are, therefore, important for Michelin. The numerical mechanics research team of the company conduced many previous research projects in this field. The capitalized results are implemented in its finite elements code BIBMEF.
The main three states of contact encountered for tire simulation are :

- Road-tire contact: in this case, the road could be considered as a rigid obstacle. This simplification is very useful to improve the robustness of the contact method.
- Deformable body-tire contact: in some cases, especially in process simulation, the rubber is in contact with other bodies that could not be modelized as rigid. The contact method needs in this case to include mapping function between the bodies. The robustness is, also, more influenced by the choice of the model parameters (notably penalty parameter).
- Self contact: Meaning that the body is highly deformed that it contacts itself (See Fig. 1.1). This configuration is present mainly at the level of the lamellae when the tire undergos several efforts. It could be also observed in the simulation of the tire manufacturing. This case could generate detection problems and, of course, it is treated as a deformable-deformable contact.

Hence, contact models in Michelin's code are mainly based on two approaches: deformable-rigid contact and deformable-deformable contact, including self-contact. The most used resolution method for the first type of contact is the nodal penalization technique. This method has the advantage of being robust in this case even though it is not consistent and allows more penetration error. Yet, for the def-def contact case this technique remains

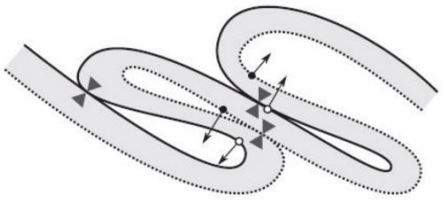

Figure 1.1: Self contact illustration

problematic in a nodal constraint. So, for the def-def contact, the mostly used method is the mortar one. Important efforts were focused on the used formulation and the solving algorithm of contact and resulted in a contact models generally accurate, robust and optimized. However, in case of self-contact or multi-body contact, mortar method has more difficulties because it is impractical to *a priori* nominate a mortar (slave) surface and a non-mortar (master) one.

On the other hand, recently, the Nitsche method (see Section 2.2), originally developed to impose Dirichlet conditions, has been adapted to friction and contact conditions. Being a segment to segment formulation, the method was interesting to be applied to def-def contact. Nitsche's method is a primal method while remaining consistent and this could make it more accurate than penalty methods without adding Lagrange multipliers. Besides, this method has the advantage of not using Lagrange multipliers to represent the contact forces what makes it more adapted to an unbiased formalism without distinguishing between slave and master surface. Thus, the method could be more adapted to self-contact case.
These advantages of Nitsche's method make it an interesting option for contact modelization that could answer Michelin's performance needs.

In this context, the first objective of the present work is to provide an adaptation of the Nitsche's method to the def-def contact problem with eventual presence of friction. To maintain convexity, allowing more efficient mathematical analysis, we would consider a Tresca type friction. This formulation has to adopt a non biased vision of the two contact surfaces, so that, it will be directly applicable to the self-contact case. Beside the implementation of the method to validate it numerically through some classic tests, we need to perform a theoretical study in order to allow a better understanding of the method.

Since the rubber is generally modelized as an hyper-elastic material undergoing very important deformations, it was mandatory to come through the restrictive frameworks of small strain and linear elasticity. Hence, the second challenge of this study was to formulate a Nitsche type method of contact and friction in the large strain framework. This Nitsche's method would be formulated for an hyper-elastic material. For the friction, it would be more efficient to construct our Nitsche's method directly with a Coulomb friction. In order to apply it to the self-contact problem, the approximation of frictional

contact has to be non biased and would constitute the continuity of the previous work in the small strain framework. For large deformations, the study would be concentrated on a numerical examination of Nitsche's method to evaluate its robustness and performance for Newton's resolution. In this study, we would validate the proposed method through some academic tests and, eventually, compare the method's performance with other classic contact methods before using it in some industrial applications.

Being an integral formulation, the accuracy and the performance of Nitsche's method depend on the used quadrature rule. For the mortar type methods, it has been preferred to adopt an exact evaluation of integrals through a segmentation of the quadrature rule when the meshes are not conformal. But the cost of this segmentation could be important in the large strain three dimensional case. Thus, it could be worthwhile to investigate the effect of numerical integration and such segmentation on the accuracy and the cost of the studied Nitsche's method. We could, as well examine the influence of the quadrature rule on the convergence order.
Therefore, a third concern of this thesis would be the study of the integration rule influence on the approximation and the comparison of several integration rules proposed in the literature for other integral methods.

1.2 Scientific context and literature review

Contact phenomena are omnipresent in biological and mechanical systems, what makes mandatory providing a better comprehension and modelization of this phenomena. Contact mechanics can be viewed from different aspects. In some cases (e.g. in nano-tribology), contact interaction is observed at an atomic scale. However, for most contact applications, a macroscopic viewpoint with a classical continuum assumptions is sufficient. Throughout this thesis, contact mechanics are considered as a subclass of continuum solid and structural mechanics. Yet, with this assumption the physics of the contact interaction is particularly rich and complicated, due to the multi-scale and multi-physical nature of the phenomenon and its associated interface effects such: sliding friction, adhesion, heat transfer, lubrication and wear.

From a mathematical point of view the contact is formulated as a boundary value problem in which the main constraint to be respected is the geometrical non-inter penetration. Besides, the effort transfer between contacting bodies has to be considered in agreement with the second Newton law.
This seemingly simple problem is actually non-trivial and complex to describe and solve mathematically as well as numerically. We are, in fact, faced to a nonlinear boundary condition, since the permitted relative displacements and efforts on the contact surface must be negative and complementary (see Fig 1.2). The contact constraints constitute a boundary inequality instead of a classic variational equality. This new mathematical structure requires new solution approach.

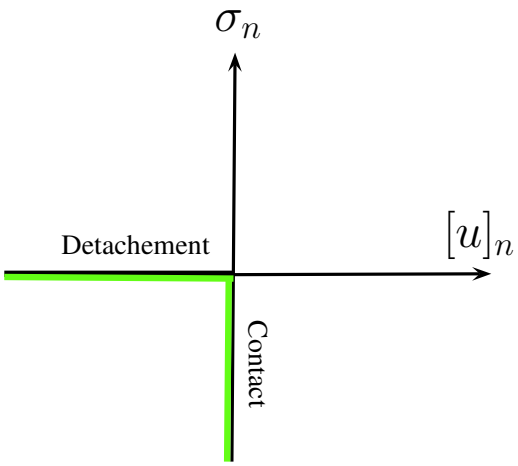

Figure 1.2: Permitted normal pressure and relative displacement on a contact interface

In addition, when considering friction the problem becomes even more complex because most of the friction laws state that tangential resistance depends on the normal contact pressure. Moreover, the nature of contact and friction law yields a non-smooth energy functional resulting even more difficulties from a numerical point of view. We can refer to the book of Kikuchi and Oden [KO88] for the mathematical formulation of contact and friction.

Due to this complexity, only very few contact settings, could be analytically solved. As an example, the work conducted by Hertz [Her82] on pressure profiles of contacting elastic bodies is commonly considered as the origin of modern contact analysis. An overview of the basic principles of contact mechanics, and the most important analytical solution techniques can be found in [Joh85, Lur70, AM83] and [TG70].

Most of the methods used for computational contact mechanics are developed in the context of the finite element method (FEM). Since the 1960s, the FEM has dominated numerical approximation of partial differential equations for solid mechanics, thermodynamics, and in particular, contact mechanics. The general FEM literature is abundant; for example we refer to [Bat96, BLM00, Hug00, Red04] and [ZT05].

Contact formulation

The first weak formulations of the computational contact began with the works of Signorini [Sig33, Sig59] who wrote the equilibrium of a linearly elastic body in frictionless contact with a rigid foundation. The existence and uniqueness of a solution to such variational inequalities problem were discussed in several works: [Fic72, KO88, MO87, MMG94, JE99] and the stability of contact problem solution have been discussed in [Kla88]. The dynamic case is treated in many publications: see e.g. [AP98, DEP11, HHLTIW12], but existence, uniqueness and energy conservation still involves many difficulties (see [Ren10]) For the standard FEM, it has been quite challenging to establish optimal convergence for contact.

The first analyses in the 1970s were sub-optimal with a convergence in $O(h^{\frac{1}{2}+\frac{\nu}{2}})$ for a solution in $H^{\frac{3}{2}+\nu}(\Omega)$ ($0 < \nu < \frac{1}{2}$): [SV77, Has77, HHN96] . The first fully optimal result, without extra assumptions, for the standard FEM has been achieved recently, in 2015, see [DH15]. We refer to, e.g., [BB00, HW05, Woh11, HR12, DH15] for more detailed reviews on *a priori* error estimates for contact problems in elasticity.

Contact resolution

The contact constraints are, generally, brought as additional terms in the objective energy functional by means of different techniques. The most common ones are:

- **Penalty method:** In this case the set of inequations associated to contact is replaced with a non-linear equation that approximates them using a penalization parameter that acts as a contact rigidity (see, e.g., [KS81, OK82b, OK82a, KO88, CS07, CH13]), This method remains primal, and is easy to implement. Nevertheless, consistency is lost, as penetration remains allowed and it is controlled by the penalty parameter.

- **Mixed method:** A Lagrange multiplier is introduced to enforce contact conditions (see, e.g., [HHN96, Hil00, BBR03, HW05, LR08, Woh11]). Resulting weak form remains consistent, and characterizes the saddle-point of the corresponding Lagrangian, but in this case, inf-sup compatibility between the primal space and the dual one must be satisfied to ensure well-posedness (see, e.g. [Woh11]).

- **Augmented Lagrangian method:** The augmented Lagrangian method is a sort of Lagrange multiplier formulation regularized by penalty functions. It yields a smooth energy functional and fully unconstrained problem. The method has been proposed in [AS58] for equality constrained optimization and then in [Roc70] and [Roc73] for inequality constraints. This technique has been considered often in the context of incompressibility constraints in, for example, [GLT89]. In [Pow69] the inf-sup condition is avoided by an independent consecutive updating of the primal and dual degrees of freedom resulting on an Uzawa's algorithm. The augmented Lagrangian method was adapted to the contact problem in [GLT89, MP85, SL92] and to frictional contact in [Ala88, AC91]. Several improvements were applied to the method to improve its robustness and convergence speed: see e.g. [ZDL12, HR10] [AC91] provides a good overview and discussion of these different enforcement techniques of contact constraints.

- **Nitsche's method:** See next paragraph.

Nitsche's method

In 1971 J. Nitsche proposed a new technique to impose Dirichlet conditions within the variational formulation without adding Lagrange multipliers [Nit71]. In this method the boundary condition is imposed weakly on the surface through a consistant term regularized by a real parameter (Nitsche's parameter). Conversely to standard penalization

techniques, the resulting method is consistent. Moreover, unlike mixed methods, no additional unknown (Lagrange multiplier) is needed. Nitsche's method has been widely applied on problems involving linear conditions on the boundary or at the correlation of sub-domains: see, e.g. [Ste95] for the Dirichlet problem or [BHS03] for domain decomposition with non-matching meshes. More recently, in [HH04a] and [HH06] it has been adapted for bilateral (persistent) contact, which is, still, a linear boundary condition. A Nitsche-based formulation of the unilateral (non-linear) contact problem was introduced in [CH13] and generalized in [CHR15c] to encompass symmetric and skew-symmetric variants. Recently, various extensions of Nitsche's method were proposed:
Some non-symmetric variants have been reconsidered recently, due to remarkable robustness properties (see, e.g., [Bur12, BB16]). A simple adaptation of the Nitsche method to Tresca's friction is proposed in [Cho14]. In [AHD14] a Nitsche stabilized approach was introduced for frictional sliding problem. The case of contact in elastodynamics is treated in [CHR15a,CHR15b]. The proposed scheme is inspired from [HLT06]. In [FPR16] Nitsche's method is combined with a cut-FEM / fictitious domain discretization, in the small deformations framework and a residual-based *a posteriori* error estimates are presented in [CFH+2]. The topic of small-sliding frictional contact on 3D interfaces is the object of [ASJ+15]. In [HRS16] a least-square stabilized augmented lagrangian method, inspired by Nitsche's method, is described for unilateral contact. This has been followed recently by some papers [BHL16a, BHLS17, BH17] that explore further the link between Nitsche and the augmented Lagrangian, for the contact problem, the obstacle problem and interface problems with adhesive contact. A penalty-free Nitsche's method has been designed and studied in [BHL16b].

An overview of the Nitsche's method for contact problems is given in [CFH+17].
The Nitsche's method was used only for small strain; but, as mentioned in section 1.2, the industrial applications require generally a large strain formulation. Therefore, a main challenge of the current work is to provide an adaptation of Nitsche's method to the large strain framework.

Contact discretization

Another difficulty of the contact problem resolution is the spatial discretization. In fact, the determination of the values involved in the model's equations is difficult when both bodies are deformable. First contributions to contact discretization within the FEM can be traced in [FZ75] and [HTS+76], where contact conditions were formulated with a very simple nodal approach, which requires node-matching meshes at the contact interface and this study was restricted to small deformations.
Thereafter, a different approach was adopted to model the contact, typically denoted as node-to-surface or node-to-segment (NTS) approach. This method is characterized by a point-wise enforcement of the non-interpenetration condition at the finite element nodes of a chosen "slave" surface. The reader is referred to [BC85, HGB85, BH90, Lau92, SL92, LS93a] and [WVS90, ZDL09b] for a comprehensive overview. The use of the NTS method involves a loss of accuracy in the calculation of displacements and stresses in the contact

area. This results from the amplification of spatial discretization errors caused by the node-wise contact constraint enforcement. A way to overcome this problem is the use of the integral mortar method. The first use of an integral constraint of contact was proposed with the called "segment-to-segment" (STS) discretization in [SWT85, PT92] and [ZW98] .
Mortar methods were originally introduced as a domain decomposition technique; see [BMP94, BB99, SS00]. They are characterized by an imposition of the interface constraints in a weak sense. Early applications of mortar finite element methods for contact mechanics can, for example, be found in [BBHL98, Hil00], and [ML00b] in the small strain case and then the method was adapted to the large deformations framework in [PL04a, PL04b, FW05, FW06, TFW09, HB11, PWGW12]. In [FHW04], a comparison between Nitsche's method and mortar-type ones is provided for linear elasticity.

Other techniques have been proposed to solve the contact problem such domain decomposition ([LT94, LTS95]). This method is used to reduce the calculation time, especially for multi-bodies contact, by treating an iterative problem instead of global solving (see [BAV01, LK03]) . We mention, also, contact domain method [OHC+09, HOW+09, HH07, WSS13] and intermediate mortar surface method [ML00b]

Other contact methods

Apart from the standard FEM, many other approximation methods were used to solve the contact problem, such as:

- **Isogeometric analysis**: introduced in 2005 by Hughes [HCB05] and applied to domain coupling in [HB12, ASWB14, DVK15] and to the contact problem in [TWH11, DLWZ12, DLWH14, DLS+14].

- **Extended finite element method (X-FEM)** (see [MDB99, DMB01, Amd13]): although this method is generally used for crack mechanics, it could be used for the modeling of nonlinear phenomena located near contact boundaries (surface roughness, damage,....).
  Meshfree methods (see [Yvo04, Liu13] and refrences therein): used for contact because of their advantage of being more malleable. So, the densification of the contact areas can be easily performed. These methods are used, especially, for forming application and thermal models.

A comprehensive introduction to most of topics related to computational contact mechanics can be found in the textbooks by Kikuchi and Oden [KO88], Laursen [Lau02] and Wriggers [Wri06].

Unbiased contact formulation

The most common paradigm to formulate contact problem of two deformable bodies is known as the master/slave formulation. In this approach one distinguishes between a master surface and a slave one on which is prescribed the non-interpenetration condition. A presentation of this formulation can be found in most of the contact literature (see for example [Lau92, Lau02]). This approach is confronted with important difficulties in the case of self-contact and multi-body contact where it is impossible or impractical to *a priori* nominate a master surface and a slave one. Automating the detection and the separation between slave and master regions in these cases may generate a lack of robustness since it may create detection problems.

Consequently, to avoid these difficulties, we need a called "unbiased" formulation of the contact. In such formulation we do not distinguish between a master surface and a slave one. Several previous works investigated the construction of unbiased methods. One can refer for example to [KROM99] for a global optimization managing contact and self-contact in the same formalism, [Pan08] where the contact constraint is approached successively by convex sets, [PA08] that solves the contact problem via a fictitious domain strategy, [HH07] for an oriented domain strategy, [OHC+09] with another fictitious domain type strategy as well as [WSS13] with the modeling of an intermediate body.
The "two-pass" method is also an often adopted strategy in which the contact conditions are imposed on both surfaces. This last over-constraints, generally, the contacting surfaces, as noted by Kikuchi and Oden [KO88],p:165. This method was formulated with penalty (see [PJS95,SL13,SD15]), and with Lagrange multipliers (see [PS98, JP01,SP05]). For the mixed methods, this kind of formulation is problematic because the use of two different multipliers for the same contact condition is not possible; then the gap constraint is prescribed in some nodes and the pressure continuity is enforced in some others. The method used in [SL13, SD15] is also called "two-half-pass" contact method because each pass accounts only for half of the contributions of common biased approaches.

Since, as mentioned in section 1.1, the application case of the method proposed by this work is, among others, self-contact, an unbiased formulation of the Nitsche's method is more adapted to the thesis objectives. Since Nitsche's method uses the contact stress instead of a Lagrange multiplier, it is very simple to divide this contact effort equitably on both of contact surfaces and a "two-half-pass" method is directly obtained. Therefore, Nitsche's method seems to be more natural to adapt to the unbiased formalism only by using the pressure continuity condition (see section 3.1).

Numerical integration

Nitsche's method is a fully integral method for which the contact conditions are imposed weakly through boundary integrals. For a two deformable bodies contact problem, one integrates fields that are discretized over two different (not necessarily matching) meshes which generates a difficulty of exactly computing boundary integrals. Typically,

the approach that is used in mortar-type methods is to mark out elements intersections (segments) between every two contact elements and evaluate the integrals on these segments (see [PL04a, PL02]). This segmentation process is challenging, especially in the large strain three dimensional case.
Due to this implementation and computation complexity, it has been seen appealing to use a higher order quadrature rule on the slave mesh without segmentation (see [FW05, TFW09]). [FPW15] provides a detailed comparison between these two integration techniques. A new segmentation approach is proposed in [WB17] to improve efficiency of the integration procedure. In [CLM97, MRW02, BBWW15] a non-symmetric integration resulting in a Petrov-Galerkin approach is proposed and tested for the mortar method.

Only few previous studies treated the influence of the quadrature error on the contact approximation and the convergence optimality. This observation suggest that an evaluation of the quadrature error for Nitsche's method, in order to quantify and control this error and to propose numeric strategies to reduce it, is an important purpose of the current study.

1.3 Overview and achievements of the thesis

In this thesis, we present a new formulation of frictional contact between two elastic bodies based on the Nitsche method. Nitsche's method is a consistent and primal method to treat contact. Its integral aspect allows it to be very suitable to deformable bodies contact with non-matching meshes.
The principal motivation of this work is the need of a simple and efficient approximation method for self-contact. To meet this requirement, we propose an unbiased method in which we do not distinguish between a master surface and a slave one and we impose the non-interpenetration and the friction conditions on both of them. Nitsche's method is more adapted to the unbiased formalism since the unbiased Nitsche's method is obtained without any additional consideration.

A first study in the framework of small strain is performed in order to adapt Nitsche's method to the two elastic bodies contact problem with an unbiased description of frictional contact. The small strain assumption allows us to obtain theoretical results proving the consistency of the method as well as its well-posedness and optimal convergence. These mathematical analysis are complemented by a numerical study of convergence. This part of the work was the subject of a first submitted and recently accepted journal article : [CMR16].

Since the analysis in the small strain case was promising, the next step was to propose a Nitsche's method for a non-linear material in the large strain framework. The proposed extension of Nitsche's method to contact and friction in the large strain framework is considered with a Coulomb friction instead of Tresca friction. A generalization parameter θ is considered to cover an entire set of methods with different numerical properties. To prove

the accuracy of the method for large deformations, we give an extended numerical study including several academic and industrial tests. The method is constructed independently of the mapping function, but its performance depends on the used mapping. Therefore, we gave a brief comparison of two mapping strategies: projection and ray-tracing. The formulation of the Nitsche's method in the large strain case was the subject of the published journal article : [MRC17].

Many integration rules were proposed in the literature for other integral methods. Being a fully integral method, the performance of Nitsche's method depends, obviously, on the used quadrature rule. Therefore, the third part of this work is devoted to the study of the integration rule influence on the approximation. This study covers a comparison of the method's accuracy and performance with different quadrature rules. The achieved work allowed the participation to the redaction of the generic overview paper on the Nitsche's method for contact: [CFH+17].

1.4 Outline

This thesis presents mathematical and numerical modelization and analysis of Nitsche's type method used to solve the frictional contact problem. It constitutes a generic presentation of all aspects of Nitsche's method for contact and provides the theoretical and numerical analysis performed along the PhD preparation. The remainder of this thesis is organized as follows:

Chapter 2 is devoted to a preliminary reminder of the governing equations of contact and friction problems for small and large strain. In addition, it presents the basic concepts of contact resolution. The second section of this chapter is an overview of Nitsche's method. We provide the derivation of Nitsche's method to treat boundary conditions, in particular contact and friction.

In **Chapter 3**, we build an unbiased formulation of the two elastic bodies contact problem with a Tresca friction. The formulation describes a whole class of methods through a generalization parameter θ. We carry out a mathematical analysis to prove the strong-weak problems equivalence, the consistency, the well-posedness and the optimal convergence. The third section of the chapter involves a numerical study of the convergence and the influence of Nitsche's parameter γ_0.

Chapter 4 extends the Nitsche–based approximation to the large strain framework with an unbiased formalism. In addition to contact, Coulomb friction is considered. Possible self–contact configuration could be taken into account. The method is built with a generic hyper-elastic material. The chapter includes, as well, a comparison between two classical mapping strategies: projection and ray-tracing. In the last section of the chapter, we provide a numerical validation of the method with several tests. The influence of Nitsche's parameter for different variants (θ) is investigated numerically.

The **Chapter 5** hands over a study of the influence of the integration error on contact approximation. This study is performed for Nitsche's method and it inspects the efficiency of segmenting the integration rule and the different alternatives to this costly operation. In this chapter, we evaluate patch test performance and the impact on the convergence order of different quadrature rules.

The manuscript is closed by a last chapter in which we remind the main conclusions drawn in this work and the possible perspectives and future works.

Chapter 2

Contact mechanics and Nitsche's method

Contents

2.1 Outline of contact mechanics

Introduction

In continuum mechanics, the small strain theory is a mathematical approach to describe the deformation in which the displacements of the material particles are assumed to be much smaller than any relevant dimension of the body. Thus, its geometry and the constitutive properties of the material (such as density and stiffness) at each point of space can be assumed to be unchanged by the deformation. With this assumption, the mechanical equations are considerably simplified because of the geometric linearity meaning that the strain tensor $\underline{\underline{\varepsilon}}(\mathbf{u})$ is a linear function of the displacement $\mathbf{u}$. This simplification will allow, especially, mathematical analysis of the contact problem.
This approach is contrasted with the "large strain" or "finite strain" theory where the geometry and material properties are changed by deformation; so that, one has to distinguish between the initial and the deformed (or actual) configuration.

The first formulations of the contact problem were performed in the small strain assumption by Signorini [Sig33] to describe a unilateral contact configuration between an

elastic body and a rigid obstacle. The Signorini conditions consist in a simple geometric description of the non-penetration, using a normal relative displacement of the contacting surfaces, as well as contact pressure that has to be compressive. These two conditions are complementary since when the contact appears the normal relative displacement have to be zero and when no contact is present the contact stress vanishes (see 2.2). Signorini problem is non linear and non differentiable at the contact boundary since the change of phase at the contact zone i.e. contact-no contact transition is highly nonlinear with respect to $\mathbf{u}$. To simplify the analysis, even more, some works consider a linear, or "bilateral ", contact were the contact is imposed on the whole contact zone and no transition could appear (see 2.4). We refer to [AC88] for a detailed study of contact in the small strain framework.

In the large strain case the non-interpenetration is imposed through a gap function $g(\mathbf{u})$ (instead of normal relative displacement) describing the normal distance between the contacting surfaces in the deformed configuration. The pressure condition is given in the deformed contact surface Γ_c^t through the Cauchy stress vector or in the initial one Γ_c using the first Piola-Kirchoff stress tensor. The contact conditions in this case are named "Karush-Kuhn-Tucker" or "Hertz-Signorini-Moreau" conditions. A comprehensive presentation of computational contact mechanics, especially for large train, can be found in the textbooks by Laursen [Lau02] and Wriggers [Wri06].

To approximate the contact problem with FEM, the strong problem is substituted by a variational one. Due to the contact conditions, the weak formulation of signorini's problem is classically written as a variational inequality (see [Fic64, KO88]). The inequality is solved in convex cone $\mathbf{K}$ of admissible displacements with respect to non-interpenetration condition.

To be solved the contact problem is in general considered from an optimization standpoint by constructing a general framework in which the contact contributions are indicated generically in a system functional to be minimized in the solution process. The functional corresponds to the virtual work of the system and the minimization is performed under the contact constraints. The optimality system can be easily extended to friction since the friction conditions are similar to contact ones. In the small strain framework, we choose to consider the Tresca friction to allow theoretical analysis. Several mathematical formulations can be applied to incorporate the contact constraints into the variational formulation. Most of them have been developed to solve generic constrained minimization problems (see e.g. [Ber84]). The penalty method and the Lagrangian multipliers formulation are commonly used. Among other relevent methods, we mention the augmented Lagrangian formulation. The Nitsche's method is described in details in the second part 2.2 of this chapter.
The obtained non-linear problem is solved in implicit applications, generally, with a generalized Newton-Raphson algorithm [AC88]. The term "generalized Newton's method" (or "semi-smooth Newton's method") comes from the fact that the optimality system is not differentiable but only Lipschitz-continuous and piecewise differentiable. However, no

special treatment is needed because from a numerical viewpoint, it is quite improbable to come across a non-differentiable point. In [Ren13], the author provides a comparison of generalized Newton's method performance with different discretization and resolution methods.

Two other major difficulty of the contact problem resolution are the spatial discretization and the contact detection. These problematics are linked since detection algorithms are developed for a discrete configuration. Many discretization techniques have been proposed and developed. The most common ones are node-to-segment methods and mortar methods. In this brief introduction to contact problem we will not broach these problematics. The presented models are described in the continuum framework.

In this first part of the chapter we provide a brief outline of the frictional contact modeling and resolution. The section 2.1.1 is devoted to the unilateral contact in the small strain assumption. In section 2.1.2, we give the contact formalism for large strain. And, finally, the third section 2.1.3 presents an outline of different classic methods to solve contact.

2.1.1 Unilateral contact with Tresca friction

In this first section we give the essential notions and concepts of the contact mechanics continuum. We make, in a first time, the assumption of small strain with linear elastic body expected to income into contact with a rigid foundation.

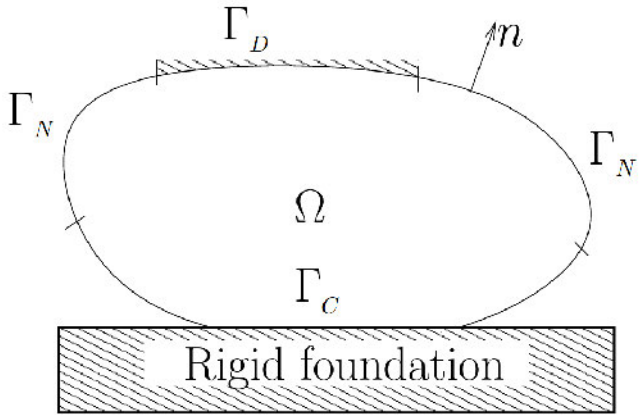

Figure 2.1: Basic notations for the unilateral contact problem.

The considered body is represented by the domain Ω in $\mathbb{R}^d$ with $d = 2$ or $d = 3$ (see Figure 2.1 when $d = 2$). Plane strain assumption is made when $d = 2$. We partition the boundary $\partial\Omega$ of Ω in three nonoverlapping parts Γ_D, Γ_N and the contact/friction boundary Γ_C, with $\text{meas}(\Gamma_D) > 0$ and $\text{meas}(\Gamma_C) > 0$. The contact/friction boundary is supposed to be a straight line segment when $d = 2$ or a planar polygon when $d = 3$ to simplify. The surface of effective contact is included in Γ_C, but not necessarily all of it.

The normal unit outward vector on $\partial\Omega$ is denoted $\mathbf{n}$. The body is clamped on Γ_D for the sake of simplicity. It is subjected to volume forces $\mathbf{f} \in (L^2(\Omega))^d$ and to surface loads $\mathbf{t} \in (L^2(\Gamma_N))^d$.

The unilateral contact problem with Tresca friction under consideration consists in finding the displacement field $\mathbf{u} : \Omega \to \mathbb{R}^d$ verifying the equations and conditions (2.1)–(2.2)–(2.3):

$$\begin{aligned} \mathbf{div}\,\sigma(\mathbf{u}) + \mathbf{f} = \mathbf{0} \quad & \text{in } \Omega, \qquad \sigma(\mathbf{u}) = \underline{\underline{\underline{\underline{\boldsymbol{A}}}}} : \underline{\underline{\boldsymbol{\varepsilon}}}(\mathbf{u}) \quad \text{in } \Omega, \\ \mathbf{u} = \mathbf{0} \quad & \text{on } \Gamma_D, \qquad \underline{\underline{\boldsymbol{\sigma}}}(\mathbf{u})\mathbf{n} = \mathbf{t} \quad \text{on } \Gamma_N, \end{aligned} \tag{2.1}$$

where $\underline{\underline{\boldsymbol{\sigma}}} = (\sigma_{ij})$, $1 \le i, j \le d$, stands for the stress tensor field and $\mathbf{div}$ denotes the divergence operator of tensor valued functions. The notation $\underline{\underline{\boldsymbol{\varepsilon}}}(\mathbf{v}) = (\underline{\underline{\boldsymbol{\nabla}}}\mathbf{v} + \underline{\underline{\boldsymbol{\nabla}}}\mathbf{v}^T)/2$ represents the linearized strain tensor field and $\underline{\underline{\underline{\underline{\mathbf{A}}}}}$ is the fourth order symmetric elasticity tensor having the usual uniform ellipticity and boundedness property. For any displacement field $\mathbf{v}$ and for any density of surface forces $\underline{\underline{\boldsymbol{\sigma}}}(\mathbf{v})\mathbf{n}$ defined on $\partial\Omega$ we adopt the following decomposition into normal and tangential components:

$$\mathbf{v} = v_n\mathbf{n} + \mathbf{v_t} \quad \text{and} \quad \underline{\underline{\boldsymbol{\sigma}}}(\mathbf{v})\mathbf{n} = \sigma_n(\mathbf{v})\mathbf{n} + \sigma_{\mathbf{t}}(\mathbf{v}).$$

The unilateral contact conditions (Signorini conditions) on Γ_C are formulated as follows:

$$u_n \le 0 \quad (i) \qquad \sigma_n(\mathbf{u}) \le 0 \quad (ii) \qquad \sigma_n(\mathbf{u})\,u_n = 0 \quad (iii) \tag{2.2}$$

The first Signorini condition simply represents the geometric constraint of non-penetration, whereas the second condition implies that no adhesive stresses are allowed in the contact zone. Finally, the third one, well-known as complementarity condition, forces the gap to be closed when non-zero contact pressure occurs (contact) and the contact pressure to be zero when the gap is open (no contact).

Let $s \in L^2(\Gamma_C)$, $s \ge 0$ be a given threshold. The Tresca friction conditions on Γ_C read:

$$\begin{cases} |\sigma_{\mathbf{t}}(\mathbf{u})| < s & \text{if } \mathbf{u_t} = \mathbf{0}, \quad (i) \\ \sigma_{\mathbf{t}}(\mathbf{u}) = -s\dfrac{\mathbf{u_t}}{|\mathbf{u_t}|} & \text{otherwise}, \quad (ii) \end{cases} \tag{2.3}$$

where $|\cdot|$ stands for the euclidean norm in $\mathbb{R}^{d-1}$. Note that conditions (2.3)–(i) and (2.3)–(ii) imply that $|\sigma_{\mathbf{t}}(\mathbf{u})| \le s$ in all cases: if $|\sigma_{\mathbf{t}}(\mathbf{u})| < s$, we must have $\mathbf{u_t} = \mathbf{0}$, and this presents the stick state and when$|\sigma_{\mathbf{t}}(\mathbf{u})| = s$ we get slip.

Remark 2.1.1. *The case of bilateral contact with Tresca friction can be considered too, simply substituting to equations* (2.2) *the following one on* Γ_C*:*

$$u_n = 0. \tag{2.4}$$

The case of frictionless contact is recovered setting $s = 0$ in (2.3).

Remark 2.1.2. *The conditions of Coulomb friction can be written similarly as:*

$$\begin{cases} |\sigma_{\mathbf{t}}(\mathbf{u})| & \leq -\mathscr{F}\sigma_n(\mathbf{u}) & \text{if } \mathbf{u_t} = \mathbf{0}, & (i) \\ \sigma_{\mathbf{t}}(\mathbf{u}) & = \mathscr{F}\sigma_n(\mathbf{u})\dfrac{\mathbf{u_t}}{|\mathbf{u_t}|} & \text{otherwise}, & (ii) \end{cases} \tag{2.5}$$

where $\mathscr{F}$ is the friction coefficient. In the Tresca friction model, we assume that the amplitude of the normal friction threshold is known (i.e., $\mathscr{F}|\sigma_n(\mathbf{u})| = s$, see, e.g., [KO88, Section 10.3]). [Ren06] provides a uniqueness criterion for Signorini problem with Colmob friction.

To get the weak formulation of the contact problem, necessary for the FEM, we introduce the Hilbert space $\mathbf{V}$ and the convex cone $\mathbf{K}$ of admissible displacements which satisfy the non-inter penetration on the contact zone Γ_C:

$$\mathbf{V} := \left\{ \mathbf{v} \in \left(H^1(\Omega)\right)^d \ : \mathbf{v} = \mathbf{0} \text{ on } \Gamma_D \right\}, \quad \mathbf{K} := \left\{ \mathbf{v} \in \mathbf{V} \ : \ v_n = \mathbf{v}\cdot\mathbf{n} \leq 0 \text{ on } \Gamma_C \right\},$$

and we define

$$a(\mathbf{u},\mathbf{v}) := \int_\Omega \underline{\underline{\boldsymbol{\sigma}}}(\mathbf{u}) : \underline{\underline{\boldsymbol{\varepsilon}}}(\mathbf{v})\, d\Omega, \quad L(\mathbf{v}) := \int_\Omega \mathbf{f}\cdot\mathbf{v}\, d\Omega + \int_{\Gamma_N} \mathbf{t}\cdot\mathbf{v}\, d\Gamma, \quad j(\mathbf{v}) := \int_{\Gamma_C} s|\mathbf{v_t}|\, d\Gamma,$$

for any $\mathbf{u}$ and $\mathbf{v}$ in $\mathbf{V}$.

The weak formulation of Problem (2.26)–(2.3) as a variational inequality of the second kind (see [Glo80]), is:

$$\begin{cases} \text{Find } \mathbf{u} \in \mathbf{K} \text{ such that:} \\ a(\mathbf{u}, \mathbf{v}-\mathbf{u}) + j(\mathbf{v}) - j(\mathbf{u}) \geq L(\mathbf{v}-\mathbf{u}), \qquad \forall\, \mathbf{v} \in \mathbf{K}. \end{cases} \tag{2.6}$$

In the frictionless case, the Stampacchia theorem ensures that this problem admits a unique solution (see, e.g., [KO88, Theorem 10.2, Chapter 10]). The frictional problem (2.6) admits, as well, a unique solution (see, e.g., [Glo84, Theorem 5.1, Remark 5.2]). Moreover this solution is the unique minimizer on the non-empty closed convex $\mathbf{K}$ of the functional

$$\mathcal{J} : \mathbf{V} \ni \mathbf{v} \mapsto \frac{1}{2}a(\mathbf{v},\mathbf{v}) - L(\mathbf{v}) + j(\mathbf{v}) \in \mathbb{R}. \tag{2.7}$$

So, to solve the contact problem we could use the available methods for constrained optimization of $\mathcal{J}$ under the constraint imposed in $\mathbf{K}$.

Remark 2.1.3. *In the case of bilateral contact (condition (2.4) instead of (2.2)), the same weak formulation (2.6) holds, replacing the convex cone $\mathbf{K}$ by the vector space:*

$$\mathbf{K}_b := \left\{ \mathbf{v} \in \mathbf{V} \ : \ v_n = 0 \text{ on } \Gamma_C \right\}.$$

The case of two contacting deformable bodies is presented in section 2.2.2. That case is more complex to treat because the contact detection and the contact discretization are

much more difficult.

2.1.2 Contact in the large strain case

2.1.2.1 Notations for the large strain framework and algebraic operators

We give in this paragraph some notations for the large strain tensors and algebraic operators. These notations will be used in the next sections as well as in the Chapter 4.

The gradient of a quantity in the deformed (resp. reference) configuration will be noted ∇ (resp. $\nabla_{\mathbf{X}}$). To describe the deformation we introduce as usual the identity tensor of size $d \times d$, denoted by $\underline{\underline{\mathbf{I}}}$ and the deformation gradient $\underline{\underline{\mathbf{F}}} = \underline{\underline{\mathbf{I}}} + \nabla_{\mathbf{X}}\mathbf{u}$. We introduce as well

$$\underline{\underline{\boldsymbol{\epsilon}}}(\mathbf{u}) = \frac{1}{2}(\nabla\mathbf{u} + \nabla\mathbf{u}^T) = \frac{1}{2}((\nabla_{\mathbf{X}}\mathbf{u})\underline{\underline{\mathbf{F}}}^{-1} + \underline{\underline{\mathbf{F}}}^{-T}(\nabla_{\mathbf{X}}\mathbf{u})^T).$$

The jacobian of the motion transformation $\boldsymbol{\varphi}$ is denoted by $J = \det \underline{\underline{\mathbf{F}}}$. We introduce also the Cauchy-Green tensor $\underline{\underline{\mathbf{C}}} = \underline{\underline{\mathbf{F}}}^T\underline{\underline{\mathbf{F}}}$, and the Green-Lagrange tensor $\underline{\underline{\mathbf{E}}} = \frac{1}{2}(\underline{\underline{\mathbf{C}}} - \underline{\underline{\mathbf{I}}})$. We will note $\underline{\underline{\boldsymbol{\sigma}}}$ the Cauchy stress tensor, $\underline{\underline{\hat{\boldsymbol{\sigma}}}} = J\underline{\underline{\boldsymbol{\sigma}}}\underline{\underline{\mathbf{F}}}^{-T}$ the first Piola-Kirchhoff stress tensor and $\underline{\underline{\mathbf{S}}} = J\underline{\underline{\mathbf{F}}}^{-1}\underline{\underline{\boldsymbol{\sigma}}}\underline{\underline{\mathbf{F}}}^{-T}$ the second Piola-Kirchhoff stress tensor. We define $\hat{\boldsymbol{\sigma}}_{\boldsymbol{N}} = \underline{\underline{\hat{\boldsymbol{\sigma}}}}\mathbf{N}$ the contact stress on $\partial\Omega$ (where $\mathbf{N}$ is the outward unit normal to $\partial\Omega$).
The operator $\underline{\underline{\mathbf{T}}}_n$ refers to the projection on the tangent plane corresponding to normal vector $\mathbf{n}$. Moreover, we consider the following notations to simplify the mathematical presentation.
The directional derivative of a quantity A with respect to the displacement $\mathbf{u}$ in direction $\delta\mathbf{u}$ will be denoted by $\mathcal{D}A(\mathbf{u})[\delta\mathbf{u}]$ or even by $\mathcal{D}A[\delta\mathbf{u}]$ if the argument of the quantity A is not ambiguous. This directional derivative is defined as

$$\mathcal{D}A(\mathbf{u})[\delta\mathbf{u}] = \lim_{\varepsilon\to 0} \frac{A(\mathbf{u} + \varepsilon\,\delta\mathbf{u}) - A(\mathbf{u})}{\varepsilon}$$

when this limit exists.
The projection onto $\mathbb{R}^-$ is defined as:

$$[a]_{\mathbb{R}^-} = \begin{cases} a & \text{if } a \leq 0\,, \\ 0 & \text{if } a > 0\,, \end{cases}$$

and the projection onto a ball centered at the origin and with a radius τ is:

$$\boldsymbol{P}_{B(\tau)}(\mathbf{q}) = \begin{cases} \mathbf{q} & \text{if } \|\mathbf{q}\| \leq \tau\,, \\ \tau\frac{\mathbf{q}}{\|\mathbf{q}\|} & \text{otherwise,} \end{cases} \tag{2.8}$$

where $\|\cdot\|$ is the euclidean norm on $\mathbb{R}^d$.

The notation $H(\cdot)$ stands for the (multivalued) Heaviside function: for any $\mathbf{x} \in \mathbb{R}$,

$$H(x) = \begin{cases} 1 & \text{if } x > 0, \\ [0,1] & \text{if } x = 0, \\ 0 & \text{if } x < 0. \end{cases}$$

2.1.2.2 Contact problem

In the large strain, the mechanical continuum is different. In this section we give the general case of two deformable bodies contact. The rigid obstacle (or Signorini) problem is easily obtained as a sub-case. In Figure 2.2, the large deformation frictional contact problem involving two bodies is shown schematically.

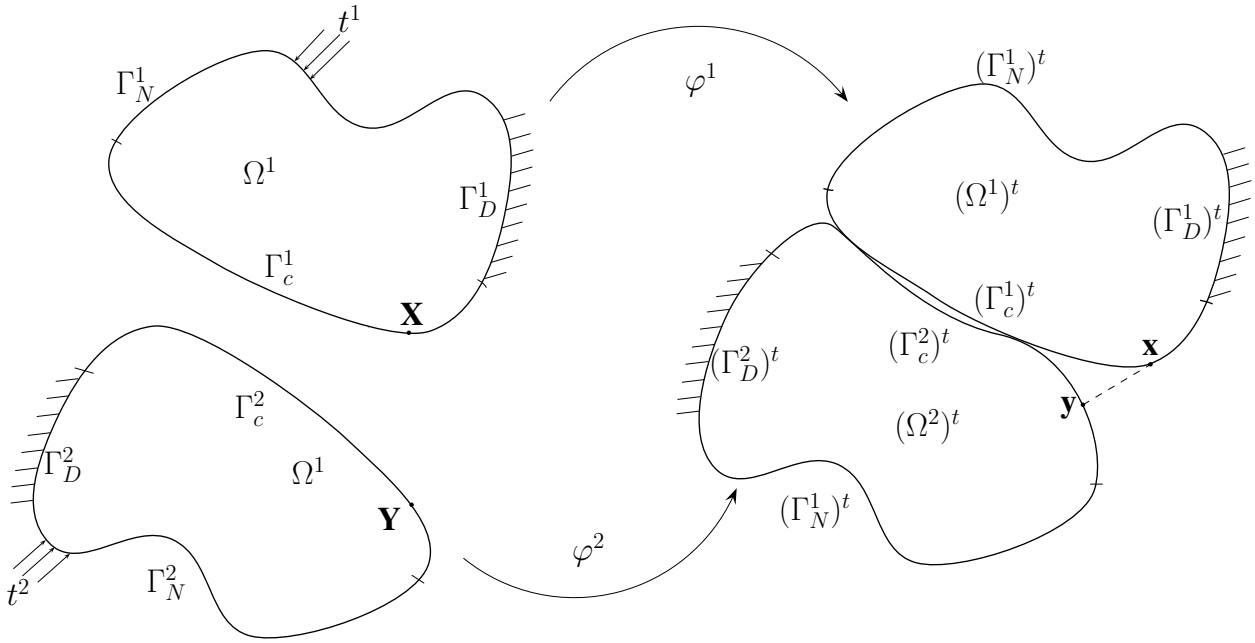

Figure 2.2: Basic notation for the two body large deformation contact problem.

As indicated in the figure, the reference configurations of the two bodies are represented by the open sets Ω^1 and Ω^2 in $\mathbb{R}^d, d = 2, 3$. To simplify the notations, a general index i is used to represent indifferently the 1st or the 2nd body. The bodies undergo motions, denoted $\boldsymbol{\varphi^i}$, which lead them to the deformed configurations $(\Omega^i)^t$, and cause them to contact and produce interactive forces on some portions of the contact surfaces Γ_c^i (deformed to $(\Gamma_c^i)^t$). As in 2.1.1, the boundary of each body $\partial\Omega^i$ consists in three non-overlapping parts Γ_D^i where displacements is imposed, Γ_N^i where a tractions $\mathbf{t}^i$ are prescribed and Γ_C^i where contact could appear. Each body could be, as well, subjected to volume forces $\mathbf{f}^i$ (such as gravity). The actual, so-called active contact surface $\Gamma_a \subseteq \Gamma_c$ is unknown, possibly continuously changing over time and thus has to be determined as part of the nonlinear solution process. A point $\mathbf{X}^i \in \Omega^i$ is related to its deformed coordinates $\mathbf{x}^i \in (\Omega^i)^t$ through the unknown displacement $\mathbf{u}^i = \boldsymbol{\varphi^i} - \mathbf{Id}$.

In the current work, we adopt a Lagrangian description of the boundary value problem (BVP) in which the the unknown of interest will be $\mathbf{u} = (\mathbf{u}^1, \mathbf{u}^2)$.
Thus, the system stress is defined through the first Piola-Kirchhoff tensor $\hat{\underline{\underline{\boldsymbol{\sigma}}}}(\mathbf{u}^i)$ and the stress on the bodies boundaries is noted $\hat{\boldsymbol{\sigma}}_{\boldsymbol{N}}(\mathbf{u}^i) = \hat{\underline{\underline{\boldsymbol{\sigma}}}}(\mathbf{u}^i)\mathbf{N}^i$. Apart of contact condition, the BVP in material description in a quasi-static approach, can be summarized as follows:

$$\begin{aligned} \mathbf{div}\, \hat{\underline{\underline{\boldsymbol{\sigma}}}}(\mathbf{u}^i) + \mathbf{f}^i = \mathbf{0} \quad & \text{in } \Omega^i, \\ \mathbf{u}^i = \mathbf{0} \quad & \text{on } \Gamma_D^i, \\ \hat{\boldsymbol{\sigma}}_{\boldsymbol{N}}(\mathbf{u}^i) = \mathbf{t}^i \quad & \text{on } \Gamma_N^i, \end{aligned} \tag{2.9}$$

In the parlance commonly used in the literature, the parameterizing surface is termed the slave (or contractor) surface, where lives the point $\mathbf{X}$ (resp. $\mathbf{x}$ in the deformed configuration), while the opposite surface is often called the master, or target surface, where is the corresponding point $\mathbf{Y}$ (resp. $\mathbf{y}$ in the deformed configuration) see, e.g., [HGB85, BH90]. If we let (1) refers to the slave side and (2) refers to the master one, $\mathbf{x}$ and $\mathbf{y}$ are related by the mapping function Π such:

$$\begin{array}{rcl} \Pi : (\Gamma_c^1)^t & \longrightarrow & (\Gamma_c^2)^t \\ \mathbf{x} & \longmapsto & \mathbf{y} = \Pi(\mathbf{x}). \end{array}$$

The choice of these two surfaces introduces a bias into the numerical approximation. Thus in Chapter 4 we discuss and deal with this difficulty. The choice of the this mapping function influence significantly the contact approximation since it has a direct impact on the detection algorithm and the expression of the normals and gap.
In section 4.1.2 of the fourth chapter, we give and compare two classical mapping strategies: projection and ray-tracing.
A fundamental geometric measure of proximity of the two bodies is the so-called gap function:

$$g(\mathbf{u}) = \mathbf{n} \cdot (\mathbf{x} - \mathbf{y}),$$

The definition of the normal vector $\mathbf{n}$ depends on the mapping function Π. Hence, the non-interpenetrability constraint is stated mathematically as $g(\mathbf{u}) \geq 0$.

The surface stress on the contact on the slave side is divided into a normal component and a tangential one such:

$$\hat{\boldsymbol{\sigma}}_{\boldsymbol{N}}(\mathbf{u}^1) = \hat{\sigma}_n(\mathbf{u}^1)\mathbf{n}_x + \underline{\underline{\mathbf{T}_{\mathbf{n}_x}}}\hat{\boldsymbol{\sigma}}_{\boldsymbol{N}}(\mathbf{u}^1) = \hat{\sigma}_n(\mathbf{u}^1)\mathbf{n}_x + \hat{\boldsymbol{\sigma}}_t(\mathbf{u}^1).$$

The quantity $\hat{\sigma}_n(\mathbf{u}^1)$ now represents the contact pressure at a slave point $\mathbf{X}$, and must be compressive (negative). In a similar way to the small strain case, Karush-Kuhn-Tucker (KKT) conditions for normal contact are:

$$g(\mathbf{u}) \geq 0 \tag{2.10a}$$
$$\hat{\sigma}_n(\mathbf{u}^1) \leq 0 \qquad \text{on } \Gamma_c^1. \tag{2.10b}$$
$$\hat{\sigma}_n(\mathbf{u}^1)g(\mathbf{u}) = 0 \tag{2.10c}$$

These conditions as well as the friction conditions (2.14) are prescribed only on the slave surface in a classic biased formulation of contact. For the unbiased version, we refer to Chapter 4.

In the presence of friction, normal and tangential stresses at the contact interface are coupled through the sliding velocity vector $\mathbf{v}$ for a quasi-static problem. As in [PR15], we use the frame indifferent definition of velocity described in [CHK95]. Adapted to the current notation $\mathbf{v}(\mathbf{X})$ reads:

$$\mathbf{v}(\mathbf{X}) = \dot{\boldsymbol{\varphi}}(\mathbf{X}) - \dot{\boldsymbol{\varphi}}(\mathbf{Y}) + g\,\dot{\mathbf{n}}\,. \tag{2.11}$$

Time discretization is based on a backward Euler approximation of the first expression in (2.11) which reads:

$$\mathbf{v}(\mathbf{X}) = \frac{1}{\Delta t}(\boldsymbol{\varphi}(\mathbf{X}) - \boldsymbol{\varphi}(\mathbf{Y}) + g\,\mathbf{n}) - \frac{1}{\Delta t}(\boldsymbol{\varphi}_0(\mathbf{X}) - \boldsymbol{\varphi}_0(\mathbf{Y}) + g\,\mathbf{n}_0)\,, \tag{2.12}$$

where $\Delta t > 0$ is the time-step, and where $\boldsymbol{\varphi}_0$, $\mathbf{n}_0$ are respectively the deformation and the surface normal at the previous time-step. Equation (2.12) can be then simplified, as in [PR15], using (4.1) and (4.2):

$$\mathbf{v}(\mathbf{X}) = -\frac{1}{\Delta t}(\boldsymbol{\varphi}_0(\mathbf{X}) - \boldsymbol{\varphi}_0(\mathbf{Y}) + g\,\mathbf{n}_0)\,. \tag{2.13}$$

It should be underlined here that the mapping between points $\mathbf{X}$ and $\mathbf{Y}$ appearing in (2.13) corresponds to the current deformation $\boldsymbol{\varphi}$ and not to the deformation $\boldsymbol{\varphi}_0$ at previous time-step.

The conditions of Coulomb friction can be written as follows (see, e.g., [KO88]):

$$\begin{cases} \|\hat{\boldsymbol{\sigma}}_t(\mathbf{u}^1)\| \leq -\mathscr{F}\hat{\sigma}_n(\mathbf{u}^1) & \text{if } \mathbf{v} = 0, \\ \hat{\boldsymbol{\sigma}}_t(\mathbf{u}^1) = \mathscr{F}\hat{\sigma}_n(\mathbf{u}^1)\dfrac{\mathbf{v}}{\|\mathbf{v}\|} & \text{otherwise.} \end{cases} \tag{2.14}$$

So, to summarize, the strong problem for frictional contact with Coulomb friction is : (2.9), (2.10) and (2.14).

In the context of the small deformation, linearly elastic theory, the statement of virtual work for contact problem is often constructed by casting the problem as one of constrained minimization. To obtain the variational inequality, the convexity of $\mathbf{K}$ is an important condition that we do not ensure in the general case of large strain. Faced with a non-convex and non-conservative frictional contact problem , one might assume directely the contact virtual work by incorporating the local equations and associated kinematic quantities. Thus, the well-known principle of virtual work (PVW) is derived here as:

$$\begin{cases} \text{Find } \mathbf{u} \in \mathbf{V} \text{ such that:} \\ G_{int,ext}(\mathbf{u}, \delta\mathbf{u}) - G_c(\mathbf{u}, \delta\mathbf{u}) = 0, \qquad \forall\, \delta\mathbf{u} \in \mathbf{V}, \end{cases} \tag{2.15}$$

where,

$$G_{int,ext}(\mathbf{u},\delta\mathbf{u}) = \sum_{i=1}^{2}\Big(\int_{\Omega^i} \underline{\underline{\nabla}}_{\mathbf{X}}\delta\mathbf{u}^i : \underline{\underline{\hat{\boldsymbol{\sigma}}}}(\mathbf{u}^i)\; d\Omega, - \int_{\Omega^i} \mathbf{f}^i\cdot\delta\mathbf{u}^i\; d\Omega - \int_{\Gamma_N^i} \mathbf{t}^i\cdot\delta\mathbf{u}^i\; d\Gamma\Big),$$

is the sum of the internal virtual work (the virtual work due to the internal stresses) and the external virtual work (the virtual work due to applied loadings) and $G_c(\mathbf{u},\delta\mathbf{u})$ are contact and friction contributions of virtual work.
The Hilbert space $\mathbf{V}$ is the space of displacements respecting the Dirichlet conditions on Γ_D^i:

$$\mathbf{V} := \Big\{\mathbf{u} = (\mathbf{u}^1,\mathbf{u}^2) : \mathbf{u}^i = \mathbf{0} \text{ on } \Gamma_D^i\Big\}.$$

The virtual work of frictional forces has the same sign as the virtual work of internal forces, since $\hat{\sigma}_n(\mathbf{u}^1) \leq 0$, and it is not conservative so all this energy dissipates. The major difficulty about (2.17) is due to the coupling between the friction threshold and the contact pressure that depends on the solution. Furthermore, the term virtual work of friction is non convex and non differentiable, consequently the questions of existence and uniqueness of the solution for the problem (2.17) remain open.

2.1.3 Contact resolution

The expression for $G_c(\mathbf{u},\delta\mathbf{u})$ includes two integrals, one over each contact surface. But all contact quantities have been assumed to be parametrized by $\mathbf{X}$. The term $G_c(\mathbf{u},\delta\mathbf{u})$ has to be converted to an expression involving only an integral over the slave surface Γ_c^1. This is achieved by enforcing the second Newton law across the contact interface, by requiring that the differential contact force induced on body (2) at $\mathbf{Y}$ is equal and opposite to that produced on body (1) at $\mathbf{X}$:

$$\mathbf{t}_c^1\cdot\delta\mathbf{u}^1(\mathbf{X})\; d\Gamma_c^1 = -\mathbf{t}_c^2\cdot\delta\mathbf{u}^2(\mathbf{Y})\; d\Gamma_c^2,$$

In other words, for all points were contact occurs, Γ_2 is thought of as being indexed by $\mathbf{X}$ through the mapping function Π. Equation (4.80) facilitates replacement of the contact contribution in the expression of $G_c(\mathbf{u},\delta\mathbf{u})$ by:

$$G_c(\mathbf{u},\delta\mathbf{u}) = \int_{\Gamma_c^1} \mathbf{t}_c^1\cdot\Big(\delta\mathbf{u}^2(\mathbf{Y}) - \delta\mathbf{u}^1(\mathbf{X})\Big)\; d\Gamma,$$

where $\mathbf{t}_c^1$ is the contact pressure which expression depends on the used resolution method. In the case of hyper-elastic materials, with a frictionless contact, the problem (2.17) becomes a constrained minimization problem. The starting point to derive equation (2.17) is the minimization of the total energy of the two bodies in contact:

$$\sum_{i=1}^{2}\Big(\int_{\Omega^i} W^i(\underline{\underline{\mathbf{E}}}) - \mathbf{f}^i\cdot\mathbf{u}^i\; d\Omega - \int_{\Gamma_N^i}\mathbf{t}^i\cdot\mathbf{u}^i\; d\Gamma\Big) - \mathcal{J}_c(\mathbf{u}),$$

where $W^i(\underline{\underline{\mathbf{E}}})$ is the energy potential of the hyper-elastic law, and $\underline{\underline{\mathbf{E}}}$ is the Green-Lagrange tensor. The term $\mathcal{J}_c(\mathbf{u})$ is contact energy, and its expression depends on the method used to constrain contact.
Introduction of dissipation, either in the form of inelasticity or friction, makes this minimzation form of the problem not valid since the dissipation makes the solution path-dependent.
In case of frictional contact, a complementary condition on tangential sliding in case of stick is:

$$\mathbf{v} = 0 \text{ if } \|\hat{\boldsymbol{\sigma}}_t(\mathbf{u}^1)\| \leq \mathscr{F}\hat{\sigma}_n(\mathbf{u}^1).$$

Several different variants for the formulation of $G_c(\mathbf{u}, \delta\mathbf{u})$ are discussed below.

2.1.3.1 Penalty method

The penalty method was one of the first to be used. It utilizes the non exactitude of the numerical resolution of the system to approximate, also, the contact conditions. The conditions of contact are thus not strictly respected and the interpenetration and reversible tangential slip are permitted. Hence, the penalty method is not consistent. In fact this method implies that the contact surface does not restrict penetration and reversible slip but resists them: the deeper the penetration the higher the resisting reaction. The physical interpretation of this method is to represent the master surface as a serie of springs with zero initial length and a rigidity equal to the penalization parameter ϵ_n. It has the advantage of being very simple for implementation what makes it, till today, one of the most widespread methods.

For the penalty method the expression of the contact and friction virtual work is:

$$\begin{cases} G_c(\mathbf{u}, \delta\mathbf{u}) = -\displaystyle\int_{\Gamma^1_{stick}} \Big(\epsilon_n[g(\mathbf{u})]_{\mathbb{R}^-}\mathbf{n} - \epsilon_t\mathbf{v}\Big) \cdot \Big(\delta\mathbf{u}^2(\mathbf{Y}) - \delta\mathbf{u}^1(\mathbf{X})\Big)\, d\Gamma, & \text{for stick,} \\ G_c(\mathbf{u}, \delta\mathbf{u}) = -\displaystyle\int_{\Gamma^1_{slip}} \Big(\epsilon_n[g(\mathbf{u})]_{\mathbb{R}^-}\mathbf{n} + \mathscr{F}\hat{\sigma}_n(\mathbf{u}^1)\frac{\mathbf{v}}{\|\mathbf{v}\|}\Big) \cdot \Big(\delta\mathbf{u}^2(\mathbf{Y}) - \delta\mathbf{u}^1(\mathbf{X})\Big)\, d\Gamma & \text{for slip.} \end{cases}$$

This two cases could be collected in a single equation using the projection operator $\boldsymbol{P}_{B(\tau)}$ and knowing that $\hat{\sigma}_n(\mathbf{u}^1) = \epsilon_n[g(\mathbf{u})]_{\mathbb{R}^-}$, we get:

$$G_c(\mathbf{u}, \delta\mathbf{u}) = -\int_{\Gamma^1_c} \Big(\epsilon_n[g(\mathbf{u})]_{\mathbb{R}^-}\mathbf{n} - \boldsymbol{P}_{B(-\mathscr{F}\epsilon_n[g(\mathbf{u})]_{\mathbb{R}^-})}(\epsilon_t\mathbf{v})\Big) \cdot \Big(\delta\mathbf{u}^2(\mathbf{Y}) - \delta\mathbf{u}^1(\mathbf{X})\Big)\, d\Gamma.$$

It is clear that the exact imposition of the contact and sliding conditions is recovered from this formulation for $\epsilon_n \to \infty$ and $\epsilon_t \to \infty$; however, large values for ϵ_n and ϵ_t will lead to an ill-conditioned numerical problem. The penalty method replaces the contact and friction laws (2.10), (2.14) by relations defining continuous contact and friction constraints as functions of normal gap $g(\mathbf{u})$ and the slip velocity($\mathbf{v}$). In other terms, the contact and friction conditions are regularized with ϵ_n and ϵ_t: see Fig. 2.3.

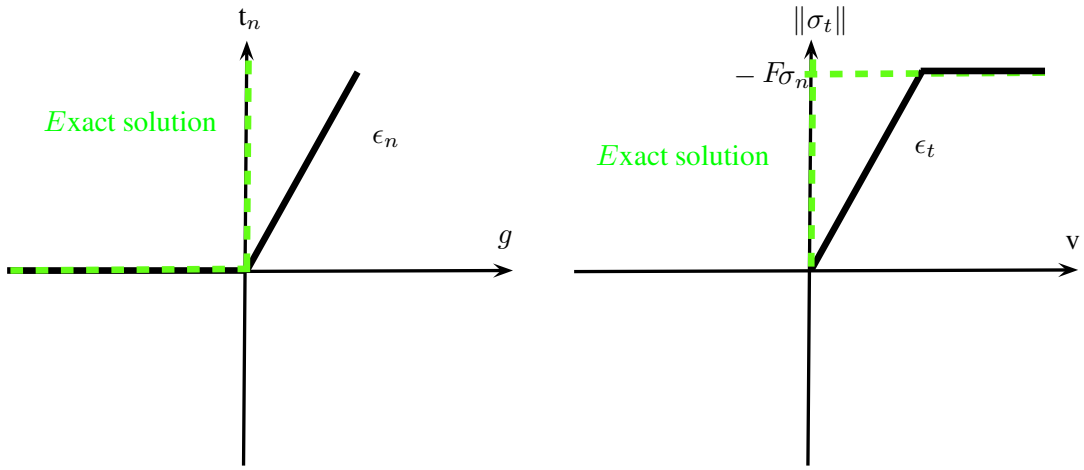

(a) Contact (b) Coulomb friction

Figure 2.3: Regularization of the contact and friction laws with the penalty method

Thus, the equation governing the mechanics of solids in the presence of frictional contact is expressed by:

$$G_{int,ext}(\mathbf{u},\delta\mathbf{u}) + \int_{\Gamma_c^1} \left(\epsilon_n [g(\mathbf{u})]_{\mathbb{R}^-}\mathbf{n} - \boldsymbol{P}_{B(-\mathscr{F}\epsilon_n[g(\mathbf{u})]_{\mathbb{R}^-})}(\epsilon_t \mathbf{v})\right) \cdot \left(\delta\mathbf{u}^2(\mathbf{Y}) - \delta\mathbf{u}^1(\mathbf{X})\right) d\Gamma = 0. \tag{2.16}$$

The resolution of this non linear problem is performed through the linearization of the equation 2.16 as part of the Newton-Raphson algorithm.

For a conservative system without friction, the virtual work of contact $G_c(\mathbf{u},\delta\mathbf{u})$ derives from the contact potential :

$$\mathcal{J}_c(\mathbf{u}) = \frac{1}{2}\int_{\Gamma_c^1} \epsilon_n([g(\mathbf{u})]_{\mathbb{R}^-})^2 \, d\Gamma,$$

The linear penalty coefficient is the most adapted from a numerical point of view, because it does not introduce additional nonlinearities to the problem. However, other non linear penalty functions could be better from the precision and robustness point of view.

Remark 2.1.4. *The small strain case could be treated in a very similar way by replacing* $g(\mathbf{u})$ *by* $-u_n$ *for unilateral contact with rigid obstacle and* $(-\mathscr{F}\hat{\sigma}_n(\mathbf{u}^1))$ *by* s *,* $\mathbf{v}$ *by* $\mathbf{u}_t$ *for Tresca friction.*

2.1.3.2 Lagrange multipier method

A classical method is the use of Lagrange multipliers to add constraints to a weak form. This method is a mixed one since it introduces new variables, the Lagrange multipliers noted $\boldsymbol{\lambda}$. They represent the contact forces preventing inter penetration at the contact

interface. The field $\boldsymbol{\lambda}$ is decomposed into a normal component λ_n and a tangential part $\boldsymbol{\lambda}_t$. The normal Lagrange multiplier λ_n is interpreted as the contact pressure and needs to fulfill the contact constraints: $\lambda_n \leq 0$. Hence, the problem (2.17) is replaced be a mixed one :

$$\begin{cases} \text{Find } \mathbf{u} \in \mathbf{V} \text{ and } \boldsymbol{\lambda} \in \mathbf{M} \text{ such that:} \\ G_{int,ext}(\mathbf{u}, \delta\mathbf{u}) - \displaystyle\int_{\Gamma_c^1} \boldsymbol{\lambda} \cdot \Big(\delta\mathbf{u}^2(\mathbf{Y}) - \delta\mathbf{u}^1(\mathbf{X})\Big)\, d\Gamma = 0, \qquad \forall\, \delta\mathbf{u} \in \mathbf{V}. \\ \displaystyle\int_{\Gamma_c^1} (\lambda_n - \delta\lambda_n) g(\mathbf{u}) \leq 0 \; d\Gamma, \\ \displaystyle\int_{\Gamma_c^1} (\boldsymbol{\lambda}_t - \delta\boldsymbol{\lambda}_t) \cdot \mathbf{v} \leq 0 \; d\Gamma \qquad \forall\, \delta\mathbf{u} \in \mathbf{M} \end{cases} \tag{2.17}$$

, where admissible variations $\delta\boldsymbol{\lambda}$ of $\boldsymbol{\lambda}$ are defined via:

$$\mathbf{M} = \Big\{ \boldsymbol{\lambda} : \Gamma_c^1 \longrightarrow \mathbb{R}^d, \lambda_n \leq 0 \text{ and } \|\boldsymbol{\lambda}_t\| \leq -\mathscr{F}\lambda_n \Big\}.$$

This inequality problem is hard to solve, especially with finite sliding and/or rotations. Different possibilities exist for the numerical solution of variational inqualities. Among them, the so-called "active set strategies" [Lue03] are the most used because they are easy to introduce in a finite element framework and do not require a totally new minimization technique.
In such strategies, we derive the framework based on variational equalities on "the active set". Active set Γ_a denotes such components of the potential contact zone Γ_c^1 which are in "active" contact at the current solution step. Naturally, the "inactive set" contains only components of the potential contact surface which are not in contact. Thus, the integration of the contact contribution to the system's work on Γ_a^1 and Γ_c^1 merges.
Once the contact interface is known we can write the weak form as an equality. This means that we know the active set of constraints within an incremental solution step.

In the frictionless case, the problem is formulated as a constrained minimization of the energy $\mathcal{J}(\mathbf{u})$:

$$\underset{g(\mathbf{u})\geq 0 \text{ on } \Gamma_c^1}{min} \mathcal{J}(\mathbf{u})$$

This problem is replaced by the search of a saddle point of the Lagrangian functional:

$$\mathscr{L}(\mathbf{u}, \lambda_n) = \mathcal{J}(\mathbf{u}) + \int_{\Gamma_c^1} \lambda_n g(\mathbf{u}) \; d\Gamma, \qquad \lambda_n \leq 0.$$

The constraint $\lambda_n \leq 0$ has still to be fulfilled, that is why the Lagrange multiplier method does not convert a minimization problem with inequality constraints to a fully unconstrained one. For a more rigorous formulation of Lagrange multiplier method for contact problems the reader is referred to [KO88, Yas11]. To get rid of this constraint,λ_n is often replaced by $[\lambda_n]_{\mathbb{R}^-}$.

However, an important drawback of mixed formulation is the mathematical conditions like the inf-sup or Babuska- Brezzi condition that have to be fulfilled in order to achieve a stable discretization scheme (see, e.g. [Woh11]).

2.1.3.3 Augmented Lagrangian method

Another method to regularize the non-differentiable normal contact and friction terms is the augmented Lagrange formulation. The main idea is to combine the penalty method with Lagrange multiplier one. The augmented Lagrange formulation yields a $\mathcal{C}^1$-differentiable saddle point functional. We present here an unconstrained integral formulation of the augmented Lagrangian method presented in [PR15, Ren13] and based on the Alart-Curnier augmented Lagrangian (see [AC88]). This is an unconstrained formulation, that is more appropriate for numerical solving.
For the frictionless contact, we get the following augmented Lagrangian:

$$\mathscr{L}_\gamma(\mathbf{u}, \lambda_n) = \mathcal{J}(\mathbf{u}) + \frac{1}{2\gamma} \int_{\Gamma_c^1} [\lambda_n + \gamma g(\mathbf{u})]_{\mathbb{R}^-}^2 - \lambda_n^2 \, d\Gamma, \tag{2.18}$$

where γ is the augmentation parameter. Note that use of $\mathscr{L}_\gamma(\mathbf{u}, \lambda_n)$ does not represent an approximation or a penalization of the contact condition as for penalty method since the penalization term vanishes in the the limit case and the augmented Lagrange formulation reduces to its Lagrange multiplier counterpart. Thus, in the continuous setting and neglecting regularity issues, this Lagrangian have the same saddle point of the Lagrangian used with the pure Lagrange multipliers method $\mathscr{L}(\mathbf{u}, \lambda_n)$. The augmented Lagrange formulation is, then, consistent.
Compared to the Lagrange multiplier method, the advantage of the augmented Lagrangian formulation is that it can be easier to treat numerically. For example, the augmented Lagrangian function penalizes violations of the kinematic constraint just as its penalty counterpart did, resulting in a "convexified" version of the objective function in the vicinity of the solution. See [Lau02] for a clear illustration of this aspect.

The optimality system of 2.18 is:

$$\begin{cases} G_{int,ext}(\mathbf{u}, \delta\mathbf{u}) + \displaystyle\int_{\Gamma_c^1} [\lambda_n + \gamma g(\mathbf{u})]_{\mathbb{R}^-} \mathcal{D}g(\mathbf{u})[\delta\mathbf{u}] \, d\Gamma = 0, & \forall\, \delta\mathbf{u} \in \mathbf{V}, \\ -\dfrac{1}{\gamma} \displaystyle\int_{\Gamma_c^1} (\lambda_n - [\lambda_n + \gamma g(\mathbf{u})]_{\mathbb{R}^-}) \delta\lambda_n \, d\Gamma = 0, & \forall\, \delta\lambda_n. \end{cases} \tag{2.19}$$

Optionally, the second line of System (2.19) can be exploited for replacing the term $[\lambda_n + \gamma g(\mathbf{u})]_{\mathbb{R}^-}$ in the first line with λ_n.
In the same way, a similar formulation can be formulated for the frictional case. For this purpose we introduce the tangential augmented Lagrange multiplier $\boldsymbol{\lambda}_t + \gamma\mathbf{v}$. As for penalty, we collect the slip and stick cases in the same expression of the contact and

friction virtual work, using the projection $\boldsymbol{P}$. The VWP reads:

$$\begin{cases} G_{int,ext}(\mathbf{u},\mathbf{v}) - \displaystyle\int_{\Gamma_c^1} \boldsymbol{\lambda}\cdot(\delta\mathbf{u}^2(\mathbf{Y}) - \delta\mathbf{u}^1(\mathbf{X}))\, d\Gamma = 0, \qquad \forall\, \mathbf{v}\in\mathbf{V}, \\ -\dfrac{1}{\gamma}\displaystyle\int_{\Gamma_c^1}\Big(\boldsymbol{\lambda} - [\lambda_n+\gamma g(\mathbf{u})]_{\mathbb{R}^-}\mathbf{n} - \boldsymbol{P}_{B(-\mathscr{F}[\lambda_n+\gamma g(\mathbf{u})]_{\mathbb{R}^-})}(\boldsymbol{\lambda}_t-\gamma\mathbf{v})\Big)\cdot\delta\boldsymbol{\lambda}\, d\Gamma = 0, \qquad \forall\,\delta\boldsymbol{\lambda}. \end{cases} \tag{2.20}$$

Remark 2.1.5. *In the case of unilateral contact with rigide obstacle problem and without friction, the optimality expression is:*

$$\begin{cases} G_{int,ext}(\mathbf{u},\delta\mathbf{u}) - \displaystyle\int_{\Gamma_c}[\lambda_n+\gamma u_n)]_{\mathbb{R}^-} v_n\, d\Gamma = 0, \qquad \forall\,\mathbf{v}\in\mathbf{V}, \\ -\dfrac{1}{\gamma}\displaystyle\int_{\Gamma_c}(\lambda_n - [\lambda_n+\gamma u_n]_{\mathbb{R}^-})\delta\lambda_n\, d\Gamma = 0, \qquad \forall\,\delta\lambda_n. \end{cases}$$

Now, remark that the second equation is a way to enforce weakly, at the discrete level, the condition (2.2), which is the aim of the Nitsche's method as well.

Another way, straightforward, to enforce this condition, is to substitute $\sigma_n(\mathbf{u})$ to λ_n in the first equation of the optimality system (and we drop the second equation). The optimality system in this case reads:

$$a(\mathbf{u},\mathbf{v}) - \int_{\Gamma_c^1}[\sigma_n(\mathbf{u})-\gamma u_n]_{\mathbb{R}^-}\, v_n\, d\Gamma = L(\mathbf{v}), \quad \forall\mathbf{v}\in\mathbf{V}.$$

We now recognize Nitsche's method (2.24) for $\theta = 0$ (See section 2.2). Moreover the Nitsche's parameter can be identified with the augmentation parameter γ. Note, in this context, that some recent works are filling the gap between Nitsche and augmented Lagrangian formulations in the case of contact and obstacle problems [BHL16a, BHLS17, HRS16].

In practice, two different implementations of the Augmented Lagrange method exist. On one hand, it is possible to keep the Lagrange multipliers $\boldsymbol{\lambda}$ as additional unknowns and apply standard Newton–Raphson iteration as nonlinear solution method. As for the Lagrange multiplier method, this leads to an undesirable saddle point formulation, however a certain "convexification" of the underlying potential around the solution is achieved. On the other hand, a simplified variant of 2.20 is provided by decoupling the displacement and the Lagrange multiplier. This leads to a double loop algorithm in which the Lagrange multiplier $\boldsymbol{\lambda}$ is fixed during an iteration loop to solve the weak form depending only on $\mathbf{u}$. Then within an outer loop the Lagrange multiplier is updated to a new value. This procedure results on an Uzawa algorithm. Therein, the penalty approach is used as kernel and the Lagrange multipliers λ are fixed within each iteration step, see Fig.2.4. This method permit to overcome the problem of ill-conditioning that arises with the penalty method since the values of γ is, in general taken smaller then penalty parameters ϵ_n, ϵ_t.

The formulation of to the Uzawa algorithm can be, easily, derived from the equation

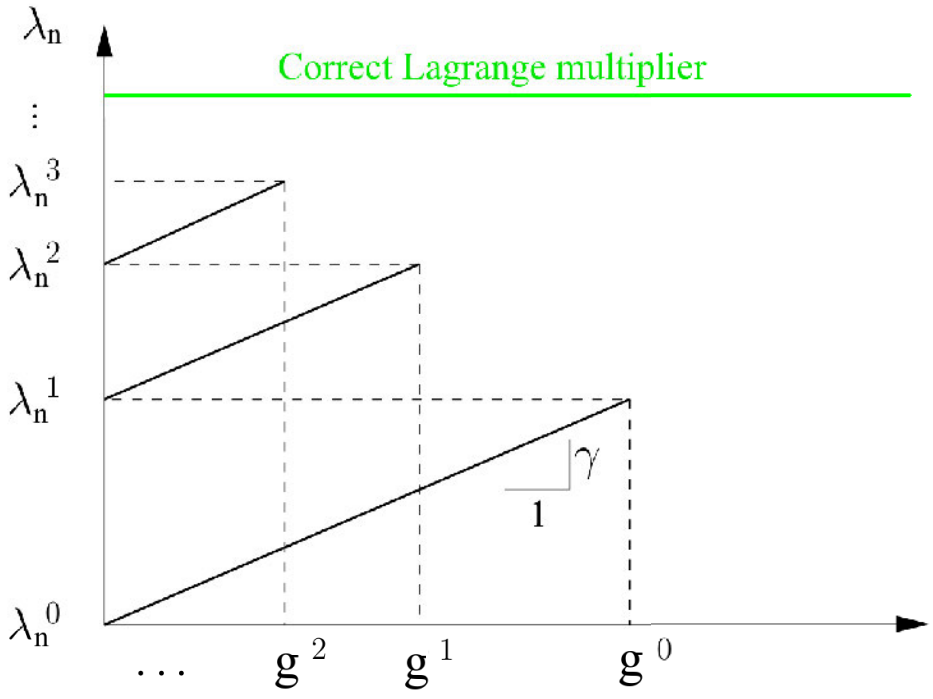

Figure 2.4: Schematic diagram of Uzawa's algorithm for the Augmented Lagrange method with normal Lagrangian λ_n

(2.20) by keeping the Lagrange multipliers constant in an inner loop and updating it in the outer loop (see Fig. 2.4) via:

$$\begin{cases} \lambda_n^{k+1} = \lambda_n^k + \gamma g(\mathbf{u}), \\ \boldsymbol{\lambda}_t^{k+1} = \boldsymbol{\lambda}_t^k + \gamma \mathbf{v}. \end{cases}$$

Another interesting method to constraint the contact and the friction conditions is the Nitsche's method. Unlike penalty methods, this method is consistent, and it remains primal without adding any additional computation steps in contrast with Lagrangian and augmented Lagrangian methods. In the Section 2.2 of this chapter we present this method in the small strain framework before generalizing it to the large strain one in Chapter 4.

2.2 Nitsche's method for boundary conditions

Introduction

Contact and friction conditions are usually formulated with a set of inequalities and non-linear equations on the boundary. Basically, contact conditions allow to enforce non-inter penetration on the whole candidate contact surface. For numerical computations, various

techniques have been used to enforce contact conditions, and the most common ones are:

- Penalty method (see, e.g., [KS81, OK82b, OK82a, KO88, CS07, CH13]), where the set of inequations associated to contact is replaced with a non-linear equation that approximates them weakly. This method remains primal, and is easy to implement. Nevertheless, consistency is lost, as penetration remains allowed and it is controlled by the penalty parameter.

- Mixed methods (see, e.g., [HHN96, Hil00, BBR03, HW05, LR08, Woh11]), where a Lagrange multiplier is introduced to enforce contact conditions. Resulting weak form remains consistent, and characterizes the saddle-point of the corresponding Lagrangian, but in this case, inf-sup compatibility between the primal space and the dual one must be satisfied to ensure well-posedness (see, e.g. [Woh11]).

Nitsche's treatment of contact is an extension of the method proposed in 1971 by J. Nitsche to impose Dirichlet conditions within the variational formulation without adding Lagrange multipliers [Nit71]. Nitsche's method has been widely applied on problems involving linear conditions on the boundary of a domain or at the interface between subdomains: see, e.g. [Ste95] for the Dirichlet problem or [BHS03] for domain decomposition with non-matching meshes. More recently, in [HH04b] and [HH06] it has been adapted for bilateral (persistent) contact, which still involves linear boundary conditions on the contact zone. An extension to large strain bilateral contact has been performed in [WZ08]. Conversely to standard penalization techniques (see section 2.1.3.1), the resulting method is consistent. Moreover, unlike mixed methods, no additional unknown (Lagrange multiplier) is needed. In recent works [CH13, CHR15c] a new Nitsche-based FEM was proposed and analyzed for Signorini's problem. Conversely to bilateral (persistent) contact, the proposed method treat directly non-linear boundary conditions associated to unilateral contact, with an unknown actual contact region. For this Nitsche-based FEM, optimal convergence in the $H^1(\Omega)$-norm of order $O(h^{\frac{1}{2}+\nu})$ has been proved, provided the solution has a regularity $H^{\frac{3}{2}+\nu}(\Omega)$, $0 < \nu \leq k - 1/2$ ($k = 1, 2$ is the polynomial degree of the Lagrange finite elements). To this purpose there is no need of additional assumption on the contact/friction zone, such as an increased regularity of the contact stress or a finite number of transition points between contact and non-contact. The proof applies in two-dimensional and three-dimensional cases, and for continuous affine and quadratic finite elements (see section 3.2.3 of Chapter 3). For many classical variants of the contact formulation such as mixed/hybrid methods or penalty methods, it has been quite challenging to establish optimal convergence in the case the solution $\mathbf{u}$ belongs to $H^{\frac{3}{2}+\nu}(\Omega)$ $(0 < \nu \leq 1/2)$, without extra assumptions. We refer to, e.g., [HW05, Woh11, HR12, DH15] for more detailed reviews on *a priori* error estimates for contact problems in elasticity.

A friction law may also be considred in the tangentiel direction and treated in a similar way as for contact. Various friction models exist and correspond to different surface properties. The most simple one is Tresca's friction (see, e.g., [AS98]) and the most common one is the Coulomb law (see, e.g., [KO88]). In this chapter we are going to use Tresca friction law for sake of simplicity to allow the theoretical analysis. A simple adaptation

of the Nitsche-based Finite Element Method to Tresca's friction is proposed in [Cho14]. All these adaptations of Nitsche's method were formulated for the contact between a deformable body and a rigid one. Thus, a first challenge of this chapter is to give an adaption of the method to the two deformable bodies contact problem.

The Nitsche-based FEM proposed in [CHR15c] and adopted in the current work encompasses symmetric and non symmetric variants depending on a generalization parameter θ. The symmetric case is recovered when $\theta = 1$. When $\theta \neq 1$ positivity of the contact term in the Nitsche variational formulation is generally lost. Nevertheless some other advantages are recovered, mostly from the numerical viewpoint. Namely, one of the variants ($\theta = 0$) involves a reduced quantity of terms, so that it is easier to implement and to extend to contact problems involving non-linear elasticity. In addition, this non symmetric variant $\theta = 0$ performs better for the Newton's loop, for a wider range of the Nitsche parameter, than the variant $\theta = 1$, see [Ren13]. Concerning the skew-symmetric variant $\theta = -1$, the well-posedness of the discrete formulation and the optimal convergence are preserved irrespectively of the value of the Nitsche parameter (See section 3.2 of chapter 3). Note that for other boundary conditions, such as non-homogeneous Dirichlet, the symmetric variant ($\theta = 1$) as originally proposed by Nitsche [Nit71] is the most widespread, since it preserves symmetry, and allows efficient solvers for linear systems with a symmetric matrix. However some non symmetric variants have been reconsidered recently, due to some remarkable robustness properties (see, e.g., [Bur12, BB16]).

In this second part of the chapter we present the Nitsche's method to treat contact: In section 2.2.1, we introduce Nitsche method for unilateral contact with a Tresca friction. Afterward an adaptation of the method to the two elastic bodies contact problem is provided in section 2.2.2. Finally, in section 2.2.3 we give a recently formulated generalization of the method that covers different type of boundary conditions.

2.2.1 Nitsche's method for unilateral contact

To discretize the problem (2.6) formulated for unilateral contact, we let $\mathbf{V}_h \subset \mathbf{V}$ be a family of finite dimensional vector spaces (see [Cia91, EG04, BS07]) indexed by h coming from a family $\mathcal{T}_h$ of triangulations of the domain Ω ($h = \max_{T\in\mathcal{T}_h} h_T$ where h_T is the diameter of T). We suppose that the family of triangulations is regular, i.e., there exists $\sigma > 0$ such that $\forall T \in \mathcal{T}_h, h_T/\rho_T \leq \sigma$ where ρ_T denotes the radius of the inscribed ball in T. Furthermore we suppose that this family is conformal to the subdivision of the boundary into Γ_D, Γ_N and Γ_C (i.e., a face of an element $T \in \mathcal{T}_h$ is not allowed to have simultaneous non-empty intersection with more than one part of the subdivision). We choose a standard Lagrange finite element method of degree k with $k = 1$ or $k = 2$, i.e.:

$$\mathbf{V}_h := \left\{ \mathbf{v}_h \in (\mathscr{C}^0(\overline{\Omega}))^d : \mathbf{v}_h|_T \in (\mathbb{P}_k(T))^d, \forall T \in \mathcal{T}_h, \mathbf{v}_h = \mathbf{0} \text{ on } \Gamma_D \right\}. \tag{2.21}$$

However, the analysis would be similar for any $\mathcal{C}^0$-conforming finite element method. We make use of the notation $[\cdot]_{\mathbb{R}^-}$ of section 2.1.2, that stands for the projection onto $\mathbb{R}^-$. To

lighten the formulas in the mathematical analysis, for the small strain case, the notation $\boldsymbol{P}_{B(\tau)}$ of projection onto the closed ball centered at the origin $\mathbf{0}$ and of radius τ, will be substituted by the notation $[\cdot]_\tau$.

The next result has been pointed out earlier in [AC88].

Proposition 2.2.1. *Let γ be a positive function defined on Γ_C. The contact conditions (2.2) can be reformulated as follows:*

$$\sigma_n(\mathbf{u}) = \left[\sigma_n(\mathbf{u}) - \gamma u_n\right]_{\mathbb{R}^-}, \tag{2.22}$$

and the condition of Tresca friction (2.3) is equivalent to :

$$\sigma_{\mathbf{t}}(\mathbf{u}) = \left[\sigma_{\mathbf{t}}(\mathbf{u}) - \gamma \mathbf{u}_{\mathbf{t}}\right]_s. \tag{2.23}$$

We consider in what follows that γ is a positive piecewise constant function on the contact and friction interface Γ_C: for any $x \in \Gamma_C$, let T be an element such that $x \in T$ and set

$$\gamma(x) = \frac{\gamma_0}{h_T}$$

where γ_0 is a positive constant. Let now $\theta \in \mathbb{R}$ be a fixed parameter. Let us introduce the discrete linear operators

$$\mathbf{P}^{\mathbf{t}}_{\theta,\gamma} : \begin{array}{ccc} \mathbf{V}_h & \to & (L^2(\Gamma_C))^{d-1} \\ \mathbf{v}_h & \mapsto & \theta\sigma_t(\mathbf{v}_h) - \gamma \mathbf{v}_{h\mathbf{t}} \end{array}, \quad \text{and} \quad \mathrm{P}^{\mathbf{n}}_{\theta,\gamma} : \begin{array}{ccc} \mathbf{V}_h & \to & L^2(\Gamma_C) \\ \mathbf{v}_h & \mapsto & \theta\sigma_n(\mathbf{v}_h) - \gamma v_{hn} \end{array}.$$

Define also the bilinear form:

$$A_{\theta\gamma}(\mathbf{u}_h, \mathbf{v}_h) := a(\mathbf{u}_h, \mathbf{v}_h) - \int_{\Gamma_C} \frac{\theta}{\gamma}\, \sigma(\mathbf{u}_h)\mathbf{n} \cdot \sigma(\mathbf{v}_h)\mathbf{n}\, d\Gamma.$$

Through an application of the Green formula on the equilibrium and boundary conditions equations (2.1) (see Section 3.1.2 for an illustration of calculation details) and inserting the contact and friction conditions (2.22),(2.23) to the problem, our Nitsche-based method for unilateral contact with Tresca friction then reads:

$$\begin{cases} \text{Find } \mathbf{u}_h \in \mathbf{V}_h \text{ such that:} \\ A_{\theta\gamma}(\mathbf{u}_h, \mathbf{v}_h) + \displaystyle\int_{\Gamma_C} \frac{1}{\gamma} \left[\mathrm{P}^{\mathbf{n}}_{1,\gamma}(\mathbf{u}_h)\right]_{\mathbb{R}^-} \mathrm{P}^{\mathbf{n}}_{\theta,\gamma}(\mathbf{v}_h)\, d\Gamma + \int_{\Gamma_C} \frac{1}{\gamma} \left[\mathbf{P}^{\mathbf{t}}_{1,\gamma}(\mathbf{u}_h)\right]_s \cdot \mathbf{P}^{\mathbf{t}}_{\theta,\gamma}(\mathbf{v}_h)\, d\Gamma \\ = L(\mathbf{v}_h), \qquad \forall\, \mathbf{v}_h \in \mathbf{V}_h. \end{cases} \tag{2.24}$$

Remark 2.2.2. *For bilateral contact with friction (equations (2.26)–(2.4)–(2.3)), the Nitsche-based formulation reads:*

$$\begin{cases} \textit{Find } \mathbf{u}_h \in \mathbf{V}^b_h \textit{ such that:} \\ A^b_{\theta\gamma}(\mathbf{u}_h, \mathbf{v}_h) + \displaystyle\int_{\Gamma_C} \frac{1}{\gamma} \left[\mathbf{P}^{\mathbf{t}}_{1,\gamma}(\mathbf{u}_h)\right]_s \cdot \mathbf{P}^{\mathbf{t}}_{\theta,\gamma}(\mathbf{v}_h)\, d\Gamma \quad = L(\mathbf{v}_h), \qquad \forall\, \mathbf{v}_h \in \mathbf{V}^b_h, \end{cases} \tag{2.25}$$

where $A^b_{\theta\gamma}(\mathbf{u}_h, \mathbf{v}_h) := a(\mathbf{u}_h, \mathbf{v}_h) - \displaystyle\int_{\Gamma_C} \frac{\theta}{\gamma}\, \sigma_{\mathbf{t}}(\mathbf{u}_h) \cdot \sigma_{\mathbf{t}}(\mathbf{v}_h)\, d\Gamma$ *and* $\mathbf{V}^b_h := \mathbf{V}_h \cap \mathbf{K}_b$.

Remark 2.2.3. *As in [CHR15c] the parameter* θ *can be set to some interesting particular values, namely:*

1. *for* $\theta = 1$ *we recover a symmetric method for which the contact term*

$$\int_{\Gamma_C} \frac{1}{\gamma}\, \left[\mathrm{P}^{\mathbf{n}}_{1,\gamma}(\mathbf{u}_h)\right]_{\mathbb{R}^-} \mathrm{P}^{\mathbf{n}}_{1,\gamma}(\mathbf{v}_h)\, d\Gamma$$

   is positive when we set $\mathbf{v}_h = \mathbf{u}_h$.

2. *for* $\theta = 0$ *we recover a simple method close to augmented Lagrangian, which involves only a few terms and may be of easiest implementation.*

3. *for* $\theta = -1$ *the method admits one unique solution and converges optimally irrespectively of the value of* $\gamma_0 > 0$.

2.2.2 Nitsche's method for contact between two elastic bodies

In this section, we formulate a Nitsche type method for contact between two elastic bodies in the small strain case. This will be a preliminary step to get the unbiased version of the method (Chapter 3). Thus, the current formulation will be, contrariwise, biased. We present, firstly, the two elastic bodies contact problem with, always, a Tresca friction.

We consider two elastic bodies expected to come into contact. To simplify notations, a general index i is used to represent indifferently the 1st or the 2nd body. Let Ω^i be the domain in $\mathbb{R}^d$ occupied by the reference configuration of the i-th body, with $d = 2$ or 3. Small strain assumption is made, as well as plane strain when $d = 2$. We suppose that the boundary $\partial\Omega^i$ of each body consists in three non-overlapping parts Γ^i_D , Γ^i_N and Γ^i_C. On Γ^i_D (resp Γ^i_N) displacements $\mathbf{u}^i$ (resp. tractions $\mathbf{t}^i$) are given. The body is clamped on Γ^i_D for the sake of simplicity. In addition each body can be subjected to a volumic force $\mathbf{f}^i$ (such as gravity). We denote by Γ^i_C a portion of the boundary of the i-th body which is a candidate contact surface with an outward unit normal vector $\mathbf{n}^i$. The actual surface on which a body comes into contact with the other one is not known in advance, but is contained in the portion Γ^i_C of $\partial\Omega^i$. Furthermore let us suppose that Γ^i_C is smooth. We let the body 1 contain the slave surface and 2 the master one. For the slave contact surface Γ^1_C, let us assume a sufficiently smooth one to one application (projection for instance) mapping each point of the first contact surface to a point of the second one:

$$\Pi^1 : \Gamma^1_C \to \Gamma^2_C.$$

Let J^1 be the Jacobian determinant of the transformation Π^1. We suppose in the following that $J^1 > 0$.

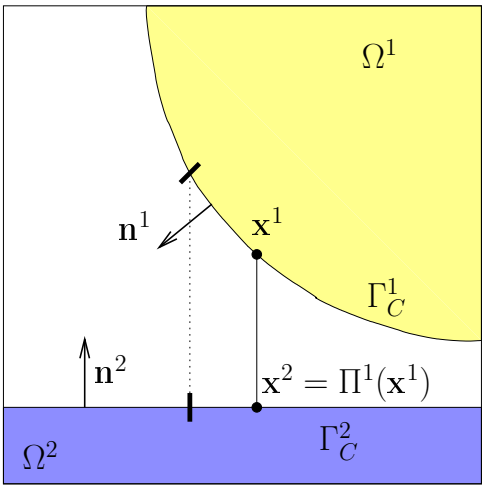

Figure 2.5: Two contacting bodies and definition of $\Pi^1(\mathbf{x})$

We define on the slave contact surface Γ_c^1 another "normal" vector $\tilde{\mathbf{n}}^1(\mathbf{x})$ such that:

$$\tilde{\mathbf{n}}^1(\mathbf{x}) = \begin{cases} \dfrac{\Pi^1(\mathbf{x}) - \mathbf{x}}{\|\Pi^1(\mathbf{x}) - \mathbf{x}\|} & \text{if } \mathbf{x} \neq \Pi^1(\mathbf{x}), \\ \mathbf{n}^1 & \text{if } \mathbf{x} = \Pi^1(\mathbf{x}). \end{cases}$$

In the small strain case such vector is needed to define the same "normal" direction for the two bodies; so that, the contact definition is consistent.
The displacements of the bodies, relatively to the fixed spatial frame are represented by $\mathbf{u} = (\mathbf{u}^1, \mathbf{u}^2)$, where $\mathbf{u}^i$ is the displacement field of the i-th body.

The contact problem in linear elasticity consists in finding the displacement field $\mathbf{u}$ satisfying the equations (2.26) and the contact conditions described hereafter:

$$\mathbf{div}\, \underline{\underline{\boldsymbol{\sigma}}}^i(\mathbf{u}^i) + \mathbf{f}^i = \mathbf{0} \quad \text{in } \Omega^i, \tag{2.26a}$$
$$\underline{\underline{\boldsymbol{\sigma}}}^i(\mathbf{u}^i) = \underline{\underline{\underline{\underline{\boldsymbol{A}}}}}^i : \underline{\underline{\boldsymbol{\varepsilon}}}(\mathbf{u}^i) \quad \text{in } \Omega^i, \tag{2.26b}$$
$$\mathbf{u}^i = \mathbf{0} \quad \text{on } \Gamma_D^i, \tag{2.26c}$$
$$\underline{\underline{\boldsymbol{\sigma}}}^i(\mathbf{u}^i)\mathbf{n}^i = \mathbf{t}^i \quad \text{on } \Gamma_N^i, \tag{2.26d}$$

where $\underline{\underline{\boldsymbol{\sigma}}}^i = \sigma^i_{(j,k)}, 1 \leq j,k \leq d$, stands for the stress tensor field and $\mathbf{div}$ denotes the divergence operator of tensor valued functions. The notation $\underline{\underline{\boldsymbol{\varepsilon}}}(\mathbf{v}) = \frac{1}{2}(\underline{\underline{\boldsymbol{\nabla}}}\mathbf{v} + \underline{\underline{\boldsymbol{\nabla}}}\mathbf{v}^T)$ represents the linearized strain tensor field and $\underline{\underline{\underline{\underline{\boldsymbol{A}}}}}^i$ is the fourth order symmetric elasticity tensor on Ω^i having the usual uniform ellipticity and boundedness property.

For any displacement field $\mathbf{v}^1$ and for any density of surface forces $\boldsymbol{\sigma}^1(\mathbf{v}^1)\mathbf{n}^1$ defined on Γ_c^1 we adopt the following notation:

$$\mathbf{v}^1 = v_n^1 \tilde{\mathbf{n}}^1 + \mathbf{v}_t^1 \text{ and } \underline{\underline{\boldsymbol{\sigma}}}^1(\mathbf{v}^1)\mathbf{n}^1 = \sigma_n^1(\mathbf{v}^1)\tilde{\mathbf{n}}^1 + \boldsymbol{\sigma}_t^1(\mathbf{v}^1),$$

where $\mathbf{v}_t^1$ (resp $\boldsymbol{\sigma}_t^1(\mathbf{v}^1)$) are the tangential components of $\mathbf{v}^1$ (resp $\boldsymbol{\sigma}^1(\mathbf{v}^1)\mathbf{n}^1$).

To simplify the expressions, we let the initial normal gap representing the normal distance between a point $\mathbf{x}$ of Γ_C^1 and its image on the other body: $g_n^1 = (\Pi^1(\mathbf{x}) - \mathbf{x}) \cdot \tilde{\mathbf{n}}^1 = 0$. We define, as well, the relative normal displacement $[\![u]\!]_n^1 = (\mathbf{u}^1 - \mathbf{u}^2 \circ \Pi^1) \cdot \tilde{\mathbf{n}}^1$.

We prescribe the contact conditions deduced from the Signorini problem conditions (see 2.1.1) on the slave surface Γ_C^1:

$$\begin{aligned} [\![u]\!]_n^1 &\leq 0 && && (2.27a)\\ \sigma_n^1(\mathbf{u}^1) &\leq 0 && \text{on } \Gamma_C^1, && (2.27b)\\ \sigma_n^1(\mathbf{u}^1)([\![u]\!]_n^1) &= 0 && && (2.27c) \end{aligned}$$

Let $s^1 \in L^2(\Gamma_C^1)$, $s^1 \geq 0$, be the Tresca friction threshold associated to the physical properties of the 1-st surface, and $[\![\mathbf{u}]\!]_t^1 = \mathbf{u}_t^1 - \mathbf{u}_t^2 \circ \Pi^1$ is the tangential relative displacement.

The Tresca friction condition on Γ_C^1 reads:

$$\begin{cases} \|\boldsymbol{\sigma}_t^1(\mathbf{u}^i)\| \leq s^1 & \text{if } [\![\mathbf{u}]\!]_t^1 = 0, \\ \boldsymbol{\sigma}_t^1(\mathbf{u}^1) = -s^1 \dfrac{[\![\mathbf{u}]\!]_t^1}{\|[\![\mathbf{u}]\!]_t^1\|} & \text{otherwise,} \end{cases} \tag{2.28}$$

where $\|\cdot\|$ stands for the Euclidean norm in $\mathbb{R}^{d-1}$.

Remark 2.2.4. *In the frictionless contact case this condition is simply replaced by* $\boldsymbol{\sigma}_t^1 = 0$.

Finally, we need to consider the second Newton law between the two contact stresses. The weak imposition of this condition gives:

$$\underline{\underline{\boldsymbol{\sigma}}}^1(\mathbf{v}^1)\mathbf{n}^1 = -J^1 \underline{\underline{\boldsymbol{\sigma}}}^2(\mathbf{v}^2)\mathbf{n}^2 \text{ on } \Gamma_C^1.$$

This condition will allow to integrate the virtual work of the master side on the slave one through the mapping function Π^1.

As in Section 2.2.1, we reformulate the contact and friction conditions (2.27)-(2.28) as follows:

$$\sigma_n^1(\mathbf{u}^1) = \left[\sigma_n^1(\mathbf{u}^1) - \gamma^1 [\![u]\!]_n^1\right]_{\mathbb{R}^-}, \tag{2.29}$$

where the notation $[\cdot]_{\mathbb{R}^-}$ refers, as in 2.22 to the projection onto $\mathbb{R}^-$ and γ^1 is a positif real function defined on the slave surface Γ_c^1. Similarly, as in (2.23), the Tresca friction condition is equivalent to the equation

$$\boldsymbol{\sigma}_t(\mathbf{u}^1) = [\boldsymbol{\sigma}_t^1(\mathbf{u}^1) - \gamma^1 [\![\mathbf{u}]\!]_t^1)]_{s^1}, \tag{2.30}$$

Using the same approach as for contact with a rigid obstacle we get a similar variational problem with the parameter θ that has the same usefulness.

We introduce the finite dimensional vector spaces as in Section 2.2.1:

$$\mathbf{V}_h = (\mathbf{V}_h^1 \times \mathbf{V}_h^2), \text{ with } \mathbf{V}_h^i = \left\{ \mathbf{v}_h^i \in \mathscr{C}^0(\overline{\Omega^i}) : \mathbf{v}_{h|T}^i \in (\mathbb{P}_k(T))^d, \forall T \in \mathcal{T}_h^i, \mathbf{v}_h^i = 0 \text{ on } \Gamma_D^i \right\}.$$

We use the Green formula and the different equations considered as well as the Nitsche's writing of the contact and friction to get the following biased finite element approximation:

$$\left\{ \begin{array}{l} \text{Find } \mathbf{u}_h \in \mathbf{V}_h \text{ such that, } \forall \mathbf{v}_h \in \mathbf{V}_h, \\ A_\theta(\mathbf{u}_h, \mathbf{v}_h) + \displaystyle\int_{\Gamma_C^1} \Big(\frac{1}{\gamma^1} P^1_{n,\theta\gamma^1}(\mathbf{v}_h) \left[P^1_{n,1\gamma^1}(\mathbf{u}_h) \right]_{\mathbb{R}^-} + \frac{1}{\gamma^1} \mathbf{P}^1_{t,\theta\gamma^1}(\mathbf{v}_h) \cdot \left[\mathbf{P}^1_{t,1\gamma^1}(\mathbf{u}_h) \right]_{s^1} \Big) \mathrm{d}\Gamma = L(\mathbf{v}_h). \end{array} \right. \tag{2.31}$$

Where:

$$P^1_{n,\theta\gamma^1}(\mathbf{v}) = \theta\sigma_n^1(\mathbf{v}^1) - \gamma^1 [\![v]\!]_n^1, \ , \qquad \mathbf{P}^1_{t,\theta\gamma^1}(\mathbf{v}) = \theta\boldsymbol{\sigma}_t^1(\mathbf{v}^1) - \gamma^1 [\![\mathbf{v}]\!]_t^1 \ ,$$

and

$$A_\theta(\mathbf{u}, \mathbf{v}) = \int_{\Omega^1} \boldsymbol{\sigma}^1(\mathbf{u}^1) : \boldsymbol{\varepsilon}(\mathbf{v}^1) \mathrm{d}\Omega + \int_{\Omega^2} \boldsymbol{\sigma}^2(\mathbf{u}^2) : \boldsymbol{\varepsilon}(\mathbf{v}^2) \mathrm{d}\Omega - \int_{\Gamma_C^1} \frac{\theta}{\gamma^1} \boldsymbol{\sigma}^1(\mathbf{u}^1)\mathbf{n} \cdot \boldsymbol{\sigma}^1(\mathbf{v}^1)\mathbf{n} \, \mathrm{d}\Gamma,$$

and

$$L(\mathbf{v}) = \int_{\Omega^1} \mathbf{f}^1 \cdot \mathbf{v}^1 \mathrm{d}\Omega + \int_{\Omega^2} \mathbf{f}^2 \cdot \mathbf{v}^2 \mathrm{d}\Omega + \int_{\Gamma_N^1} \mathbf{t}^1 \cdot \mathbf{v}^1 \mathrm{d}\Gamma + \int_{\Gamma_N^2} \mathbf{t}^2 \cdot \mathbf{v}^2 \mathrm{d}\Gamma,$$

All the mathematical properties that will be presented in Chapter 3 for the unbiased formulation case can be transposed to this biased deformable/deformable Nitsche formulation.

Remark 2.2.5. *Nitsche method for frictionless contact was, also, adapted to the framework of a fictitious domain discretization using cut-elements in [FPR16].*

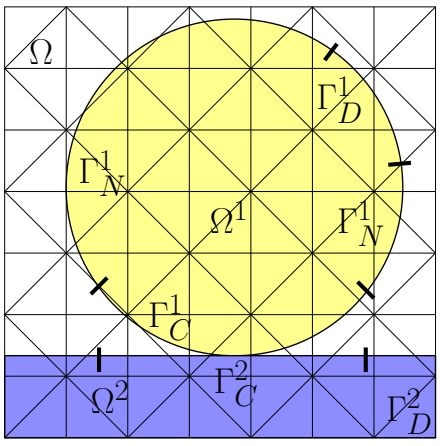

Figure 2.6: Two bodies Ω^1 and Ω^2 in contact with a single mesh of the fictitious domain Ω.

In this study, A fictitious domain Ω that contains both Ω^1 and Ω^2 is considered, generally with a simple geometry such that a structured mesh $\mathcal{T}^h$ of Ω can be used (see the example in Fig. 2.6). Then a single finite element space

$$\mathbf{W}_h := \left\{ \mathbf{v}^h \in \mathscr{C}^0(\overline{\Omega}) : \mathbf{v}^{h,i}_{|T} \in (\mathbb{P}_k(T))^d, \forall T \in \mathcal{T}^h \right\},$$

is used to approximate the displacement of the two bodies, in the sense that we consider the following approximations space

$$\mathbf{V}_h := \mathbf{W}^h{}_{|\Omega^1} \times \mathbf{W}^h{}_{|\Omega^2}.$$

in the discrete problem (2.32), where $\mathbf{W}^h{}_{|\Omega^i}$ is the space of restrictions to Ω^i of functions of $\mathbf{W}_h$. This yields the following approximation (in the frictionless case):

$$\left\{ \begin{array}{l} \text{Find } \mathbf{u}_h \in \mathbf{V}_h \text{ such that,} \\ \overline{A}^1_{\theta\gamma}(\mathbf{u}_h, \mathbf{v}_h) + \displaystyle\int_{\Gamma^1_C} \frac{1}{\gamma^1} \left[\overline{P}_{n,1\gamma^1}(\mathbf{u}_h)\right]_{\mathbb{R}^-} \overline{P}_{n,\theta\gamma^1}(\mathbf{v}_h)\, \mathrm{d}\Gamma = L(\mathbf{v}_h), \quad \forall \mathbf{v}_h \in \mathbf{V}_h, \end{array} \right. \tag{2.32}$$

where now

$$\overline{P}_{n,\theta\gamma^i}(\mathbf{v}) \;:=\; \theta \mathbf{R}_{\hat{\rho}}(\mathbf{v}^i) - \gamma^i [\![v]\!]^i_n \;,$$

and

$$\overline{A}^1_{\theta\gamma}(\mathbf{u}, \mathbf{v}) \;:=\; \sum_{i=1}^{2} \left(\int_{\Omega^i} \sigma(\mathbf{u}^i) : \boldsymbol{\varepsilon}(\mathbf{v}^i)\, d\Omega \right) - \int_{(\Gamma^1_C \cup \Gamma^1_D \cup \Gamma^2_D)} \frac{\theta}{\gamma^1} \mathbf{R}_{\hat{\rho}}(\mathbf{u}^1) \cdot \mathbf{R}_{\hat{\rho}}(\mathbf{v}^1)\, \mathrm{d}\Gamma.$$

The new term $\mathbf{R}_{\hat{\rho}}(\mathbf{v}^{h,i})$ is an approximation of $\underline{\underline{\boldsymbol{\sigma}}}^i(\mathbf{v}^i)\mathbf{n}^i$ built in order to recover an optimal order of convergence. In [FPR16] this operator is defined as the polynomial extension of the displacement field of neighbor elements having a sufficiently large intersection with the domain Ω^i, as proposed initially in [HR09]. Note that an alternative is the use of the so-called ghost penalty introduced in [BH12].

Remark finally that the presentation here differs slightly from [FPR16] in which the second Newton's law is used to reformulate differently the contact conditions (2.27). This second Newton's law reveals as well to be a key ingredient for the derivation of the unbiased formulation, as detailed before.

2.2.3 A generic formulation of the Nitsche's method for boundary conditions

We present in this section the Nitsche method within an abstract setting, and then we illustrate the application of the method to some classic problems in computational mechanics (Dirirchlet conditions and domain coupling). This abstract formulation was inspired by the one proposed in [HCCB17] to genereralize Nitsche's type methods for different boundary and interface conditions. As for contact, we will consider a whole family of Nitsche's methods indexed by the real parameter θ. Consider in the following we want to compute a

field $\mathbf{u} : \Omega \longrightarrow \mathbb{R}^d, (d \geq 1)$, that is solution to a given set of partial differential equations with prescribed boundary/interface conditions. We will denote by $\mathbf{v}$ an arbitrary test function corresponding to $\mathbf{u}$. We let Γ a portion of the boundary of Ω or an interface that subdivides Ω into two sub-domains. Two main equations are necessary to build a Nitsche-based formulation. The first one is a Green formula, that we provide below in an abstract setting:

$$a(\mathbf{u}, \mathbf{v}) - \langle \boldsymbol{\tau}(\mathbf{u}), \mathbf{B}\mathbf{v} \rangle_\Gamma = L(\mathbf{v}), \tag{2.33}$$

where $a(\cdot, \cdot)$ is a bilinear form , $\langle \cdot, \cdot \rangle_\Gamma$, is an appropriate duality product for functions on Γ(the boundary/interface work), and $L(\cdot)$ a linear form. The linear operator $\mathbf{Bv}$ is a trace-like operator (for instance $\mathbf{Bv}$ can be the value of $\mathbf{v}$ on the interface, or of its normal component). The term $\boldsymbol{\tau}(\mathbf{u})$ is to be defined for each application, and is generally related to the boundary/interface stress (if $\mathbf{u}$ is a displacement). We suppose that both $\tau(\mathbf{u})$ and $\mathbf{B}$ can be represented at almost every point of the boundary as vectors of dimension $k(1 \leq k \leq d)$. $\boldsymbol{\tau}(\mathbf{u}) : \Gamma \longrightarrow \mathbb{R}^k$; $\mathbf{Bv} : \Gamma \longrightarrow \mathbb{R}^k$.
The second equation is a reformulation of the boundary / interface conditions as follows:

$$\boldsymbol{\tau}(\mathbf{u}) = [\boldsymbol{\tau}(\mathbf{u}) - \gamma(\mathbf{Bv} - \bar{\mathbf{B}})]_S, \tag{2.34}$$

where $\gamma > 0$ is a stabilization parameter called the Nitsche parameter, $\bar{\mathbf{B}}$ is a known quantity, and $[\cdot]_S$ is the projection onto S, a closed convex set of $\mathbb{R}^k$.

To get a Nitsche-based discretization we apply the following steps (which are mathematicaly valid only for sufficiently smooth fields $\mathbf{u}$ and $\mathbf{v}$):

1. Apply the following decomposition:

$$\mathbf{Bv} = -\frac{1}{\gamma}(\theta\boldsymbol{\tau}(\mathbf{v}) - \gamma\mathbf{Bv}) + \frac{\theta}{\gamma}\boldsymbol{\tau}(\mathbf{v})$$

2. Put it into(2.33) which yields:

$$a(\mathbf{u}, \mathbf{v}) - \frac{\theta}{\gamma}\langle \boldsymbol{\tau}(\mathbf{u}), \boldsymbol{\tau}(\mathbf{v}) \rangle_\Gamma + \frac{1}{\gamma}\langle \boldsymbol{\tau}(\mathbf{u}), \theta\boldsymbol{\tau}(\mathbf{v}) - \gamma\mathbf{Bv} \rangle_\Gamma = L(\mathbf{v}).$$

3. Inject condition (2.34) into the above formula, so as to impose it weakly:

$$a(\mathbf{u}, \mathbf{v}) - \frac{\theta}{\gamma}\langle \boldsymbol{\tau}(\mathbf{u}), \boldsymbol{\tau}(\mathbf{v}) \rangle_\Gamma + \frac{1}{\gamma}\langle [\boldsymbol{\tau}(\mathbf{u}) - \gamma(\mathbf{Bu} - \bar{\mathbf{B}})]_S, \theta\boldsymbol{\tau}(\mathbf{v}) - \gamma\mathbf{Bv} \rangle_\Gamma = L(\mathbf{v}).$$

When all the fields are discretized, we obtain the Nitsche-based formulation below:

$$A_\theta(\mathbf{u}_h, \mathbf{v}_h) + \frac{1}{\gamma}\langle [P_1(\mathbf{u}_h) + \gamma\bar{\mathbf{B}})]_S, P_\theta(\mathbf{v}_h) \rangle_\Gamma = L(\mathbf{v}_h), \tag{2.35}$$

with the notations

$$A_\theta(\mathbf{u}_h, \mathbf{v}_h) = a(\mathbf{u}, \mathbf{v}) - \frac{\theta}{\gamma}\langle \boldsymbol{\tau}(\mathbf{u}_h), \boldsymbol{\tau}(\mathbf{v}_h) \rangle_\Gamma,$$

and

$$P_\theta(\mathbf{v}_h) = \theta\boldsymbol{\tau}(\mathbf{v}_h) - \gamma\mathbf{B}\mathbf{v}_h.$$

An interesting case to consider is when boundary/interface conditions are linear, which means that the convex set S is the whole sub-space ($S = \mathbb{R}^k$) and so the projection operator is merely the identity. Then (2.35) reads:

$$A_\theta(\mathbf{u}_h, \mathbf{v}_h) + \frac{1}{\gamma}\langle P_1(\mathbf{u}_h) + \gamma\bar{\mathbf{B}}), P_\theta(\mathbf{v}_h)\rangle_\Gamma = L(\mathbf{v}_h).$$

and, after re-ordering and simplifications:

$$a(\mathbf{u}_h, \mathbf{v}_h) - \theta\langle\mathbf{B}\mathbf{u}_h, \boldsymbol{\tau}(\mathbf{v}_h)\rangle_\Gamma - \langle\boldsymbol{\tau}(\mathbf{u}_h), \mathbf{B}(\mathbf{v}_h)\rangle_\Gamma + \gamma\langle, \mathbf{B}\mathbf{u}_h, \mathbf{B}\mathbf{v}_h\rangle_\Gamma = L(\mathbf{v}_h) \tag{2.36}$$

We recognize here the standard formulation presented for instance in [Han05].

Dirichlet conditions

To illustrate how the above framework can be applied to deal with various boundary conditions, we consider in a first time an elastic body Ω, subjected to Dirichlet conditions on the boundary Γ_D. The PVW reads:

$$a(\mathbf{u}, \mathbf{v}) = L(\mathbf{v}), \qquad \mathbf{u} = \bar{\mathbf{u}} \text{ on } \Gamma_D, \tag{2.37}$$

where $a(\mathbf{u}, \mathbf{v}) = \displaystyle\int_\Omega \underline{\underline{\boldsymbol{\sigma}}}(\mathbf{u}) : \underline{\underline{\boldsymbol{\varepsilon}}}(\mathbf{v})\, d\Omega$ and $L(\mathbf{v})$ is the virtual work of external forces. Taking:

$$\mathbf{B}\mathbf{u} = \mathbf{u}, \quad \boldsymbol{\tau}(\mathbf{u}) = \underline{\underline{\boldsymbol{\sigma}}}(\mathbf{u})\mathbf{n}, \quad \bar{\mathbf{B}} = \bar{\mathbf{u}} \quad \text{and } S = \mathbb{R}^d,$$

we obtain from (2.36) the following Nitsche-based formulation:

$$a(\mathbf{u}_h, \mathbf{v}_h) - \theta\langle\mathbf{u}_h, \boldsymbol{\sigma}(\mathbf{v}_h)\mathbf{n}\rangle_\Gamma - \langle\boldsymbol{\sigma}(\mathbf{u}_h)\mathbf{n}, \mathbf{v}_h\rangle_\Gamma + \gamma\langle\mathbf{u}_h, \mathbf{v}_h\rangle_\Gamma = L(\mathbf{v}_h) - \langle\bar{\mathbf{u}}, \theta\boldsymbol{\sigma}(\mathbf{v}_h)\mathbf{n} - \gamma\mathbf{v}_h)\rangle_\Gamma.$$

This last correspond to the Nitsche's method for Dirichlet conditions discribed in [Han05]

Subdomain interface coupling

We consider now an interface problem in which the domain Ω is decomposed into two sub-domains $\Omega^i, i = 1, 2$ (see Fig. 2.7). The shared boundary between Ω^1 andΩ^2 is denoted by Γ, and $\mathbf{n}^i$ is the unit normal along the interface, pointing out of Ω^i.

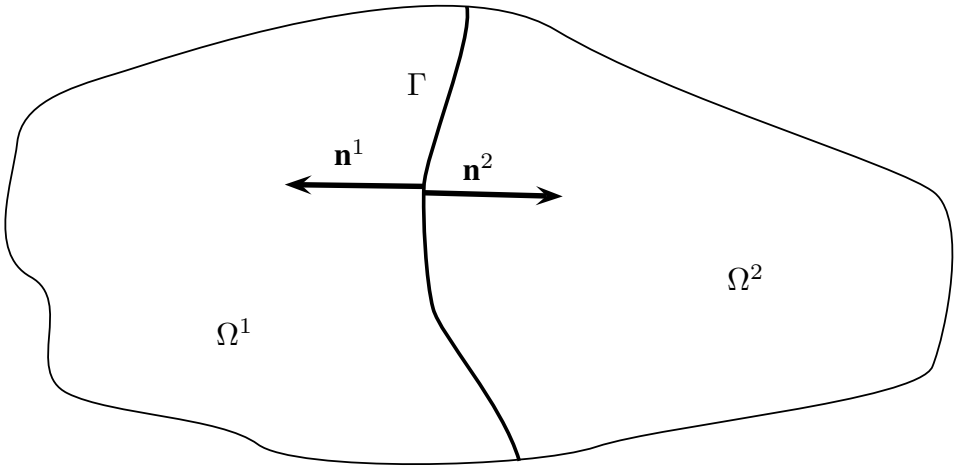

Figure 2.7: Two sub-domains Ω^1 and Ω^2 divided by the boundary Γ.

We still consider elastic body in small strains. The continuity of displacement and pressure along the interface reads:

$$\begin{cases} \mathbf{u}^1 - \mathbf{u}^2 = \mathbf{0}, \\ \underline{\underline{\boldsymbol{\sigma}}}^1 \mathbf{n}^1 + \underline{\underline{\boldsymbol{\sigma}}}^2 \mathbf{n}^2 = \mathbf{0}. \end{cases} \quad \text{on } \Gamma \tag{2.38}$$

Let us define as usual the jump and average operators along the interface:

$$\begin{cases} [\![\mathbf{u}]\!] = \mathbf{u}^1 - \mathbf{u}^2, \\ \langle \boldsymbol{\sigma} \rangle = \dfrac{1}{2}(\underline{\underline{\boldsymbol{\sigma}}}^1 \mathbf{n}^1 - \underline{\underline{\boldsymbol{\sigma}}}^2 \mathbf{n}^2) \end{cases}$$

Green formula for elasticity equations yields:

$$a(\mathbf{u}, \mathbf{v}) - \int_\Gamma \underline{\underline{\boldsymbol{\sigma}}}^1 \mathbf{n}^1 \cdot \mathbf{v}^1 \, d\Gamma - \int_\Gamma \underline{\underline{\boldsymbol{\sigma}}}^2 \mathbf{n}^2 \cdot \mathbf{v}^2 \, d\Gamma = L(\mathbf{v})$$

Using the second equation of (2.38) we get the needed Green formula for our Nitsche's method:

$$a(\mathbf{u}, \mathbf{v}) - \int_\Gamma \langle \boldsymbol{\sigma} \rangle \cdot [\![\mathbf{v}]\!] \, d\Gamma = L(\mathbf{v}). \tag{2.39}$$

With the choice

$$\mathbf{B}\mathbf{u} = [\![\mathbf{u}]\!], \quad \boldsymbol{\tau}(\mathbf{u}) = \langle \boldsymbol{\sigma}(\mathbf{u}) \rangle, \quad \bar{\mathbf{B}} = \mathbf{0} \quad \text{and } S = \mathbb{R}^d,$$

formulation (2.36) reads:

$$a(\mathbf{u}_h, \mathbf{v}_h) - \theta \int_\Gamma [\![\mathbf{u}_h]\!] \cdot \langle \boldsymbol{\sigma}(\mathbf{v}_h) \rangle \, d\Gamma - \int_\Gamma \langle \boldsymbol{\sigma}(\mathbf{u}_h) \rangle \cdot [\![\mathbf{v}_h]\!] \, d\Gamma + \int_\Gamma \gamma [\![\mathbf{u}_h]\!] \cdot [\![\mathbf{v}_h]\!] \, d\Gamma = L(\mathbf{v}_h).$$

The case of contact and friction are recovred by the formulation (2.35) as well when taking :

$$\mathbf{Bu} = [\![\mathbf{u}]\!]_n^1, \quad \boldsymbol{\tau}(\mathbf{u}) = \hat{\sigma}^1(\mathbf{u}^1), \quad \bar{\mathbf{B}} = \mathbf{0} \quad \text{and } S = \mathbb{R}^-,$$

for contact and

$$\mathbf{Bu} = [\![\mathbf{u}]\!]_t^1, \quad \boldsymbol{\tau}(\mathbf{u}) = \boldsymbol{\sigma}_t^1(\mathbf{u}^1), \quad \bar{\mathbf{B}} = \mathbf{0} \quad \text{and } S = \mathcal{B}_s,$$

for friction; where $\mathcal{B}_s$ is the closed ball of radius s equal to the friction threshold depending on the friction law.

Chapter 3

Unbiased Nitsche's method in the small strain framework

Contents

Introduction

The most common paradigm to treat the problem of two deformable bodies in contact is known as the master/slave formulation. In this approach one distinguishes between a master surface and a slave one on which is prescribed the non-interpenetration condition. A presentation of this formulation and the contact problem can be found in Laursen's work [Lau92, Lau02] (see also [LS93b]). In section 2.2.2, we presented a classical Nitsche

formulation of the contact between two elastic bodies. This formulation uses a biased master/slave description of the problem.

This approach is confronted with important difficulties especially in the case of self-contact and multi-body contact where it is impossible or impractical to a priori nominate a master surface and a slave one. Automating the detection and the separation between slave and master surfaces in these cases may generate a lack of robustness since it may create detection problems.

If the master/slave formulation consists in a natural extension of the contact treatment between a deformable body and a rigid ground, it has no complete theoretical justification. Consequently, to avoid these difficulties, we provide in this chapter an unbiased formulation of the two elastic bodies contact problem in the small strain framework. In this formulation we do not distinguish between a master surface and a slave one since we impose the non-inter penetration and the friction conditions on both of them. Unbiased contact and friction formulation have been considered before in [SD15] and references therein. There, the authors present a numerical study of the method and make use of a penalized formulation of contact and friction. The terms two-pass and two-half-pass are also used in literature to describe this type of methods.

This study can be seen as a first step in the construction of a method taking into account contact between two elastic solids and self-contact in large transformations in the same formalism. The present formulation, in small deformations, allows us to ensure the consistency, the convergence and the optimality of the method. In this context, the aim of this chapter is to provide an unbiased description of the contact and Tresca friction conditions, that relies upon a Nitsche's treatment of contact conditions.

Other possibilities for contact discretization are for instance node-to-segment techniques or the mortar method. Note that the mortar method is an efficient alternative that has been widely applied to contact problem (see [BBHL99, ML00a, PWGW12]). The mortar technique allows to match independent discretization of the contacting solids and takes into account the unilateral contact conditions in a convenient way. The procedure provides variationally consistent contact pressures. But mortar methods normally represent asymmetric formulations, by distinguishing between a master (or mortar) and a slave (or non-mortar) surface. Thus, the adaptation to an unbiased contact description is quite easier with Nitsche's method than a mortar one. In fact, since Nitsche's method uses the contact stress as a multiplier, it is very simple to divide this contact effort equitably on both of contact surfaces. A comparaision between Nitsche's method and mortar-type ones for linear elasticity is provided in [FHW04].

The formulation described in this chapter uses an additional parameter θ as in [CHR15c] and the previous chapter, allowing us to introduce some variants acting on the symmetry / skew-symmetry / non-symmetry of the discrete formulation. Moreover, a unified analysis of all these variants can be performed. We provide, as well, theoretical and numerical verifications of the proposed method. First, we prove the consistency of the method, its well-posedness and its optimal convergence. And then, a numerical verification is performed to confirm the theoretical results.

In section 3.1 we build an unbiased formulation of the two elastic bodies frictional (Tresca) contact problem. To prove the efficiency of the method (3.16), we carry out some

mathematical analysis in section 3.2. In the last section 3.3 of this chapter, we present the results of several two/three-dimensional numerical tests. The tests cover a convergence study of the global relative error of displacement in H^1-norm and the contact pressure error in L^2-norm with different values of the parameter θ and the Nitsche's parameter γ_0. The open source environment GetFEM++[1] is used to perform the tests.

3.1 Construction of the unbiased Nitsche's method

3.1.1 Formal statement of the two bodies contact problem

As for the classic (biased) formulation, we consider the two elastic bodies configuration with the same notations and considerations of section 2.2.2.
The displacements of the bodies, relatively to the fixed spatial frame are represented by $\mathbf{u} = (\mathbf{u}^1, \mathbf{u}^2)$, where $\mathbf{u}^i$ is the displacement field of the i-th body.

In the same way for the biased formulation, we assume a sufficiently smooth one to one application (projection for instance) mapping each point of the first contact surface to a point of the second one:

$$\Pi^1 : \Gamma_C^1 \to \Gamma_C^2.$$

Let J^1 be the Jacobian determinant of the transformation Π^1. But for the non biased case we define also the mapping Π^2 as the inverse function of Π^1 ($\Pi^2 = (\Pi^1)^{-1}$). Then, the Jacobian determinant of $\Pi^2 =$ will be $J^2 = \dfrac{1}{J^1}$. We suppose in the following that $J^i > 0$.

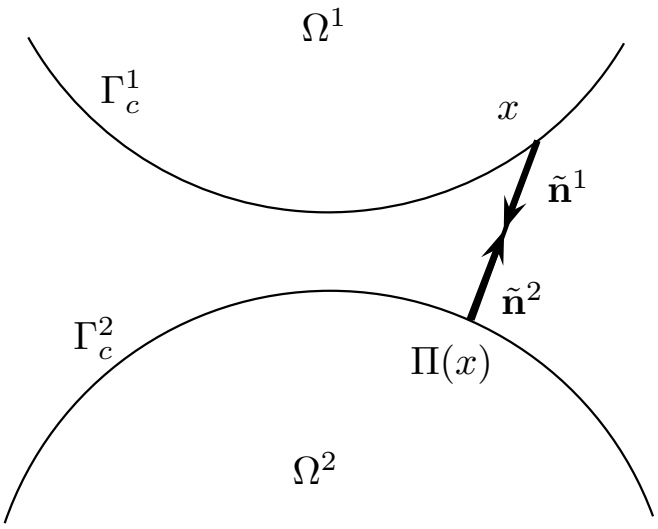

Figure 3.1: Example of definition of $\tilde{\mathbf{n}}^i$

We define, this time two normal vectors $\tilde{\mathbf{n}}^i$, on each contact surface (see Figure 3.1)

[1] http://getfem.org/

such that:

$$\tilde{\mathbf{n}}^i(\mathbf{x}) = \begin{cases} \dfrac{\Pi^i(\mathbf{x}) - \mathbf{x}}{\|\Pi^i(\mathbf{x}) - \mathbf{x}\|} & \text{if } \mathbf{x} \neq \Pi^i(\mathbf{x}), \\ \mathbf{n}^i & \text{if } \mathbf{x} = \Pi^i(\mathbf{x}). \end{cases}$$

Note that $\tilde{\mathbf{n}}^1 = -\tilde{\mathbf{n}}^2 \circ \Pi^1$ and $\tilde{\mathbf{n}}^2 = -\tilde{\mathbf{n}}^1 \circ \Pi^2$.

We consider the same equilibirum and boundary conditions (2.26) given for the biased version.

As in 2.2.2, displacement field $\mathbf{v}^i$ and for any density of surface forces $\boldsymbol{\sigma}^i(\mathbf{v}^i)\mathbf{n}^i$ defined on Γ_c^i we adopt the following notation:

$$\mathbf{v}^i = v_n^i \tilde{\mathbf{n}}^i + \mathbf{v}_t^i \text{ and } \underline{\boldsymbol{\sigma}}^i(\mathbf{v}^i)\mathbf{n}^i = \sigma_n^i(\mathbf{v}^i)\tilde{\mathbf{n}}^i + \boldsymbol{\sigma}_t^i(\mathbf{v}^i),$$

where $\mathbf{v}_t^i$ (resp $\boldsymbol{\sigma}_t^i(\mathbf{v}^i)$) are the tangential components of $\mathbf{v}^i$ (resp $\boldsymbol{\sigma}^i(\mathbf{v}^i)\mathbf{n}^i$).
We define an initial normal gap representing the normal distance between a point $\mathbf{x}$ of Γ_C^i and its image on the other body: $g_n^i = (\Pi^i(\mathbf{x}) - \mathbf{x}) \cdot \tilde{\mathbf{n}}^i$. We define, as well, the relative normal and tangential displacements :

$$\begin{cases} [\![u]\!]_n^1 = (\mathbf{u}^1 - \mathbf{u}^2 \circ \Pi^1) \cdot \tilde{\mathbf{n}}^1 \text{ and } [\![u]\!]_n^2 = (\mathbf{u}^2 - \mathbf{u}^1 \circ \Pi^2) \cdot \tilde{\mathbf{n}}^2, \\ \text{ and} \\ [\![\mathbf{u}]\!]_t^1 = \mathbf{u}_t^1 - \mathbf{u}_t^2 \circ \Pi^1 \text{ and } [\![\mathbf{u}]\!]_t^2 = \mathbf{u}_t^2 - \mathbf{u}_t^1 \circ \Pi^2. \end{cases}$$

Remark 3.1.1. *Note that:* $g_n^1 \circ \Pi^2 = g_n^2$ *and* $g_n^2 \circ \Pi^1 = g_n^1$ *;* $[\![u]\!]_n^1 \circ \Pi^2 = [\![u]\!]_n^2$ *and* $[\![u]\!]_n^2 \circ \Pi^1 = [\![u]\!]_n^1$. *And* $[\![\mathbf{u}]\!]_t^1 = -[\![\mathbf{u}]\!]_t^2 \circ \Pi^1$ *and* $[\![\mathbf{u}]\!]_t^2 = -[\![\mathbf{u}]\!]_t^1 \circ \Pi^2$.

In order to obtain an unbiased formulation of the contact problem we prescribe the contact conditions deduced from the Signorini problem conditions (see [KO88]) on the two surfaces in a symmetric way. Thus, the conditions describing contact on Γ_C^1 and Γ_C^2 are:

$$[\![u]\!]_n^i \leq g_n^i \tag{3.1a}$$
$$\sigma_n^i(\mathbf{u}^i) \leq 0 \qquad \text{on } \Gamma_C^i, \tag{3.1b}$$
$$\sigma_n^i(\mathbf{u}^i)([\![u]\!]_n^i - g_n^i) = 0 \tag{3.1c}$$

Let $s^i \in L^2(\Gamma_C^i)$, $s^i \geq 0$, be the Tresca friction threshold associated to the physical properties of the i-th surface.

The Tresca friction condition on Γ_C^1 and Γ_C^2 reads:

$$\begin{cases} \|\boldsymbol{\sigma}_t^i(\mathbf{u}^i)\| \leq s^i & \text{if } [\![\mathbf{u}]\!]_t^i = 0, \\ \boldsymbol{\sigma}_t^i(\mathbf{u}^i) = -s^i \dfrac{[\![\mathbf{u}]\!]_t^i}{\|[\![\mathbf{u}]\!]_t^i\|} & \text{otherwise,} \end{cases} \tag{3.2}$$

where $\|\cdot\|$ stands for the Euclidean norm in $\mathbb{R}^{d-1}$.

Remark 3.1.2. *In the frictionless contact case this condition is simply replaced by* $\boldsymbol{\sigma}_t^i = 0$.

Finally, we need to consider the second Newton law between the two bodies:

$$\begin{cases} \displaystyle\int_{\gamma_C^1} \sigma_n^1(\mathbf{u}^1)\mathrm{d}s - \int_{\gamma_C^2} \sigma_n^2(\mathbf{u}^2)\mathrm{d}s = 0, \\ \displaystyle\int_{\gamma_C^1} \boldsymbol{\sigma}_t^1(\mathbf{u}^1)\mathrm{d}s + \int_{\gamma_C^2} \boldsymbol{\sigma}_t^2(\mathbf{u}^2)\mathrm{d}s = 0, \end{cases}$$

where γ_C^1 is any subset of Γ_C^1 and $\gamma_C^2 = \Pi^1(\gamma_C^1)$. Mapping all terms on γ_C^1 allows writing:

$$\begin{cases} \displaystyle\int_{\gamma_C^1} \sigma_n^1(\mathbf{u}^1) - J^1\sigma_n^2(\mathbf{u}^2 \circ \Pi^1)\mathrm{d}s = 0, \\ \displaystyle\int_{\gamma_C^1} \boldsymbol{\sigma}_t^1(\mathbf{u}^1) + J^1\boldsymbol{\sigma}_t^2(\mathbf{u}^2 \circ \Pi^1)\mathrm{d}s = 0, \end{cases} \qquad \forall \gamma_C^1 \subset \Gamma_C^1$$

so we obtain:

$$\begin{cases} \sigma_n^1(\mathbf{u}^1) - J^1\sigma_n^2(\mathbf{u}^2 \circ \Pi^1) = 0, \\ \boldsymbol{\sigma}_t^1(\mathbf{u}^1) + J^1\boldsymbol{\sigma}_t^2(\mathbf{u}^2 \circ \Pi^1) = 0, \end{cases} \quad \text{on } \Gamma_C^1. \tag{3.3}$$

Remark 3.1.3. *: A similar condition holds on* Γ_c^2*:*

$$\begin{cases} \sigma_n^2(\mathbf{u}^2) - J^2\sigma_n^1(\mathbf{u}^1 \circ \Pi^2) = 0, \\ \boldsymbol{\sigma}_t^2(\mathbf{u}^2) + J^2\boldsymbol{\sigma}_t^1(\mathbf{u}^1 \circ \Pi^2) = 0. \end{cases}$$

It is important to mention that, due to second Newton law, we need to fix s^1 and s^2 such that: $-s^1 \dfrac{[\![\mathbf{u}]\!]_t^1}{\|[\![\mathbf{u}]\!]_t^1\|} = \boldsymbol{\sigma}_t^1(\mathbf{u}^1) = -J^1\boldsymbol{\sigma}_t^2(\mathbf{u}^2 \circ \Pi^1) = J^1 s^2 \dfrac{[\![\mathbf{u}]\!]_t^2 \circ \Pi^1}{\|[\![\mathbf{u}]\!]_t^2 \circ \Pi^1\|} = -J^1 s^2 \dfrac{[\![\mathbf{u}]\!]_t^1}{|[\![\mathbf{u}]\!]_t^1|}$.
And so:

$$s^1 = J^1 s^2. \tag{3.4}$$

3.1.2 Variational formulation using Nitsche's method

In this section, we establish the weak formulation of problem (2.26)–(3.3) using Nitsche's method and the unbiased form of the contact and the friction conditions given in Section 3.1.1.

As in [CHR15c], we introduce an additional parameter θ. This generalization will allow several variants, depending on the value of θ. The symmetric case is obtained when $\theta = 1$. The advantage of the symmetric formulation is that it derives from an energy potential (see 3.1.3). These features are lost when $\theta \neq 1$. Nevertheless the variants $\theta = -1$ and 0 presents some other advantages, mostly from the numerical viewpoint. In particular, the case $\theta = 0$ involves a reduced number of terms, which makes it easier to implement and to extend to contact problems involving non-linear elasticity. Also, for $\theta = -1$,

the well-posedness of the discrete formulation and the optimal convergence are preserved irrespectively of the value of the Nitsche parameter γ^i. Some general guidelines on how to choose γ_0 and θ are provided in the section 3.3.5. First, we introduce the Hilbert space

$$\mathbf{V} = \Big\{ \mathbf{v} = (\mathbf{v}^1, \mathbf{v}^2) \in H^1(\Omega^1)^d \times H^1(\Omega^2)^d : \quad \mathbf{v}^1 = \mathbf{0} \text{ on } \Gamma_D^1 \text{ and } \mathbf{v}^2 = \mathbf{0} \text{ on } \Gamma_D^2 \Big\}.$$

Let $\mathbf{u} = (\mathbf{u}^1, \mathbf{u}^2)$ be the solution of the contact problem in its strong form (2.26)–(3.3). We assume that $\mathbf{u}$ is sufficiently regular so that all the following calculations make sense.

As shown in Chapter 2, the derivation of a Nitsche-based method comes from a reformulation of the contact conditions (4.16a)-(4.16b)-(4.16c) (see for instance [CH13] and [CHR15c]). This reformulation is similar to the augmented Lagrangian formulation of contact problems. The contact conditions (4.16a)-(4.16b)-(4.16c) are equivalent to the equation (3.5) for a given positive function γ^i :

$$\sigma_n^i(\mathbf{u}^i) = [\sigma_n^i(\mathbf{u}^i) - \gamma^i([\![u]\!]_n^i - g_n^i)]_{\mathbb{R}^-}, \tag{3.5}$$

where the notation $[\cdot]_{\mathbb{R}^-}$ refers to the the projection on $\mathbb{R}^-$ of a scalar quantity. Similarly, as in chapter 2, the Tresca friction condition is equivalent to the equation

$$\boldsymbol{\sigma}_t(\mathbf{u}^i) = [\boldsymbol{\sigma}_t(\mathbf{u}^i) - \gamma^i [\![\mathbf{u}]\!]_t^i]_{s^i}, \tag{3.6}$$

where, as in section 2.2.1, the notation $[\cdot]_\tau$ refers to the orthogonal projection onto, the closed ball centered at the origin and of radius τ. In what follows some properties of the positive part and the projection are mentioned. Those properties will be useful in the analysis of the method.
Note that, for $x, y \in \mathbb{R}$:

$$(y - x)([y]_{\mathbb{R}^-} - [x]_{\mathbb{R}^-}) \geq ([y]_{\mathbb{R}^-} - [x]_{\mathbb{R}^-})^2. \tag{3.7}$$

We note, also, the following classical property for a projection for all $\mathbf{x}, \mathbf{y} \in \mathbb{R}^{d-1}$:

$$(\mathbf{y} - \mathbf{x}).([\mathbf{y}]_\tau - [\mathbf{x}]_\tau) \geq \|[\mathbf{y}]_\tau - [\mathbf{x}]_\tau\|^2. \tag{3.8}$$

From the Green formula and equations (2.26), we get for every $\mathbf{v} \in \mathbf{V}$:

$$\int_{\Omega^1} \underline{\underline{\boldsymbol{\sigma}}}^1(\mathbf{u}^1) : \underline{\underline{\boldsymbol{\varepsilon}}}(\mathbf{v}^1) \mathrm{d}\Omega + \int_{\Omega^2} \underline{\underline{\boldsymbol{\sigma}}}^2(\mathbf{u}^2) : \underline{\underline{\boldsymbol{\varepsilon}}}(\mathbf{v}^2) \mathrm{d}\Omega = \int_{\Omega^1} \mathbf{f}^1 \cdot \mathbf{v}^1 \mathrm{d}\Omega + \int_{\Omega^2} \mathbf{f}^2 \cdot \mathbf{v}^2 \mathrm{d}\Omega$$
$$+ \int_{\Gamma_N^1} \mathbf{t}^1 \cdot \mathbf{v}^1 \mathrm{d}\Gamma + \int_{\Gamma_N^2} \mathbf{t}^2 \cdot \mathbf{v}^2 \mathrm{d}\Gamma + \int_{\Gamma_C^1} \underline{\underline{\boldsymbol{\sigma}}}^1(\mathbf{u}^1)\mathbf{n}^1 \cdot \mathbf{v}^1 \mathrm{d}\Gamma + \int_{\Gamma_C^2} \underline{\underline{\boldsymbol{\sigma}}}^2(\mathbf{u}^2)\mathbf{n}^2 \cdot \mathbf{v}^2 \mathrm{d}\Gamma.$$

We define

$$\begin{aligned} a(\mathbf{u},\mathbf{v}) &= \int_{\Omega^1} \underline{\underline{\boldsymbol{\sigma}}}^1(\mathbf{u}^1) : \underline{\underline{\boldsymbol{\varepsilon}}}(\mathbf{v}^1)\mathrm{d}\Omega + \int_{\Omega^2} \underline{\underline{\boldsymbol{\sigma}}}^2(\mathbf{u}^2) : \underline{\underline{\boldsymbol{\varepsilon}}}(\mathbf{v}^2)\mathrm{d}\Omega, \\ &\text{and} \\ L(\mathbf{v}) &= \int_{\Omega^1} \mathbf{f}^1 \cdot \mathbf{v}^1 \mathrm{d}\Omega + \int_{\Omega^2} \mathbf{f}^2 \cdot \mathbf{v}^2 \mathrm{d}\Omega + \int_{\Gamma_N^1} \mathbf{t}^1 \cdot \mathbf{v}^1 \mathrm{d}\Gamma + \int_{\Gamma_N^2} \mathbf{t}^2 \cdot \mathbf{v}^2 \mathrm{d}\Gamma. \end{aligned}$$

So, there holds:

$$a(\mathbf{u},\mathbf{v}) - \int_{\Gamma_C^1} \sigma_n^1(\mathbf{u}^1) v_n^1 \mathrm{d}\Gamma - \int_{\Gamma_C^2} \sigma_n^2(\mathbf{u}^2) v_n^2 \mathrm{d}\Gamma - \int_{\Gamma_C^1} \boldsymbol{\sigma}_t^1(\mathbf{u}^1) \cdot \mathbf{v}_t^1 \mathrm{d}\Gamma - \int_{\Gamma_C^2} \boldsymbol{\sigma}_t^2(\mathbf{u}^2) \cdot \mathbf{v}_t^2 \mathrm{d}\Gamma = L(\mathbf{v}).$$

Using condition (3.3) we can write

$$\begin{aligned} &a(\mathbf{u},\mathbf{v}) - \frac{1}{2}\int_{\Gamma_C^1} (\sigma_n^1(\mathbf{u}^1) + J^1\sigma_n^2(\mathbf{u}^2 \circ \Pi^1)) v_n^1 \mathrm{d}\Gamma - \frac{1}{2}\int_{\Gamma_C^2} (\sigma_n^2(\mathbf{u}^2) + J^2\sigma_n^1(\mathbf{u}^1 \circ \Pi^2)) v_n^2 \mathrm{d}\Gamma \\ &-\frac{1}{2}\int_{\Gamma_C^1} (\boldsymbol{\sigma}_t^1(\mathbf{u}^1) - J^1\boldsymbol{\sigma}_t^2(\mathbf{u}^2 \circ \Pi^1)) \cdot \mathbf{v}_t^1 \mathrm{d}\Gamma - \frac{1}{2}\int_{\Gamma_C^2} (\boldsymbol{\sigma}_t^2(\mathbf{u}^2) - J^2\boldsymbol{\sigma}_t^1(\mathbf{u}^1 \circ \Pi^2)) \cdot \mathbf{v}_t^2 \mathrm{d}\Gamma = L(\mathbf{v}). \end{aligned}$$

So, using the property $\displaystyle\int_{\Gamma_C^1} J^1 f \mathrm{d}\Gamma = \int_{\Gamma_C^2} f \circ \Pi^2 \mathrm{d}\Gamma$, we have

$$\begin{aligned} &a(\mathbf{u},\mathbf{v}) - \frac{1}{2}\int_{\Gamma_C^1} \sigma_n^1(\mathbf{u}^1) v_n^1 \mathrm{d}\Gamma - \frac{1}{2}\int_{\Gamma_C^1} \sigma_n^1(\mathbf{u}^1)(v_n^2 \circ \Pi^1)\mathrm{d}\Gamma - \frac{1}{2}\int_{\Gamma_C^2} \sigma_n^2(\mathbf{u}^2) v_n^2 \mathrm{d}\Gamma \\ &-\frac{1}{2}\int_{\Gamma_C^2} \sigma_n^2(\mathbf{u}^2)(v_n^1 \circ \Pi^2)\mathrm{d}\Gamma - \frac{1}{2}\int_{\Gamma_C^1} \boldsymbol{\sigma}_t^1(\mathbf{u}^1) \cdot \mathbf{v}_t^1 + \frac{1}{2}\int_{\Gamma_C^1} \boldsymbol{\sigma}_t^1(\mathbf{u}^1) \cdot (\mathbf{v}_t^2 \circ \Pi^1)\mathrm{d}\Gamma \\ &-\frac{1}{2}\int_{\Gamma_C^2} \boldsymbol{\sigma}_t^2(\mathbf{u}^2) \cdot \mathbf{v}_t^2 + \frac{1}{2}\int_{\Gamma_C^2} \boldsymbol{\sigma}_t^2(\mathbf{u}^2) \cdot (\mathbf{v}_t^1 \circ \Pi^2)\mathrm{d}\Gamma = L(\mathbf{v}). \end{aligned}$$

This leads to:

$$\begin{aligned} &a(\mathbf{u},\mathbf{v}) - \frac{1}{2}\int_{\Gamma_C^1} \sigma_n^1(\mathbf{u}^1)(v_n^1 + v_n^2 \circ \Pi^1)\mathrm{d}\Gamma - \frac{1}{2}\int_{\Gamma_C^2} \sigma_n^2(\mathbf{u}^2)(v_n^2 + v_n^1 \circ \Pi^2)\mathrm{d}\Gamma \\ &-\frac{1}{2}\int_{\Gamma_C^1} \boldsymbol{\sigma}_t^1(\mathbf{u}^1) \cdot (\mathbf{v}_t^1 - \mathbf{v}_t^2 \circ \Pi^1)\mathrm{d}\Gamma - \frac{1}{2}\int_{\Gamma_C^2} \boldsymbol{\sigma}_t^2(\mathbf{u}^2) \cdot (\mathbf{v}_t^2 - \mathbf{v}_t^1 \circ \Pi^2)\mathrm{d}\Gamma = L(\mathbf{v}). \end{aligned}$$

Using the writings, for $\theta \in \mathbb{R}$,

$$\begin{cases} v_n^1 + v_n^2 \circ \Pi^1 = -\dfrac{1}{\gamma^1}\big(\theta\sigma_n^1(\mathbf{v}^1) - \gamma^1(v_n^1 + v_n^2 \circ \Pi^1)\big) + \dfrac{\theta}{\gamma^1}\sigma_n^1(\mathbf{v}^1) \\ v_n^2 + v_n^1 \circ \Pi^2 = -\dfrac{1}{\gamma^2}\big(\theta\sigma_n^2(\mathbf{v}^2) - \gamma^2(v_n^2 + v_n^1 \circ \Pi^2)\big) + \dfrac{\theta}{\gamma^2}\sigma_n^2(\mathbf{v}^2) \end{cases}$$

$$\begin{cases} \mathbf{v}_t^1 - \mathbf{v}_t^2 \circ \Pi^1 = -\dfrac{1}{\gamma^1}\big(\theta\boldsymbol{\sigma}_t^1(\mathbf{v}^1) - \gamma^1(\mathbf{v}_t^1 - \mathbf{v}_t^2 \circ \Pi^1)\big) + \dfrac{\theta}{\gamma^1}\boldsymbol{\sigma}_t^1(\mathbf{v}^1) \\ \mathbf{v}_t^2 - \mathbf{v}_t^1 \circ \Pi^2 = -\dfrac{1}{\gamma^2}\big(\theta\boldsymbol{\sigma}_t^2(\mathbf{v}^2) - \gamma^2(\mathbf{v}_t^2 - \mathbf{v}_t^1 \circ \Pi^2)\big) + \dfrac{\theta}{\gamma^2}\boldsymbol{\sigma}_t^2(\mathbf{v}^2), \end{cases}$$

we obtain:

$$\begin{aligned} & a(\mathbf{u},\mathbf{v}) - \frac{1}{2}\int_{\Gamma_C^1}\frac{\theta}{\gamma^1}\sigma_n^1(\mathbf{u}^1)\sigma_n^1(\mathbf{v}^1)\mathrm{d}\Gamma - \frac{1}{2}\int_{\Gamma_C^2}\frac{\theta}{\gamma^2}\sigma_n^2(\mathbf{u}^2)\sigma_n^2(\mathbf{v}^2)\mathrm{d}\Gamma \\ & -\frac{1}{2}\int_{\Gamma_C^1}\frac{\theta}{\gamma^1}\boldsymbol{\sigma}_t^1(\mathbf{u}^1)\cdot\boldsymbol{\sigma}_t^1(\mathbf{v}^1)\mathrm{d}\Gamma - \frac{1}{2}\int_{\Gamma_C^2}\frac{\theta}{\gamma^2}\boldsymbol{\sigma}_t^2(\mathbf{u}^2)\cdot\boldsymbol{\sigma}_t^2(\mathbf{v}^2)\mathrm{d}\Gamma \\ & +\frac{1}{2}\int_{\Gamma_C^1}\frac{\sigma_n^1(\mathbf{u}^1)}{\gamma^1}\big(\theta\sigma_n^1(\mathbf{v}^1) - \gamma^1(v_n^1 + v_n^2\circ\Pi^1)\big)\mathrm{d}\Gamma \\ & +\frac{1}{2}\int_{\Gamma_C^2}\frac{\sigma_n^2(\mathbf{u}^2)}{\gamma^2}\big(\theta\sigma_n^2(\mathbf{v}^2) - \gamma^2(v_n^2 + v_n^1\circ\Pi^2)\big)\mathrm{d}\Gamma \\ & +\frac{1}{2}\int_{\Gamma_C^1}\frac{\boldsymbol{\sigma}_t^1(\mathbf{u}^1)}{\gamma^1}\cdot\big(\theta\boldsymbol{\sigma}_t^1(\mathbf{v}^1) - \gamma^1(\mathbf{v}_t^1 - \mathbf{v}_t^2\circ\Pi^1)\big)\mathrm{d}\Gamma \\ & +\frac{1}{2}\int_{\Gamma_C^2}\frac{\boldsymbol{\sigma}_t^2(\mathbf{u}^2)}{\gamma^2}\cdot\big(\theta\boldsymbol{\sigma}_t^2(\mathbf{v}^2) - \gamma^2(\mathbf{v}_t^2 - \mathbf{v}_t^1\circ\Pi^2)\big)\mathrm{d}\Gamma \\ & = L(\mathbf{v}). \end{aligned} \tag{3.9}$$

Let us define:

$$\begin{aligned} P_{n,\gamma^i}^i(\mathbf{u}) &= \sigma_n^i(\mathbf{u}^i) - \gamma^i([\![u]\!]_n^i - g_n^i), & \mathbf{P}_{t,\gamma^i}^i(\mathbf{u}) &= \boldsymbol{\sigma}_t^i(\mathbf{u}^i) - \gamma^i[\![\mathbf{u}]\!]_t^i, \\ P_{n,\theta\gamma^i}^i(\mathbf{v}) &= \theta\sigma_n^i(\mathbf{v}^i) - \gamma^i[\![v]\!]_n^i, & \mathbf{P}_{t,\theta\gamma^i}^i(\mathbf{v}) &= \theta\boldsymbol{\sigma}_t^i(\mathbf{v}^i) - \gamma^i[\![\mathbf{v}]\!]_t^i \end{aligned} \tag{3.10}$$

and

$$\begin{aligned} A_\theta(\mathbf{u},\mathbf{v}) &= a(\mathbf{u},\mathbf{v}) - \frac{1}{2}\int_{\Gamma_C^1}\frac{\theta}{\gamma^1}\sigma_n^1(\mathbf{u}^1)\sigma_n^1(\mathbf{v}^1)\mathrm{d}\Gamma - \frac{1}{2}\int_{\Gamma_C^2}\frac{\theta}{\gamma^2}\sigma_n^2(\mathbf{u}^2)\sigma_n^2(\mathbf{v}^2)\mathrm{d}\Gamma \\ &\quad -\frac{1}{2}\int_{\Gamma_C^1}\frac{\theta}{\gamma^1}\boldsymbol{\sigma}_t^1(\mathbf{u}^1)\cdot\boldsymbol{\sigma}_t^1(\mathbf{v}^1)\mathrm{d}\Gamma - \frac{1}{2}\int_{\Gamma_C^2}\frac{\theta}{\gamma^2}\boldsymbol{\sigma}_t^2(\mathbf{u}^2)\cdot\boldsymbol{\sigma}_t^2(\mathbf{v}^2)\mathrm{d}\Gamma \\ &= \mathbf{a}(\mathbf{u},\mathbf{v}) - \sum_{i=1}^{2}\frac{1}{2}\Big(\int_{\Gamma_C^i}\frac{\theta}{\gamma^i}\underline{\underline{\boldsymbol{\sigma}}}^i(\mathbf{u}^i)\mathbf{n}\cdot\underline{\underline{\boldsymbol{\sigma}}}^i(\mathbf{v}^i)\mathbf{n}\,\mathrm{d}\Gamma\Big). \end{aligned}$$

Now we insert the expressions (3.5) of $\sigma_n^i(\mathbf{u}^i)$ and (3.6) of $\boldsymbol{\sigma}_t^i(\mathbf{u}^i)$ in (3.9) and the variational problem could be formally written as follows:

$$\left\{\begin{array}{l} \text{Find a sufficiently regular } \mathbf{u}\in\mathbf{V} \text{ such that for all sufficiently regular } \mathbf{v}\in\mathbf{V},\\ \\ A_\theta(\mathbf{u},\mathbf{v})+\frac{1}{2}\displaystyle\int_{\Gamma_C^1}\frac{1}{\gamma^1}[P^1_{n,\gamma^1}(\mathbf{u})]_{\mathbb{R}^-}P^1_{n,\theta\gamma^1}(\mathbf{v})\mathrm{d}\Gamma+\frac{1}{2}\int_{\Gamma_C^2}\frac{1}{\gamma^2}[P^2_{n,\gamma^2}(\mathbf{u})]_{\mathbb{R}^-}P^2_{n,\theta\gamma^2}(\mathbf{v})\mathrm{d}\Gamma\\ +\frac{1}{2}\displaystyle\int_{\Gamma_C^1}\frac{1}{\gamma^1}[\mathbf{P}^1_{t,\gamma^1}(\mathbf{u})]_{s^1}\cdot\mathbf{P}^1_{t,\theta\gamma^1}(\mathbf{v})\mathrm{d}\Gamma+\frac{1}{2}\int_{\Gamma_C^2}\frac{1}{\gamma^2}[\mathbf{P}^2_{t,\gamma^2}(\mathbf{u})]_{s^2}\cdot\mathbf{P}^2_{t,\theta\gamma^2}(\mathbf{v})\mathrm{d}\Gamma=L(\mathbf{v}). \end{array}\right. \tag{3.11}$$

Remark 3.1.4. *In the frictionless contact case the formulation reads:*

$$\left\{\begin{array}{l} \textit{Find a sufficiently regular } \mathbf{u}\in\mathbf{V} \textit{ such that for all sufficiently regular } \mathbf{v}\in\mathbf{V}\\ \\ A_\theta(\mathbf{u},\mathbf{v})+\frac{1}{2}\displaystyle\int_{\Gamma_C^1}\frac{1}{\gamma^1}[P^1_{n,\gamma^1}(\mathbf{u})]_{\mathbb{R}^-}P^1_{n,\theta\gamma^1}(\mathbf{v})\mathrm{d}\Gamma+\frac{1}{2}\int_{\Gamma_C^2}\frac{1}{\gamma^2}[P^2_{n,\gamma^2}(\mathbf{u})]_{\mathbb{R}^-}P^2_{n,\theta\gamma^2}(\mathbf{v})\mathrm{d}\Gamma=L(\mathbf{v}). \end{array}\right.$$

.

3.1.3 Derivation of the method from a potential

In this section we show, through a formal demonstration, that the method derives from a potential in the frictional symmetric ($\theta=1$) case. Let us define the potential:

$$J(\mathbf{u})=\boldsymbol{\varepsilon}_\Omega(\mathbf{u})+\sum_{i=1}^{2}(\boldsymbol{\varepsilon}_n^i(\mathbf{u})+\boldsymbol{\varepsilon}_t^i(\mathbf{u})),$$

with:

$$\begin{array}{rcl} \boldsymbol{\varepsilon}_\Omega(\mathbf{u}) &=& \frac{1}{2}a(\mathbf{u},\mathbf{u})-\displaystyle\sum_{i=1}^{2}\Big(\frac{1}{4}\int_{\Gamma_C^i}\frac{(\sigma_n^i(\mathbf{u}^i))^2}{\gamma^i}+\frac{1}{4}\int_{\Gamma_C^i}\frac{\|\boldsymbol{\sigma}_t^i(\mathbf{u}^i)\|^2}{\gamma^i}\mathrm{d}\Gamma\Big)-L(\mathbf{u})\\ &=& \frac{1}{2}A_1(\mathbf{u},\mathbf{u})-L(\mathbf{u}),\\ \boldsymbol{\varepsilon}_n^i(\mathbf{u}) &=& \frac{1}{4}\displaystyle\int_{\Gamma_C^i}\frac{1}{\gamma^i}[P^i_{n,\gamma^i}(\mathbf{u})]^2_{\mathbb{R}^-}\mathrm{d}\Gamma,\\ \boldsymbol{\varepsilon}_t^i(\mathbf{u}) &=& \frac{1}{4}\displaystyle\int_{\Gamma_C^i}\frac{1}{\gamma^i}\|\mathbf{P}^i_{t,\gamma^i}(\mathbf{u})\|^2\mathrm{d}\Gamma-\frac{1}{4}\int_{\Gamma_C^i}\frac{1}{\gamma^i}\|\mathbf{P}^i_{t,\gamma^i}(\mathbf{u})-[\mathbf{P}^i_{t,\gamma^i}(\mathbf{u})]_{s^i}\|^2\mathrm{d}\Gamma. \end{array}$$

We compute now the derivative of this potential. We have:

$$\mathcal{D}\boldsymbol{\varepsilon}_\Omega(\mathbf{u})[\mathbf{v}] \quad = A_1(\mathbf{u},\mathbf{v})-L(\mathbf{v}) \quad (L \text{ is linear and } A_\theta \text{ is bilinear}),$$

$$\begin{aligned}\mathcal{D}\boldsymbol{\varepsilon}_n^i(\mathbf{u})[\mathbf{v}] &= \frac{1}{2}\int_{\Gamma_C^i}\frac{1}{\gamma^i}[P_{n,\gamma^i}^i(\mathbf{u})]_{\mathbb{R}^-}\mathcal{D}\big([P_{n,\gamma^i}^i(\mathbf{u})]_{\mathbb{R}^-}\big)[\mathbf{v}]\mathrm{d}\Gamma \\ &= \frac{1}{2}\int_{\Gamma_C^i}\frac{1}{\gamma^i}[P_{n,\gamma^i}^i(\mathbf{u})]_{\mathbb{R}^-}H\big(-P_{n,\gamma^i}^i(\mathbf{u})\big)\big(\mathcal{D}\big(P_{n,\gamma^i}^i(\mathbf{u})\big)[\mathbf{v}]\mathrm{d}\Gamma,\end{aligned}$$

where H is the Heaviside step function. Using the equalities: $H(-x)[x]_{\mathbb{R}^-} = [x]_{\mathbb{R}^-}$, for any $x \in \mathbb{R}$, and $\mathcal{D}[A(\mathbf{u})]_{\mathbb{R}^-}[\mathbf{v}] = H(-A(\mathbf{u}))\mathcal{D}A(\mathbf{u})[\mathbf{v}]$, for any application $A : \mathbf{u} \mapsto A(\mathbf{u}) \in \mathbb{R}$, and since $\mathcal{D}\big(P_{n,\gamma^i}^i(\mathbf{u})\big)[\mathbf{v}] = P_{n,\gamma^i}^i(\mathbf{v})$ (P_{n,γ^i}^i is affine), we get:

$$\mathcal{D}\boldsymbol{\varepsilon}_n^i(\mathbf{u})[\mathbf{v}] = \frac{1}{2}\int_{\Gamma_C^i}\frac{1}{\gamma^i}[P_{n,\gamma^i}^i(\mathbf{u})]_{\mathbb{R}^-}P_{n,\gamma^i}^i(\mathbf{v})\mathrm{d}\Gamma.$$

For the tangential term, we have:

$$\begin{aligned}\mathcal{D}\boldsymbol{\varepsilon}_t^i(\mathbf{u})[\mathbf{v}] &= \frac{1}{2}\int_{\Gamma_C^i}\frac{1}{\gamma^i}\mathbf{P}_{t,\gamma^i}^i(\mathbf{u})\cdot\mathbf{P}_{t,\gamma^i}^i(\mathbf{v})\mathrm{d}\Gamma \\ &\quad -\frac{1}{2}\int_{\Gamma_C^i}\frac{1}{\gamma^i}(\mathbf{P}_{t,\gamma^i}^i(\mathbf{u}) - [\mathbf{P}_{t,\gamma^i}^i(\mathbf{u})]_{s^i})\cdot(\mathbf{P}_{t,\gamma^i}^i(\mathbf{v}) - D\big([\mathbf{P}_{t,\gamma^i}^i(\mathbf{u})]_{s^i}\big)[\mathbf{v}])\mathrm{d}\Gamma\end{aligned}$$

$$\begin{cases}\text{if } \|\mathbf{P}_{t,\gamma^i}^i(\mathbf{u})\| \le \gamma^i s^i, \text{then } \mathbf{P}_{t,\gamma^i}^i(\mathbf{u}) - [\mathbf{P}_{t,\gamma^i}^i(\mathbf{u})]_{s^i} = 0 \\ \\ \text{if } \|\mathbf{P}_{t,\gamma^i}^i(\mathbf{u})\| > \gamma^i s^i, \text{then } \mathcal{D}\big([\mathbf{P}_{t,\gamma^i}^i(\mathbf{u})]_{s^i}\big)[\mathbf{v}] \text{ is tangential to } \mathcal{B}(0,\gamma^i s^i) \text{ and} \\ \mathcal{D}\big([\mathbf{P}_{t,\gamma^i}^i(\mathbf{u})]_{s^i}\big)[\mathbf{v}]\cdot(\mathbf{P}_{t,\gamma^i}^i(\mathbf{u}) - [\mathbf{P}_{t,\gamma^i}^i(\mathbf{u})]_{s^i}) = 0.\end{cases}$$

So, in both cases we get:

$$\mathcal{D}\boldsymbol{\varepsilon}_t^i(\mathbf{u})[\mathbf{v}] = \frac{1}{2}\int_{\Gamma_C^i}\frac{1}{\gamma^i}[\mathbf{P}_{t,\gamma^i}^i(\mathbf{u})]_{s^i}\cdot\mathbf{P}_{t,\gamma^i}^i(\mathbf{v})\mathrm{d}\Gamma$$

so, if we consider the first order optimality condition $D\boldsymbol{\varepsilon}(\mathbf{u})[\mathbf{v}] = 0\ \forall\mathbf{v} \in \mathbf{V}$, we get:

$$A_1(\mathbf{u},\mathbf{v}) + \sum_{i=1}^{2}\Big(\frac{1}{2}\int_{\Gamma_C^i}\frac{1}{\gamma^i}[P_{n,\gamma^i}^i(\mathbf{u})]_{\mathbb{R}^-}P_{n,\gamma^i}^i(\mathbf{v})\mathrm{d}\Gamma + \frac{1}{2}\int_{\Gamma_C^i}\frac{1}{\gamma^i}[\mathbf{P}_{t,\gamma^i}^i(\mathbf{u})]_{s^i}\cdot\mathbf{P}_{t,\gamma^i}^i(\mathbf{v})\mathrm{d}\Gamma\Big) = L(\mathbf{v}).$$

This is exactly (3.11) when $\theta = 1$.

3.1.4 Strong-weak formulation equivalence

In this section, we are going to establish the formal equivalence between (3.11) and (2.26)-(3.3). Since the construction of (3.11) is quite elaborated and consists in particular in the splitting of the contact terms into two parts, this step is necessary to ensure the coherence of the formulation.

Theorem 3.1.5. *Let* $\mathbf{u} = (\mathbf{u}^1, \mathbf{u}^2)$ *be a sufficiently regular solution to the problem (3.11), then* $\mathbf{u}$ *solves the problem (2.26)-(3.3) for all* $\theta \in \mathbb{R}$.

Proof. Let $\mathbf{u} = (\mathbf{u}^1, \mathbf{u}^2)$ be a sufficiently regular solution to the problem (3.11). Using the definitions of $A_\theta, P^i_{\gamma^i}(\mathbf{u})$ and $P^i_{\theta\gamma^i}(\mathbf{v})$, we obtain:

$$
\begin{aligned}
&\mathbf{a}(\mathbf{u},\mathbf{v}) - \frac{1}{2}\int_{\Gamma_C^1}\frac{\theta}{\gamma^1}\sigma_n^1(\mathbf{u}^1)\sigma_n^1(\mathbf{v}^1)\mathrm{d}\Gamma - \frac{1}{2}\int_{\Gamma_C^2}\frac{\theta}{\gamma^2}\sigma_n^2(\mathbf{u}^2)\sigma_n^2(\mathbf{v}^2)\mathrm{d}\Gamma - \frac{1}{2}\int_{\Gamma_C^1}\frac{\theta}{\gamma^1}\boldsymbol{\sigma}_t^1(\mathbf{u}^1)\cdot\boldsymbol{\sigma}_t^1(\mathbf{v}^1)\mathrm{d}\Gamma\\
&-\frac{1}{2}\int_{\Gamma_C^2}\frac{\theta}{\gamma^2}\boldsymbol{\sigma}_t^2(\mathbf{u}^2)\cdot\boldsymbol{\sigma}_t^2(\mathbf{v}^2)\mathrm{d}\Gamma + \frac{1}{2}\int_{\Gamma_C^1}\frac{1}{\gamma^1}[\sigma_n^1(\mathbf{u}^1) - \gamma^1([\![u]\!]_n^1 - g_n^1)]_{\mathbb{R}^-}\big(\theta\sigma_n^1(\mathbf{v}^1) - \gamma^1(v_n^1 + v_n^2\circ\Pi^1)\big)\mathrm{d}\Gamma\\
&+\frac{1}{2}\int_{\Gamma_C^2}\frac{1}{\gamma^2}[\sigma_n^2(\mathbf{u}^2) - \gamma^2([\![u]\!]_n^2 - g_n^2)]_{\mathbb{R}^-}\big(\theta\sigma_n^2(\mathbf{v}^2) - \gamma^2(v_n^2 + v_n^1\circ\Pi^2)\big)\mathrm{d}\Gamma\\
&+\frac{1}{2}\int_{\Gamma_C^1}\frac{1}{\gamma^1}[\boldsymbol{\sigma}_t^1(\mathbf{u}^1) - \gamma^1[\![\mathbf{u}]\!]_t^1]_{s^1}\cdot\big(\theta\boldsymbol{\sigma}_t^1(\mathbf{v}^1) - \gamma^1(\mathbf{v}_t^1 - \mathbf{v}_t^2\circ\Pi^1)\big)\mathrm{d}\Gamma\\
&+\frac{1}{2}\int_{\Gamma_C^2}\frac{1}{\gamma^2}[\boldsymbol{\sigma}_t^2(\mathbf{u}^2) - \gamma^2[\![\mathbf{u}]\!]_t^2]_{s^2}\cdot\big(\theta\boldsymbol{\sigma}_t^2(\mathbf{v}^2) - \gamma^2(\mathbf{v}_t^2 - \mathbf{v}_t^1\circ\Pi^2)\big)\mathrm{d}\Gamma = L(\mathbf{v}).
\end{aligned}
$$

Using Green's formula we can write

$$
\begin{aligned}
\mathbf{a}(\mathbf{u},\mathbf{v}) \;&= -\int_{\Omega^1}\mathbf{div}\underline{\underline{\boldsymbol{\sigma}}}^1(\mathbf{u}^1)\cdot\mathbf{v}^1\mathrm{d}\Omega - \int_{\Omega^2}\mathbf{div}\underline{\underline{\boldsymbol{\sigma}}}^2(\mathbf{u}^2)\cdot\mathbf{v}^2\mathrm{d}\Omega\\
&\quad+\int_{\partial\Omega^1}\underline{\underline{\boldsymbol{\sigma}}}^1(\mathbf{u}^1)\mathbf{n}^1\cdot\mathbf{v}^1\mathrm{d}\Gamma + \int_{\partial\Omega^2}\underline{\underline{\boldsymbol{\sigma}}}^2(\mathbf{u}^2)\mathbf{n}^2\cdot\mathbf{v}^2\mathrm{d}\Gamma.
\end{aligned}
$$

If we take $\mathbf{v} = (\mathbf{v}^1, \mathbf{0})$ with $\mathbf{v}^1 = \mathbf{0}$ on $\partial\Omega^1$, we obtain:

$$
\int_{\Omega^1}\mathbf{div}\underline{\underline{\boldsymbol{\sigma}}}^1(\mathbf{u}^1)\cdot\mathbf{v}^1\mathrm{d}\Omega = \int_{\Omega^1}\mathbf{f}^1\cdot\mathbf{v}^1\mathrm{d}\Omega\ \forall\mathbf{v}^1,
$$

which yields (4.22) for i=1. In the same way we establish (4.22) for i=2.
To establish (4.16),(4.18) and (3.3), we consider a displacement field $\mathbf{v}$ that vanishes on the boundary except on the contact surfaces where $\mathbf{v} = (\mathbf{v}^1, \mathbf{v}^2)$. Then (3.11) and (4.22) gives

$$
\begin{aligned}
&\int_{\Gamma_C^1}\sigma_n^1(\mathbf{u}^1)v_n^1\mathrm{d}\Gamma + \int_{\Gamma_C^2}\sigma_n^2(\mathbf{u}^2)v_n^2\mathrm{d}\Gamma + \int_{\Gamma_C^1}\boldsymbol{\sigma}_t^1(\mathbf{u}^1)\cdot\mathbf{v}_t^1\mathrm{d}\Gamma + \int_{\Gamma_C^2}\boldsymbol{\sigma}_t^2(\mathbf{u}^2)\cdot\mathbf{v}_t^2\mathrm{d}\Gamma\\
&-\frac{1}{2}\int_{\Gamma_C^1}\frac{\theta}{\gamma^1}\sigma_n^1(\mathbf{u}^1)\sigma_n^1(\mathbf{v}^1)\mathrm{d}\Gamma - \frac{1}{2}\int_{\Gamma_C^2}\frac{\theta}{\gamma^2}\sigma_n^2(\mathbf{u}^2)\sigma_n^2(\mathbf{v}^2)\mathrm{d}\Gamma - \frac{1}{2}\int_{\Gamma_C^1}\frac{\theta}{\gamma^1}\boldsymbol{\sigma}_t^1(\mathbf{u}^1)\cdot\boldsymbol{\sigma}_t^1(\mathbf{v}^1)\mathrm{d}\Gamma\\
&-\frac{1}{2}\int_{\Gamma_C^2}\frac{\theta}{\gamma^2}\boldsymbol{\sigma}_t^2(\mathbf{u}^2)\cdot\boldsymbol{\sigma}_t^2(\mathbf{v}^2)\mathrm{d}\Gamma + \frac{1}{2}\int_{\Gamma_C^1}\frac{1}{\gamma^1}[\sigma_n^1(\mathbf{u}^1) - \gamma^1([\![u]\!]_n^1 - g_n^1)]_{\mathbb{R}^-}\big(\theta\sigma_n^1(\mathbf{v}^1)\\
&-\gamma^1(v_n^1 + v_n^2\circ\Pi^1)\big)\mathrm{d}\Gamma + \frac{1}{2}\int_{\Gamma_C^2}\frac{1}{\gamma^2}[\sigma_n^2(\mathbf{u}^2) - \gamma^2([\![u]\!]_n^2 - g_n^2)]_{\mathbb{R}^-}\big(\theta\sigma_n^2(\mathbf{v}^2) - \gamma^2(v_n^2 + v_n^1\circ\Pi^2)\big)\mathrm{d}\Gamma\\
&+\frac{1}{2}\int_{\Gamma_C^1}\frac{1}{\gamma^1}[\boldsymbol{\sigma}_t^1(\mathbf{u}^1) - \gamma^1[\![\mathbf{u}]\!]_t^1]_{s^1}\cdot\big(\theta\boldsymbol{\sigma}_t^1(\mathbf{v}^1) - \gamma^1(\mathbf{v}_t^1 - \mathbf{v}_t^2\circ\Pi^1)\big)\mathrm{d}\Gamma\\
&+\frac{1}{2}\int_{\Gamma_C^2}\frac{1}{\gamma^2}[\boldsymbol{\sigma}_t^2(\mathbf{u}^2) - \gamma^2[\![\mathbf{u}]\!]_t^2]_{s^2}\cdot\big(\theta\boldsymbol{\sigma}_t^2(\mathbf{v}^2) - \gamma^2(\mathbf{v}_t^2 - \mathbf{v}_t^1\circ\Pi^2)\big)\mathrm{d}\Gamma = 0.
\end{aligned}
\tag{3.12}
$$

We need to discuss two cases: $\theta \neq 0$ and $\theta = 0$.

Case 1 $\theta \neq 0$**:**
In (3.12), let us consider $\mathbf{v} = (\mathbf{v}^1, \mathbf{v}^2)$ such that:

$$\begin{cases} \mathbf{v}^1 = \mathbf{0} \text{ and } \boldsymbol{\sigma}_t^1(\mathbf{v}^1) = \mathbf{0} \ , \ \sigma_n^1(\mathbf{v}^1) \neq 0 & \text{on } \Gamma_C^1 \text{ and} \\ \mathbf{v}^2 = \mathbf{0} \text{ and } \boldsymbol{\sigma}^2(\mathbf{v}^2)\mathbf{n}^2 = \mathbf{0} & \text{on } \Gamma_C^2, \end{cases} \tag{3.13}$$

so,

$$\frac{\theta}{2}\int_{\Gamma_C^1}\Big([\sigma_n^1(\mathbf{u}^1) - \gamma^1([\![u]\!]_n^1 - g_n^1)]_{\mathbb{R}^-} - \sigma_n^1(\mathbf{u}^1)\Big)\frac{1}{\gamma^1}\sigma_n^1(\mathbf{v}^1)\mathrm{d}\Gamma = 0 \qquad \forall \mathbf{v} \text{ satisfying (3.13)}.$$

Then:

$$\sigma_n^1(\mathbf{u}^1) = [\sigma_n^1(\mathbf{u}^1) - \gamma^1([\![u]\!]_n^1 - g_n^1)]_{\mathbb{R}^-},$$

which implies (4.16) for $i = 1$. Arguing in the same way we obtain (4.16) for i =2 and the friction conditions (4.18).

Remark 3.1.6. *We can show that* $\mathbf{v}$ *satisfying (3.13) can be built by considering* $s(x)$ *the curvilinear coordinate system on the boundary* Γ_C *and* $d(x)$ *the signed distance to* Γ_C*. Then, for* $\mathbf{g}$ *a given vector field of* $\mathbb{R}^d$*,* $u(x) = B^{-1}(s(x))g(s(x))d(x)$ *satisfies* $u(x) = 0$ *and* $\boldsymbol{\sigma}(u)n = g$ *on* Γ_C*, with* $B_{il} = A_{ijkl}n_k n_j$*,* A *being the elasticity tensor.*

To obtain the second Newton law, we use Nitsche's writing of (4.16) in (3.12) with: $\mathbf{v}_t = 0$ and $\boldsymbol{\sigma}_t = 0$ and $v_n^2 = -v_n^1 \circ \Pi^2$:

$$\int_{\Gamma_C^1}\sigma_n^1(\mathbf{u}^1)v_n^1\mathrm{d}\Gamma - \int_{\Gamma_C^2}\sigma_n^2(\mathbf{u}^2)v_n^1 \circ \Pi^2\mathrm{d}\Gamma = 0 \qquad \forall v_n^1.$$

Then:

$$\int_{\Gamma_C^1}[\sigma_n^1(\mathbf{u}^1) - J^1\sigma_n^2(\mathbf{u}^2 \circ \Pi^1)]v_n^1\mathrm{d}\Gamma = 0 \qquad \forall v_n^1.$$

For $v_n^1 = v_n^2 = 0$ and $\mathbf{v}_t^2 = \mathbf{v}_t^1 \circ \Pi^2$ and using (4.18) in (3.12), we have similary

$$\int_{\Gamma_C^1}[\boldsymbol{\sigma}_t^1(\mathbf{u}^1) + J^1\boldsymbol{\sigma}_t^2(\mathbf{u}^2 \circ \Pi^1)] \cdot \mathbf{v}_t^1\mathrm{d}\Gamma = 0 \qquad \forall \mathbf{v}_t^1,$$

and we have (3.3).

Case 2 $\theta = 0$**:**
Let us take $\mathbf{v}_t^1 = \mathbf{v}_t^2 = \mathbf{0}$ and $v_n^2 = -v_n^1 \circ \Pi^2$, $v_n^1 = -v_n^2 \circ \Pi^1$, then (3.12) reads:

$$\int_{\Gamma_C^1}[\sigma_n^1(\mathbf{u}^1) - J^1\sigma_n^2(\mathbf{u}^2 \circ \Pi^1)]v_n^1\mathrm{d}\Gamma = 0 \qquad \forall v_n^1.$$

Let us take,now $v_n^1 = v_n^2 = 0$ and $\mathbf{v}_t^2 = \mathbf{v}_t^1 \circ \Pi^2$, $\mathbf{v}_t^1 = \mathbf{v}_t^2 \circ \Pi^1$, then (3.12) reads:

$$\int_{\Gamma_C^1}[\boldsymbol{\sigma}_t^1(\mathbf{u}^1) + J^1\boldsymbol{\sigma}_t^2(\mathbf{u}^2 \circ \Pi^1)] \cdot \mathbf{v}_t^1\mathrm{d}\Gamma = 0 \qquad \forall \mathbf{v}_t^1,$$

and we have (3.3).

Let $\mathbf{v}^2 = 0$ on Γ_C^2. Taking $\mathbf{v}_t^1 = 0$, we get:

$$\int_{\Gamma_C^1} \Big[\sigma_n^1(\mathbf{u}^1) - \frac{1}{2}[\sigma_n^1(\mathbf{u}^1) - \gamma^1([\![u]\!]_n^1 - g_n^1)]_{\mathbb{R}^-} - J^1\frac{1}{2}[\sigma_n^2(\mathbf{u}^2 \circ \Pi^1) - \gamma^2([\![u]\!]_n^2 \circ \Pi^1 - g_n^2 \circ \Pi^1)]_{\mathbb{R}^-}\Big] v_n^1 \mathrm{d}\Gamma = 0$$

$$, \forall v_n^1.$$

Then, noting the Remark3.1.1:

$$\sigma_n^1(\mathbf{u}^1) = \frac{1}{2}\Big([\sigma_n^1(\mathbf{u}^1) - \gamma^1([\![u]\!]_n^1 - g_n^1)]_{\mathbb{R}^-} + J^1[\sigma_n^2(\mathbf{u}^2 \circ \Pi^1) - \gamma^2([\![u]\!]_n^1 - g_n^1)]_{\mathbb{R}^-}\Big).$$

Since $J^1 > 0$, $\sigma_n^1(\mathbf{u}^1) \leq 0$ and so we obtain (4.16b). The second Newton law (3.3) yields:

$$\sigma_n^1(\mathbf{u}^1) = \frac{1}{2}\Big([\sigma_n^1(\mathbf{u}^1) - \gamma^1([\![u]\!]_n^1 - g_n^1)]_{\mathbb{R}^-} + [\sigma_n^1(\mathbf{u}^1) - J^1\gamma^2([\![u]\!]_n^1 - g_n^1)]_{\mathbb{R}^-}\Big). \tag{3.14}$$

We discuss both cases:
If $\sigma_n^1(\mathbf{u}^1) = 0$:

$$(\gamma^1 + J^1\gamma^2)[-([\![u]\!]_n^1 - g_n^1)]_{\mathbb{R}^-} = 0 \text{ then } [\![u]\!]_n^1 \leq g_n^1.$$

If $\sigma_n^1(\mathbf{u}^1) < 0$:

$$\sigma_n^1(\mathbf{u}^1) - \gamma^1([\![u]\!]_n^1 - g_n^1) < 0 \qquad \text{or} \qquad \sigma_n^1(\mathbf{u}^1) - J^1\gamma^2([\![u]\!]_n^1 - g_n^1) < 0 \qquad \text{or both .}$$

1. If we suppose first that: $\sigma_n^1(\mathbf{u}^1) - \gamma^1([\![u]\!]_n^1 - g_n^1) < 0$ and $\sigma_n^1(\mathbf{u}^1) - J^1\gamma^2([\![u]\!]_n^1 - g_n^1) < 0$, the equation (3.14) holds :

$$\sigma_n^1(\mathbf{u}^1) = \frac{1}{2}\Big(2\sigma_n^1(\mathbf{u}^1) - (\gamma^1 + J^1\gamma^2)([\![u]\!]_n^1 - g_n^1)\Big) \qquad \text{then} \qquad [\![\mathbf{u}]\!]_n^1 = g_n^1.$$

2. If now there only holds $\sigma_n^1(\mathbf{u}^1) - \gamma^1([\![u]\!]_n^1 - g_n^1) < 0$ and $\sigma_n^1(\mathbf{u}^1) - J^1\gamma^2([\![u]\!]_n^1 - g_n^1) > 0$, we can write (3.14):

$$\begin{aligned} \sigma_n^1(\mathbf{u}^1) &= \frac{1}{2}\sigma_n^1(\mathbf{u}^1) - \frac{\gamma^1}{2}([\![u]\!]_n^1 - g_n^1). \\ \text{So } \sigma_n^1(\mathbf{u}^1) &= -\gamma^1([\![u]\!]_n^1 - g_n^1). \end{aligned}$$

Then, since $\sigma_n(\mathbf{u}^1) < 0$: $[\![u]\!]_n^1 > g_n^1$. But in this case,

$$\sigma_n^1(\mathbf{u}^1) - J^1\gamma^2([\![u]\!]_n^1 - g_n^1) < 0,$$

and this contradicts the assumption $\sigma_n^1(\mathbf{u}^1) - J^1\gamma^2([\![u]\!]_n^1 - g_n^1) > 0$. So, this case is absurd. In a similar way we get contradiction for the case $\sigma_n^1(\mathbf{u}^1) - J^1\gamma^2([\![u]\!]_n^1 - g_n^1) < 0$.

To conclude, we establish that: if $\sigma_n^1(\mathbf{u}^1) = 0$, $[\![u]\!]_n^1 \leq g_n^1$ and if $\sigma_n^1(\mathbf{u}^1) < 0$, $[\![u]\!]_n^1 = g_n^1$; and this is equivalent to (4.16a) and (4.16c).

We suppose, now, that $v_n^1 = 0$ and $\mathbf{v}^2 = \mathbf{0}$. We get:

$$\int_{\Gamma_C^1}\Big[\boldsymbol{\sigma}_t^1(\mathbf{u}^1)-\frac{1}{2}[\boldsymbol{\sigma}_t^1(\mathbf{u}^1)-\gamma^1[\![\mathbf{u}]\!]_t^1]_{s^1}+\frac{J^1}{2}[\boldsymbol{\sigma}_t^2(\mathbf{u}^2\circ\Pi^1)-\gamma^2[\![\mathbf{u}]\!]_t^2\circ\Pi^1]_{s^2}\Big]\cdot\mathbf{v}_t^1\mathrm{d}\Gamma=0\ \forall\mathbf{v}_t^1.$$

Then, using the property: $\forall\gamma>0$, $[x]_{\gamma s}=\gamma\big[\frac{x}{\gamma}\big]_s$ and the condition (3.4) , it yields:

$$\boldsymbol{\sigma}_t^1(\mathbf{u}^1)-\frac{1}{2}\Big[\boldsymbol{\sigma}_t^1(\mathbf{u}^1)-\gamma^1[\![\mathbf{u}]\!]_t^1\Big]_{s^1}+\frac{1}{2}\Big[J^1\boldsymbol{\sigma}_t^2(\mathbf{u}^2\circ\Pi^1)-J^1\gamma^2[\![\mathbf{u}]\!]_t^2\circ\Pi^1\Big]_{s^1}=0.$$

We use the Newton law (3.3) and the Remark3.1.1 to obtain:

$$\boldsymbol{\sigma}_t^1(\mathbf{u}^1)-\frac{1}{2}\Big[\boldsymbol{\sigma}_t^1(\mathbf{u}^1)-\gamma^1[\![\mathbf{u}]\!]_t^1\Big]_{s^1}-\frac{1}{2}\Big[\boldsymbol{\sigma}_t^1(\mathbf{u}^1)-J^1\gamma^2[\![\mathbf{u}]\!]_t^1\Big]_{s^1}=0.$$

1. If $\|\boldsymbol{\sigma}_t^1(\mathbf{u}^1)-\gamma^1[\![\mathbf{u}]\!]_t^1\|<s^1$ and $\|\boldsymbol{\sigma}_t^1(\mathbf{u}^1)-J^1\gamma^2[\![\mathbf{u}]\!]_t^1\|<s^1$:
   $\frac{[\![\mathbf{u}]\!]_t^1}{2}(\gamma^1+J^1\gamma^2)=0$; so $[\![\mathbf{u}]\!]_t^1=0$. In this case we obtain: $\boldsymbol{\sigma}_t^1(\mathbf{u}^1)=\Big[\boldsymbol{\sigma}_t^1(\mathbf{u}^1)\Big]_{s^1}$,
   and so: $\|\boldsymbol{\sigma}_t^1(\mathbf{u}^1)\|<s^1$.

2. If $\|\boldsymbol{\sigma}_t^1(\mathbf{u}^1)-\gamma^1[\![\mathbf{u}]\!]_t^1\|\geq s^1$ and $\|\boldsymbol{\sigma}_t^1(\mathbf{u}^1)-J^1\gamma^2[\![\mathbf{u}]\!]_t^1\|\geq s^1$:

$$\boldsymbol{\sigma}_t^1(\mathbf{u}^1)-\frac{s^1}{2}\frac{\boldsymbol{\sigma}_t^1(\mathbf{u}^1)-\gamma^1[\![\mathbf{u}]\!]_t^1}{\|\boldsymbol{\sigma}_t^1(\mathbf{u}^1)-\gamma^1[\![\mathbf{u}]\!]_t^1\|}-\frac{s^1}{2}\frac{\boldsymbol{\sigma}_t^1(\mathbf{u}^1)-J^1\gamma^2[\![\mathbf{u}]\!]_t^1}{\|\boldsymbol{\sigma}_t^1(\mathbf{u}^1)-J^1\gamma^2[\![\mathbf{u}]\!]_t^1\|}=0. \tag{3.15}$$

   The equation (3.15) shows that $\boldsymbol{\sigma}_t^1(\mathbf{u}^1)$ and $[\![\mathbf{u}]\!]_t^1$ are collinear.

   So: $\begin{cases}\dfrac{\boldsymbol{\sigma}_t^1(\mathbf{u}^1)-\gamma^1[\![\mathbf{u}]\!]_t^1}{\|\boldsymbol{\sigma}_t^1(\mathbf{u}^1)-\gamma^1[\![\mathbf{u}]\!]_t^1\|}=\dfrac{\boldsymbol{\sigma}_t^1(\mathbf{u}^1)-J^1\gamma^2[\![\mathbf{u}]\!]_t^1}{\|\boldsymbol{\sigma}_t^1(\mathbf{u}^1)-J^1\gamma^2[\![\mathbf{u}]\!]_t^1\|},\\ \text{or}\\ \dfrac{\boldsymbol{\sigma}_t^1(\mathbf{u}^1)-\gamma^1[\![\mathbf{u}]\!]_t^1}{\|\boldsymbol{\sigma}_t^1(\mathbf{u}^1)-\gamma^1[\![\mathbf{u}]\!]_t^1\|}=-\dfrac{\boldsymbol{\sigma}_t^1(\mathbf{u}^1)-J^1\gamma^2[\![\mathbf{u}]\!]_t^1}{\|\boldsymbol{\sigma}_t^1(\mathbf{u}^1)-J^1\gamma^2[\![\mathbf{u}]\!]_t^1\|}(*),\end{cases}$

   and we obtain, from (3.15) : $\begin{cases}\boldsymbol{\sigma}_t^1(\mathbf{u}^1)=-s^1\frac{\boldsymbol{\sigma}_t^1(\mathbf{u}^1)-\gamma^1[\![\mathbf{u}]\!]_t^1}{\|\boldsymbol{\sigma}_t^1(\mathbf{u}^1)-\gamma^1[\![\mathbf{u}]\!]_t^1\|}=-\frac{1}{\gamma^1}[\boldsymbol{\sigma}_t^1(\mathbf{u}^1)-\gamma^1[\![\mathbf{u}]\!]_t^1]_{s^1},\\ \quad\text{and, according to (3.6) ,this is equivalent to (3.2).}\\ \text{or}\\ \boldsymbol{\sigma}_t^1(\mathbf{u}^1)=0\text{ which means }[\![\mathbf{u}]\!]_t^1=0\text{ in }(*).\end{cases}$

3. If now $\|\boldsymbol{\sigma}_t^1(\mathbf{u}^1)-\gamma^1[\![\mathbf{u}]\!]_t^1\|<s^1$ and $\|\boldsymbol{\sigma}_t^1(\mathbf{u}^1)-J^1\gamma^2[\![\mathbf{u}]\!]_t^1\|\geq s^1$:

$$\boldsymbol{\sigma}_t^1(\mathbf{u}^1)+\gamma^1[\![\mathbf{u}]\!]_t^1-s^1\frac{\boldsymbol{\sigma}_t^1(\mathbf{u}^1)-J^1\gamma^2[\![\mathbf{u}]\!]_t^1}{\|\boldsymbol{\sigma}_t^1(\mathbf{u}^1)-J^1\gamma^2[\![\mathbf{u}]\!]_t^1\|}=0.$$

   Projecting on $\frac{\boldsymbol{\sigma}_t^1(\mathbf{u}^1)}{\|\boldsymbol{\sigma}_t^1(\mathbf{u}^1)\|}$ and setting $a=\|\boldsymbol{\sigma}_t^1(\mathbf{u}^1)\|$; $b=\dfrac{\gamma^1\boldsymbol{\sigma}_t^1(\mathbf{u}^1)\cdot[\![\mathbf{u}]\!]_t^1}{\|\boldsymbol{\sigma}_t^1(\mathbf{u}^1)\|}$,

we get:

$$\begin{cases} & |a-b| < s^1 \text{ and } |a - bJ^1\frac{\gamma^2}{\gamma^1}| \geq s^1 \\ \text{and} & \\ & a+b-\epsilon s^1 = 0 \text{ ; where } \epsilon = \text{sign}(a - bJ^1\frac{\gamma^2}{\gamma^1}) = \pm 1. \end{cases}$$

Let $\epsilon = -1$; so, $a = -b - s^1$ and we obtain:

$$\begin{cases} & b - a = 2b + s^1 \text{ and } |b-a| < s^1 \\ \text{and} & \\ & a - bJ^1\frac{\gamma^2}{\gamma^1} = -(J^1\frac{\gamma^2}{\gamma^1}+1)b - s^1 \text{ and } a - bJ^1\frac{\gamma^2}{\gamma^1} \leq -s^1. \end{cases}$$

So:

$$\begin{cases} & -s^1 < b < 0 \\ \text{and} & \\ & (J^1\frac{\gamma^2}{\gamma^1}+1)b \geq 0 \end{cases}$$

which is absurd.

Let $\epsilon = 1$; so $a = -b + s^1$ and we obtain:

$$\begin{cases} & b - a = 2b - s^1 \text{ and } |b-a| < s^1 \\ \text{and} & \\ & a - bJ^1\frac{\gamma^2}{\gamma^1} = -(J^1\frac{\gamma^2}{\gamma^1}+1)b + s^1 \text{ and } a - bJ^1\frac{\gamma^2}{\gamma^1} \geq s^1, \end{cases}$$

so:

$$\begin{cases} & 0 < b < s^1 \\ \text{and} & \\ & (J^1\frac{\gamma^2}{\gamma^1}+1)b \leq 0, \end{cases}$$

which is absurd.

4. If $\|\boldsymbol{\sigma}_t^1(\mathbf{u}^1) - \gamma^1[\![\mathbf{u}]\!]_t^1\| \geq s^1$ and $\|\boldsymbol{\sigma}_t^1(\mathbf{u}^1) - J^1\gamma^2[\![\mathbf{u}]\!]_t^1\| < s^1$:
   We argue in the same way laying $a = \|\boldsymbol{\sigma}_t^1(\mathbf{u}^1)\|$; $b = J^1\dfrac{\gamma^2\boldsymbol{\sigma}_t^1(\mathbf{u}^1)\cdot[\![\mathbf{u}]\!]_t^1}{\|\boldsymbol{\sigma}_t^1(\mathbf{u}^1)\|}$.

Thus, we establish the friction condition (4.18) for i=1. In the same way, when supposing $\mathbf{v}^1 = 0$, we get (4.16a)-(4.16b)-(4.16c) and (4.18) for i=2. □

3.1.5 Discretization of the variational formulation

Let $(\mathcal{T}_h^i)_{h>0}$ be a family of triangulations of the domain Ω^i supposed regular and conformal to the subdivisions of the boundaries into Γ_D^i, Γ_N^i and Γ_C^i. We introduce

$$\mathbf{V}_h = (\mathbf{V}_h^1 \times \mathbf{V}_h^2), \text{ with } \mathbf{V}_h^i = \left\{ \mathbf{v}_h^i \in \mathscr{C}^0(\overline{\Omega^i}) : \mathbf{v}_{h|T}^i \in (\mathbb{P}_k(T))^d, \forall T \in \mathcal{T}_h^i, \mathbf{v}_h^i = \mathbf{0} \text{ on } \Gamma_D^i \right\},$$

the family of finite dimensional vector spaces indexed by h and coming from $\mathcal{T}_h^i$.
We consider in what follows that γ^i is a positive piecewise constant function on the contact interface Γ_C^i which satisfies

$$\gamma^i_{|K^i \cap \Gamma_C^i} = \frac{\gamma_0}{h_{K^i}},$$

for every $K^i \in \mathcal{T}_h^i$ that has a non-empty intersection of dimension $d-1$ with Γ_C^i, and where γ_0 is a positive given constant. Note that the value of γ^i on element intersections has no influence. This allows to define a discrete counterpart of (3.11). Let us use, for this purpose, the same notations for the linear operators as given by 3.10.

Then the unbiased formulation of the two bodies contact in the discrete setting reads:

$$\left\{ \begin{array}{l} \text{Find } \mathbf{u}_h \in \mathbf{V}_h \text{ such that, for all } \mathbf{v}_h \in \mathbf{V}_h, \\ \\ A_\theta(\mathbf{u}_h, \mathbf{v}_h) + \dfrac{1}{2}\displaystyle\int_{\Gamma_C^1} \frac{1}{\gamma^1} P^1_{n,\theta\gamma^1}(\mathbf{v}_h)[P^1_{n,\gamma^1}(\mathbf{u}_h)]_{\mathbb{R}^-} \mathrm{d}\Gamma + \frac{1}{2}\displaystyle\int_{\Gamma_C^2} \frac{1}{\gamma^2} P^2_{n,\theta\gamma^2}(\mathbf{v}_h)[P^2_{n,\gamma^2}(\mathbf{u}_h)]_{\mathbb{R}^-} \mathrm{d}\Gamma \\ + \dfrac{1}{2}\displaystyle\int_{\Gamma_C^1} \frac{1}{\gamma^1} \mathbf{P}^1_{t,\theta\gamma^1}(\mathbf{v}_h) \cdot [\mathbf{P}^1_{t,\gamma^1}(\mathbf{u}_h)]_{s^1} \mathrm{d}\Gamma + \frac{1}{2}\displaystyle\int_{\Gamma_C^2} \frac{1}{\gamma^2} \mathbf{P}^2_{t,\theta\gamma^2}(\mathbf{v}_h) \cdot [\mathbf{P}^2_{t,\gamma^2}(\mathbf{u}_h)]_{s^2} \mathrm{d}\Gamma = L(\mathbf{v}_h). \end{array} \right. \tag{3.16}$$

Remark 3.1.7. *Note that Nitsche's method is not a standard penalty method, since it is consistent. In fact the Nitsche's method is closer to Barbosa & Hughes stabilization (see [Ste95] and [CH13, Section 2.3]), so the Nitsche parameter γ_0 is in fact a stabilization parameter. As a result, making γ_0 high does not increase necessarily precision, conversely to standard penalty (see as well Figures 3.16 and 3.17 in section 3.3.5 for a numerical illustration here). The parameter γ_0 must therefore be just larger than a threshold value ensuring the coercivity so that the problem is well posed (and not too large not to cause ill-conditioning). This threshold value depends on the variant (θ).*

3.2 Mathematical analysis of the method

A major difference between Nitsche's method and standard penalty methods is the consistency demonstrated in 3.2.1. Using the same arguments as in [CH13] we prove the well-posedness and the optimal convergence of (3.16) when the mesh size h vanishes. To insure well-posedness and convergence of the method we need to impose γ_0 to be sufficiently large when $\theta \neq -1$. This condition is avoided when $\theta = -1$ which is a major

advantage of this version.

3.2.1 Consistency

Similarly to Nitsche's method for unilateral contact problems [CH13], our Nitsche-based formulation (3.16) is consistent:

Lemma 3.2.1. *Suppose that the solution* $\mathbf{u}$ *of (2.26)-(3.3) lies in* $(H^{\frac{3}{2}+\nu}(\Omega^1))^d \times (H^{\frac{3}{2}+\nu}(\Omega^2))^d$ *with* $\nu > 0$*, then* $\mathbf{u}$ *is also solution to:*

$$\begin{aligned}
&A_\theta(\mathbf{u},\mathbf{v}_h) + \frac{1}{2}\int_{\Gamma_C^1} \frac{1}{\gamma^1} P^1_{n,\theta\gamma^1}(\mathbf{v}_h)[P^1_{n,\gamma^1}(\mathbf{u})]_{\mathbb{R}^-}\mathrm{d}\Gamma + \frac{1}{2}\int_{\Gamma_C^2} \frac{1}{\gamma^2} P^2_{n,\theta\gamma^2}(\mathbf{v}_h)[P^2_{n,\gamma^2}(\mathbf{u})]_{\mathbb{R}^-}\mathrm{d}\Gamma \\
&+ \frac{1}{2}\int_{\Gamma_C^1} \frac{1}{\gamma^1} \mathbf{P}^1_{t,\theta\gamma^1}(\mathbf{v}_h)\cdot[\mathbf{P}^1_{t,\gamma^1}(\mathbf{u})]_{s^1}\mathrm{d}\Gamma + \frac{1}{2}\int_{\Gamma_C^2} \frac{1}{\gamma^2} \mathbf{P}^2_{t,\theta\gamma^2}(\mathbf{v}_h)\cdot[\mathbf{P}^2_{t,\gamma^2}(\mathbf{u})]_{s^2}\mathrm{d}\Gamma \\
&= L(\mathbf{v}_h), \quad \forall \mathbf{v}_h \in \mathbf{V}_h.
\end{aligned} \tag{3.17}$$

Proof. Let $\mathbf{u}$ be a solution of (2.26)–(3.3) and set $\mathbf{v}_h \in \mathbf{V}_h$. Since $\mathbf{u}^i \in (H^{\frac{3}{2}+\nu}(\Omega^i))^d$, we have $\sigma_n^i(\mathbf{u}^i) \in (H^\nu(\Gamma_C^i))^d$ and $P_{n\gamma^i}$ and $\mathbf{P}_{t\gamma^i}$ are well-defined and belong to $L^2(\Gamma_C^i)$.

With equations (2.26)–(3.2) and integration by parts, it holds:

$$\mathbf{a}(\mathbf{u},\mathbf{v}_h) - \int_{\Gamma_C^1}\sigma_n^1(\mathbf{u}^1)v_{hn}^1\mathrm{d}\Gamma - \int_{\Gamma_C^2}\sigma_n^2(\mathbf{u}^2)v_{hn}^2\mathrm{d}\Gamma - \int_{\Gamma_C^1}\boldsymbol{\sigma}_t^1(\mathbf{u}^1)\cdot\mathbf{v}_{ht}^1\mathrm{d}\Gamma - \int_{\Gamma_C^2}\boldsymbol{\sigma}_t^2(\mathbf{u}^2)\cdot\mathbf{v}_{ht}^2\mathrm{d}\Gamma = L(\mathbf{v}_h).$$

We use now (3.3) to write:

$$\begin{aligned}
&\mathbf{a}(\mathbf{u},\mathbf{v}) - \frac{1}{2}\int_{\Gamma_C^1}\sigma_n^1(\mathbf{u}^1)(v_{hn}^1 + v_{hn}^2\circ\Pi^1)\mathrm{d}\Gamma - \frac{1}{2}\int_{\Gamma_C^2}\sigma_n^2(\mathbf{u}^2)(v_{hn}^2 + v_{hn}^1\circ\Pi^2)\mathrm{d}\Gamma \\
&- \frac{1}{2}\int_{\Gamma_C^1}\boldsymbol{\sigma}_t^1(\mathbf{u}^1)\cdot(\mathbf{v}_{ht}^1 - \mathbf{v}_{ht}^2\circ\Pi^1)\mathrm{d}\Gamma - \frac{1}{2}\int_{\Gamma_C^2}\boldsymbol{\sigma}_t^2(\mathbf{u}^2)\cdot(\mathbf{v}_{ht}^2 - \mathbf{v}_{ht}^1\circ\Pi^2)\mathrm{d}\Gamma = L(\mathbf{v}_h).
\end{aligned}$$

For any $\theta \in \mathbb{R}$, we can write:

$$\begin{aligned}
&\begin{cases} v_{hn}^1 + v_{hn}^2\circ\Pi^1 = -\dfrac{1}{\gamma^1}\big(\theta\sigma_n^1(\mathbf{v}_h^1) - \gamma^1(v_{hn}^1 + v_{hn}^2\circ\Pi^1)\big) + \dfrac{\theta}{\gamma^1}\sigma_n^1(\mathbf{v}_h^1) \\ v_{hn}^2 + v_{hn}^1\circ\Pi^2 = -\dfrac{1}{\gamma^2}\big(\theta\sigma_n^2(\mathbf{v}_h^2) - \gamma^2(v_{hn}^2 + v_{hn}^1\circ\Pi^2)\big) + \dfrac{\theta}{\gamma^2}\sigma_n^2(\mathbf{v}_h^2) \end{cases} \\
&\begin{cases} \mathbf{v}_{th}^1 - \mathbf{v}_{th}^2\circ\Pi^1 = -\dfrac{1}{\gamma^1}\big(\theta\boldsymbol{\sigma}_t^1(\mathbf{v}_h^1) - \gamma^1(\mathbf{v}_{th}^1 - \mathbf{v}_{th}^2\circ\Pi^1)\big) + \dfrac{\theta}{\gamma^1}\boldsymbol{\sigma}_t^1(\mathbf{v}_h^1) \\ \mathbf{v}_{th}^2 - \mathbf{v}_{th}^1\circ\Pi^2 = -\dfrac{1}{\gamma^2}\big(\theta\boldsymbol{\sigma}_t^2(\mathbf{v}_h^2) - \gamma^2(\mathbf{v}_{th}^2 - \mathbf{v}_{th}^1\circ\Pi^2)\big) + \dfrac{\theta}{\gamma^2}\boldsymbol{\sigma}_t^2(\mathbf{v}_h^2), \end{cases}
\end{aligned} \tag{3.18}$$

Using (3.18), formulations (3.5) and (3.6) of the contact and friction conditions and the notations (3.10), we obtain (3.17). □

Remark 3.2.2. *The regularity assumption that we made in Lemma 3.2.1 is standard for Signorini contact. It was proved for an elliptic scalar problem in [MK92] and noted*

numerically for linear elasticity. In fact the singularities that appear with contact-non-contact transitions allow us, generally, to expect a Sobolev regularity between $3/2$ *and* $5/2$.

3.2.2 Well-posedness

To prove well-posedness of our formulation, we first need the following discrete trace inequality.

Lemma 3.2.3. *There exists* $C > 0$, *independent of the parameter* γ_0 *and of the mesh size* h, *such that:*

$$\|(\gamma^i)^{-\frac{1}{2}}\boldsymbol{\sigma}_t^i(\mathbf{v}_h^i)\|_{0,\Gamma_c^i}^2 + \|(\gamma^i)^{-\frac{1}{2}}\sigma_n^i(\mathbf{v}_h^i)\|_{0,\Gamma_c^i}^2 \leq \frac{C}{\gamma_0}\|\mathbf{v}_h^i\|_{1,\Omega^i}^2 , \tag{3.19}$$

for all $\mathbf{v}_h^i \in \mathbf{V}_h^i$.

Proof. The inequality (3.19) is obtained using a scaling argument as in [Cho14, Lemma 3.2] . □

We then show in Theorem 3.2.4 that the problem (3.16) is well-posed using an argument from [Bre68] for M-type and pseudo-monotone operators. In the proof of the well-posedness, two cases are discused: $\theta = 1$ and $\theta \neq 1$.

Theorem 3.2.4. *Suppose that* $\gamma_0 > 0$ *is sufficiently large or* $\theta = -1$, *then Problem (3.16) admits one unique solution* $\mathbf{u}_h$ *in* $\mathbf{V}_h$. *When* $\theta = -1$ *we do not need the assumption of largeness of* γ_0.

Proof. Using the Riesz representation theorem, we define a (non-linear) operator $\mathbf{B} : \mathbf{V}_h \to \mathbf{V}_h$, by means of the formula:

$$\begin{aligned}(\mathbf{B}\mathbf{u}_h, \mathbf{v}_h)_1 = A_\theta(\mathbf{u}_h, \mathbf{v}_h) + \sum_{i=1}^{2}\Big(&\frac{1}{2}\int_{\Gamma_C^i}\frac{1}{\gamma^i}P_{n,\theta\gamma^i}^i(\mathbf{v}_h)[P_{n,\gamma^i}^i(\mathbf{u}_h)]_{\mathbb{R}^-}\mathrm{d}\Gamma \\ &+ \frac{1}{2}\int_{\Gamma_C^i}\frac{1}{\gamma^i}\mathbf{P}_{t,\theta\gamma^i}^i(\mathbf{v}_h)\cdot[\mathbf{P}_{t,\gamma^i}^i(\mathbf{u}_h)]_{s^i}\mathrm{d}\Gamma\Big),\end{aligned}$$

for all $\mathbf{u}_h, \mathbf{v}_h \in \mathbf{V}_h$, and where $(.,.)_1$ stands for the scalar product in $\mathbf{V}$and the notations P_{n,γ^i}^i, $\mathbf{P}_{t,\gamma^i}^i$, $P_{n,\theta\gamma^i}^i$ and $\mathbf{P}_{t,\theta\gamma^i}^i$ are given by (3.10).
Note that Problem (3.16) is well-posed if and only if $\mathbf{B}$ is a one-to-one operator. Let $\mathbf{v}_h, \mathbf{w}_h \in \mathbf{V}_h$, using the writings $P_{n,\theta\gamma^i}^i(\cdot) = P_{n,\gamma^i}^i(\cdot) + \gamma^i g_n^i + (1-\theta)\sigma_n^i(\cdot)$ and $\mathbf{P}_{t,\theta\gamma^i}^i(\cdot) =$

$\mathbf{P}^i_{t,\gamma^i}(\cdot) + (1-\theta)\boldsymbol{\sigma}^i_t(\cdot)$, we have:

$$
\begin{aligned}
&(\mathbf{B}\mathbf{v}_h - \mathbf{B}\mathbf{w}_h, \mathbf{v}_h - \mathbf{w}_h)_1 = \mathbf{a}(\mathbf{v}_h - \mathbf{w}_h, \mathbf{v}_h - \mathbf{w}_h)\\
&+\sum_{i=1}^{2}\Big(-\frac{\theta}{2}\|(\gamma^i)^{-\frac{1}{2}}\boldsymbol{\sigma}(\mathbf{v}^i_h - \mathbf{w}^i_h)\mathbf{n}\|^2_{0,\Gamma^i_C}\\
&+\frac{1}{2}\int_{\Gamma^i_C}\frac{1}{\gamma^i}P^i_{n,\gamma^i}(\mathbf{v}_h - \mathbf{w}_h)\big([P^i_{n,\gamma^i}(\mathbf{v}_h)]_{\mathbb{R}^-} - [P^i_{n,\gamma^i}(\mathbf{w}_h)]_{\mathbb{R}^-}\big)\mathrm{d}\Gamma\\
&+\frac{(1-\theta)}{2}\int_{\Gamma^i_C}\frac{1}{\gamma^i}\sigma^i_n(\mathbf{v}^i_h - \mathbf{w}^i_h)\big([P^i_{n,\gamma^i}(\mathbf{v}_h)]_{\mathbb{R}^-} - [P^i_{n,\gamma^i}(\mathbf{w}_h)]_{\mathbb{R}^-}\big)\mathrm{d}\Gamma\\
&+\frac{1}{2}\int_{\Gamma^i_C}\frac{1}{\gamma^i}\mathbf{P}^i_{t,\gamma^i}(\mathbf{v}_h - \mathbf{w}_h).\big([\mathbf{P}^i_{t,\gamma^i}(\mathbf{v}_h)]_{s^i} - [\mathbf{P}^i_{t,\gamma^i}(\mathbf{w}_h)]_{s^i}\big)\mathrm{d}\Gamma\\
&+\frac{(1-\theta)}{2}\int_{\Gamma^i_C}\frac{1}{\gamma^i}\boldsymbol{\sigma}^i_t(\mathbf{v}^i_h - \mathbf{w}^i_h).\big([\mathbf{P}^i_{t,\gamma^i}(\mathbf{v}^i_h)]_{s^i} - [\mathbf{P}^i_{t,\gamma^i}(\mathbf{w}_h)]_{s^i}\big)\mathrm{d}\Gamma\Big).
\end{aligned}
$$

We use Cauchy-Schwarz inequality and the proprieties (3.7) and (3.8) to get:

$$
\begin{aligned}
&(\mathbf{B}\mathbf{v}_h - \mathbf{B}\mathbf{w}_h, \mathbf{v}_h - \mathbf{w}_h)_1 \geq \mathbf{a}(\mathbf{v}_h - \mathbf{w}_h, \mathbf{v}_h - \mathbf{w}_h) + \sum_{i=1}^{2}\Big(-\frac{\theta}{2}\|(\gamma^i)^{-\frac{1}{2}}\boldsymbol{\sigma}(\mathbf{v}^i_h - \mathbf{w}^i_h)\mathbf{n}\|^2_{0,\Gamma^i_C}\\
&+\frac{1}{2}\|(\gamma^i)^{-\frac{1}{2}}\big([P^i_{n,\gamma^i}(\mathbf{v}_h)]_{\mathbb{R}^-} - [P^i_{n,\gamma^i}(\mathbf{w}_h)]_{\mathbb{R}^-}\big)\|^2_{0,\Gamma^i_C} + \frac{1}{2}\|(\gamma^i)^{-\frac{1}{2}}\big([\mathbf{P}^i_{t,\gamma^i}(\mathbf{v}_h)]_{s^i} - [\mathbf{P}^i_{t,\gamma^i}(\mathbf{w}_h)]_{s^i}\big)\|^2_{0,\Gamma^i_C}\\
&-\frac{|1-\theta|}{2}\|(\gamma^i)^{-\frac{1}{2}}\big([P^i_{n,\gamma^i}(\mathbf{v}_h)]_{\mathbb{R}^-} - [P^i_{n,\gamma^i}(\mathbf{w}_h)]_{\mathbb{R}^-}\big)\|_{0,\Gamma^i_C}\|(\gamma^i)^{-\frac{1}{2}}\sigma^i_n(\mathbf{v}^i_h - \mathbf{w}^i_h)\|_{0,\Gamma^i_C}\\
&-\frac{|1-\theta|}{2}\|(\gamma^i)^{-\frac{1}{2}}\big([\mathbf{P}^i_{t,\gamma^i}(\mathbf{v}_h)]_{s^i} - [\mathbf{P}^i_{t,\gamma^i}(\mathbf{w}_h)]_{s^i}\big)\|_{0,\Gamma^i_C}\|(\gamma^i)^{-\frac{1}{2}}\boldsymbol{\sigma}^i_t(\mathbf{v}^i_h - \mathbf{w}^i_h)\|_{0,\Gamma^i_C}\Big).
\end{aligned}
$$

If $\theta = 1$, we use the coercivity of $a(\cdot,\cdot)$ and the property (3.19) to get:

$$
\begin{aligned}
&(\mathbf{B}\mathbf{v}_h - \mathbf{B}\mathbf{w}_h, \mathbf{v}_h - \mathbf{w}_h)_1 \geq \mathbf{a}(\mathbf{v}_h - \mathbf{w}_h, \mathbf{v}_h - \mathbf{w}_h) - \sum_{i=1}^{2}\frac{1}{2}\|(\gamma^i)^{-\frac{1}{2}}\boldsymbol{\sigma}^i(\mathbf{v}^i_h - \mathbf{w}^i_h)\mathbf{n}^i\|^2_{0,\Gamma^i_C}\\
&\geq \mathbf{a}(\mathbf{v}_h - \mathbf{w}_h, \mathbf{v}_h - \mathbf{w}_h) - \sum_{i=1}^{2}\frac{1}{2}\Big(\|(\gamma^i)^{-\frac{1}{2}}\sigma^i_n(\mathbf{v}^i_h - \mathbf{w}^i_h)\|^2_{0,\Gamma^i_C} + \|(\gamma^i)^{-\frac{1}{2}}\boldsymbol{\sigma}^i_t(\mathbf{v}^i_h - \mathbf{w}^i_h)\|^2_{0,\Gamma^i_C}\Big)\\
&\geq C\|\mathbf{v}_h - \mathbf{w}_h\|^2_1
\end{aligned}
$$

when γ_0 is sufficiently large.

We suppose now that $\theta \neq 1$; let $\beta > 0$. Applying Young inequality yields:

$$
\begin{aligned}
&(\mathbf{B}\mathbf{v}_h - \mathbf{B}\mathbf{w}_h, \mathbf{v}_h - \mathbf{w}_h)_1 \geq \mathbf{a}(\mathbf{v}_h - \mathbf{w}_h, \mathbf{v}_h - \mathbf{w}_h) + \sum_{i=1}^{2} \Big(- \frac{\theta}{2} \|(\gamma^i)^{-\frac{1}{2}} \boldsymbol{\sigma}^i(\mathbf{v}_h^i - \mathbf{w}_h^i)\mathbf{n}^i\|^2_{0,\Gamma_C^i} \\
&+\frac{1}{2}\|(\gamma^i)^{-\frac{1}{2}} \big([P^i_{n,\gamma^i}(\mathbf{v}_h)]_{\mathbb{R}^-} - [P^i_{n,\gamma^i}(\mathbf{w}_h)]_{\mathbb{R}^-}\big)\|^2_{0,\Gamma_C^i} + \frac{1}{2}\|(\gamma^i)^{-\frac{1}{2}} \big([\mathbf{P}^i_{t,\gamma^i}(\mathbf{v}_h)]_{s^i} - [\mathbf{P}^i_{t,\gamma^i}(\mathbf{w}_h)]_{\gamma^i s^i}\big)\|^2_{0,\Gamma_C^i} \\
&-\frac{|1-\theta|}{4\beta}\|(\gamma^i)^{-\frac{1}{2}} \big([P^i_{n,\gamma^i}(\mathbf{v}_h)]_{\mathbb{R}^-} - [P^i_{n,\gamma^i}(\mathbf{w}_h)]_{\mathbb{R}^-}\big)\|^2_{0,\Gamma_C^i} - \frac{|1-\theta|\beta}{4}\|(\gamma^i)^{-\frac{1}{2}} \sigma^i_n(\mathbf{v}_h^i - \mathbf{w}_h^i)\|^2_{0,\Gamma_C^i} \\
&-\frac{|1-\theta|}{4\beta}\|(\gamma^i)^{-\frac{1}{2}} \big(\mathbf{P}^i_{t,\gamma^i}(\mathbf{v}_h)]_{s^i} - [\mathbf{P}^i_{t,\gamma}(\mathbf{w}_h)]_{s^i}\big)\|^2_{0,\Gamma_C^i} - \frac{|1-\theta|\beta}{4}\|(\gamma^i)^{-\frac{1}{2}} \boldsymbol{\sigma}^i_t(\mathbf{v}_h^i - \mathbf{w}_h^i)\|^2_{0,\Gamma_C^i}\Big) \\
&= \mathbf{a}(\mathbf{v}_h - \mathbf{w}_h, \mathbf{v}_h - \mathbf{w}_h) + \sum_{i=1}^{2} \Big(- \frac{1}{2}\Big(\theta + \frac{|1-\theta|\beta}{2}\Big)\Big(\|(\gamma^i)^{-\frac{1}{2}} \sigma^i_n(\mathbf{v}_h^i - \mathbf{w}_h^i)\|^2_{0,\Gamma_C^i} \\
&+\|(\gamma^i)^{-\frac{1}{2}} \boldsymbol{\sigma}^i_t(\mathbf{v}_h^i - \mathbf{w}_h^i)\|^2_{0,\Gamma_C^i}\Big) + \frac{1}{2}\Big(1 - \frac{|1-\theta|}{2\beta}\Big)\Big(\|(\gamma^i)^{-\frac{1}{2}} \big([P^i_{n,\gamma^i}(\mathbf{v}_h)]_{\mathbb{R}^-} - [P^i_{n,\gamma^i}(\mathbf{w}_h)]_{\mathbb{R}^-}\big)\|^2_{0,\Gamma_C^i} \\
&+\|(\gamma^i)^{-\frac{1}{2}} \big([\mathbf{P}^i_{t,\gamma^i}(\mathbf{v}_h)]_{s^i} - [\mathbf{P}^i_{t,\gamma^i}(\mathbf{w}_h)]_{s^i}\big)\|^2_{0,\Gamma_C^i}\Big)\Big).
\end{aligned}
$$

Choosing $\beta = \dfrac{|1-\theta|}{2}$ and γ_0 sufficiently large we get:

$$
\begin{aligned}
(\mathbf{B}\mathbf{v}_h - \mathbf{B}\mathbf{w}_h, \mathbf{v}_h - \mathbf{w}_h)_1 &\geq \mathbf{a}(\mathbf{v}_h - \mathbf{w}_h, \mathbf{v}_h - \mathbf{w}_h) \\
&\quad - \frac{(1+\theta)^2}{8} \sum_{i=1}^{2} \Big(\|(\gamma^i)^{-\frac{1}{2}} \sigma^i_n(\mathbf{v}_h^i - \mathbf{w}_h^i)\|^2_{0,\Gamma_C^i} \\
&\quad + \|(\gamma^i)^{-\frac{1}{2}} \boldsymbol{\sigma}^i_t(\mathbf{v}_h^i - \mathbf{w}_h^i)\|^2_{0,\Gamma_C^i}\Big). \\
(\mathbf{B}\mathbf{v}_h - \mathbf{B}\mathbf{w}_h, \mathbf{v}_h - \mathbf{w}_h)_1 &\geq C\|\mathbf{v} - \mathbf{w}\|_1^2
\end{aligned}
$$

Note that, when $\theta = -1$ we do not need the assumption of largeness of γ_0.

Let us show, now, that $\mathbf{B}$ is hemicontinuous. Since $\mathbf{V}^h$ is a vector space, it is sufficient to show that:

$$
\begin{aligned}
\phi : \quad [0,1] &\to \mathbb{R} \\
t &\mapsto (\mathbf{B}(\mathbf{v}_h - t\mathbf{w}_h), \mathbf{w}_h)_1
\end{aligned}
$$

is a continuous real function for all $\mathbf{v}_h, \mathbf{w}_h \in \mathbf{V}_h$. Let $t, s \in [0,1]$, we compute:

$$
\begin{aligned}
&|\phi(t)-\phi(s)| \\
&= \Big|(\mathbf{B}(\mathbf{v}_h - t\mathbf{w}_h) - \mathbf{B}(\mathbf{v}_h - s\mathbf{w}_h), \mathbf{w}_h)_1\Big| \\
&= \Big|A_\theta((s-t)\mathbf{w}_h, \mathbf{w}_h) + \sum_{i=1}^{2}\Big(\frac{1}{2}\int_{\Gamma_C^i}\frac{1}{\gamma^i}P^i_{n,\theta\gamma^i}(\mathbf{w}_h)\big([P^i_{n\gamma^i}(\mathbf{v}_h - t\mathbf{w}_h)]_{\mathbb{R}^-} - [P^i_{n\gamma^i}(\mathbf{v}_h - s\mathbf{w}_h)]_{\mathbb{R}^-}\big)\mathrm{d}\Gamma \\
&+ \frac{1}{2}\int_{\Gamma_C^i}\frac{1}{\gamma^i}\mathbf{P}^i_{t,\theta\gamma^i}(\mathbf{w}_h)\big([\mathbf{P}^i_{t\gamma^i}(\mathbf{v}_h - t\mathbf{w}_h)]_{s^i} - [\mathbf{P}^i_{t\gamma^i}(\mathbf{v}_h - s\mathbf{w}_h)]_{s^i}\big)\mathrm{d}\Gamma\Big)\Big| \\
&\leq |s-t|A_\theta(\mathbf{w}_h, \mathbf{w}_h) + \sum_{i=1}^{2}\Big(\frac{1}{2}\int_{\Gamma_C^i}\frac{1}{\gamma^i}|P^i_{n,\theta\gamma^i}(\mathbf{w}_h)|\Big|[P^i_{n\gamma^i}(\mathbf{v}_h - t\mathbf{w}_h)]_{\mathbb{R}^-} - [P^i_{n\gamma^i}(\mathbf{v}_h - s\mathbf{w}_h)]_{\mathbb{R}^-}\Big|\mathrm{d}\Gamma \\
&+ \frac{1}{2}\int_{\Gamma_C^i}\frac{1}{\gamma^i}\|\mathbf{P}^i_{t,\theta\gamma^i}(\mathbf{w}_h)\|\Big\|[\mathbf{P}^i_{t\gamma^i}(\mathbf{v}_h - t\mathbf{w}_h)]_{s^i} - [\mathbf{P}^i_{t\gamma^i}(\mathbf{v}_h - s\mathbf{w}_h)]_{s^i}\Big\|\mathrm{d}\Gamma\Big).
\end{aligned}
$$

We use the bounds $|[a]_{\mathbb{R}^-} - [b]_{\mathbb{R}^-}| \leq |a-b|$ for all $a, b \in \mathbb{R}$ and $\big\|[a]_{g^i} - [b]_{g^i}\big\| \leq \|a-b\|$ for all $a, b \in \mathbb{R}^{d-1}$ to deduce that:

$$
\begin{aligned}
&\int_{\Gamma_C^i}\frac{1}{\gamma^i}|P^i_{n,\theta\gamma^i}(\mathbf{w}_h)|\Big|[P^i_{n\gamma^i}(\mathbf{v}_h - t\mathbf{w}_h)]_{\mathbb{R}^-} - [P^i_{n\gamma^i}(\mathbf{v}_h - s\mathbf{w}_h)]_{\mathbb{R}^-}\Big|\mathrm{d}\Gamma \\
&\quad + \int_{\Gamma_C^i}\frac{1}{\gamma^i}\|\mathbf{P}^i_{t,\theta\gamma^i}(\mathbf{w}_h)\|\Big\|[\mathbf{P}^i_{t\gamma^i}(\mathbf{v}_h - t\mathbf{w}_h)]_{s^i} - [\mathbf{P}^i_{t\gamma^i}(\mathbf{v}_h - s\mathbf{w}_h)]_{s^i}\Big\|\mathrm{d}\Gamma \\
&\leq \int_{\Gamma_C^i}\frac{1}{\gamma^i}|P^i_{n,\theta\gamma^i}(\mathbf{w}_h)|\Big|P^i_{n\gamma^i}(\mathbf{v}_h - t\mathbf{w}_h) - P^i_{n\gamma^i}(\mathbf{v}_h - s\mathbf{w}_h)\Big|\mathrm{d}\Gamma \\
&\quad + \int_{\Gamma_C^i}\frac{1}{\gamma^i}\|\mathbf{P}^i_{t,\theta\gamma^i}(\mathbf{w}_h)\|\Big\|\mathbf{P}^i_{t\gamma^i}(\mathbf{v}_h - t\mathbf{w}_h) - \mathbf{P}^i_{t\gamma^i}(\mathbf{v}_h - s\mathbf{w}_h)\Big\|\mathrm{d}\Gamma \\
&\leq |s-t|\Big(\int_{\Gamma_C^i}\frac{1}{\gamma^i}|P^i_{n,\theta\gamma^i}(\mathbf{w}_h)||P^i_{n\gamma^i}(\mathbf{w}_h)|\mathrm{d}\Gamma + \int_{\Gamma_C^i}\frac{1}{\gamma^i}\|\mathbf{P}^i_{t,\theta\gamma^i}(\mathbf{w}_h)\|\|\mathbf{P}^i_{t\gamma^i}(\mathbf{w}_h)\|\mathrm{d}\Gamma\Big).
\end{aligned}
$$

It results that:

$$
\begin{aligned}
|\phi(t)-\phi(s)| \quad \leq \quad & |s-t|\Big(A_\theta(\mathbf{w}_h, \mathbf{w}_h) + \sum_{i=1}^{2}\Big(\int_{\Gamma_C^i}\frac{1}{2\gamma^i}|P^i_{n,\theta\gamma^i}(\mathbf{w}_h)||P^i_{n\gamma^i}(\mathbf{w}_h)|\mathrm{d}\Gamma \\
& + \int_{\Gamma_C^i}\frac{1}{2\gamma^i}\|\mathbf{P}^i_{t,\theta\gamma^i}(\mathbf{w}_h)\|\|\mathbf{P}^i_{t\gamma^i}(\mathbf{w}_h)\|\mathrm{d}\Gamma\Big)\Big).
\end{aligned}
$$

Which means that ϕ is Lipschitz, so that $\mathbf{B}$ is hemicontinuous. We finally apply the Corollary 15 (p.126) of [Bre68] to conclude that $\mathbf{B}$ is a one to one operator. □

3.2.3 A priori error analysis

Our Nitsche-based method (3.16) converges in a optimal way as the mesh parameter h vanishes. This is proved in the Theorem 3.2.6, where we provide an estimate of the

displacement error in H^1-norm and of the contact error in $L^2(\Gamma_C^i)$-norm. We establish, first, the following abstract error estimate.

Theorem 3.2.5. *Suppose that* $\mathbf{u}$ *is a solution to (2.26-3.3) and belongs to* $(H^{\frac{3}{2}+\nu}(\Omega^1))^d \times (H^{\frac{3}{2}+\nu}(\Omega^2))^d$ *with* $\nu > 0$.

1. We suppose γ_0 *sufficiently large. The solution* $\mathbf{u}_h$ *to the discrete problem (3.16) satisfies the following error estimate:*

$$\begin{aligned}
&\sum_{i=1}^{2}\Big(\|\mathbf{u}^i-\mathbf{u}_h^i\|_{1,\Omega^i}^2+\frac{1}{2}\|(\gamma^i)^{-\frac{1}{2}}\big(\sigma_n^i(\mathbf{u}^i)-[P_{n,\gamma}^i(\mathbf{u}_h)]_{\mathbb{R}^-}\big)\|_{0,\Gamma_C^i}^2\\
&+\frac{1}{2}\|(\gamma^i)^{-\frac{1}{2}}\big(\boldsymbol{\sigma}_t^i(\mathbf{u}^i)-[\mathbf{P}_{t,\gamma^i}^i(\mathbf{u}_h)]_{s^i}\big)\|_{0,\Gamma_C^i}^2\Big)\\
&\leq C\inf_{\mathbf{v}_h\in\mathbf{V}_h}\Big(\sum_{i=1}^{2}\|\mathbf{u}^i-\mathbf{v}_h^i\|_{1,\Omega^i}^2+\frac{1}{2}\|(\gamma^i)^{\frac{1}{2}}(\mathbf{u}^i-\mathbf{v}_h^i)\|_{0,\Gamma_C^i}^2+\frac{1}{2}\|(\gamma^i)^{-\frac{1}{2}}\underline{\underline{\boldsymbol{\sigma}}}(\mathbf{u}^i-\mathbf{v}_h^i)\mathbf{n}^i\|_{0,\Gamma_C^i}^2\Big),
\end{aligned}\tag{3.20}$$

where $C > 0$ *is a constant independent of* h, $\mathbf{u}$ *and* γ_0.

2. If $\theta = -1$, *for all* $\gamma_0 > 0$, *the solution* $\mathbf{u}_h$ *to the problem (3.16) satisfies the estimate (3.20) with* $C > 0$ *a constant independent of* h *and* $\mathbf{u}$, *but eventually dependent of* γ_0.

Proof. The proof of this theorem is inspired by [CHR15c, Theorem 3.6] for unilateral contact and [Cho14, Theorem 3.4] for the frictional case.

Let $\mathbf{v}_h \in \mathbf{V}_h$, using the coercivity and the continuity of the form $a(\cdot,\cdot)$ as well as Young's inequality, we obtain:

$$\begin{aligned}
\alpha\sum_{i=1}^{2}\|\mathbf{u}^i-\mathbf{u}_h^i\|_{1,\Omega^i}^2 &\leq a(\mathbf{u}-\mathbf{u}_h,\mathbf{u}-\mathbf{u}_h)\\
&= a(\mathbf{u}-\mathbf{u}_h,\mathbf{u}-\mathbf{v}_h)+a(\mathbf{u}-\mathbf{u}_h,\mathbf{v}_h-\mathbf{u}_h)\\
&\leq C\sum_{i=1}^{2}\|\mathbf{u}^i-\mathbf{u}_h^i\|_{1,\Omega^i}\|\mathbf{u}^i-\mathbf{v}_h^i\|_{1,\Omega^i}+a(\mathbf{u}-\mathbf{u}_h,\mathbf{v}_h-\mathbf{u}_h)\\
&\leq \frac{\alpha}{2}\sum_{i=1}^{2}\|\mathbf{u}^i-\mathbf{u}_h^i\|_{1,\Omega^i}^2+\frac{C^2}{2\alpha}\sum_{i=1}^{2}\|\mathbf{u}^i-\mathbf{v}_h^i\|_{1,\Omega^i}^2\\
&\quad +a(\mathbf{u},\mathbf{v}_h-\mathbf{u}_h)-a(\mathbf{u}_h,\mathbf{v}_h-\mathbf{u}_h).
\end{aligned}$$

Therefore, we get:

$$\frac{\alpha}{2}\sum_{i=1}^{2}\|\mathbf{u}^i-\mathbf{u}_h^i\|_{1,\Omega^i}^2\leq\frac{C^2}{2\alpha}\sum_{i=1}^{2}\|\mathbf{u}^i-\mathbf{v}_h^i\|_{1,\Omega^i}^2+a(\mathbf{u},\mathbf{v}_h-\mathbf{u}_h)-a(\mathbf{u}_h,\mathbf{v}_h-\mathbf{u}_h).$$

Since $\mathbf{u}$ solves (2.26-3.3) and $\mathbf{u}_h$ solves (3.16), using the Lemma 3.2.1 yields:

$$\begin{aligned}\frac{\alpha}{2}\sum_{i=1}^{2}\|\mathbf{u}^i-\mathbf{u}_h^i\|_{1,\Omega^i}^2 \;\leq\; & \frac{C^2}{2\alpha}\sum_{i=1}^{2}\|\mathbf{u}^i-\mathbf{v}_h^i\|_{1,\Omega^i}^2 \\ & +\sum_{i=1}^{2}\Big(-\frac{\theta}{2}\int_{\Gamma_C^i}\frac{1}{\gamma^i}\boldsymbol{\sigma}^i(\mathbf{u}_h^i-\mathbf{u}^i)\mathbf{n}^i\cdot\boldsymbol{\sigma}^i(\mathbf{v}_h^i-\mathbf{u}_h^i)\mathbf{n}^i\mathrm{d}\Gamma \\ & +\frac{1}{2}\int_{\Gamma_C^i}\frac{1}{\gamma^i}\mathbf{P}^i_{t,\theta\gamma^i}(\mathbf{v}_h-\mathbf{u}_h)\cdot\big([\mathbf{P}^i_{t,\gamma^i}(\mathbf{u}_h)]_{s^i}-[\mathbf{P}^i_{t,\gamma^i}(\mathbf{u})]_{s^i}\big)\mathrm{d}\Gamma \\ & +\frac{1}{2}\int_{\Gamma_C^i}\frac{1}{\gamma^i}P^i_{n,\theta\gamma^i}(\mathbf{v}_h-\mathbf{u}_h)\big([P^i_{n,\gamma^i}(\mathbf{u}_h)]_{\mathbb{R}^-}-[P^i_{n,\gamma^i}(\mathbf{u})]_{\mathbb{R}^-}\big)\mathrm{d}\Gamma\Big).\end{aligned} \tag{3.21}$$

Let $\beta_1>0$. The first integral term in (3.21) is bounded, using Cauchy-Schwarz and Young's inequalities, as follows:

$$\begin{aligned}&-\frac{\theta}{2}\int_{\Gamma_C^i}\frac{1}{\gamma^i}\boldsymbol{\sigma}^i(\mathbf{u}_h^i-\mathbf{u}^i)\mathbf{n}^i\cdot\boldsymbol{\sigma}^i(\mathbf{v}_h^i-\mathbf{u}_h^i)\mathbf{n}^i\mathrm{d}\Gamma \\ &=\frac{\theta}{2}\int_{\Gamma_C^i}\frac{1}{\gamma^i}\boldsymbol{\sigma}^i(\mathbf{v}_h^i-\mathbf{u}_h^i)\mathbf{n}^i\cdot\boldsymbol{\sigma}^i(\mathbf{v}_h^i-\mathbf{u}_h^i)\mathbf{n}^i\mathrm{d}\Gamma-\frac{\theta}{2}\int_{\Gamma_C^i}\frac{1}{\gamma^i}\boldsymbol{\sigma}^i(\mathbf{v}_h^i-\mathbf{u}^i)\mathbf{n}^i\cdot\boldsymbol{\sigma}^i(\mathbf{v}_h^i-\mathbf{u}_h^i)\mathbf{n}^i\mathrm{d}\Gamma \\ &\leq\frac{\theta}{2}\|(\gamma^i)^{-\frac{1}{2}}\boldsymbol{\sigma}^i(\mathbf{v}_h^i-\mathbf{u}_h^i)\mathbf{n}^i\|_{0,\Gamma_C^i}^2+\frac{|\theta|}{2}\|(\gamma^i)^{-\frac{1}{2}}\boldsymbol{\sigma}^i(\mathbf{v}_h^i-\mathbf{u}^i)\mathbf{n}^i\|_{0,\Gamma_C^i}\|(\gamma^i)^{-\frac{1}{2}}\boldsymbol{\sigma}^i(\mathbf{v}_h^i-\mathbf{u}_h^i)\mathbf{n}^i\|_{0,\Gamma_C^i} \\ &\leq\frac{\beta_1\theta^2}{4}\|(\gamma^i)^{-\frac{1}{2}}\boldsymbol{\sigma}^i(\mathbf{v}_h^i-\mathbf{u}^i)\mathbf{n}^i\|_{0,\Gamma_C^i}^2+\frac{1}{2}\big(\theta+\frac{1}{2\beta_1}\big)\|(\gamma^i)^{-\frac{1}{2}}\boldsymbol{\sigma}^i(\mathbf{v}_h^i-\mathbf{u}_h^i)\mathbf{n}^i\|_{0,\Gamma_C^i}^2.\end{aligned} \tag{3.22}$$

For the second integral term in (3.21), we can write:

$$\begin{aligned}&\int_{\Gamma_C^i}\frac{1}{\gamma^i}\mathbf{P}^i_{t,\theta\gamma^i}(\mathbf{v}_h-\mathbf{u}_h)\cdot\big([\mathbf{P}^i_{t,\gamma^i}(\mathbf{u}_h)]_{s^i}-[\mathbf{P}^i_{t,\gamma^i}(\mathbf{u})]_{s^i}\big)\mathrm{d}\Gamma \\ &=\int_{\Gamma_C^i}\frac{1}{\gamma^i}\mathbf{P}^i_{t,\gamma^i}(\mathbf{v}_h-\mathbf{u})\cdot\big([\mathbf{P}^i_{t,\gamma^i}(\mathbf{u}_h)]_{s^i}-[\mathbf{P}^i_{t,\gamma^i}(\mathbf{u})]_{s^i}\big)\mathrm{d}\Gamma \\ &+\int_{\Gamma_C^i}\frac{1}{\gamma^i}\mathbf{P}^i_{t,\gamma^i}(\mathbf{u}-\mathbf{u}_h)\cdot\big([\mathbf{P}^i_{t,\gamma^i}(\mathbf{u}_h)]_{s^i}-[\mathbf{P}^i_{t,\gamma^i}(\mathbf{u})]_{s^i}\big)\mathrm{d}\Gamma \\ &+\int_{\Gamma_C^i}(1-\theta)\boldsymbol{\sigma}_t^i(\mathbf{v}_h^i-\mathbf{u}_h^i)\cdot\big([\mathbf{P}^i_{t,\gamma^i}(\mathbf{u}_h)]_{s^i}-[\mathbf{P}^i_{t,\gamma^i}(\mathbf{u})]_{s^i}\big)\mathrm{d}\Gamma.\end{aligned}$$

Using the bound (3.8) and applying two times Cauchy-Schwarz and Young's inequalities,

we obtain for $\beta_2 > 0$ and $\beta_3 > 0$:

$$\begin{aligned}
&\int_{\Gamma_C^i} \frac{1}{\gamma^i} \mathbf{P}^i_{t,\theta\gamma^i}(\mathbf{v}_h - \mathbf{u}_h) \cdot \big([\mathbf{P}^i_{t,\gamma^i}(\mathbf{u}_h)]_{s^i} - [\mathbf{P}^i_{t,\gamma^i}(\mathbf{u})]_{s^i}\big) \mathrm{d}\Gamma \\
&\leq \frac{1}{2\beta_2} \Big\| (\gamma^i)^{-\frac{1}{2}} \Big(\boldsymbol{\sigma}^i_t(\mathbf{u}^i) - [\mathbf{P}^i_{t,\gamma^i}(\mathbf{u}_h)]_{s^i} \Big) \Big\|^2_{0,\Gamma_C^i} + \frac{\beta_2}{2} \| (\gamma^i)^{-\frac{1}{2}} [\mathbf{P}^i_{t,\gamma^i}(\mathbf{v}_h - \mathbf{u})]_{s^i} \|^2_{0,\Gamma_C^i} \\
&- \Big\| (\gamma^i)^{-\frac{1}{2}} \Big(\boldsymbol{\sigma}^i_t(\mathbf{u}^i) - [\mathbf{P}^i_{t,\gamma^i}(\mathbf{u}_h)]_{s^i} \Big) \Big\|^2_{0,\Gamma_C^i} + \frac{|1-\theta|}{2\beta_3} \Big\| (\gamma^i)^{-\frac{1}{2}} \Big(\boldsymbol{\sigma}^i_t(\mathbf{u}^i) - [\mathbf{P}^i_{t,\gamma^i}(\mathbf{u}_h)]_{s^i} \Big) \Big\|^2_{0,\Gamma_C^i} \\
&+ \frac{|1-\theta|\beta_3}{2} \| (\gamma^i)^{-\frac{1}{2}} \boldsymbol{\sigma}^i_t(\mathbf{v}^i_h - \mathbf{u}^i_h) \|^2_{0,\Gamma_C^i}.
\end{aligned} \tag{3.23}$$

In a similar way, we can upper bound the third integral term of (3.21).
Noting that:

$$\begin{aligned}
&\| (\gamma^i)^{-\frac{1}{2}} [\mathbf{P}^i_{t,\gamma^i}(\mathbf{v}_h - \mathbf{u})]_{s^i} \|^2_{0,\Gamma_C^i} + \| (\gamma^i)^{-\frac{1}{2}} [P^i_{n,\gamma^i}(\mathbf{v}_h - \mathbf{u})]_{\mathbb{R}^-} \|^2_{0,\Gamma_C^i} \\
&\leq 2 \| (\gamma^i)^{\frac{1}{2}} (\llbracket u - v_h \rrbracket^i_n + \llbracket \mathbf{u} - \mathbf{v}_h \rrbracket^i_t) \|^2_{0,\Gamma_C^i} + 2 \| (\gamma^i)^{-\frac{1}{2}} \boldsymbol{\sigma}^i(\mathbf{u}^i - \mathbf{v}^i_h) \mathbf{n}^i \|^2_{0,\Gamma_C^i} \\
&\leq 2 \sum_{i=1}^{2} \Big(\| (\gamma^i)^{\frac{1}{2}} (\mathbf{u}^i - \mathbf{v}^i_h) \|^2_{0,\Gamma_C^i} \Big) + 2 \| (\gamma^i)^{-\frac{1}{2}} \boldsymbol{\sigma}^i(\mathbf{u}^i - \mathbf{v}^i_h) \mathbf{n}^i \|^2_{0,\Gamma_C^i},
\end{aligned} \tag{3.24}$$

and using estimates (3.22) and (3.23) in (3.21), we obtain:

$$\begin{aligned}
&\frac{\alpha}{2} \sum_{i=1}^{2} \| \mathbf{u}^i - \mathbf{u}^i_h \|^2_{1,\Omega^i} \leq \frac{C^2}{2\alpha} \sum_{i=1}^{2} \| \mathbf{u}^i - \mathbf{v}^i_h \|^2_{1,\Omega^i} \\
&+ \frac{1}{2} \sum_{i=1}^{2} \Big((\frac{\beta_1 \theta^2}{2} + \beta_2) \| (\gamma^i)^{-\frac{1}{2}} \boldsymbol{\sigma}^i(\mathbf{u}^i - \mathbf{v}^i_h) \mathbf{n}^i \|^2_{0,\Gamma_C^i} + 2\beta_2 \| (\gamma^i)^{\frac{1}{2}} (\mathbf{u}^i - \mathbf{v}^i_h) \|^2_{0,\Gamma_C^i} \\
&+ \big(-1 + \frac{1}{2\beta_2} + \frac{|1-\theta|}{2\beta_3} \big) \big(\| (\gamma^i)^{-\frac{1}{2}} (\boldsymbol{\sigma}^i_t(\mathbf{u}^i) - \mathbf{P}^i_{t,\gamma^i}(\mathbf{u}_h))_{s^i}) \|^2_{0,\Gamma_C^i} + \\
&\| (\gamma^i)^{-\frac{1}{2}} (\sigma^i_n(\mathbf{u}^i) - [P^i_{n,\gamma^i}(\mathbf{u}_h)]_{\mathbb{R}^-}) \|^2_{0,\Gamma_C^i} \big) + \big(\frac{1}{2\beta_1} + \theta + \frac{|1-\theta|\beta_3}{2} \big) \| (\gamma^i)^{-\frac{1}{2}} \boldsymbol{\sigma}^i(\mathbf{v}^i_h - \mathbf{u}^i_h) \mathbf{n}^i \|^2_{0,\Gamma_C^i} \Big).
\end{aligned} \tag{3.25}$$

We use now the estimate (3.19) to get:

$$\| (\gamma^i)^{-\frac{1}{2}} \boldsymbol{\sigma}^i(\mathbf{v}^i_h - \mathbf{u}^i_h) \mathbf{n}^i \|^2_{0,\Gamma_C^i} \leq C \gamma_0^{-\frac{1}{2}} \| \mathbf{v}^i_h - \mathbf{u}^i_h \|^2_{1,\Omega^i} \leq C \gamma_0^{-\frac{1}{2}} (\| \mathbf{v}^i_h - \mathbf{u}^i \|^2_{1,\Omega^i} + \| \mathbf{u}^i_h - \mathbf{u}^i \|^2_{1,\Omega^i}) \tag{3.26}$$

For a fixed $\theta \in \mathbb{R}$ we choose β_2 and β_3 large enough that:

$$-1 + \frac{1}{2\beta_2} + \frac{|1-\theta|}{2\beta_3} < -\frac{1}{2}$$

Choosing γ_0 large enough in (3.26) and putting the estimate in (3.25), we establish the first statement of the theorem.

We consider now the case $\theta = -1$ in which (3.25) becomes:

$$\begin{aligned}
&\frac{\alpha}{2}\sum_{i=1}^{2}\|\mathbf{u}^i-\mathbf{u}_h^i\|_{1,\Omega^i}^2 \leq \frac{C^2}{2\alpha}\sum_{i=1}^{2}\|\mathbf{u}^i-\mathbf{v}_h^i\|_{1,\Omega^i}^2\\
&+\frac{1}{2}\sum_{i=1}^{2}\Big((\frac{\beta_1}{2}+\beta_2)\|(\gamma^i)^{-\frac{1}{2}}\boldsymbol{\sigma}^i(\mathbf{u}^i-\mathbf{v}_h^i)\mathbf{n}^i\|_{0,\Gamma_C^i}^2+2\beta_2\|(\gamma^i)^{\frac{1}{2}}(\mathbf{u}^i-\mathbf{v}_h^i)\|_{0,\Gamma_C^i}^2\\
&+\big(-1+\frac{1}{2\beta_2}+\frac{1}{\beta_3}\big)\big(\|(\gamma^i)^{-\frac{1}{2}}(\boldsymbol{\sigma}_t^i(\mathbf{u}^i)-[\mathbf{P}_{t,\gamma^i}^i(\mathbf{u}_h)]_{s^i})\|_{0,\Gamma_C^i}^2+\|(\gamma^i)^{-\frac{1}{2}}(\sigma_n^i(\mathbf{u}^i)-[P_{n,\gamma^i}^i(\mathbf{u}_h)]_{\mathbb{R}^-})\|_{0,\Gamma_C^i}^2\big)\\
&+\big(\frac{1}{2\beta_1}-1+\beta_3\big)\big(\|(\gamma^i)^{-\frac{1}{2}}\boldsymbol{\sigma}^i(\mathbf{v}_h^i-\mathbf{u}_h^i)\mathbf{n}^i\|_{0,\Gamma_C^i}^2\big)\Big).
\end{aligned}$$

Let be given $\eta>0$. Set $\beta_1=\frac{1}{2\eta}$, $\beta_2=1+\frac{1}{\eta}$, $\beta_3=1+\eta$. And so we arrive at:

$$\begin{aligned}
&\frac{\alpha}{2}\sum_{i=1}^{2}\|\mathbf{u}^i-\mathbf{u}_h^i\|_{1,\Omega^i}^2 \leq \frac{C^2}{2\alpha}\sum_{i=1}^{2}\|\mathbf{u}^i-\mathbf{v}_h^i\|_{1,\Omega^i}^2\\
&+\frac{1}{2}\sum_{i=1}^{2}\Big((\frac{5}{4\eta}+1)\|(\gamma^i)^{-\frac{1}{2}}\boldsymbol{\sigma}^i(\mathbf{u}^i-\mathbf{v}_h^i)\mathbf{n}^i\|_{0,\Gamma_C^i}^2+2\frac{1+\eta}{\eta}\|(\gamma^i)^{\frac{1}{2}}(\mathbf{u}^i-\mathbf{v}_h^i)\|_{0,\Gamma_C^i}^2\\
&-\frac{\eta}{2(1+\eta)}\big(\|(\gamma^i)^{-\frac{1}{2}}(\boldsymbol{\sigma}_t^i(\mathbf{u}^i)-[\mathbf{P}_{t,\gamma^i}^i(\mathbf{u}_h)]_{s^i})\|_{0,\Gamma_C^i}^2+\|(\gamma^i)^{-\frac{1}{2}}(\sigma_n^i(\mathbf{u}^i)-[P_{n,\gamma^i}^i(\mathbf{u}_h)]_{\mathbb{R}^-})\|_{0,\Gamma_C^i}^2\big)\\
&+2\eta\|(\gamma^i)^{-\frac{1}{2}}\underline{\underline{\boldsymbol{\sigma}}}^i(\mathbf{v}_h^i-\mathbf{u}_h^i)\mathbf{n}^i\|_{0,\Gamma_C^i}^2\Big)
\end{aligned}$$

Set $\eta=\dfrac{\alpha}{16C^2\gamma_0}$, where C is the constant in (3.26) to conclude the proof of the theorem. □

Theorem 3.2.6. *Suppose that* $\mathbf{u}=(\mathbf{u}^1,\mathbf{u}^2)$ *is a solution to problem (2.26-3.3) and belongs to* $(H^{\frac{3}{2}+\nu}(\Omega^1))^d\times(H^{\frac{3}{2}+\nu}(\Omega^2))^d$ *with* $0<\nu\leq\dfrac{1}{2}$ *if* $k=1$ *and* $0<\nu\leq 1$ *if* $k=2$ *(k is the degree of the finite element method). If* $\theta=-1$ *or* γ_0 *is sufficiently large, the solution* $\mathbf{u}_h$ *to the problem (3.16) satisfies the following estimate:*

$$\begin{aligned}
&\sum_{i=1}^{2}\Big(\|\mathbf{u}^i-\mathbf{u}_h^i\|_{1,\Omega^i}^2+\frac{1}{2}\|(\gamma^i)^{-\frac{1}{2}}\big(\sigma_n^i(\mathbf{u}^i)-[P_{n,\gamma^i}^i(\mathbf{u}_h)]_{\mathbb{R}^-}\big)\|_{0,\Gamma_C^i}^2\\
&+\frac{1}{2}\|(\gamma^i)^{-\frac{1}{2}}\big(\boldsymbol{\sigma}_t^i(\mathbf{u}^i)-[\mathbf{P}_{t,\gamma^i}^i(\mathbf{u}_h)]_{s^i}\big)\|_{0,\Gamma_C^i}^2\Big)\leq Ch^{1+2\nu}\sum_{i=1}^{2}\|\mathbf{u}^i\|_{\frac{3}{2}+\nu,\Omega^i}^2
\end{aligned}\tag{3.27}$$

where C is a constant independent of $\mathbf{u}$ *and* h.

Proof. To establish (3.27) we need to bound the right terms in estimate (3.20). We choose $\mathbf{v}_h^i=\mathcal{I}_h^i\mathbf{u}^i$ where $\mathcal{I}_h^i$ stands for the Lagrange interpolation operator mapping onto $\mathbf{V}_h^i$. The estimation of the Lagrange interpolation error in the H^1-norm on a domain is classical (see, e.g., [DS80], [BS07] and [EG04])

$$\|\mathbf{u}^i-\mathcal{I}_h^i\mathbf{u}^i\|_{1,\Omega^i}\leq Ch^{\frac{1}{2}+\nu}\|\mathbf{u}^i\|_{\frac{3}{2}+\nu,\Omega^i}\tag{3.28}$$

for $-\frac{1}{2} < \nu \leq k - \frac{1}{2}$.

Let E in Γ_C^i be an edge of triangle $K \in T_h^i$, we have:

$$\|(\gamma^i)^{\frac{1}{2}}(\mathbf{u}^i - \mathcal{I}_h^i \mathbf{u}^i)\|_{0,E} \leq Ch^{\frac{1}{2}+\nu}\|\mathbf{u}^i\|_{1+\nu,E}$$

A summation on all the edges E , with the trace theorem yields:

$$\|(\gamma^i)^{\frac{1}{2}}(\mathbf{u}^i - \mathcal{I}_h^i \mathbf{u}^i)\|_{0,\Gamma_C^i} \leq Ch^{\frac{1}{2}+\nu}\|\mathbf{u}^i\|_{1+\nu,\Gamma_C^i} \leq Ch^{\frac{1}{2}+\nu}\|\mathbf{u}^i\|_{\frac{3}{2}+\nu,\Omega^i} \tag{3.29}$$

From Appendix A of [CHR15c] (see also [FHW04]), we get the following estimate:

$$\|(\gamma^i)^{-\frac{1}{2}}\boldsymbol{\sigma}(\mathbf{u}^i - \mathcal{I}_h^i \mathbf{u}^i)\mathbf{n}^i\|_{0,\Gamma_C^i} \leq Ch^{\frac{1}{2}+\nu}\|\mathbf{u}^i\|_{\frac{3}{2}+\nu,\Omega^i} \tag{3.30}$$

By inserting (3.28), (3.29) and (3.30) onto (3.20) we get (3.27). □

3.3 Numerical experiments

In this section, we test the Nitsche unbiased method (3.16) for two/three-dimensional contact between two elastic bodies Ω^1 and Ω^2. The first body is a disk/sphere and the second is a rectangle/rectangular cuboid. This situation is not strictly a Hertz type contact problem because Ω^2 is bounded.

The tests are performed with P_1 and P_2 Lagrange finite elements. The finite element library Getfem++ is used. The discrete contact problem is solved by using a generalized Newton method. Further details on generalized Newton's method applied to contact problems can be found for instance in [Ren13] and the references therein. The accuracy of the method is discussed for the different cases with respect to the finite element used, the mesh size, and the value of the parameters θ and γ_0. We perform experiments with a frictionless contact to compare the results of the formulation with other ones using Nitsche's method (given mainly in [CHR15c,FPR16]). Moreover, we present the convergence curves for frictional contact in figures 3.11 and 3.12.

The numerical tests in two dimensions (resp. three dimensions) are performed on a domain $\Omega =]-0.5, 0.5[^2$ (resp. $\Omega =]-0.5, 0.5[^3$) containing the two bodies Ω^1 and Ω^2 . The first body is a disk of radius 0.25 and center (0,0) (resp. a sphere of radius 0.25 and center (0,0,0)), and the second is a rectangle $]-0.5, 0.5[\times]-0.5, -0.25[$ (resp. $\Omega^2 =]-0.5, 0.5[^2 \times]-0.5, 0.25[$). The contact surface Γ_C^1 is the lower semicircle and Γ_C^2 is the top surface of Ω^2 (i.e. $\Gamma_C^1 = \{\mathbf{x} \in \partial\Omega^1; x_2 \leq 0\}$ and $\Gamma_C^2 = \{\mathbf{x} \in \partial\Omega^2; x_2 = -0.25\}$ (resp. $\Gamma_C^1 = \{\mathbf{x} \in \partial\Omega^1; x_3 \leq 0\}$ and $\Gamma_C^2 = \{\mathbf{x} \in \partial\Omega^2; x_3 = -0.25\}$)). A Dirichlet condition is prescribed at the bottom of the rectangle (resp. cuboid). Since no Dirichlet condition is applied on Ω^1 the problem is only semi-coercive. To overcome the non-definiteness coming from the free rigid motions, the horizontal displacement is prescribed to be zero on the two points of coordinates (0,0) and (0,0.1) (resp. (0,0,0) and (0,0,0.1)) which blocks the horizontal translation and the rigid rotation. The projector Π^1 is defined from Γ_C^1 to Γ_C^2 in the vertical direction. All remaining parts of the boundaries are considered traction free.

For simplicity, we consider a dimensionless configuration with Lamé coefficients $\lambda = 1$ and $\mu = 1$ and a volume density of vertical force $f_v = -0.25$.

The expression of the exact solution being unknown, the convergence is studied with respect to a reference solution computed with a P_2 element on a very fine mesh for $\theta = -1$ (see Figures 3.2 and 3.3).

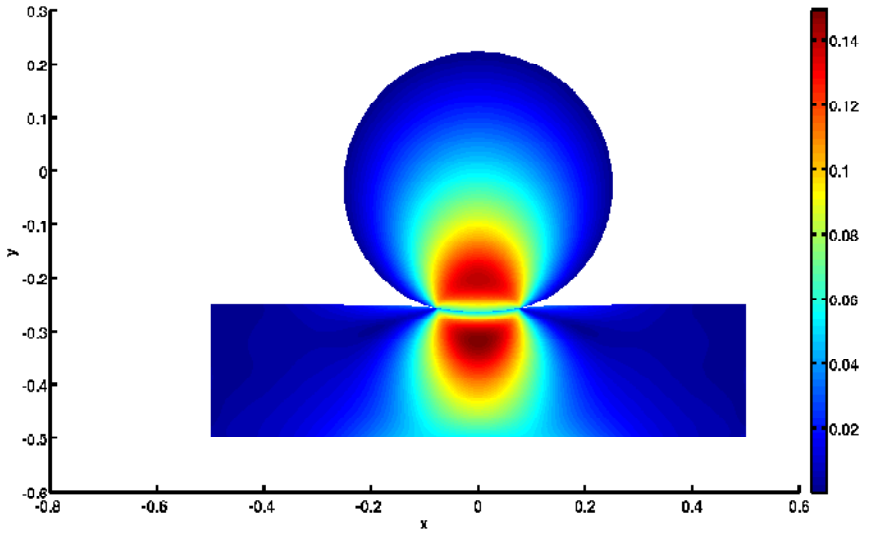

Figure 3.2: 2D Numerical reference solution with contour plot of Von Mises stress. $h = 1/400, \gamma_0 = 100$ and P_2 elements.

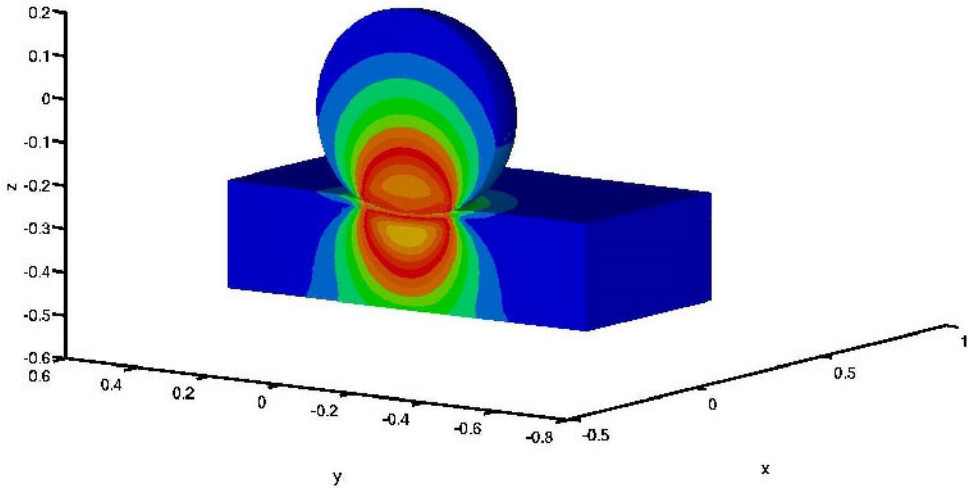

Figure 3.3: Cross-section of 3D numerical reference solution with contour plot of Von Mises stress. $h = 1/50, \gamma_0 = 100$ and P_2 elements.

To show the quality of the approximation method we plot in Figure 4.5 the contact stress profile on the second boundary and we compare it to Hertz's solution. The diagrams

in Figure 4.5 correspond to the pressure profiles for the reference fine mesh with quadratic elements. The vertical green arrows correspond to values of the contact pressure field at quadrature points. The blue solid line represents the analytically calculated Hertz's pressure profile. The left diagram correspond to the bi-dimensional case and the right one is the obtained pressure at quadrature points of the elements crossing the plan $y = 0$ in the three dimensional case.

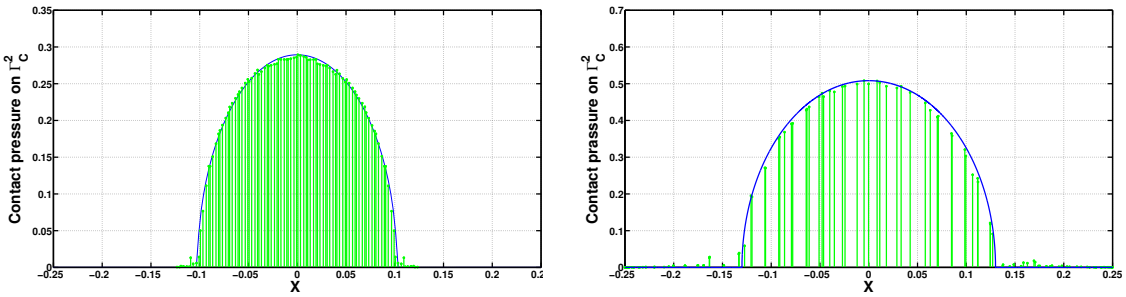

(a) 2D (b) 3D (for y=0)

Figure 3.4: Contact pressure profile for the 2D and 3D cases (Hertz solution in blue solid line and computed solution in vertical green lines).

3.3.1 Convergence in the two dimensional frictionless case

We perform a numerical convergence study on the three methods $\theta = 1$, $\theta = 0$ and $\theta = -1$ for a fixed parameter $\gamma_0 = 100$ (chosen large in order to obtain convergence for the three cases) and friction coefficients $s^1 = s^2 = 0$. In each case we plot the relative error in percentage in the H^1-norm of the displacement in the two bodies and the error of the L^2 norm of the Nitsche's contact condition on Γ_C^1 and Γ_C^2. The error of the Nitsche's contact condition is equal to:

$$\frac{\|(\gamma^i)^{-\frac{1}{2}}\left(\sigma_n^i(\mathbf{u}_{ref}^{hi}) - [P_{n,\gamma}^i(\mathbf{u}_h)]_{\mathbb{R}^-}\right)\|_{0,\Gamma_C^i}}{\|(\gamma^i)^{-\frac{1}{2}}\sigma_n^i(\mathbf{u}_{ref}^{hi})\|_{0,\Gamma_C^i}}, \text{ where } \mathbf{u}_{ref}^{hi} \text{ is the reference solution on } \Omega^i.$$

On figures 3.5, 3.6 and 3.7 the curves of relative error in percentage for Lagrange P_1 finite elements are plotted. The convergence rate in a H^1-norm is about 1 for the three values of θ which is in this case optimal, according to Theorem 3.2.6. On figures 3.8, 3.9 and 3.10 the same experiments are reported for Lagrange P_2 finite elements. The convergence rate for the three cases is about 1.5 which correspond to optimality as well.

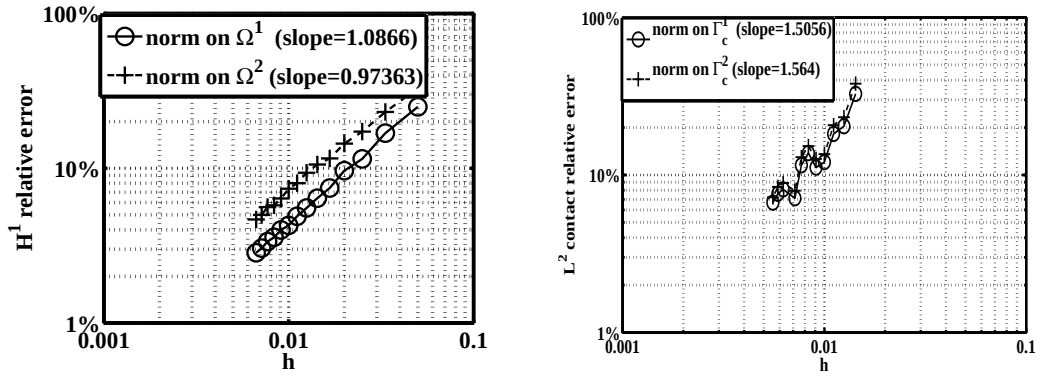

(a) (b)

Figure 3.5: Convergence curves in 2D for the method $\theta = 1$, with $\gamma_0 = 100$ and P_1 finite elements for the relative H^1-norm of the error (a) and the relative $L^2(\Gamma_C)$-norm of the error (b).

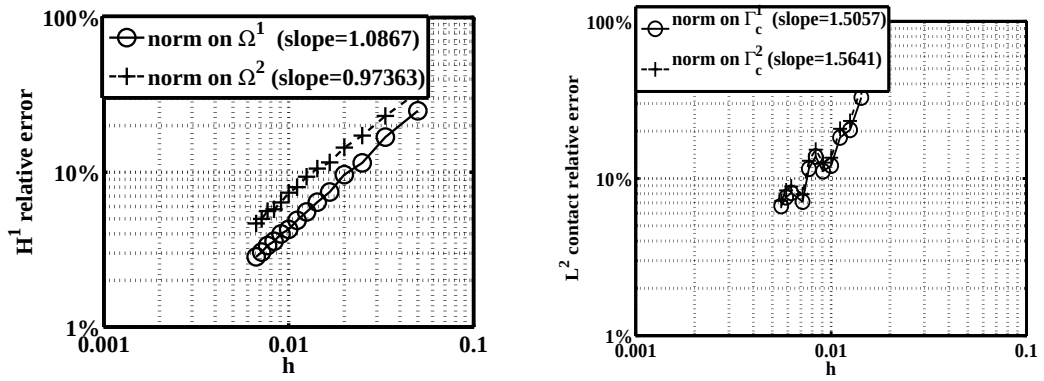

(a) (b)

Figure 3.6: Convergence curves in 2D for the method $\theta = 0$, with $\gamma_0 = 100$ and P_1 finite elements for the relative H^1-norm of the error (a) and the relative $L^2(\Gamma_C)$-norm of the error (b).

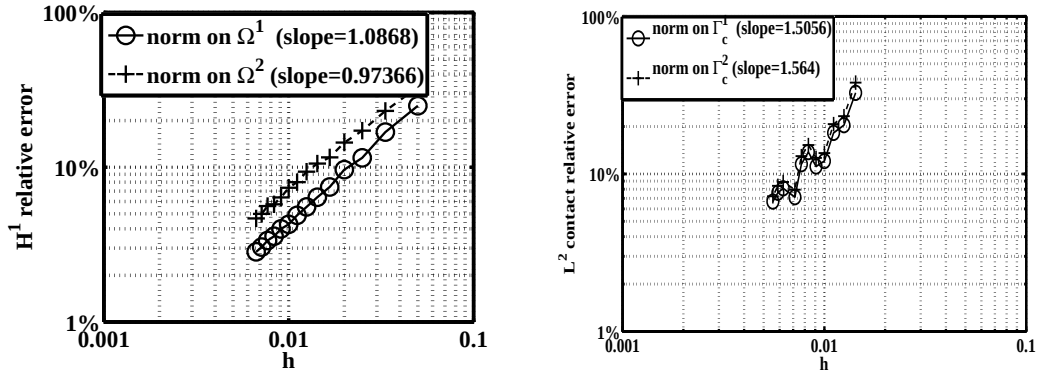

(a) (b)

Figure 3.7: Convergence curves in 2D for the method $\theta = -1$, with $\gamma_0 = 100$ and P_1 finite elements for the relative H^1-norm of the error (a) and the relative $L^2(\Gamma_C)$-norm of the error (b).

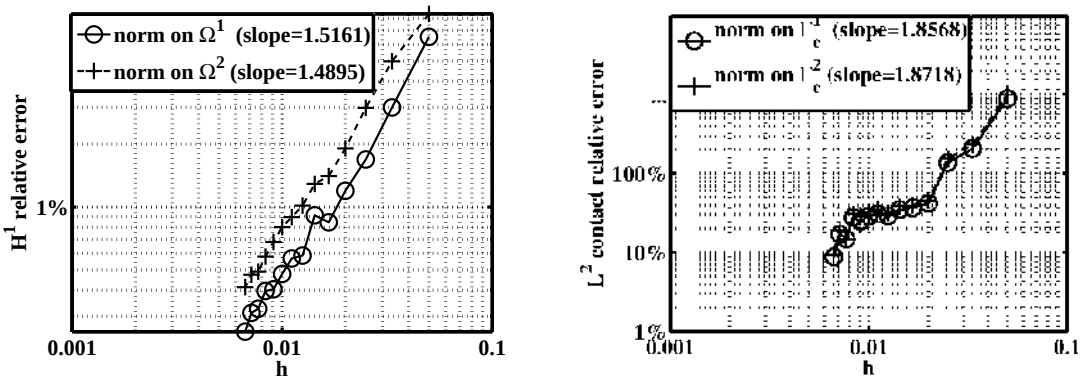

(a) (b)

Figure 3.8: Convergence curves in 2D for the method $\theta = 1$, with $\gamma_0 = 100$ and P_2 finite elements for the relative H^1-norm of the error (a) and the relative $L^2(\Gamma_C)$-norm of the error (b).

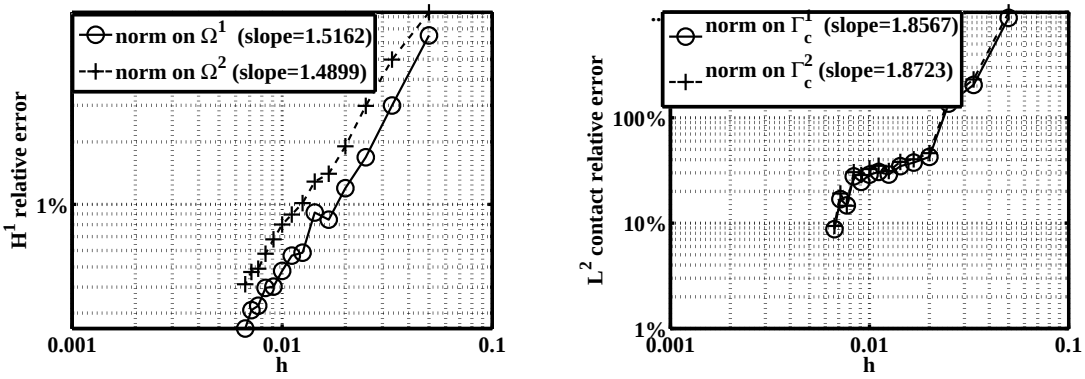

(a) (b)

Figure 3.9: Convergence curves in 2D for the method $\theta = 0$, with $\gamma_0 = 100$ and P_2 finite elements for the relative H^1-norm of the error (a) and the relative $L^2(\Gamma_C)$-norm of the error (b).

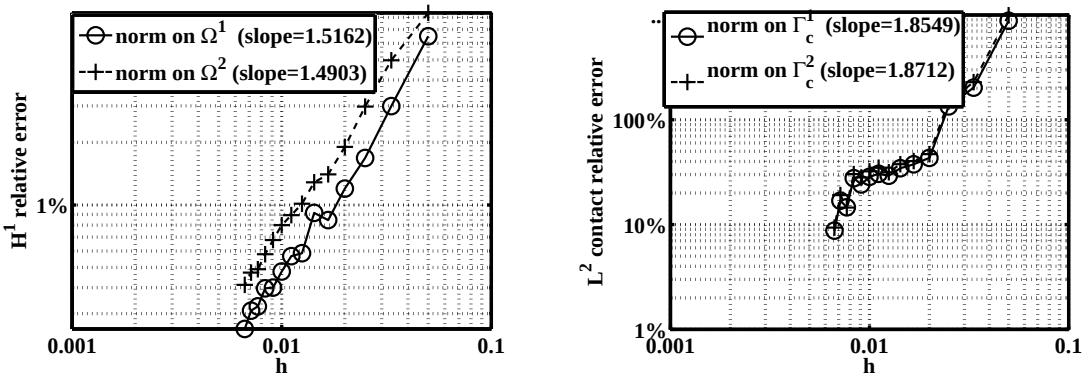

(a) (b)

Figure 3.10: Convergence curves in 2D for the method $\theta = -1$, with $\gamma_0 = 100$ and P_2 finite elements for the relative H^1-norm of the error (a) and the relative $L^2(\Gamma_C)$-norm of the error (b).

3.3.2 Convergence in 2D frictional contact case

We establish, as well, the convergence curves for a frictional contact (Tresca friction) with a friction coefficient $s^1 = 0.1$ with the method $\theta = -1$, for a Nitsche's parameter $\gamma_0 = 100$. The frictional contact curves are presented for P_1 and P_2 Lagrange elements in figures 3.11 and 3.12. Similar curves are obtained with other values of θ. We mention here that this numerical validation is the first one for Nitsche's method with frictional contact since in [Cho14] no numerical study was performed. This validation confirms optimal convergence with a convergence rate close to the frictionless case.

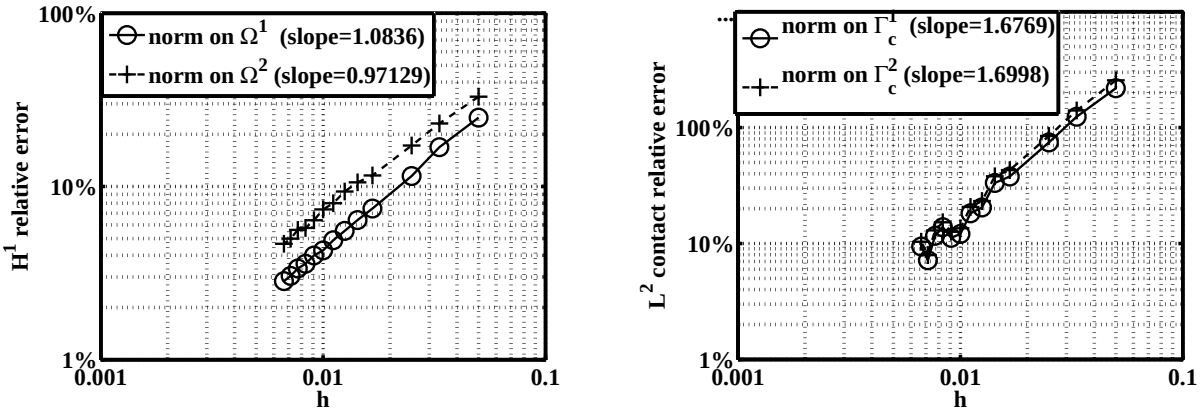

(a) (b)

Figure 3.11: Convergence curves in 2D frictional case for the method $\theta = -1$, with $\gamma_0 = 100$ with P_1 finite elements for the relative H^1-norm of the error (a) for the $L^2(\Gamma_C)$-norm of the error(b).

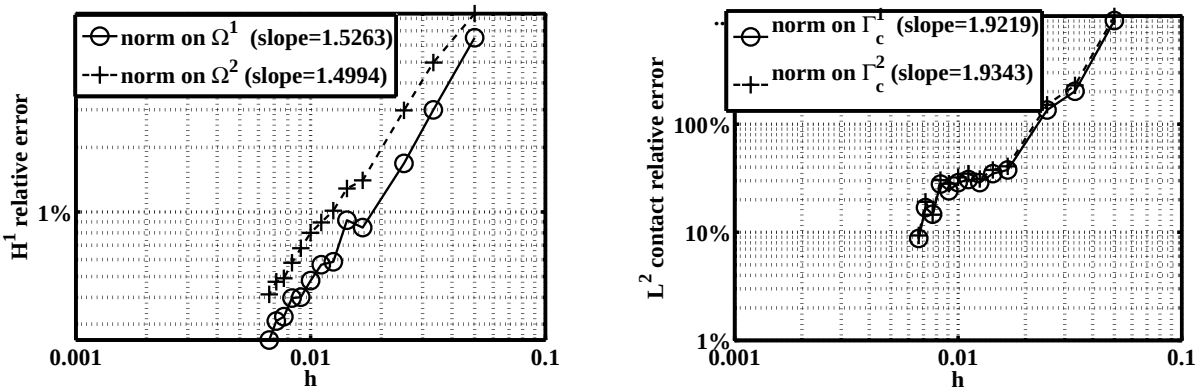

(a) (b)

Figure 3.12: Convergence curves in 2D frictional case for the method $\theta = -1$, with $\gamma_0 = 100$ with P_2 finite elements for the relative H^1-norm of the error (a) for the $L^2(\Gamma_C)$-norm of the error (b).

3.3.3 Convergence in the three dimensional case

The three-dimensional tests are similar to the two-dimensional ones. The error curves with $\theta = -1$ and P_1 Lagrange elements are presented in Fig. 3.13. Very similar conclusions can be drawn compared with the two-dimensional case.

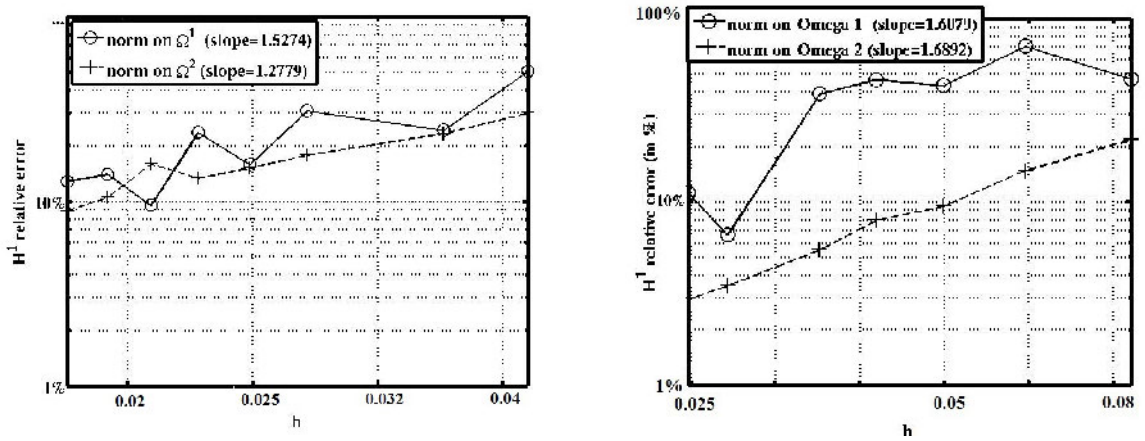

(a) (b)

Figure 3.13: Convergence curves in 3D for the method $\theta = -1$, with $\gamma_0 = 100$ for the relative H^1-norm of the error with P_1 finite elements (a) and P_2 finite elements (b).

As expected the optimal convergence is obtained in H^1 and $L^2(\Gamma_C)$-norm for all methods in good accordance with Theorem 3.2.6.

3.3.4 Comparison with other methods

To better compare the proposed method with other ones we present in the following the convergence curves of our test case with the convergence curves of the biased Nitsche's formulation and the augmented Lagrangian method [CHR15c, HR10], see Figure 3.14 and Figure 3.15. As for the proposed Nitsche's method, for augmented Lagrangian method the augmentation parameter r is taken as linear function of the mesh size : $r = \gamma_0 h$.
The curves are exactly the same for P_1 elements and very similar for P_2 ones and the convergence rate of the unbiased Nitsche's method is equal to other formulations' rate. We note that, for different values of θ the convergence is obtained for Nitsche's method (biased and unbiased) and the augmented Lagrangian method generally with a close number of iterations of the Newton algorithm.

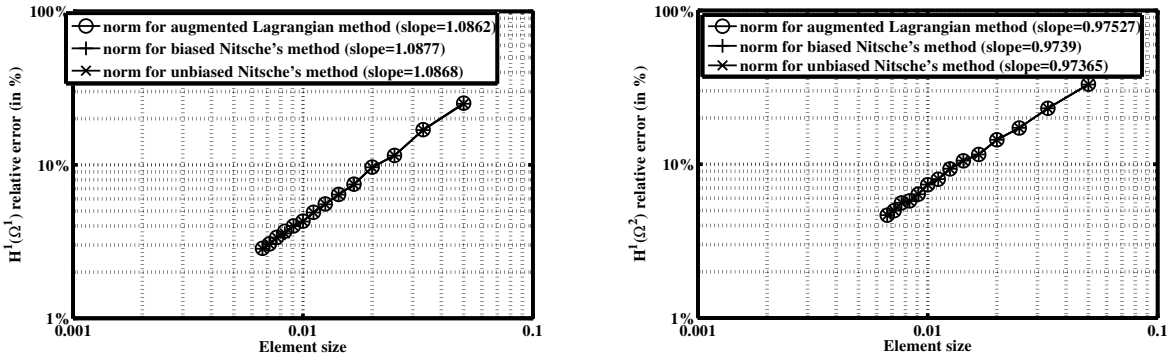

(a) (b)

Figure 3.14: Comparison of convergence curves in 2D frictionless case for the method $\theta = -1$, with $\gamma_0 = 100$ and P_1 finite elements for the relative H^1-norm of the error on Ω^1 (a) and on Ω^2 (b) for different formulations of contact.

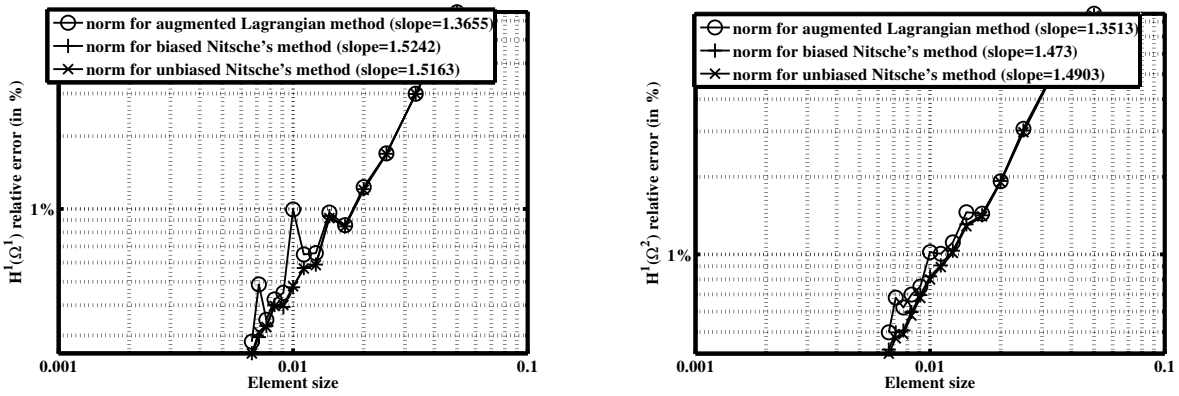

(a) (b)

Figure 3.15: Comparison of convergence curves in 2D frictionless case for the method $\theta = -1$, with $\gamma_0 = 100$ and P_2 finite elements for the relative H^1-norm of the error on Ω^1 (a) and on Ω^2 (b) for different formulations of contact.

3.3.5 Influence of the Nitsche's parameter

The influence of γ_0 on the H^1-norm of the error for P_2 elements is plotted for a mesh size $h = 0.01$ in Figure 3.16 in the frictionless case and on Figure 3.17 with a friction coefficient $s^1 = 0.1$. It is remarkable that the error curves for the largest value of γ_0 are rather the same for the three values of θ.

The variant $\theta = 1$ is the most influenced by the value of γ_0. It converges only for γ_0 large (≥ 10). The method for $\theta = 0$ gives a much large window of choice of γ_0 though it has to remain large to keep a good solution. In agreement with the theoretical result of Theorem 3.2.6, the influence of γ_0 on the method $\theta = -1$ is limited.

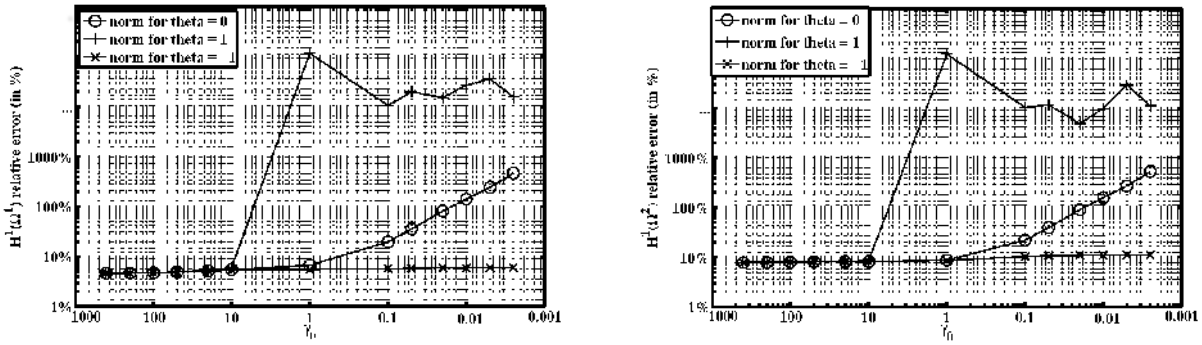

(a) (b)

Figure 3.16: Influence of γ_0 on the H^1-norm error for different values of θ in the 2D frictionless case and with P_2 finite elements on Ω^1 (a) and on Ω^2 (b).

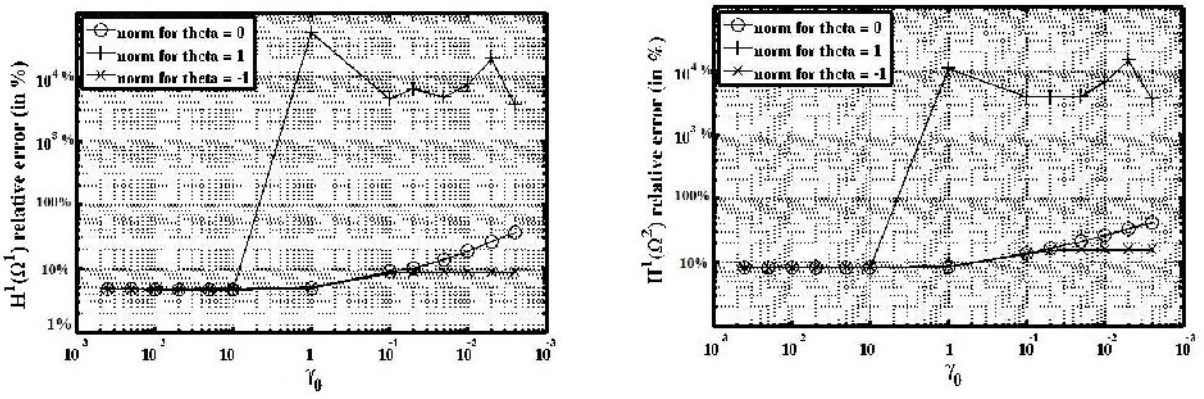

(a) (b)

Figure 3.17: Influence of γ_0 on the H^1-norm error for different values of θ in the 2D frictional case and with P_2 finite elements on Ω^1 (a) and on Ω^2 (b).

So the choice of γ_0 depends on the considered version. We can always choose $\theta = -1$ to insure the stability and convergence independently on γ_0. In this case we loose symmetry and we need to introduce $\underline{\underline{\boldsymbol{\sigma}}}(\mathbf{v}_h)$ into the weak formulation. The version $\theta = 1$ allows to keep symmetry, however it requires that γ_0 be rather large. The version $\theta = 0$ can be seen as good compromise since it is the simplest and it remains stable and converges optimally even for moderate values of γ_0. A strategy to guarantee the coercivity of the problem and then an optimal convergence is of course to consider a sufficiently large γ_0 . However, the price to pay is an ill-conditioned discrete problem. The study presented in [Ren13] shows that Newton's method has important difficulties to converge when γ_0 is very large because the nonlinear discrete system (3.16) becomes very stiff in this case.

Conclusion

A theoretical and numerical study of Nitsche's method were carried out for the Signorini problem in [CH13, CHR15c]. These analysis prove the performance of this type of formulation for contact between an elastic body and a rigid support. In this chapter we adapt Nitsche's method to the two elastic bodies contact problem through an unbiased method that could be directly applicable to multi-body contact and self-contact. The method was analyzed and we proved its consistency, well-posedness and optimal convergence. For the numerical study, the accuracy of the method was discussed for the Hertz problem with different types of finite elements, for variations of the mesh size and the value of the parameters θ and γ_0. Frictionless and frictional situations have been considered, as well as two- and three-dimensional cases. The theoretical results are, generally, confirmed by numerical tests, especially the optimal convergence and the influence of the parameter γ_0. As well, other solvers than semi-smooth Newton could be considered for improved computational efficiency. For instance highly efficient multi-grid methods have been designed for mortar-type discretization of contact problems in [WK03]. The adaptation of multigrid techniques to Nitsche's discretization of contact is still an open issue and could be considered as a perspective (see [FHW04] for multi-grid with Nitsche's method for interface problems).

Since the analysis in the small strain case are promising, the next chapter will concern Nitsche's method for the non-linear materials in the large deformation framework. In this case, our goal is to provide a construction of the method similar to the linear case and the corresponding numerical study.

Chapter 4

Nitsche's formulation of large strain contact and self-contact

Contents

Introduction

Frictional contact problems involve difficulties from both theoretical and numerical viewpoints, especially in large deformations, where complex geometrical and mechanical quantities depend on an a priori unknown mapping between contact surfaces. Contact problems are inherently non–linear, even non–smooth, and involve variational inequalities and constrained minimization. In the literature, many attempts have been developed to deal with such problems using the finite element method. In most cases, the difficulty caused

by the non-differentiability of contact and friction laws is resolved with either a method of regularization, such as penalization or augmented Lagrangian [KO88, SL92], or a mixed method [HR10, BS05].

Moreover, the spatial discretization of the problem produces difficulties at level of the calculation of mechanical contact. Evaluating the quantities involved in the equations of mechanical contact is difficult when the two boundaries are discretized. The most commonly used method is the node-to-surface (NTS) approach under a master-slave configuration [LS93b, PL02]. Then, mortar method has been successfully applied to solve contact problems with finite deformations [FW06, PL04a, PWGW12]. In this method, the enforcement of contact constraints is applied in a weak sense throughout the contact interface.

In this chapter we introduce an extention of Nitsche's method to the large deformation contact problem. Nitsche's method was originally proposed in [Nit71] to take into account a Dirichlet condition weakly. It was adapted to bilateral contact in [HH04a, WZ08] and to unilateral contact in [CH13, CHR15c]. This method aims at treating the interface conditions in a weak sense, thanks to a consistent penalty term. So it differs from standard penalization techniques which are non-consistent. Conversely to mixed method and augmented Lagrangian method, the proposed approach is primal; this allows us to eliminate an outer augmentation loop as well as additional unknowns (Lagrange multiplier) and there is no inf-sup condition to satisfy. In [CH13, CHR15c] a complete study of Nitsche's method for frictionless unilateral contact undergoing small deformations is presented. The well-posedness as well as the nominal convergence for the H^1–norm were proved. In [AHD14] a Nitsche stabilized approach was introduced for frictional sliding problem.

In Chapter 3 were introduced some variants of the method, that a real parameter θ allows to encompass. Namely, $\theta = 0$ yields a non-symmetric simple version of Nitsche; when $\theta = 1$ we recover a symmetric method and to $\theta = -1$ corresponds a skew-symmetric method that is much more robust regarding Nitsche's parameter. In this adaptation to the large strain case, we use a similar parameter to recover all the different variants. The above remarks concerning this parameter θ remain true to some extent for large deformation contact. The main difference between large and small strain is that, when $\theta \neq 0$, the weak formulation and the tangent problem are more difficult to obtain since they involve additional derivatives of the stress tensor.

The standard paradigm to treat the problem of two deformable bodies in contact is known as the master/slave formulation (see, e.g., [Lau02, LS93b, Wri06]): one distinguishes between a master surface and a slave one on which one prescribes the non–penetration condition. With this paradigm important difficulties appear in the case of self–contact and multi–body contact where it is difficult to *a priori* nominate a master surface and a slave one. Automating the detection and the separation between slave and master surfaces in these cases may generate a lack of robustness since it may create detection problems. To avoid these difficulties some unbiased formulations for contact were proposed, see for instance [SD15].

In Chapter 3, the Nitsche's method was formulated for a two deformables bodies contact problem with a Tresca type friction. In order to prepare its adaptation to the

self-contact problem, an unbiased version for contact and Tresca friction in the small strain framework was presented and analysed. In this previous work, the two contact surfaces were treated symmetrically and the integration of contact/friction condition was made along the two surfaces. This current chapter could be seen as the continuity of the previous one, since in this chapter, we present also an unbiased approximation of contact but in the large strain formalism.
The extension is also made for the friction law, since Coulomb friction is considered instead of Tresca friction. The reformulation of Coulomb friction follows the same path as in [Cho14, CMR16]. Of course no proof of well-posedness or convergence can be obtained with standard techniques for the problem under consideration, but we test numerically the performance of our method in various situations. The formulation involves boundary integrals of fields that are discretized over two different meshes what generates a difficulty for the numerical quadrature. Typically, the approach that is used in mortar-type methods is to compute elements intersections between the two contact surfaces and subdivide the integration rule in order to accurately integrate the contributions to the algebraic system using standard Gauss quadrature techniques. This segmentation process is challenging, especially in the three dimensional case (see [PL04a, PL02]). Due to this computational complexity, it has been seen appealing to use a higher order quadrature rule on the slave mesh without segmentation (see [FW05, TFW09]). Following [FPW15], we call this technique "element-based integration" and the segmentation technique " segment-based integration". In section 4.3.1,we compare the two methods: the error generated by using element-based integration, though much larger than with segment-based integration, remains small. This is in agreement with the study [FPW15] that concludes that both methods provide acceptable results. Though segment-based integration leads to an improved quality of the solution for quadratic elements and/or friction (see [FPW15]), we carried out the remaining part of the study with element-based integration because this method is simpler and cheaper.

Another major difficulty for large deformation contact comes from the mapping function relating the two contact surfaces. Classically, a point of the first contact surface is mapped to the closest projection point on the second one. Hence, the second surface normals $\mathbf{n}_y$ govern the definition of the gap function and its kinematics. This classical mapping will in the following be simply referred to as the projection strategy. In [PR15] this strategy is compared with another one named ray-tracing, where a point of the first surface is mapped to the closest intersection with the other surface along the first surface normal. Unlike projection the definition of the gap and related quantities are governed by the first surface normal $\mathbf{n}_x$. The formulations presented for instance in [FW06, KS13] employ the classic projection approach, while [PL04a, TFW09] present formulations that rely on the ray-tracing strategy. According to [PR15] the ray-tracing is more stable since the expression of the directional derivative of the mapping is quite simpler and expected to be smoother. Moreover, there are generally less special cases to treat when dealing with ray-tracing rather than projection since the probability to come across a non regular point, like a corner of the geometry or simply an element boundary, is negligible for the ray-tracing strategy while it is very frequent for the projection. In Section 4.1.2 of this chapter, we remind the advantages of using ray-tracing, and we provide a numerical

comparison between them in Section 4.3.6.

In Section 4.1 we present the setting and notations for the problem under consideration: large deformation contact with Coulomb friction and possibly self–contact. In Section 4.2 the Nitsche–based approximation is detailed, particularly the variational formulation and the tangent problem. Section 4.3 is a numerical validation of the method with several tests. The influence of Nitsche's parameter for different variants is investigated numerically.

4.1 Problem setting

4.1.1 Notations

In this chapter, we use the same notations of tensors and operators defined in the section 2.1.2.1 of chapter2.

We let, moreover, $\Omega \subset \mathbb{R}^d$ be an open bounded set that denotes the reference configuration of one or several deformable solids in a space of dimension $d = 2$ or 3. A deformed configuration Ω^t of the considered solids can be defined through a transformation $\boldsymbol{\varphi}$ which maps any point $\mathbf{X}$ of the reference configuration to a point $\mathbf{x}$ of the deformed one (see Figure 4.1):

$$\begin{array}{rcl} \boldsymbol{\varphi} : \overline{\Omega} & \longrightarrow & \mathbb{R}^d \\ \mathbf{X} & \longmapsto & \mathbf{x} = \boldsymbol{\varphi}(\mathbf{X}). \end{array}$$

We define the displacement $\mathbf{u}$ relatively to the reference configuration as:

$$\mathbf{u}(\mathbf{X}) = \boldsymbol{\varphi}(\mathbf{X}) - \mathbf{X}.$$

Deformation of the solid can be considered either in equilibrium or as part of a quasi-static evolution. To deal with Coulomb friction, a quasi-static process will be considered, and the static case can be viewed as a particular case.

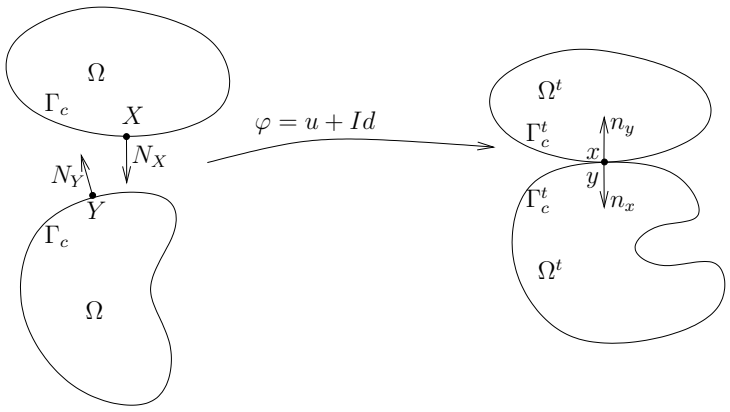

Figure 4.1: Basic notations for different quantities in reference and deformed configurations.

In the deformed configuration Ω^t, at time t, different portions of the boundary $\partial\Omega$ of

Ω may come into contact and interact with each other. In order to express this interaction mathematically, it is convenient to consider a restricted part of $\partial\Omega$ as the contact surface Γ, i.e. the surface where contact/friction phenomena may occur. As in [CMR16] we consider an unbiased formulation that does not distinguish between a master and a slave surface. The case of self–contact is treated implicitly and there is no need to divide the self–contact surface. A non-penetration condition on the deformed contact surface Γ^t can be expressed with the help of a mapping function relating a point $\mathbf{x}$ to its mapping $\mathbf{y}$. We denote by $\Gamma_c^t \subset \Gamma^t$ (resp. $\Gamma_c \subset \Gamma$) the set of points $\mathbf{x}$ (resp. $\mathbf{X}$) in the deformed (resp. reference) configuration, for which such a mapping Π exists:

$$\begin{array}{rcl} \Pi : \Gamma_c^t & \longrightarrow & \Gamma^t \\ \mathbf{x} & \longmapsto & \mathbf{y} = \Pi(\mathbf{x}). \end{array}$$

Recall that surface points $\mathbf{X}$, $\mathbf{Y}$, $\mathbf{x}$ and $\mathbf{y}$ are of dimension d as well as the corresponding unit outward normal vectors: $\mathbf{N_X}$, $\mathbf{N_Y}$ in the reference configuration and $\mathbf{n}_x$, $\mathbf{n}_y$ in the deformed one.

To fix ideas we will consider a general hyperelastic constitutive law, derived from a potential W that depends on the deformation through $\underline{\underline{\mathbf{E}}}$ (or $\underline{\underline{\mathbf{C}}}$) (see, e.g., [BW08,FG11]), so that the second Piola-Kirchhoff stress is

$$\underline{\underline{\mathbf{S}}} = \frac{\partial W}{\partial \underline{\underline{\mathbf{E}}}}(\underline{\underline{\mathbf{E}}}) = 2\frac{\partial W}{\partial \underline{\underline{\mathbf{C}}}}(\underline{\underline{\mathbf{C}}}),$$

with corresponding fourth-order elasticity tensor

$$\underline{\underline{\underline{\underline{\boldsymbol{\mathcal{C}}}}}} = \frac{\partial \underline{\underline{\mathbf{S}}}}{\partial \underline{\underline{\mathbf{E}}}} = \frac{\partial^2 W}{\partial \underline{\underline{\mathbf{E}}} \partial \underline{\underline{\mathbf{E}}}}.$$

We will need as well the isotropic tensor

$$\underline{\underline{\underline{\underline{\boldsymbol{\mathcal{I}}}}}} = \frac{1}{2}(\mathbf{e}_i \otimes \mathbf{e}_j \otimes \mathbf{e}_i \otimes \mathbf{e}_j + \mathbf{e}_i \otimes \mathbf{e}_j \otimes \mathbf{e}_j \otimes \mathbf{e}_i),$$

where $\otimes$ denotes the tensor product of two vectors, $(\mathbf{e}_i)_{i=1,\dots,d}$ is the canonical basis of $\mathbb{R}^d$ and where Einstein's summation convention is used. The tensor $\underline{\underline{\underline{\underline{\boldsymbol{\mathcal{I}}}}}}$ has the property $\underline{\underline{\underline{\underline{\boldsymbol{\mathcal{I}}}}}} : \underline{\underline{\mathbf{A}}} = \underline{\underline{\mathbf{A}}}$ for any symmetric second-order tensor $\underline{\underline{\mathbf{A}}}$ (: denotes the double-dot product between two tensors).

Since the choice of a constitutive law is not central in the description of the proposed contact approximation, we will simply denote the global potential energy by $\mathcal{J}(\cdot)$. For example, if considering simple equilibrium under a gravity force, the potential energy is

$$\mathcal{J}(\mathbf{u}) = \int_\Omega W(\underline{\underline{\mathbf{E}}})\ dX - \int_\Omega \rho\ \mathbf{g} \cdot \mathbf{u}\ dX,$$

where ρ is the density in the reference configuration and $\mathbf{g}$ is the gravity acceleration

vector. Of course, additional terms such as boundary loads, can be considered as well. Dirichlet conditions can also be prescribed, but, to simplify the formulation, the treatment of Dirichlet conditions will be omitted in the following.

4.1.2 The mapping and the gap function

In the problem setting above, it is assumed that a point $\mathbf{x}$ of the deformed contact surface is mapped to a point $\mathbf{y}$. Regarding this mapping, there are several possibilities. The most classic strategy is to define $\mathbf{y}$ as the closest point projection of $\mathbf{x}$ onto the deformed surface Γ_c, like shown in Figure 4.2(a). We can refer to [Lau02] for this mapping. The main difficulty for using projection is the complicated expression of the tangent problem, that is due to the derivative of the unit normal vector $\mathbf{n}_y$. The expression of this derivative can be found in [Lau02, chapter 4]. However, this expression does not take into account the inter-element jumps.

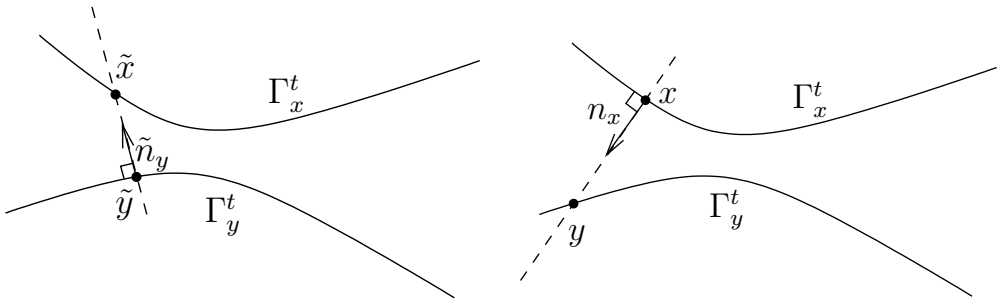

(a) Projection strategy (b) Ray-tracing strategy

Figure 4.2: Illustration of projection and ray-tracing strategies.

An alternative strategy, corresponding to Fig. 4.2(b), is to define $\mathbf{y}$ as the closest intersection of the contact surface with the line passing through point $\mathbf{x}$ and having direction vector $\mathbf{n}_x$. The latter strategy, which can be referred to as ray-tracing, was studied in [PR15].

The two strategies are in fact closely related since the orthogonality of $\mathbf{n}_x$ to the contact surface implies that in the ray-tracing strategy, the point $\mathbf{x}$ is the projection of the corresponding point $\mathbf{y}$ on the deformed slave surface. For this reason, this strategy can also be characterized as an inverse projection. The main motivation for using it instead of the classical projection is for achieving a simpler expression for the weak formulation, due to the fact that the unit normal vector $\mathbf{n}_x$ has a simpler derivative than $\mathbf{n}_y$. In this section, we give the expressions of the derivatives of $\mathbf{y}$ and $\mathbf{n}_x$ to prove that those expressions are much simpler for ray-tracing. We investigate also the performance of each strategy. This theoretical comparison is inspired by [PR15] and completed by a numerical one on Section 4.3.6.

Contact kinematics are actually for both methods very similar. In order to make similarities and differences easier to recognize, the most important equations for both ray-tracing and projection are presented in parallel, with quantities referring to the projection method identified by an additional tilde symbol.

Gap functions corresponding to ray-tracing and projection are respectively defined by:

$$g = \mathbf{n}_x \cdot (\mathbf{y} - \mathbf{x}) \,, \tag{4.1}$$

$$\tilde{g} = \tilde{\mathbf{n}}_y \cdot (\tilde{\mathbf{x}} - \tilde{\mathbf{y}}) \,. \tag{4.2}$$

Those expressions allow us to write:

$$\mathbf{y} = \mathbf{x} + g \ \mathbf{n}_x \,, \tag{4.3}$$

$$\tilde{\mathbf{y}} = \tilde{\mathbf{x}} - \tilde{g} \ \tilde{\mathbf{n}}_y \,. \tag{4.4}$$

To obtain and linearize a weak formulation representing the non-penetration condition, not only the definition of a gap function is required, but also the directional derivatives of all quantities involved in Eqs. (4.3) and (4.4) with respect to the current deformation $\boldsymbol{\varphi}$ in any direction $\delta\mathbf{u}$.

With $\mathbf{X}$ or $\tilde{\mathbf{X}}$ considered as the independent variable, the directional derivatives of $\mathbf{x}$ or $\tilde{\mathbf{x}}$ and $\mathbf{n}_x$ are straightforward to determine, whether corresponding quantities at the point $\mathbf{y}$ are difficult to evaluate. This is because $\mathbf{y}$ depends on both deformation $\boldsymbol{\varphi}$ and coordinate $\mathbf{Y}$, with the latter depending on $\boldsymbol{\varphi}$ itself and having its own directional derivative $\mathcal{D}Y[\delta\mathbf{u}]$. Thus, we write, on a first time the directional derivatives of $\mathbf{y}$ and $\tilde{\mathbf{y}}$ with respect to $\delta\mathbf{u}$:

$$\mathcal{D}\mathbf{y}[\delta\mathbf{u}] = \delta\mathbf{u}(\mathbf{Y}) + \underline{\underline{\mathbf{F}}}_Y \ \mathcal{D}\mathbf{Y}[\delta\mathbf{u}] \,, \tag{4.5}$$

$$\mathcal{D}\tilde{\mathbf{y}}[\delta\mathbf{u}] = \delta\mathbf{u}(\tilde{\mathbf{Y}}) + \underline{\underline{\tilde{\mathbf{F}}}}_Y \ \mathcal{D}\tilde{\mathbf{Y}}[\delta\mathbf{u}] \,, \tag{4.6}$$

with $\mathcal{D}\mathbf{Y}[\delta\mathbf{u}]$ and $\mathcal{D}\tilde{\mathbf{Y}}[\delta\mathbf{u}]$ being tangential to Γ_Y, so that $\underline{\underline{\mathbf{F}}}_Y \ \mathcal{D}\mathbf{Y}[\delta\mathbf{u}]$ and $\underline{\underline{\tilde{\mathbf{F}}}}_Y \ \mathcal{D}\tilde{\mathbf{Y}}[\delta\mathbf{u}]$ are tangential to the deformed surface Γ_y^t, which means:

$$\mathbf{n}_y \cdot \mathbf{F}_Y \ \mathcal{D}\mathbf{Y}[\delta\mathbf{u}] = \tilde{\mathbf{n}}_y \cdot \underline{\underline{\tilde{\mathbf{F}}}}_Y \ \mathcal{D}\tilde{\mathbf{Y}}[\delta\mathbf{u}] = 0 \,. \tag{4.7}$$

Other expressions of the directional derivatives of $\mathbf{y}$ and $\tilde{\mathbf{y}}$ can be obtained from Eqs. (4.3) and (4.4) as:

$$\mathcal{D}\mathbf{y}[\delta\mathbf{u}] = \delta\mathbf{u}(\mathbf{X}) + \mathcal{D}g[\delta\mathbf{u}] \ \mathbf{n}_x + g \ \mathcal{D}\mathbf{n}_x[\delta\mathbf{u}] \,, \tag{4.8}$$

$$\mathcal{D}\tilde{\mathbf{y}}[\delta\mathbf{u}] = \delta\mathbf{u}(\tilde{\mathbf{X}}) - \mathcal{D}\tilde{g}[\delta\mathbf{u}] \ \tilde{\mathbf{n}}_y - \tilde{g} \ \mathcal{D}\tilde{\mathbf{n}}_y[\delta\mathbf{u}] \,. \tag{4.9}$$

Assuming sufficient regularity, the directional derivatives of the gap functions can be written after combining Eqs. (4.5) and (4.8) or Eqs. (4.6) and (4.9), multiplying respec-

tively by $\mathbf{n}_y$ or $\tilde{\mathbf{n}}_y$ and exploiting Eq. (4.7), as:

$$\mathcal{D}g[\delta\mathbf{u}] = -\frac{\mathbf{n}_y}{\mathbf{n}_x \cdot \mathbf{n}_y} \cdot (\delta\mathbf{u}(\mathbf{X}) - \delta\mathbf{u}(\mathbf{Y}) + g\ \mathcal{D}\mathbf{n}_x[\delta\mathbf{u}]) \ , \tag{4.10}$$

$$\mathcal{D}\tilde{g}[\delta\mathbf{u}] = \tilde{\mathbf{n}}_y \cdot \left(\delta\mathbf{u}(\tilde{\mathbf{X}}) - \delta\mathbf{u}(\tilde{\mathbf{Y}})\right) \ . \tag{4.11}$$

The simpler expression in the case of projection is due to the fact that $\tilde{\mathbf{n}}_y \cdot \mathcal{D}\tilde{\mathbf{n}}_y[\delta\mathbf{u}] = 0$, but no similar relation can be utilized in case of ray-tracing. The directional derivative of the unit normal vector $\mathbf{n}_x$ in Eq. (4.10) is given by:

$$\mathcal{D}\mathbf{n}_x[\delta\mathbf{u}] = -\underline{\underline{\mathbf{T}}}_{\mathbf{n}_x} \underline{\underline{\mathbf{F}}}_X^{-T} \nabla\delta\mathbf{u}^T(\mathbf{X})\, \mathbf{n}_x \, . \tag{4.12}$$

At this point, despite the more complex expression obtained for $\mathcal{D}g[\delta\mathbf{u}]$, the basic kinematic analysis of ray-tracing can be considered as completed. Substituting Eqs. (4.10) and (4.12) into Eq. (4.8) permits evaluation of $\mathcal{D}\mathbf{y}[\delta\mathbf{u}]$ while Eq. (4.5) can be used in a further step for evaluating $\mathcal{D}\mathbf{Y}[\delta\mathbf{u}]$ as:

$$\mathcal{D}\mathbf{Y}[\delta\mathbf{u}] = \underline{\underline{\mathbf{F}}}_Y^{-1} \left(\underline{\underline{\mathbf{I}}} - \frac{\mathbf{n}_x \otimes \mathbf{n}_y}{\mathbf{n}_x \cdot \mathbf{n}_y}\right) \left(\delta\mathbf{u}(\mathbf{X}) - \delta\mathbf{u}(\mathbf{Y}) - g\, \underline{\underline{\mathbf{F}}}_X^{-T} \nabla\delta\mathbf{u}^T(\mathbf{X})\, \mathbf{n}_x\right) \ . \tag{4.13}$$

In the case of the projection strategy, Eq. (4.9) cannot be evaluated yet, since the expression of $\mathcal{D}\tilde{\mathbf{n}}_y[\delta\mathbf{u}]$ can not be established in a similar way to Eq. (4.12). Apart from a term similar to Eq. (4.12), $\mathcal{D}\tilde{\mathbf{n}}_y[\delta\mathbf{u}]$ involves $\mathcal{D}\tilde{\mathbf{Y}}[\delta\mathbf{u}]$ and the curvature of the deformed surface Γ_y^t at point $\tilde{\mathbf{y}}$. With such an expression and combining Eqs. (4.6) and (4.9), it is possible to determine $\mathcal{D}\tilde{\mathbf{Y}}[\delta\mathbf{u}]$ and consequently also $\mathcal{D}\tilde{\mathbf{y}}[\delta\mathbf{u}]$ as described, for instance, in [LS93a, Wri95, Lau02, KS13]. We note also that for projection, even when calculating the exact expression of the derivatives, the discrete method will not be stable because of the non-continuity of the normal vector $\mathbf{n}_y(\mathbf{X})$ in terms of the position $\mathbf{X}$ since the projection is not a continuous operator.

Thus, for ray-tracing, $\mathbf{y}$ is continuous with respect to $\boldsymbol{\varphi}$ and the directional derivative does not depend on the curvature of the projected (master) surface. This is a crucial advantage compared to the projection strategy for which the projected point is discontinuous in several situations and the directional derivative involves the computation of the surface curvature.

Besides, from a computational viewpoint, ray-tracing allows a more efficient algorithm implementation than projection. The intersection equation for determining point $\mathbf{Y}$ in ray-tracing is:

$$(\boldsymbol{\varphi}(\mathbf{Y}) - \boldsymbol{\varphi}(\mathbf{X})) \cdot \mathbf{t}_i(\mathbf{X}) = 0 \, , \tag{4.14}$$

while the projection equation for specifying point $\tilde{\mathbf{Y}}$ is:

$$(\boldsymbol{\varphi}(\tilde{\mathbf{Y}}) - \boldsymbol{\varphi}(\tilde{\mathbf{X}})) \cdot \tilde{\mathbf{t}}_i(\tilde{\mathbf{Y}}) = 0 \, , \tag{4.15}$$

where vectors $\mathbf{t}_i$ and $\tilde{\mathbf{t}}_i$, for $i = 1, \ldots d-1$, form orthonormal bases of the planes tangent to

$\mathbf{n}_x$ and $\tilde{\mathbf{n}}_y$ respectively. After expressing $\mathbf{Y}$ through $d-1$ coordinates on an element face of the discretized body, applying Newton's method for solving Eq. (4.14) is straightforward and efficient since its tangent system only involves $\underline{\underline{\mathbf{F}}}_Y$. The tangent system of Eq. (4.15) additionally involves the nonlinearity between the tangent basis vectors and the unknown $\tilde{\mathbf{Y}}$.

Moreover, there are generally less special cases to treat when dealing with ray-tracing rather than projection. The probability to come across a non regular point, like a corner of the geometry or simply an element boundary, is negligible for the ray-tracing strategy while it is very frequent for the projection. Fig. 4.3(a), illustrates how the projection from a significant portion of the slave surface can be somehow attracted by convex non-regular points, complicating the definition of $\tilde{\mathbf{n}}_y$. The probability that a ray-traced point $\mathbf{y}$ in Fig. 4.3(b) falls on a non-regular point is negligible.

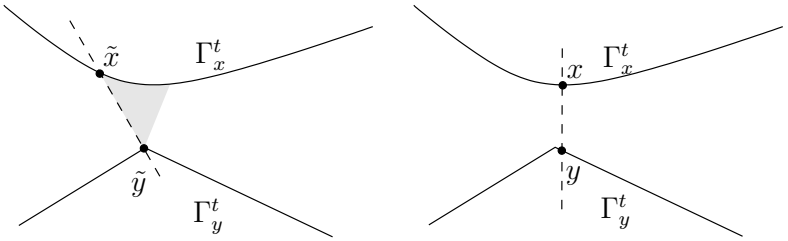

(a) Projection strategy (b) Ray-tracing strategy

Figure 4.3: *Set of points $\tilde{x}$ projected onto a convex non-regular point $\tilde{y}$ (a). Negligible probability of a ray-traced point y falling on a non-regular point (b).*

Those advantages of the ray-tracing strategy seems to increase its numerical performance compared to the projection. The strategy is more performing according to Section 4.3.6.

4.1.3 Formulation of contact and friction conditions

The impenetrability constraint is stated mathematically as $g(\mathbf{u}) \geq 0$. To formulate the associated complementarity conditions, we need to consider the contact traction $\hat{\boldsymbol{\sigma}}_{\boldsymbol{N}}(\mathbf{u})$ which we take to be the Piola traction at point $\mathbf{X}$. This traction is resolved as follows:

$$\hat{\boldsymbol{\sigma}}_{\boldsymbol{N}}(u) = \hat{\sigma}_n(\mathbf{u})\mathbf{n}_x + \underline{\underline{\mathbf{T}}}_{\mathbf{n}_x}\hat{\boldsymbol{\sigma}}_{\boldsymbol{N}}(\mathbf{u}) = \hat{\sigma}_n(\mathbf{u})\mathbf{n}_x + \hat{\boldsymbol{\sigma}}_t,$$

where $\mathbf{n}_x$ is the outward normal to Γ_c^t at $\mathbf{x}$. When contact occurs ($\hat{\sigma}_n < 0$) the outward normal vectors $\mathbf{n}_x$ and $\mathbf{n}_y$ are opposite. Thus, for projection the stress vector $\hat{\boldsymbol{\sigma}}_{\boldsymbol{N}}$ is resolved at the projected point $\tilde{\mathbf{y}}$ according the normal vector $-\tilde{\mathbf{n}}_y$, instead of $\mathbf{n}_x$. The quantity $\hat{\sigma}_n(\mathbf{u})$ now represents the contact pressure at $\mathbf{X}$, and must be negative. The

conditions for normal contact are:

$$\begin{aligned} g(\mathbf{u}) &\geq 0 && && (4.16a)\\ \hat{\sigma}_n(\mathbf{u}) &\leq 0 && \text{on } \Gamma_c. && (4.16b)\\ \hat{\sigma}_n(\mathbf{u})g(\mathbf{u}) &= 0 && && (4.16c) \end{aligned}$$

Let γ be a given positive function. As for small strain in [AC88, CH13, CHR15c] and Chapter 3, the contact conditions (4.16) are reformulated as

$$\hat{\sigma}_n(\mathbf{u}) = [\hat{\sigma}_n(\mathbf{u}) + \gamma g(\mathbf{u})]_{\mathbb{R}^-}. \tag{4.17}$$

Using the vilocity $\mathbf{v}$ defined in section 2.1.2, the conditions of Coulomb friction can be written as follows:

$$\begin{cases} \|\hat{\boldsymbol{\sigma}}_t(\mathbf{u})\| \leq -\mathscr{F}\hat{\sigma}_n(\mathbf{u}) & \text{if } \mathbf{v} = 0, \\ \hat{\boldsymbol{\sigma}}_t(\mathbf{u}) = \mathscr{F}\hat{\sigma}_n(\mathbf{u})\dfrac{\mathbf{v}}{\|\mathbf{v}\|} & \text{otherwise.} \end{cases} \tag{4.18}$$

As presented in Capter 3 for Tresca friction, we could reformulate the Coulomb friction condition using the projection $\boldsymbol{P}_{B(\tau)}$. In fact, for a given positive function γ, the friction condition is equivalent to the non-smooth equation:

$$\hat{\boldsymbol{\sigma}}_t(\mathbf{u}) = \boldsymbol{P}_{B(-\mathscr{F}\hat{\sigma}_n(\mathbf{u}))}(\hat{\boldsymbol{\sigma}}_t(\mathbf{u}) - \gamma\mathbf{v}). \tag{4.19}$$

To simplify the formulation, and following [PR15], we define the non-smooth operator $\mathcal{C}_{\gamma,\mathscr{F}}$ as:

$$\boldsymbol{\mathcal{C}}_{\gamma,\mathscr{F}}(\boldsymbol{\sigma}, g, \mathbf{v}, \mathbf{n}) = [\boldsymbol{\sigma}\cdot\mathbf{n} + \gamma\, g]_{\mathbb{R}^-}\,\mathbf{n} + \boldsymbol{\mathcal{P}}_{B(\mathbf{n}, -\mathscr{F}[\boldsymbol{\sigma}\cdot\mathbf{n}+\gamma g]_{\mathbb{R}^-})}(\boldsymbol{\sigma} - \gamma\,\mathbf{v}).$$

Unlike $\boldsymbol{P}_{B(\tau)}$ that represents a simple ball projection, here $\boldsymbol{\mathcal{P}}_{B(\mathbf{n},\tau)}$ is the projection onto the tangent plane defined by the normal $\mathbf{n}$, followed by the projection onto a ball of radius τ, i.e. :

$$\boldsymbol{\mathcal{P}}_{B(\mathbf{n},\tau)}(\mathbf{q}) = \begin{cases} \underline{\underline{\mathbf{T}_n}}\mathbf{q} & \text{if } \|\underline{\underline{\mathbf{T}_n}}\mathbf{q}\| \leq \tau\,, \\ \tau\dfrac{\underline{\underline{\mathbf{T}_n}}\mathbf{q}}{\|\underline{\underline{\mathbf{T}_n}}\mathbf{q}\|} & \text{otherwise.} \end{cases} \tag{4.20}$$

As a result, contact and friction conditions, in the case of ray-tracing, are formulated as:

$$\hat{\boldsymbol{\sigma}}_{\boldsymbol{N}} = \boldsymbol{\mathcal{C}}_{\gamma,\mathscr{F}}(\hat{\boldsymbol{\sigma}}_{\boldsymbol{N}}, g, \mathbf{v}, \mathbf{n}_x). \tag{4.21}$$

4.2 A Nitsche-based formulation for frictional contact

4.2.1 Weak formulation

We consider test functions $\delta\mathbf{u} \in \mathbf{V}$, with $\mathbf{V}$ the space of all (smooth) admissible variations of $\mathbf{u}$ satisfying possibly homogeneous Dirichlet conditions on the appropriate part of $\partial\Omega$. The abstract weak formulation for (frictional) contact is:

$$G(\mathbf{u}, \delta\mathbf{u}) = \int_{\Gamma_c} \hat{\boldsymbol{\sigma}}_{\boldsymbol{N}} \cdot \delta\mathbf{u} \, d\Gamma, \qquad \forall \delta\mathbf{u} \in \mathbf{V}.$$

The expression $G(\mathbf{u}, \delta\mathbf{u})$ is the sum of the internal virtual work and of the virtual work of body or surface external forces. This work is seen to balance the virtual work of the contact and friction forces acting on Γ_c. In the considered case of hyperelastic bodies and simple equilibrium under a gravity force, there holds $G(\mathbf{u}; \delta\mathbf{u}) = \mathcal{DJ}(\mathbf{u})[\delta\mathbf{u}]$. Thus, the above weak formulation reads:

$$\mathcal{DJ}(\mathbf{u})[\delta\mathbf{u}] - \int_{\Gamma_c} \hat{\boldsymbol{\sigma}}_{\boldsymbol{N}} \cdot \delta\mathbf{u} \, d\Gamma = 0, \qquad \forall \delta\mathbf{u} \in \mathbf{V}. \tag{4.22}$$

Moreover, we apply the second Newton law: to each point $X \in \Gamma_c$, we require that the differential contact force induced on Γ_c at the corresponding point Y be equal and opposite to that produced at $\mathbf{X}$, i.e.

$$\hat{\boldsymbol{\sigma}}_{\boldsymbol{N}}(\mathbf{X}) \, d\Gamma_X = -\hat{\boldsymbol{\sigma}}_{\boldsymbol{N}}(\mathbf{Y}) \, d\Gamma_Y. \tag{4.23}$$

Integrating with respect to Y instead of X, we obtain the following identities:

$$\begin{aligned}\int_{\Gamma_c} \hat{\boldsymbol{\sigma}}_{\boldsymbol{N}}(\mathbf{X}) \cdot \delta\mathbf{u}(\mathbf{X}) \, d\Gamma_X &= \int_{\Gamma_c} \hat{\boldsymbol{\sigma}}_{\boldsymbol{N}}(\mathbf{Y}) \cdot \delta\mathbf{u}(\mathbf{Y}) \, d\Gamma_Y \\ &= \frac{1}{2}\Big(\int_{\Gamma_c} \hat{\boldsymbol{\sigma}}_{\boldsymbol{N}}(\mathbf{X}) \cdot \delta\mathbf{u}(\mathbf{X}) \, d\Gamma_X + \int_{\Gamma_c} \hat{\boldsymbol{\sigma}}_{\boldsymbol{N}}(\mathbf{Y}) \cdot \delta\mathbf{u}(\mathbf{Y}) \, d\Gamma_Y \Big).\end{aligned}$$

Using (4.23) we get:

$$\int_{\Gamma_c} \hat{\boldsymbol{\sigma}}_{\boldsymbol{N}}(\mathbf{X}) \cdot \delta\mathbf{u}(\mathbf{X}) \, d\Gamma_X = \frac{1}{2} \int_{\Gamma_c} \hat{\boldsymbol{\sigma}}_{\boldsymbol{N}}(\mathbf{X}) \cdot \Big(\delta\mathbf{u}(\mathbf{X}) - \delta\mathbf{u}(\mathbf{Y}) \Big) \, d\Gamma_X.$$

We inject the above expression into (4.22) and get:

$$\mathcal{DJ}(\mathbf{u})[\delta\mathbf{u}] - \frac{1}{2} \int_{\Gamma_c} \hat{\boldsymbol{\sigma}}_{\boldsymbol{N}} \cdot \Big(\delta\mathbf{u}(\mathbf{X}) - \delta\mathbf{u}(\mathbf{Y}) \Big) \, d\Gamma \; = 0, \qquad \forall \delta\mathbf{u} \in \mathbf{V}.$$

Let now $\theta \in \mathbb{R}$ be a fixed parameter that we use to recover different variants of the Nitsche method, as in the linear elastic setting (see, e.g., [CHR15c] and Chapter 3). With the

splitting

$$\begin{aligned}\delta\mathbf{u}(\mathbf{X})-\delta\mathbf{u}(\mathbf{Y}) &= -\frac{1}{\gamma}\Big(\gamma(\delta\mathbf{u}(\mathbf{Y})-\delta\mathbf{u}(\mathbf{X}))+\theta\mathcal{D}\hat{\boldsymbol{\sigma}}_{N}[\delta\mathbf{u}]\Big)+\frac{\theta}{\gamma}\mathcal{D}\hat{\boldsymbol{\sigma}}_{N}[\delta\mathbf{u}]\\ &= -\frac{1}{\gamma}\mathcal{D}\Big(\theta\hat{\boldsymbol{\sigma}}_{N}+\gamma(\mathbf{u}(\mathbf{Y})-\mathbf{u}(\mathbf{X}))\Big)[\delta\mathbf{u}]+\frac{\theta}{\gamma}\mathcal{D}\hat{\boldsymbol{\sigma}}_{N}[\delta\mathbf{u}],\end{aligned}$$

we obtain, for all $\delta\mathbf{u}\in\mathbf{V}$,

$$\mathcal{D}\mathcal{J}(u)[\delta\mathbf{u}]-\frac{1}{2}\int_{\Gamma_c}\frac{\theta}{\gamma}\hat{\boldsymbol{\sigma}}_{N}\cdot\mathcal{D}\hat{\boldsymbol{\sigma}}_{N}[\delta\mathbf{u}]\,d\Gamma+\frac{1}{2}\int_{\Gamma_c}\frac{1}{\gamma}\hat{\boldsymbol{\sigma}}_{N}\cdot\mathcal{D}\Big(\theta\hat{\boldsymbol{\sigma}}_{N}+\gamma(\mathbf{u}(\mathbf{Y})-\mathbf{u}(\mathbf{X}))\Big)[\delta\mathbf{u}]\,d\Gamma=0. \tag{4.24}$$

We inject finally the expression (4.21) into (4.24) and obtain, formally, our Nitsche's based formulation for frictional contact and the ray-tracing strategy:

$$\begin{cases}\mathcal{D}\mathcal{J}(\mathbf{u})[\delta\mathbf{u}]-\dfrac{1}{2}\displaystyle\int_{\Gamma_c}\frac{\theta}{\gamma}\hat{\boldsymbol{\sigma}}_{N}\cdot\mathcal{D}\hat{\boldsymbol{\sigma}}_{N}[\delta\mathbf{u}]\,d\Gamma\\ +\dfrac{1}{2}\displaystyle\int_{\Gamma_c}\frac{1}{\gamma}\boldsymbol{\mathcal{C}}_{\gamma,\mathscr{F}}(\hat{\boldsymbol{\sigma}}_{N},g,\mathbf{v},\mathbf{n}_x)\cdot\mathcal{D}\Big(\theta\hat{\boldsymbol{\sigma}}_{N}+\gamma(\mathbf{u}(\mathbf{Y})-\mathbf{u}(\mathbf{X}))\Big)[\delta\mathbf{u}]\,d\Gamma=0 \quad \forall\,\delta\mathbf{u}\in\mathbf{V}\,.\end{cases} \tag{4.25}$$

The expression of $\mathcal{D}\hat{\boldsymbol{\sigma}}_{N}[\delta\mathbf{u}]$ is provided in Appendix A. Note that, for the numerical solving, when $\theta\neq 0$, the tangent system involves the second order derivative: $\mathcal{D}^2\underline{\hat{\boldsymbol{\sigma}}}(\mathbf{u})[\delta\mathbf{u},\Delta\mathbf{u}]$ (see Section 4.2.3). This emphasizes the interest of the non-symmetric variant $\theta=0$ for which the method is simpler. As in the small strain case ([CHR15c, CMR16]) the interest of the symmetric variant $\theta=1$ consists mostly in its derivation from a potential (see Section 4.2.2) and the symmetry of the tangent problem, while the interest of the skew-symmetric variant $\theta=-1$ is its robustness respectively to the Nitsche parameter γ (see Section 4.3).

Remark 4.2.1. *For projection we decompose $\hat{\boldsymbol{\sigma}}_{N}$ at point $\tilde{\mathbf{y}}$ instead of $\mathbf{x}$ and using the normal $\tilde{\mathbf{n}}_y$. The yielding formulation reads:*

$$\begin{cases}\mathcal{D}\mathcal{J}(\mathbf{u})[\delta\mathbf{u}]-\dfrac{1}{2}\displaystyle\int_{\Gamma_c}\frac{\theta}{\gamma}\hat{\boldsymbol{\sigma}}_{N}\cdot\mathcal{D}\hat{\boldsymbol{\sigma}}_{N}[\delta\mathbf{u}]\,d\Gamma\\ +\dfrac{1}{2}\displaystyle\int_{\Gamma_c}\frac{1}{\gamma}\boldsymbol{\mathcal{C}}_{\gamma,\mathscr{F}}(\hat{\boldsymbol{\sigma}}_{N},\tilde{g},\tilde{\mathbf{v}},\tilde{\mathbf{n}}_y)\cdot\mathcal{D}\Big(\theta\hat{\boldsymbol{\sigma}}_{N}+\gamma(\mathbf{u}(\tilde{\mathbf{Y}})-\mathbf{u}(\tilde{\mathbf{X}}))\Big)[\delta\mathbf{u}]\,d\Gamma=0 \quad \forall\,\delta\mathbf{u}\in\mathbf{V}\,.\end{cases} \tag{4.26}$$

In this case, the derivative of the gap is (according to (4.11)):

$$\mathcal{D}\tilde{g}[\delta\mathbf{u}]=\tilde{\mathbf{n}}_y\cdot(\delta\mathbf{u}(\tilde{\mathbf{X}})-\delta\mathbf{u}(\tilde{\mathbf{Y}})).$$

This results allows us to get a symmetric variant of the Nitsche's formulation in the frictionless case and when $\theta=1$. This variant is similar to the formulation described in

Proposition 4.2.3. When projecting on $\mathbf{n} = -\tilde{\mathbf{n}}_y$*, the method reads indeed:*

$$\begin{cases} \mathcal{D}\mathcal{J}(\mathbf{u})[\delta\mathbf{u}] - \dfrac{1}{2}\displaystyle\int_{\Gamma_c} \frac{1}{\gamma}\hat{\sigma}_n \mathcal{D}\hat{\sigma}_n[\delta\mathbf{u}]\ d\Gamma \\ +\dfrac{1}{2}\displaystyle\int_{\Gamma_c} \frac{1}{\gamma}\Big[\hat{\sigma}_n + \gamma\, g\Big]_{\mathbb{R}^-}\Big(\mathcal{D}\hat{\sigma}_n[\delta\mathbf{u}] + \gamma\mathcal{D}g[\delta\mathbf{u}]\Big)\ d\Gamma\ = 0 \quad \forall\, \delta\mathbf{u} \in \mathbf{V}\,. \end{cases}$$

Remark 4.2.2. *A biased version of our Nitsche's method is obtained by dividing the domain* Ω *into two bodies* Ω^1 *and* Ω^2 *and the contact surface* Γ_c *into a master surface* Γ_c^M *and a slave one* Γ_c^S*. In this case the factor* $\frac{1}{2}$ *disappears when applying the second Newton law because the integration is applied only on the slave surface. In this case the method reads:*

$$\begin{cases} \mathcal{D}\mathcal{J}(\mathbf{u})[\delta\mathbf{u}] - \displaystyle\int_{\Gamma_c^S} \frac{\theta}{\gamma}\hat{\boldsymbol{\sigma}}_{\boldsymbol{N}} \cdot \mathcal{D}\hat{\boldsymbol{\sigma}}_{\boldsymbol{N}}[\delta\mathbf{u}]\ d\Gamma \\ +\displaystyle\int_{\Gamma_c^S} \frac{1}{\gamma}\boldsymbol{\mathcal{C}}_{\gamma,\mathscr{F}}(\hat{\boldsymbol{\sigma}}_{\boldsymbol{N}}, g, \mathbf{v}, \mathbf{n}_x) \cdot \mathcal{D}\Big(\theta\hat{\boldsymbol{\sigma}}_{\boldsymbol{N}} + \gamma(\mathbf{u}(\mathbf{Y}) - \mathbf{u}(\mathbf{X}))\Big)[\delta\mathbf{u}]\ d\Gamma\ = 0 \quad \forall\, \delta\mathbf{u} \in \mathbf{V}. \end{cases} \tag{4.27}$$

4.2.2 Energy potential and symmetric formulation for frictionless contact

In this section, as in Section 3.1.3 for small strain, we show, that, at least formally, a symmetric variant $\theta = 1$ of Nitsche's formulation, close to (4.25), for frictionless contact derives from an energy potential. This result is summarized as:

Proposition 4.2.3. *Let us define the energy potential* $\mathcal{J}_{\mathrm{N}}(\cdot)$ *that takes into account the body deformation as well as non-penetration formulated in a Nitsche's manner:*

$$\mathcal{J}_{\mathrm{N}}(\mathbf{u}) = \mathcal{J}(\mathbf{u}) - \frac{1}{4}\int_{\Gamma_c} \frac{1}{\gamma}\hat{\sigma}_n^2\ d\Gamma\ + \frac{1}{4}\int_{\Gamma_c} \frac{1}{\gamma}[\hat{\sigma}_n + \gamma g]_{\mathbb{R}^-}^2\ d\Gamma\,, \tag{4.28}$$

where $\gamma > 0$ *is the Nitsche's parameter,* $\hat{\sigma}_n$ *is the normal stress in reference configuration (see Section 4.1.3) and* g *is the gap function (see Section 4.1.2). The first-order optimality system associated to* $\mathcal{J}_{\mathrm{N}}(\cdot)$ *reads:*

$$\begin{cases} \mathcal{D}\mathcal{J}(\mathbf{u})[\delta\mathbf{u}] - \dfrac{1}{2}\displaystyle\int_{\Gamma_c} \frac{1}{\gamma}\hat{\sigma}_n \mathcal{D}\hat{\sigma}_n[\delta\mathbf{u}]\ d\Gamma \\ +\dfrac{1}{2}\displaystyle\int_{\Gamma_c} \frac{1}{\gamma}[\hat{\sigma}_n + \gamma g]_{\mathbb{R}^-}\mathcal{D}(\hat{\sigma}_n + \gamma g)[\delta\mathbf{u}]\ d\Gamma\ = 0 \quad \forall\, \delta\mathbf{u} \in \mathbf{V}. \end{cases} \tag{4.29}$$

Proof: Let us write the optimality system associated to $\mathcal{J}_{\mathrm{N}}(\cdot)$:

$$\mathcal{D}\mathcal{J}_{\mathrm{N}}(\mathbf{u})[\delta\mathbf{u}] = \mathcal{D}\mathcal{J}(\mathbf{u})[\delta\mathbf{u}] - \frac{1}{2}\int_{\Gamma_c} \frac{1}{\gamma}\hat{\sigma}_n \mathcal{D}\hat{\sigma}_n[\delta\mathbf{u}]\ d\Gamma + \frac{1}{4}\int_{\Gamma_c} \frac{1}{\gamma}\mathcal{D}[\hat{\sigma}_n + \gamma g]_{\mathbb{R}^-}^2[\delta\mathbf{u}]\ d\Gamma\ = 0 \quad \forall\, \delta\mathbf{u} \in \mathbf{V}.$$

To obtain (4.29) there remains to compute:

$$\begin{aligned}\mathcal{D}[\hat{\sigma}_n+\gamma g]^2_{\mathbb{R}^-}[\delta\mathbf{u}] &= 2[\hat{\sigma}_n+\gamma g]_{\mathbb{R}^-}\mathcal{D}[\hat{\sigma}_n+\gamma g]_{\mathbb{R}^-}[\delta\mathbf{u}]\\ &= 2[\hat{\sigma}_n+\gamma g]_{\mathbb{R}^-}H\big(-(\hat{\sigma}_n+\gamma g)\big)\mathcal{D}\big(\hat{\sigma}_n+\gamma g\big)[\delta\mathbf{u}]\\ &= 2[\hat{\sigma}_n+\gamma g]_{\mathbb{R}^-}\mathcal{D}(\hat{\sigma}_n+\gamma g)[\delta\mathbf{u}],\end{aligned}$$

where we used properties $\mathcal{D}[A(\mathbf{u})]_{\mathbb{R}^-}[\delta\mathbf{u}] = H(-A(\mathbf{u}))\mathcal{D}A(\mathbf{u})[\delta\mathbf{u}]$, for any application $A:\mathbf{u}\mapsto A(\mathbf{u})\in\mathbb{R}$ as well as $H(-x)[x]_{\mathbb{R}^-}=[x]_{\mathbb{R}^-}$ for any $x\in\mathbb{R}$. □

The expression of the derivative $\mathcal{D}\hat{\sigma}_n[\delta\mathbf{u}]$ is detailed in Appendix A while for $\mathcal{D}g[\delta\mathbf{u}]$, we can refer to Section 4.1.2 or [PR15, Section 3] both for ray-tracing and projection techniques.

Remark 4.2.4. *We can introduce $\theta\in\mathbb{R}$, as in section 4.1.3. We only modify slightly system (4.29) as below:*

$$\left\{\begin{array}{l}\mathcal{D}\mathcal{J}(\mathbf{u})[\delta\mathbf{u}]-\dfrac{1}{2}\displaystyle\int_{\Gamma_c}\frac{\theta}{\gamma}\hat{\sigma}_n\mathcal{D}\hat{\sigma}_n[\delta\mathbf{u}]\;d\Gamma\\ +\dfrac{1}{2}\displaystyle\int_{\Gamma_c}\frac{1}{\gamma}[\hat{\sigma}_n+\gamma g]_{\mathbb{R}^-}\mathcal{D}(\theta\hat{\sigma}_n+\gamma g)[\delta\mathbf{u}]\;d\Gamma=0\qquad\forall\,\delta u\in\mathbf{V}\,.\end{array}\right. \tag{4.30}$$

4.2.3 Finite element approximation and tangent system

A standard Galerkin procedure can be applied by choosing a finite element space for the displacement, i.e., $\mathbf{V}_h\subset\mathbf{V}$ to account for any possible Dirichlet condition. We consider in what follows, as in Section 3.1.5, that γ is a positive piecewise constant function on the contact interface Γ_c which satisfies

$$\gamma_{|K\cap\Gamma_c}=\frac{\gamma_0}{h_K},$$

for every element K that has a non-empty intersection of dimension $d-1$ with Γ_c, where h_K is the size of the element K and γ_0 is a positive given constant. Note that the value of γ on element intersections has no influence.

Then, the finite element approximation of System (4.25) reads:

$$\left\{\begin{array}{l}\mathcal{D}\mathcal{J}(\mathbf{u}^h)[\delta\mathbf{u}^h]-\dfrac{1}{2}\displaystyle\int_{\Gamma_c}\frac{\theta}{\gamma}\hat{\boldsymbol{\sigma}}_{\boldsymbol{N}}{}^h\cdot\mathcal{D}\hat{\boldsymbol{\sigma}}_{\boldsymbol{N}}{}^h[\delta\mathbf{u}^h]\;d\Gamma\\ +\dfrac{1}{2}\displaystyle\int_{\Gamma_c}\frac{1}{\gamma}\boldsymbol{\mathcal{C}}_{\gamma,\mathscr{F}}(\hat{\boldsymbol{\sigma}}_{\boldsymbol{N}}{}^h,g,\mathbf{v}^h,\mathbf{n}_x)\cdot\mathcal{D}\Big(\theta\hat{\boldsymbol{\sigma}}_{\boldsymbol{N}}{}^h+\gamma(\mathbf{u}^h(\mathbf{Y})-\mathbf{u}^h(\mathbf{X}))\Big)[\delta\mathbf{u}^h]\;d\Gamma=0\;\forall\,\delta\mathbf{u}^h\in\mathbf{V}_h,\end{array}\right. \tag{4.31}$$

where $\hat{\boldsymbol{\sigma}}_{\boldsymbol{N}}{}^h=\hat{\boldsymbol{\sigma}}_{\boldsymbol{N}}(\mathbf{u}^h)$, $\mathcal{D}\hat{\boldsymbol{\sigma}}_{\boldsymbol{N}}{}^h[\delta\mathbf{u}^h]=\mathcal{D}\hat{\boldsymbol{\sigma}}_{\boldsymbol{N}}(u^h)[\delta\mathbf{u}^h]$ and $\mathbf{v}^h$ is a finite element approximation of the velocity $\mathbf{v}$. The system (4.31) is Lipschitz-continuous with respect to $\mathbf{u}^h$ and piecewise C^1–continuous. This means that it is sufficiently regular to be solved with a generalized Newton method. The tangent system is provided below. Each Newton step

consists in finding $\Delta\mathbf{u}^h$ solution to:

$$\left\{\begin{array}{l}
\mathcal{D}^2\mathcal{J}(\mathbf{u}^h)[\delta\mathbf{u}^h,\Delta\mathbf{u}^h]\\
-\dfrac{1}{2}\displaystyle\int_{\Gamma_c}\frac{\theta}{\gamma}\mathcal{D}\hat{\boldsymbol{\sigma}}_{\boldsymbol{N}}{}^h[\Delta\mathbf{u}^h]\cdot\mathcal{D}\hat{\boldsymbol{\sigma}}_{\boldsymbol{N}}{}^h[\delta\mathbf{u}^h]\;d\Gamma\;-\frac{1}{2}\displaystyle\int_{\Gamma_c}\frac{\theta}{\gamma}\hat{\boldsymbol{\sigma}}_{\boldsymbol{N}}{}^h\cdot\mathcal{D}^2\hat{\boldsymbol{\sigma}}_{\boldsymbol{N}}{}^h[\delta\mathbf{u}^h,\Delta\mathbf{u}^h]\;d\Gamma\\
+\dfrac{1}{2}\displaystyle\int_{\Gamma_c}\frac{1}{\gamma}\Big(\partial_\sigma\boldsymbol{\mathcal{C}}_{\gamma,\mathscr{F}}\;\mathcal{D}\hat{\boldsymbol{\sigma}}_{\boldsymbol{N}}{}^h[\Delta\mathbf{u}^h]+\partial_g\boldsymbol{\mathcal{C}}_{\gamma,\mathscr{F}}\;\mathcal{D}g[\Delta\mathbf{u}^h]+\partial_{\mathbf{v}}\boldsymbol{\mathcal{C}}_{\gamma,\mathscr{F}}\;\mathcal{D}\mathbf{v}^h[\Delta\mathbf{u}^h]\\
+\partial_{\mathbf{n}}\boldsymbol{\mathcal{C}}_{\gamma,\mathscr{F}}\;\mathcal{D}\mathbf{n}_x[\Delta\mathbf{u}^h]\Big)\cdot\mathcal{D}\Big(\theta\hat{\boldsymbol{\sigma}}_{\boldsymbol{N}}{}^h+\gamma(\mathbf{u}^h(\mathbf{Y})-\mathbf{u}^h(\mathbf{X}))\Big)[\delta\mathbf{u}^h]\;d\Gamma\\
+\dfrac{1}{2}\displaystyle\int_{\Gamma_c}\frac{1}{\gamma}\boldsymbol{\mathcal{C}}_{\gamma,\mathscr{F}}(\hat{\boldsymbol{\sigma}}_{\boldsymbol{N}}{}^h,g,\mathbf{v}^h,\mathbf{n}_x)\cdot\Big(\theta\mathcal{D}^2\hat{\boldsymbol{\sigma}}_{\boldsymbol{N}}{}^h[\delta\mathbf{u}^h,\Delta\mathbf{u}^h]+\gamma\nabla_X\delta\mathbf{u}^h(\mathbf{Y})\,\mathcal{D}\mathbf{Y}[\Delta\mathbf{u}^h]\Big)\;d\Gamma\\
=-\mathcal{D}\mathcal{J}(\mathbf{u}^h)[\delta\mathbf{u}^h]+\dfrac{1}{2}\displaystyle\int_{\Gamma_c}\frac{\theta}{\gamma}\hat{\boldsymbol{\sigma}}_{\boldsymbol{N}}{}^h\cdot\mathcal{D}\hat{\boldsymbol{\sigma}}_{\boldsymbol{N}}{}^h[\delta\mathbf{u}^h]\;d\Gamma\\
-\dfrac{1}{2}\displaystyle\int_{\Gamma_c}\frac{1}{\gamma}\boldsymbol{\mathcal{C}}_{\gamma,\mathscr{F}}(\hat{\boldsymbol{\sigma}}_{\boldsymbol{N}}{}^h,g,\mathbf{v}^h,\mathbf{n}_x)\cdot\mathcal{D}\Big(\theta\hat{\boldsymbol{\sigma}}_{\boldsymbol{N}}{}^h+\gamma(\mathbf{u}^h(\mathbf{Y})-\mathbf{u}^h(\mathbf{X}))\Big)[\delta\mathbf{u}^h]\;d\Gamma\qquad\forall\,\delta\mathbf{u}^h\in\mathbf{V}_h,
\end{array}\right.\tag{4.32}$$

where $\mathcal{D}^2\mathcal{J}(\mathbf{u}^h)[\delta\mathbf{u}^h,\Delta\mathbf{u}^h]$ is the second directional derivative of $\mathcal{J}(\mathbf{u}^h)$. From (2.13) the derivative $\mathcal{D}\mathbf{v}^{\mathrm{h}}[\Delta\mathbf{u}^h]$ can be evaluated as:

$$\mathcal{D}\mathbf{v}^{\mathrm{h}}[\Delta\mathbf{u}^h]=\frac{1}{\Delta t}\left(\underline{\underline{\mathbf{F}}}_{\mathbf{Y}_0}\,\mathcal{D}\mathbf{Y}[\Delta\mathbf{u}^h]-\mathcal{D}g[\Delta\mathbf{u}^h]\,\mathbf{n}_0\right),\tag{4.33}$$

where $\underline{\underline{\mathbf{F}}}_{\mathbf{Y}_0}$ is the deformation gradient at the previous time-step, evaluated at point $\mathbf{Y}$. All partial derivatives $\partial_\sigma\boldsymbol{\mathcal{C}}$, $\partial_g\boldsymbol{\mathcal{C}}$, $\partial_{\mathbf{v}}\boldsymbol{\mathcal{C}}$ and $\partial_n\boldsymbol{\mathcal{C}}$ of the function $\boldsymbol{\mathcal{C}}$ are provided in Appendix B.

For the ray-tracing strategy, we refer to section 4.1.2 and [PR15] for the exact expression of $\mathcal{D}g[\Delta\mathbf{u}^h]$, $\mathcal{D}\mathbf{n}_x[\Delta\mathbf{u}^h]$ and and $\mathcal{D}\mathbf{Y}[\Delta\mathbf{u}^h]$.

For the projection strategy, the tangent system is the same, replacing $\mathbf{n}_x$ by $\tilde{\mathbf{n}}_y$. In this case $\mathcal{D}\tilde{g}[\Delta\mathbf{u}^h]$ is simple to compute but the expression of $\mathcal{D}\tilde{\mathbf{n}}_y[\Delta\mathbf{u}^h]$ is quite intricated. Therefore we neglect this term in the tangent system and in the expression of $\mathcal{D}\tilde{\mathbf{Y}}[\Delta\mathbf{u}^h]$. Using (4.2) $\mathcal{D}\tilde{\mathbf{y}}[\delta\mathbf{u}]$ reads:

$$\mathcal{D}\tilde{\mathbf{y}}[\delta\mathbf{u}]=\delta\mathbf{u}(\tilde{\mathbf{X}})-\mathcal{D}g[\delta\mathbf{u}]\;\tilde{\mathbf{n}}_y-g\;\mathcal{D}\tilde{\mathbf{n}}_y[\delta\mathbf{u}]\simeq\delta\mathbf{u}(\tilde{\mathbf{X}})-\mathcal{D}\tilde{g}[\delta\mathbf{u}]\;\tilde{\mathbf{n}}_y\,.$$

Moreover, using(4.11), (4.6) and neglecting $\mathcal{D}\tilde{\mathbf{n}}_y[\delta\mathbf{u}]$, we can take:

$$\mathcal{D}\tilde{\mathbf{Y}}[\delta\mathbf{u}]\simeq\underline{\underline{\mathbf{F}}}_{\tilde{\mathbf{Y}}}^{-1}\;(\underline{\underline{\mathbf{I}}}-\tilde{\mathbf{n}}_y\otimes\tilde{\mathbf{n}}_y)\left(\delta\mathbf{u}(\tilde{\mathbf{X}})-\delta\mathbf{u}(\tilde{\mathbf{Y}})\right)\,.\tag{4.34}$$

Remark 4.2.5. *For the non-symmetric variant $\theta=0$, the tangent system can be sub-*

stantially simplified as:

$$\left\{\begin{array}{l}\mathcal{D}^2\mathcal{J}(\mathbf{u}^h)[\delta\mathbf{u}^h,\Delta\mathbf{u}^h]\\ +\frac{1}{2}\displaystyle\int_{\Gamma_c}\Big(\partial_\sigma\boldsymbol{\mathcal{C}}_{\gamma,\mathscr{F}}\ \mathcal{D}\hat{\boldsymbol{\sigma}}_{\boldsymbol{N}}{}^h[\Delta\mathbf{u}^h]+\partial_g\boldsymbol{\mathcal{C}}_{\gamma,\mathscr{F}}\ \mathcal{D}g[\Delta\mathbf{u}^h]+\partial_{\mathbf{v}}\boldsymbol{\mathcal{C}}_{\gamma,\mathscr{F}}\ \mathcal{D}\mathbf{v}^h[\Delta\mathbf{u}^h]+\partial_{\mathbf{n}}\boldsymbol{\mathcal{C}}_{\gamma,\mathscr{F}}\ \mathcal{D}\mathbf{n}_x[\Delta\mathbf{u}^h]\Big)\\ \qquad\cdot\Big(\delta\mathbf{u}^h(\mathbf{Y})-\delta\mathbf{u}^h(\mathbf{X})\Big)\ d\Gamma+\frac{1}{2}\displaystyle\int_{\Gamma_c}\boldsymbol{\mathcal{C}}_{\gamma,\mathscr{F}}(\hat{\boldsymbol{\sigma}}_{\boldsymbol{N}}{}^h,g,\mathbf{v}^h,\mathbf{n}_x)\cdot\Big(\nabla_X\delta\mathbf{u}^h(\mathbf{Y})\,\mathcal{D}\mathbf{Y}[\Delta\mathbf{u}^h]\Big)\ d\Gamma\\ =-\mathcal{D}\mathcal{J}(\mathbf{u}^h)[\delta\mathbf{u}^h]-\frac{1}{2}\displaystyle\int_{\Gamma_c}\boldsymbol{\mathcal{C}}_{\gamma,\mathscr{F}}(\hat{\boldsymbol{\sigma}}_{\boldsymbol{N}}{}^h,g,\mathbf{v}^h,\mathbf{n}_x)\cdot\Big(\delta\mathbf{u}^h(\mathbf{Y})-\delta\mathbf{u}^h(\mathbf{X}))\Big)\ d\Gamma\quad\forall\,\delta\mathbf{u}^h\in\mathbf{V}_h.\end{array}\right.\tag{4.35}$$

4.3 Numerical tests and validation

Formulation (4.31) has been implemented in our open-source finite element library GetFEM++ (see http://getfem.org/). It corresponds to solving System (4.32) within a (semi–smooth) Newton loop. We test and compare both unbiased and biased versions, as well as variants corresponding to different values of $\theta=-1,0,1$. Except in Section 4.3.6, the mapping strategy used is always the ray-tracing.

As a first example, the simulation of a two-dimensional patch test with non-matching meshes allows to check the capability of the formulation to exactly transmit constant normal stresses between two contacting surfaces, regardless of their discretization. With this first example, we provide numerical evidence that element-based integration leads to acceptable accuracy, provided enough Gauss points are used. So we keep this choice for the remaining numerical tests, following [FW05] and [PR15]. For the unbiased version of the method, in each contact boundary Γ_c^i, we use the corresponding Gauss rule to evaluate the contact intgral. The second test is the two-dimensional Hertz contact problem that assesses the capability of the approximation to capture a known contact pressure profile in a restricted contact area with non-matching meshes. Further two-dimensional examples are classic problems found in the large sliding contact literature and aim at testing the performance of the proposed method. Finally, simulation of contact between two hollow cylindrical tubes, including self-contact, is presented in order to evaluate the performance of the method in three dimensions and for the self-contact case. In reference [PR15] the projection and the ray-tracing strategies are presented with a general discussion. We complement here this discussion with a numerical comparison between the two mapping strategies.

4.3.1 Taylor patch test

The patch test originally proposed in [TP91], investigates the ability of contact formulations to exactly transmit constant normal tractions between two contacting surfaces, regardless of their discretization. However, note that a patch test does not provide any information about the stability of an algorithm and and is not relevant when considering contact between deformable and rigid bodies. In this section we compare the obtained

error with element-based and segment-based quadrature. Among available patch tests, we choose the one depicted in Figure 4.4, that is similar to the test used in [Cri00] and [Hil00]. An elastic body rests on a smooth elastic foundation having the same dimensions. A uniform distributed load $p = 10$ KPa is applied on the upper surface of the solid. A two dimensional plain strain analysis is considered with a Saint Venant-Kirchhoff material. Corresponding elastic parameters are: $E = 2 \cdot 10^5$ MPa and $\nu = 0.3$. Frictionless contact is considered. We compare the performance of our Nitsche-based method with some other

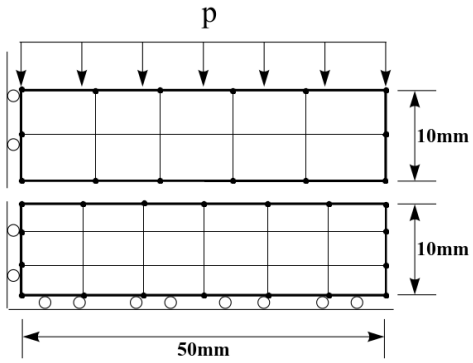

Figure 4.4: Taylor patch test configuration.

discretizations of contact. The transferred contact stress is measured on the lower contact surface. We compare the obtained pressure profile with those computed using a simple nodal (node-to-segment) approximation, with an integral augmented lagrangian method (see [PR15]) as well as a mortar method (see [TFW09, PL04a]). For Nitsche's method, we compare biased and unbiased versions. For the biased method, as well as for other contact methods, the slave surface is the upper one. The parameters for Nitsche's method are: $\theta = 0$ and $\gamma_0 = 100E$. At first, we perform the test with a subdivision of the quadrature method according to the elements intersections (segment-based integration). The maximum relative stress errors for different methods is shown in Table 4.1 with 4 integration points per element and Lagrange $\mathbb{Q}_2$ elements. All of Nitsche's methods, augmented Lagrangian and mortar ones produce a resulting axial stress exactly satisfied to more than ten decimal places and a zero penetration up to the truncation error. As expected the nodal method results in a much higher error.

Approximation method	Biased Nitsche	Unbiased Nitsche	Augmented Lag	Mortar	Nodal
Max pressure relative error	$7.5 \cdot 10^{-12}$	$3.7 \cdot 10^{-12}$	$8.8 \cdot 10^{-9}$	$1.7 \cdot 10^{-13}$	$1.1 \cdot 10^{-1}$
Max gap(mm)	$-8.5 \cdot 10^{-16}$	$-6.4 \cdot 10^{-16}$	$-2.5 \cdot 10^{-12}$	$-6.5 \cdot 10^{-19}$	$-9 \cdot 10^{-6}$

Table 4.1: Maximum of contact pressure relative error and gap for segment-based integration.

If, now, performing same measures using the Gauss integration rule without cutting (element-base integration) we get the following results:

Approximation method	Biased Nitsche	Unbiased Nitsche	Augmented Lag	Mortar	Nodal
Max pressure relative error	$6.3 \cdot 10^{-3}$	$9.6 \cdot 10^{-3}$	$7.6 \cdot 10^{-3}$	$7.4 \cdot 10^{-3}$	$8.9 \cdot 10^{-2}$
Max gap(mm)	$-2.6 \cdot 10^{-7}$	$-2.9 \cdot 10^{-7}$	$-3.9 \cdot 10^{-6}$	$-3.9 \cdot 10^{-6}$	$-7.6 \cdot 10^{-6}$

Table 4.2: Maximum of contact pressure relative error and gap for element-based integration.

It is clear that segment-based integration is more precise and using element based integration technique generates a quadrature error. But this error remains still very small and can be considered acceptable in practice and it vanishes when refining the integration method (see Table 4.3). We observe from Table 4.2 that, despite the coarse mesh and the use of only 4 integration points per segment, the rate of quadrature error is low for Nitsche's method in its two versions. For both versions the accuracy is comparable even though the biased method seems to generate a lower error since the integration is performed only on one surface for this variant. Remark that changing the integration method does not affect the nodal method. The augmented lagrangian integral method and the mortar method have almost the same accuracy.

Approximation method	Biased Nitsche	Unbiased Nitsche	Augmented Lag	Mortar	Nodal
Max pressure relative error	$1.7 \cdot 10^{-3}$	$2.2 \cdot 10^{-3}$	$0.6 \cdot 10^{-3}$	$0.6 \cdot 10^{-3}$	$9.7 \cdot 10^{-2}$
Max gap(mm)	$-0.7 \cdot 10^{-7}$	$-1.5 \cdot 10^{-7}$	$-1.6 \cdot 10^{-6}$	$-1.6 \cdot 10^{-6}$	$-7.5 \cdot 10^{-6}$

Table 4.3: Maximum of contact pressure relative error and gap for element-based integration and a finer inegration rule (8 integration points).

In Table 4.3, we use the element based integration with 8 Gauss points per segment. The results show that for all integral formulations the integration error decreases significantly when refining numerical integration.

4.3.2 Hertz contact

We consider the case of a half-disc of radius R = 10 mm pressed onto a plane elastic foundation. For the sake of simplicity, we consider a material law of Saint-Venant-Kirchhoff type. The elastic modulus is $E = 10^5$ MPa, and the Poisson ratio is set to $\nu = 0.3$ for both bodies. The half-disc's top side is clamped and lowered vertically. For all the tests we compare the approximated solution to the Hertz one for a small rate of loading going from 0 to 0.5 mm in ten steps equally spaced. The tests were performed with both Lagrange linear and quadratic triangular finite elements and non matching interface meshes. The test is performed first with $\gamma_0 = E$, $\theta = 0$ and the unbiased variant.
The diagrams in Figure 4.5 correspond to the pressure profiles at the 10th load-step obtained with two and three quadrature points per element while Figure 4.6 corresponds to

the penetration error measured on the contact surface (in mm) when taking 3 integration points per element. Figure 4.6 allow to measure and locate the penetration on the contact surface with the proposed weak imposition of contact constraints. The vertical red arrows in Figure 4.5 correspond to values of the contact pressure field at quadrature points. The blue line represents the analytically calculated Hertz's pressure profile for the corresponding normal load obtained in the simulation. In both figures, diagrams in the left column correspond to a linear approximation of the displacement while the results in the right column refer to a quadratic one.

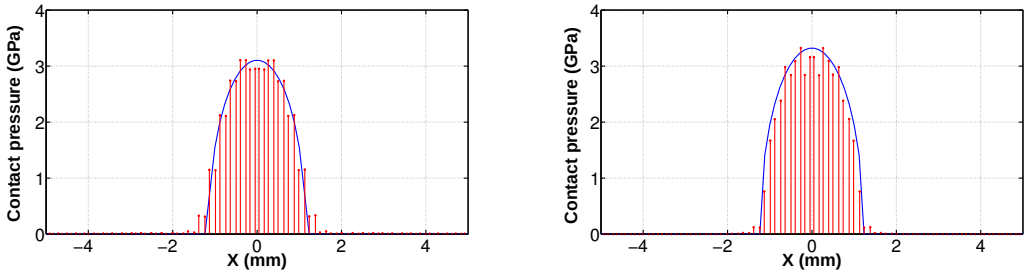

(a) Linear approximation (2 integration points) (b) Quadratic approximation (2 integration points)

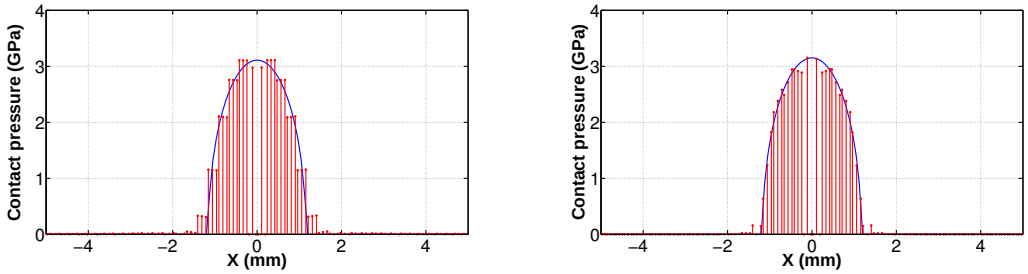

(c) Linear approximation (3 integration points) (d) Quadratic approximation (3 integration points)

Figure 4.5: Contact pressure for Hertz problem with unbiased Nitsche's method.

A first observation is that the method approximates well the Hertz solution: the exact pressure profile is reproduced and no problem is encountered with the release of the nodes for inactive contact elements. For linear approximation, two quadrature points per element edge appear to be sufficient for numerical integration whereas 3 points allow a better accuracy for the quadratic approximation. The linear approximation is accurate only for a sufficiently fine mesh because the pressure profile is not linear along the contact surface.

Figure 4.6 shows that the measured penetration is very low with linear and quadratic elements: less than 0.4% of the element size. To better see the convergence of this error when refining the mesh, we plot on Figure 4.7 the evolution of the measured penetration norm with the mesh size for Lagrange quadratic elements. This curve shows clearly that

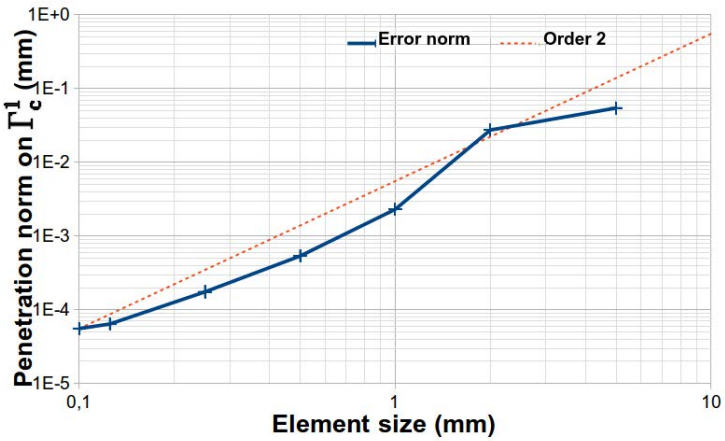

Figure 4.7: Evolution of gap error norm along Γ_c^1 with elements size.

the gap error vanishes by refining the mesh. The order of convergence is approximately 2 in L^2-norm. Increasing the approximation order reduces as well the gap error.

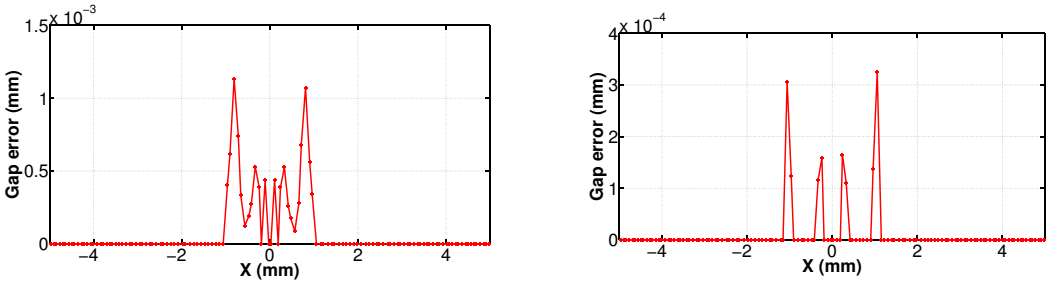

(a) Linear approximation

(b) Quadratic approximation

Figure 4.6: Gap error for Hertz problem with 3 integration points per element and unbiased Nitsche's method.

The solution of this problem depends on Nitsche's parameter γ in the sense that similarly to the small strain case studied in [CHR15c, CMR16] the convergence of the method is influenced by the parameter γ_0 and this dependency differs for different values of θ. We provide in Table 4.4 the average (along the loading steps) of the pressure error and of the required Newton iterations yielding convergence with a maximum of 50 iterations for all steps, for different values of γ_0 and θ. The test is performed for Lagrange quadratic triangular elements, with and without friction.

Frictionless				Friction coefficient $\mathscr{F} = 0.3$			
Value of θ	Nitsche's parameter γ_0	Newton's iterations	Average contact pressure error (in %)	Value of θ	Nitsche's parameter γ_0	Newton's iterations	Average contact pressure error(in %)
0	$\frac{E}{100}$	7.24	17	0	$\frac{E}{100}$	8.5	14.4
	E	3.5	2.4		E	4.6	2.4
	$100 \cdot E$	4.6	2.7		$100 \cdot E$	20.7	6.8
-1	$\frac{E}{100}$	4.8	3.7	-1	$\frac{E}{100}$	5.3	3.3
	E	4.3	3.0		E	4.3	3.1
	$100 \cdot E$	4.6	4.1		$100 \cdot E$	9.2	4
1	$\frac{E}{100}$	14.8	54.8	1	$\frac{E}{100}$	29.8	59
	E	26.8	52.2		E	30	64
	$100 \cdot E$	4	4.2		$100 \cdot E$	11.2	4.1

Table 4.4: Average of contact pressure error and number of Newton's iterations for Hertz contact.

As for small strain [CHR15c, CMR16] the influence of Nitsche's parameter γ_0 depends on θ. It is remarkable that the skew-symmetric version $\theta = -1$ remains the most robust one and converges whatever is the value of γ_0. In this case the obtained pressure profile approximates well the theoretical one. This is also observed in [CHR15c] for small deformations and a mathematical proof is provided in that case. The symmetric version $\theta = 1$ is the most sensitive one and it converges only when γ_0 is large enough. Comparing $\theta = 0$ to $\theta = 1$, we remark that the simple version $\theta = 0$ is more robust regarding γ_0 since it converges for a wider range of values for γ_0. Nevertheless, convergence is lost when γ_0 becomes too small. The same behavior is observed in the frictional case. Additionally let us mention that when γ_0 is very large, convergence of the Newton algorithm is more difficult to achieve, especially for frictional contact. This is related to the fact that, when taking γ_0 too large, the problem becomes stiff and ill-conditioned (see, e.g., [Ren13]).

Remark 4.3.1. *Note that a recent attempt has been made to adapt a penalty-free Nitsche method originally analyzed in [Bur12] to the Signorini problem (see [BHL16a]). However it does not correspond to the case $\gamma_0 = 0$ and there remains an additional numerical parameter, conversely to the case of Dirichlet boundary conditions which is parameter-free.*

4.3.3 Shallow ironing

The third numerical example to be presented is the so-called shallow ironing test. An indenter with a circular arc shaped bottom edge is pressed against an elastic block and is forced to slide along the block length. This example can also be found for instance in [FW06, HOW+09, TFW09, PR15]. In this test we investigate the transmission of the force in vertical and horizontal directions when the contact surface evolves. We compare essentially the frictionless and the frictional case to test the accuracy of method when approximating a friction problem. Figure 4.8 shows the initial geometry with the different dimensions in mm. For the two contacting bodies a neo-Hookean material behavior is considered, with Young's moduli equal to $68.96 \cdot 10^8$ MPa and $68.96 \cdot 10^7$ MPa for the indenter and the block, respectively, and Poisson's ratio of 0.32 for both parts. The considered two-dimensional system is solved under the plane strain assumption. As in [PR15], we consider a quasi-static load. For $t \in [0, 1]$, a vertical displacement of 1 mm is performed in 10 steps. Then, when $t \in [1, 2]$, we perform an horizontal displacement along the block in 500 equal steps, each of 0.02 mm. The three computed deformed configurations are presented in Figure 4.8 with a plot of the Von-Mises stress distribution, which demonstrate the finite deformations involved in the ironing process. This result and the curves of Figure 4.9 correspond to a friction coefficient $\mathscr{F} = 0.3$ and quadratic rectangular finite elements. We use the simple version of the method ($\theta = 0$) and three quadrature points per segment for numerical integration. Since the material parameters of the two bodies are different, we consider, for the unbiased version, two different Nitsche's parameters $\gamma_0^i = E^i$.

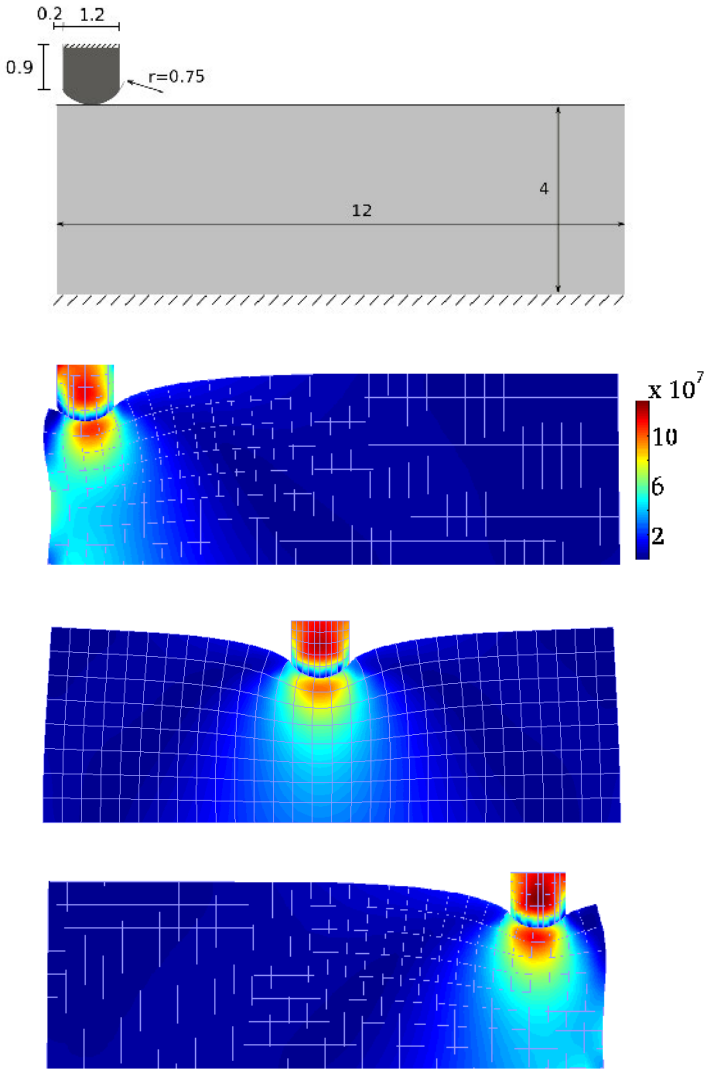

Figure 4.8: Initial geometry and deformed configuration of the shallow ironing example with contour plot of the Von-Mises stress in the frictionless case, at $t = 1$, $t = 1.5$ and $t = 2$.

Figure 4.9 shows the evolution of the total horizontal and vertical force components between the contacting bodies during the whole simulation. During the first phase of pressing the indenter into the slab, the curves are smooth and the two bodies stick together. Starting the horizontal movement, the vertical as well as the horizontal reaction forces increase a bit until a limit is reached. At this stage the block starts sliding over the slab. An oscillation is observed for the vertical and horizontal reaction forces. This oscillation decreases when refining the mesh. This is due to the fact that the finite element mesh of the block has to slip around the right corner of the indenting body. Note however that these observed oscillations for vertical and horizontal force, even with only three quadrature points, remain still small, compared to similar results presented in [FW06]. Comparing the results of the present study with those reported in [PR15, FW06], one

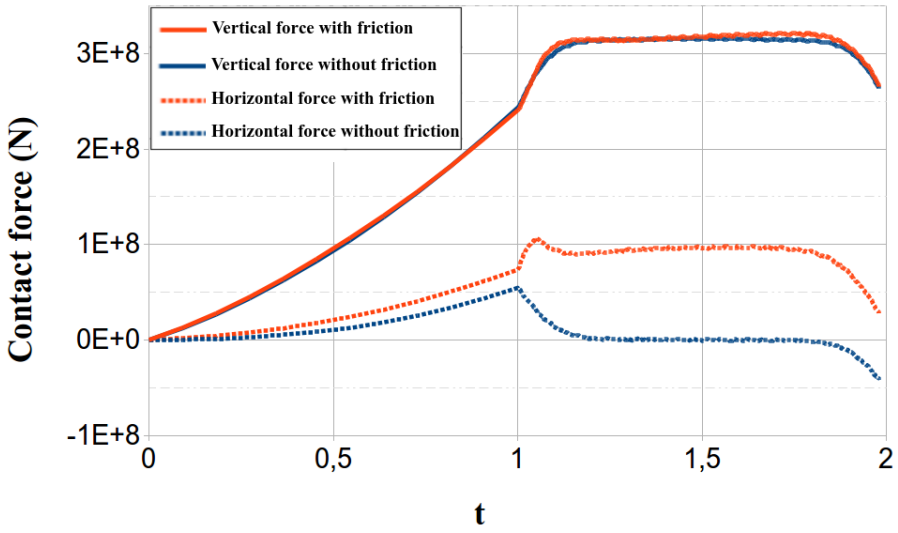

Figure 4.9: Evolution of the vertical and horizontal components of the contact forces for shallow ironing.

can note that the qualitative behavior is very well captured. The results are close to those obtained in [PR15] but there are important quantitative differences with [FW06]. The vertical force in Figure 4.9 is slightly lower than in [FW06], while the reported horizontal force is significantly lower compared to the aforementioned reference. At time 1.5 s for example, the ratio between the horizontal and vertical force can be estimated to 0.53, based on the results reported in [FW06] and 0.304 according to [PR15]. The obtained ratio with our Nitsche's unbiased method is 0.3014, which is very close to the result of [PR15] and [TFW09] where an integral augmented mixed method and a mrotar one are respectively used. The contact stress distribution is in agreement with common understanding of system mechanics and if we calculate the angle between the resulting stress vector along the contact surface at $t = 1.5$ and the resulting surface normal, we get 15.36°. This appears to be very close to the friction angle of 16.7° corresponding to the given coefficient of friction of 0.3. For the frictionless case, a zero horizontal force is predicted correctly for the symmetric position at $t = 1.5$, and it goes for negative values near the edge.

4.3.4 Contact of an elastic half-ring

In the fourth example, contact between an elastic ring undergoing large deformations and an elastic block is considered. As in reference [FW05, TFW09], both parts are assumed to exhibit neo-Hookean material behavior with Poisson's ratio equal to 0.3. As introduced in [TFW09], in this test, the elastic half-ring is assembled from outer and inner rings with the same thickness of 5 mm. The outer ring has a Young modulus of 10^3 MPa and the inner one is assumed to be 100 times stiffer. The Young modulus is of 300 MPa for the block. The inner radius of the half-ring is equal to 90 mm. The block is 260 mm long and 50 mm high. The rectangular block is fixed at its bottom edge, while the ends of the half-ring

are horizontally fixed and vertically displaced by a total distance of 70 mm in 140 steps of size 0.5 mm. Figure 4.10 shows the initial geometry and four deformed configurations at different time-steps. The deformations are obtained without and with friction coefficient $\mathscr{F} = 0.5$. The coarsest mesh used in the calculations is made of 64 elements along the ring circumference and 1 element across each ring layer, while the block is discretized with 52 by 10 quadrilateral elements, in length and height directions respectively. On each body, Nitsche parameter will be equal to its Young modulus: $\gamma_{0_R} = E_{\text{Rext}}$, $\gamma_{0_B} = E_{\text{B}}$. We consider the version $\theta = 0$.

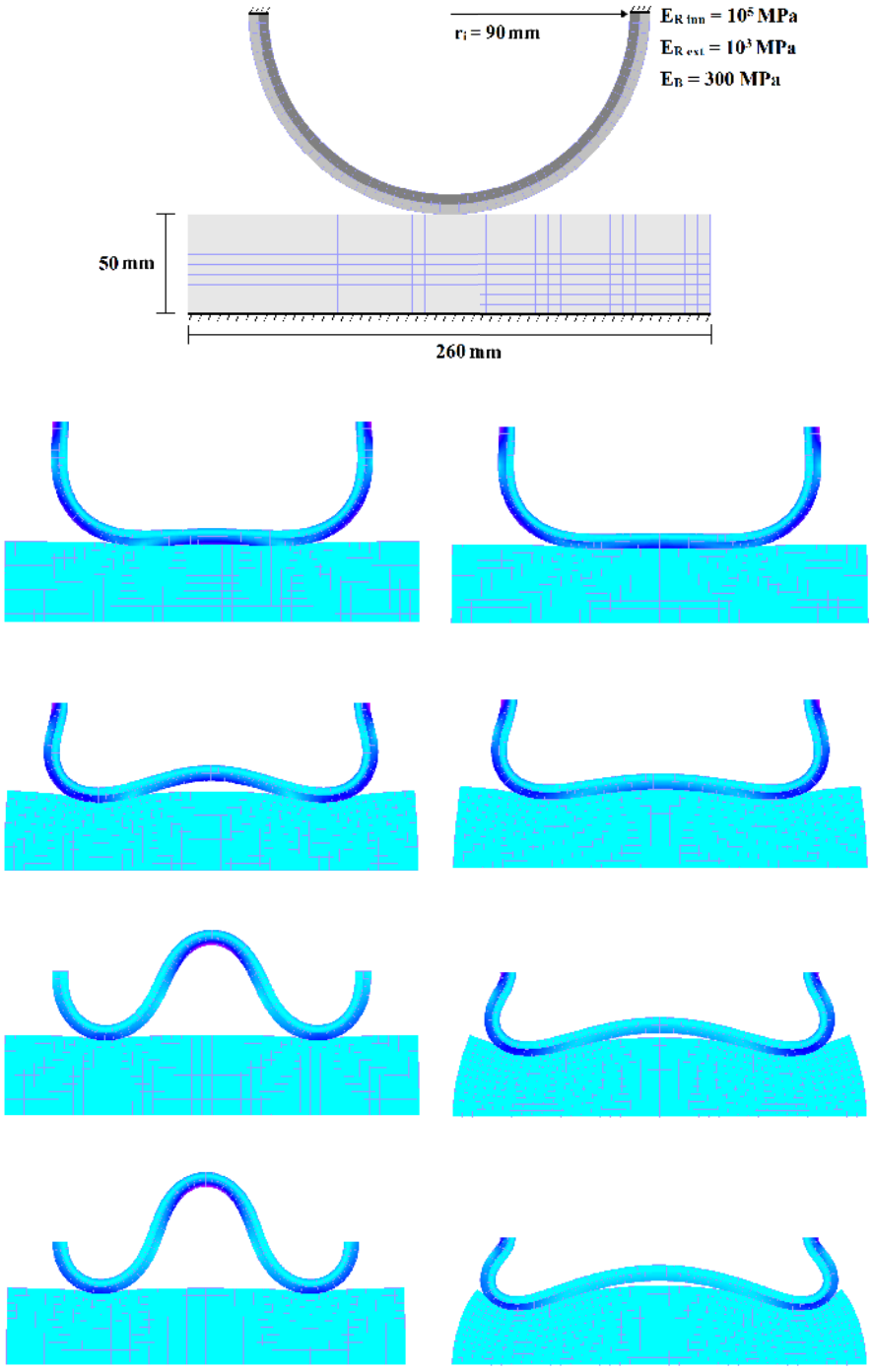

Figure 4.10: Deformation of the elastic half ring without friction (left) and with $\mathscr{F} = 0.5$ (right) for $\mathbb{Q}_2$ elements, after a loading of 25, 45, 60 and 70 mm.

This example allows us to test the accuracy of the Nitsche method in the case of heterogeneous materials and high friction forces. To compare the computed deformation with previous results from other methods, we measure the vertical displacement of the ring's mid-point. This displacement along the load steps is plotted in Figure 4.11, both

for frictionless and frictional contact.

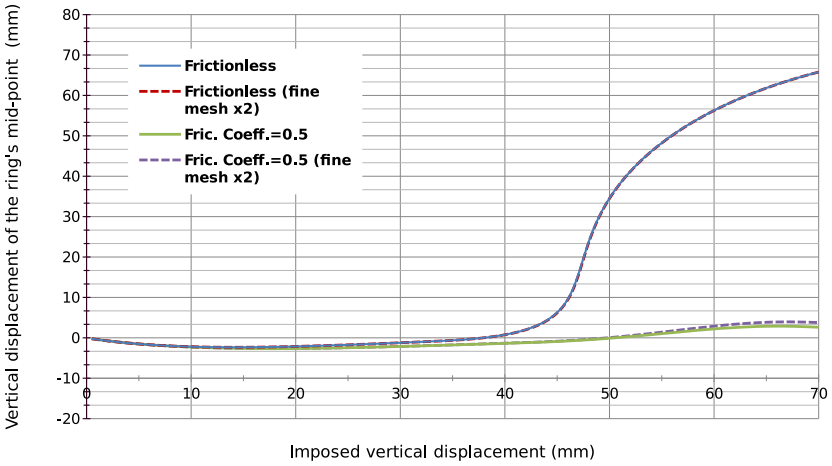

Figure 4.11: Vertical displacement of the half-ring middle point for different mesh sizes.

Figure 4.10 shows that the loaded half-ring compresses initially the elastic block on its central contact surface, as expected. At this stage the frictional and frictionless cases are quite similar and the central mid-point of the half-ring moves downwards. This is observable on Figure 4.11 until an amount of imposed displacement of 20 to 25mm is reached. This corresponds to the first deformed configuration in Figure 4.10. Subsequently, the tracked point is lifted progressively until 45mm of displacement. Then, in the interval between 45mm and 60mm , the lifting speed of the half-ring middle point peaks in absence of friction when it remains low in the frictional case because of extensive sliding between the ring and the block. In the remaining part of the simulation the tracked point keep on moving up, but with a lower speed in both cases. The results with coarse and refined meshes are very similar for the frictionless case, and also for the frictional one but only until 50 mm of displacement. In the last 20 mms of the simulation, a remarkable difference between the two approximations is observed, when considering friction. This could be due to the important sliding forces since we do not get that error in the frictionless case. As for Hertzian contact, Nitsche's parameter γ_0 needs to be large enough for stability and convergence, but when it is too large the problem stiffens: some elements are inverted and convergence is difficult to achieve. The optimal values of γ_0 on each material are those near its Young modulus E. For $\gamma_0 = E$ we obtain an average of Newton's iterations of 4.45 for frictionless contact and 4.44 for frictional contact. With a fine mesh the convergence speed is similar with a slight difference for the frictional case since the average in that case is 5.05.

To test the method with large contrast of stiffness between the contacting bodies, we measure the average of Newton's iterations with different values of the ratio $E_{\text{Rext}}/E_{\text{B}}$ in the frictional case. The Young modulus of the inner ring is constant ($=10^5$ MPa) and as for previous tests, Nitsche's parameter is equal to the Young modulus on each body.

$E_{\text{Rext}}/E_{\text{B}}$	10^{-5}	10^{-3}	10^{-2}	10^{-1}	1	10	10^{2}	10^{3}
Average of Newton's iterations	No convergence	6,43	6,07	6,35	7,66	6,36	5,73	No convergence

Table 4.5: Average of Newton's iterations with different values of $E_{\text{Rext}}/E_{\text{B}}$.

We observe that a large difference of stiffness does not influence the accuracy of the unbiased method. The convergence is obtained with a close number of iterations for different values of the stiffness ratio. We loose convergence only when going to extreme values because, when the block is too much flabby, some elements are inverted; and when it is too rigid the problem becomes stiff and ill-conditioned.

4.3.5 Crossed Tubes with self-contact

The last numerical example is the crossed tubes test. In this example we simulate contact between two crossed hollow elastic cylinders. Each of the tubes has an outer diameter of 24 mm, a wall thickness equal to 0.8 mm and a length equal to 100 mm. Neo-Hookean material behavior is considered for both tubes, with material parameters corresponding to Poisson's ratio equal to 0.3 and Young moduli of $E_1 = 10^5$ MPa for the lower tube and $E_2 = 10^4$ MPa for the upper one. The tubes are forced into contact through Dirichlet conditions applied at their ends. The upper tube is displaced vertically for a total distance of 40 mm divided into 80 equal load steps. Since the enforced displacement is large, the deformations of the tubes are large and we observe a self-contact configuration on the less rigid tube. So this test allows us to validate our method in case of self-contact. Since the geometry as well as the boundary conditions are symmetric, it is sufficient to model only one quarter of the considered structure. The actually modeled portion of each tube is colored in Figure 4.12 and it is discretized using 16 by 24 by 2 three-dimensional elements in the length, circumferential and radial directions respectively.

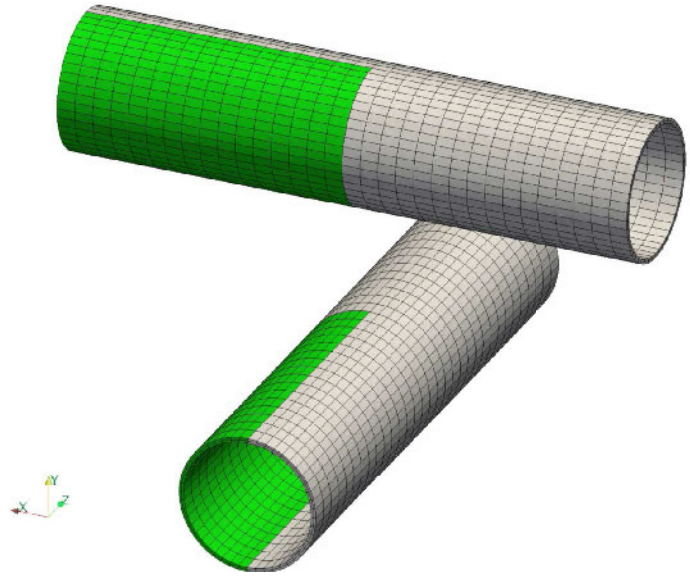

Figure 4.12: Geometry and mesh of the crossed tubes in their initial configuration.

The presented solution is based on an approximation of the geometry and of the displacement with quadratic hexahedral elements. The unbiased Nitsche method with $\theta = 0$ is considered to deal with self-contact. The results of Figure 4.13 correspond to the frictionless case with a Nitsche's parameter $\gamma_0 = E_1$ for the lower tube and $\gamma_0 = E_2$ for the upper one. Figure 4.13 depicts the calculated deformed configurations for the 30th, 60th and 80th load steps. Figure 4.14 shows the evolution along the loading steps of required Newton's iterations for the frictionless case and for a friction coefficient $\mathscr{F} = 0.3$. Despite the increase of the required iterations when self-contact occurs, Newton's algorithm converges in general within a few iterations. The required iterations number for convergence increases from the 45th load step. This is due to the onset of self-contact.

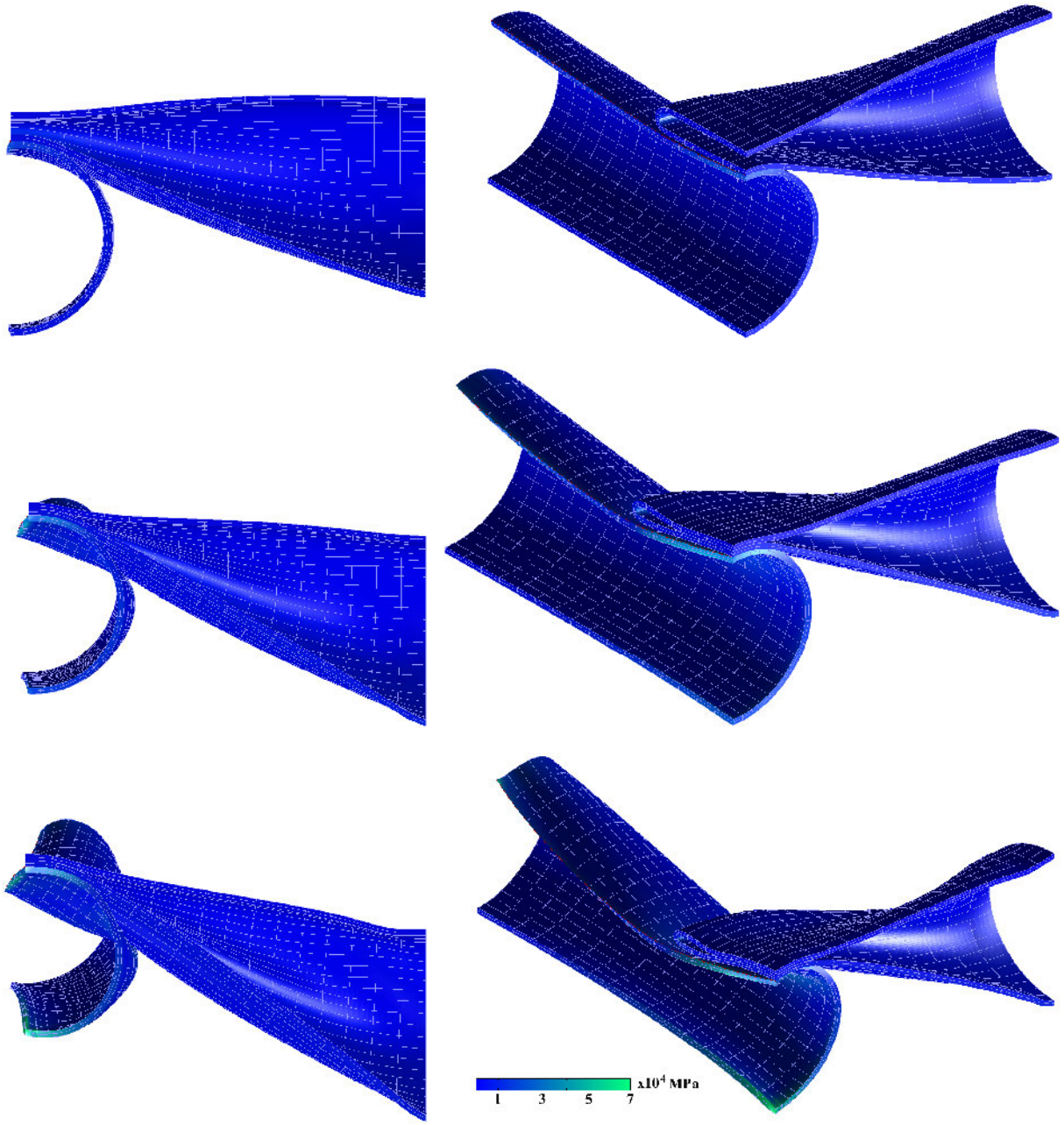

Figure 4.13: Deformation and Von-Mises contour plot of the two crossed tubes test without friction for a loading of 20, 30 and 40 mm.

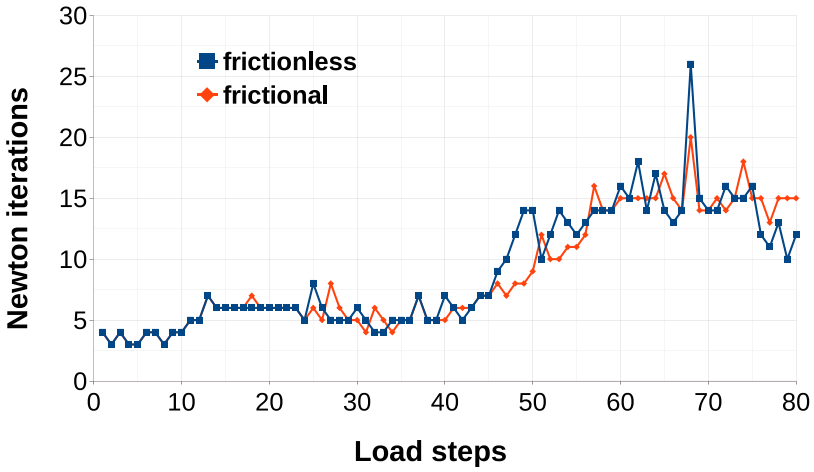

Figure 4.14: Crossed tubes test: required Newton's iterations per load step with ($\mathscr{F} = 0.3$) and without friction.

4.3.6 Projection and ray-tracing

For contact problems, the choice of mapping strategy influences directly the performance and the robustness of the method. In section 4.1.2, we provided a theoratical comparaision between two classic strategies of mapping: orthogonal projection and ray-tracing. In this last part we compare the two mappings from a numerical viewpoint. The comparison is made through two tests: two-dimensional Hertz's contact and three-dimensional crossed tubes.

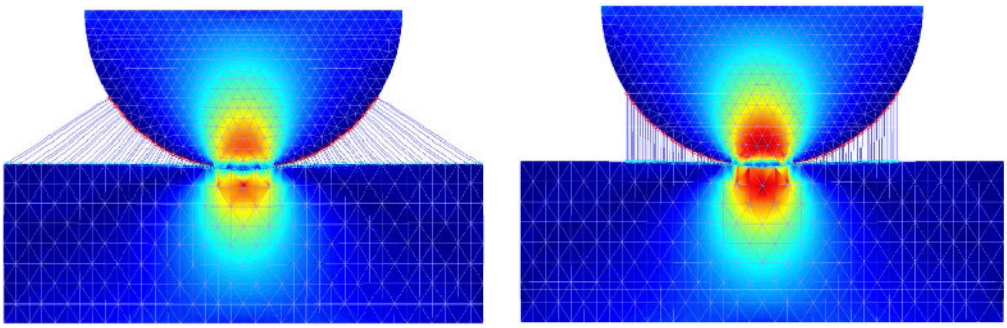

(a) Ray-tracing (b) Projection

Figure 4.15: Illustration of ray-tracing and projection from the upper interface to the lower one and Von mises pressure profiles for Hertz contact.

At first, we illustrate in Figure 4.15 the difference between ray-tracing and projection for Hertz problem and we present the deformation and the effort distribution obtained by using the two mappings. The two strategies solve well Hertz contact problem, but to compare them, we provide for each one the average number of Newton iterations yielding convergence as well as the mean pressure error along the ten steps of loading. The test is

performed with different values of θ, with and without friction. For sake of briefness, we choose only the value of γ_0 equal to E and the unbiased version of the method.

Ray-tracing			
Value of θ	Friction Coefficient	Newton's iterations average	Average contact pressure error (in %)
0	0	2.7	3.34
	0.3	2.8	3.4
-1	0	3.4	3.36
	0.3	3.3	3.46
1	0	No convergence	-
	0.3	No convergence	-

Projection			
Value of θ	Friction Coefficient	Newton's iterations average	Average contact pressure error(in %)
0	0	5.9	3.39
	0.3	6.5	3.35
-1	0	6.3	3.36
	0.3	6.5	3.45
1	0	No convergence	-
	0.3	No convergence	-

Table 4.6: Mean contact pressure and number of Newton's iterations for projection and ray-tracing strategy, for the Hertz test with $\gamma_0 = E$ and the unbiased Nitsche's method.

A first observation is that the accuracy of the approximation is the same for the two mappings, meaning that the choice of the mapping does not influence strongly the quality of the solution. When $\theta = 1$ we do not reach convergence since γ_0 is not large enough. So the two strategies seem to have the same response regarding Nitsche's parameter. In addition, the difference in terms of Newton's iterations is clearly observable for different values of θ. Ray-tracing allows a convergence twice faster than projection. This may be due to the non-exactitude of the tangent problem for projection in which we neglected the directional derivative of $\mathbf{n}_y$ term. A similar difference of convergence speed is observed for the crossed tubes test in Figure 4.16. If we apart the influence of self-contact, the number of iterations is almost two times higher for projection. The smoothness of the contact surfaces in both tests does not allow to study robustness regarding some special cases detailed in [PR15].

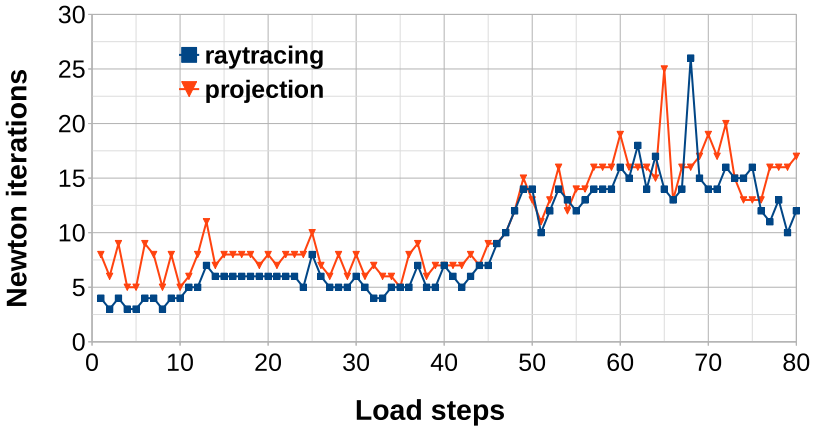

Figure 4.16: Required Newton's iterations per load step for the crossed tubes test without friction, for the ray-tracing and projection mapping strategies.

4.3.7 Industrial validation

In this section we give, briefly, the simulation results of some tests more severe and more representative of industrial applications. Through these tests we validate the Nitsche's method, especially in the large strain framework, in an industrial context. After being analyzed with academic tests on the Getfem++ environment, the Nitsche's method was implemented on the FEM code of Michelin. In a first step, the method was implemented for a contact with a rigid ground. This configuration is not the interesting application of the Nitsche's method but it will enable the evaluation of the method's ability to simulate contact and friction for an advanced geometry and behavior laws. The method was implemented, in this first application, for $\theta = 0$. For a unilateral contact, in the large strain case, the method reads, where the red terms are deleted:

$$\left\{\begin{array}{l} \mathcal{D}J(\mathbf{u})[\delta\mathbf{u}] + \dfrac{1}{2}\displaystyle\int_{\Gamma_c} ([\sigma_{\mathbf{n}}(\mathbf{u}) + \gamma_n\, g(\mathbf{u})]_{\mathbb{R}^-} n) \cdot \mathcal{D}\Big(\mathbf{u}(\mathbf{Y}) - \mathbf{u}(\mathbf{X})\Big)[\delta\mathbf{u}]\; d\Gamma \\ + \dfrac{1}{2}\displaystyle\int_{\Gamma_c} P_{B(-\mathscr{F}[\hat{\sigma}_n(\mathbf{u}) + \gamma_n\, g(\mathbf{u})]_{\mathbb{R}^-})}(\boldsymbol{\sigma}_t(\mathbf{u}) - \gamma\mathbf{v}) \cdot \mathcal{D}\Big(\mathbf{u}(\mathbf{Y}) - \mathbf{u}(\mathbf{X})\Big)[\delta\mathbf{u}]\; d\Gamma \;= 0 \;\forall\, \delta\mathbf{u}\,. \end{array}\right. \tag{4.36}$$

This, simplifies significatly the tangent system.

The first performed test is a contact between a simplified model of the tire and a rigid ground. The tire is composed of 4 different materials and discretized with 9424 nodes. To test normal contact, we impose a vertical displacement of 5 mm on the center of the tire. The inner side is submitted to a pumping pressure of 2 bars. All the extern side of the tire is considered as a contact surface. The obtained deformation using Nitsche's method as well as a contact stress contour plot are given in Fig. 4.17

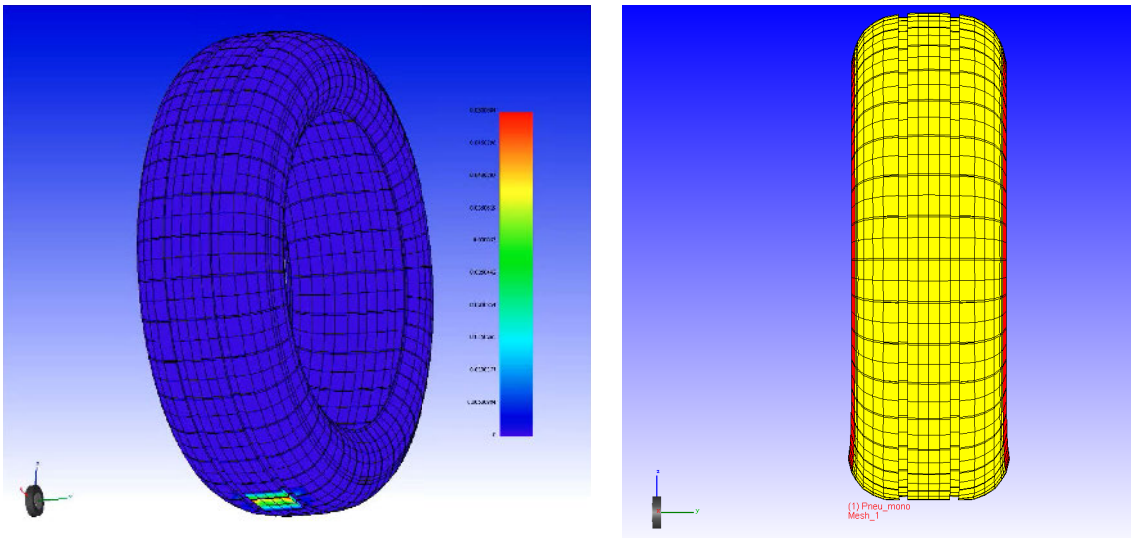

Figure 4.17: Obtained deformation and contact stress contour plot of the bi-stripe tire with the Nitsche method and $\gamma = 10^3$

A first observation is the ability of Nitsche's method to approximate the contact even with a large number of elements and complex behaviour laws. The number of Newton iterations is close to the one got with the penalty method but, the method do not converge with very small values of γ (see Fig. 4.18). This was expected for the tested variant $\theta = 0$. To study the robustness of the method regrading the Nitsche's parameter we give in Fig. 4.18 the needed iterations to get convergence when variating γ between 10^{-3} and 10^{12}.

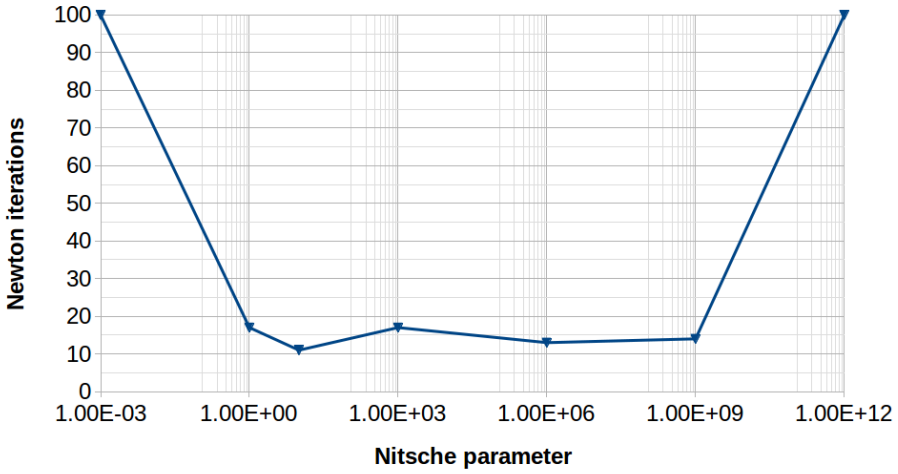

Figure 4.18: Required Newton's iterations for differents values of γ.

As expected, the small values of γ prevent the convergence since the coercivity is lost. For high values of γ the convergence is got for a large interval of values and the problem become ill-conditioned only when γ exceeds 10^9.

To test friction, we consider the same test configuration and we add a rolling of the tire over five time steps. In fact the tire is charged progressively on the normal direction along 5 first time steps and then rolled along 5 second steps.
For this test, we variate this time the friction coefficient $\mathscr{F}$ and we repport the total number of Newton iterations along the 10 time steps (see Fig 4.19). For the simulation we used 3 different integration rules: in blue: Newton-côte rule, in red: Gauss rule with 4 Gauss points per face and in yellow Gauss rule with 8 Gauss points. This test will allow us to validate the method for slip and stick states. We consider here $\gamma_N = 100$ and $\gamma_T = 1$

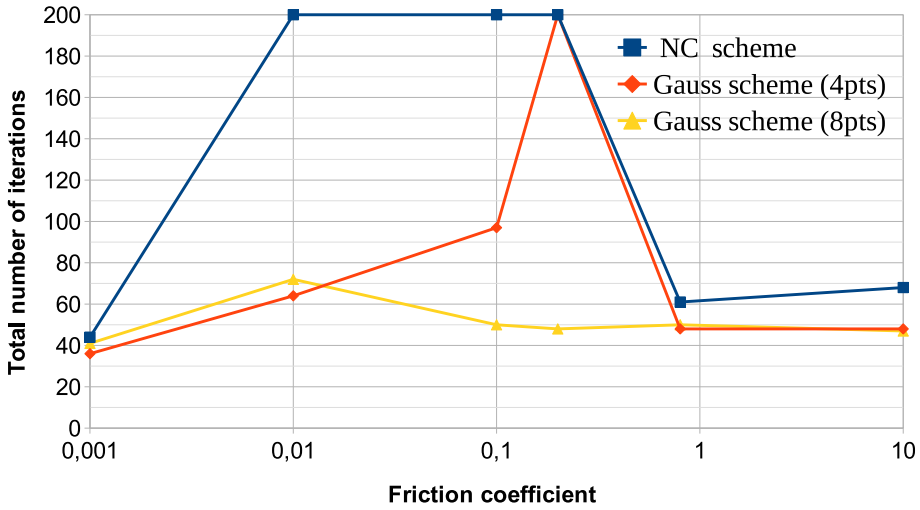

Figure 4.19: Required Newton's iterations for different values of $\mathscr{F}$.

We remark that the Nitche's method converges well when the friction coefficient $\mathscr{F}$ is very low or very high: pure slip and pure stick configurations. When the two phenomenas took place the convergence is lost with Newton-côte integration. This may be caused by the non-smooth transition of the Coulomb law. However, when considering a Gauss integration with a sufficient number of integration points, the convergence is obtained for all values of $\mathscr{F}$. We note here that the augmented Lagrangian method (with Uzawa type algorithm), when $\mathscr{F} = 0.8$ and $\gamma_N = 10^6$, tooks 71 iterations. So that, Nitsche's method is as performing as this last.

Conclusion

In Chapter 3, we proposed and studied an unbiased Nitsche method for the contact between two elastic bodies in the small strain framework. We proved theoretically its consistence, stability and optimal convergence, and studied numerically its robustness. The aim of this Chapter is to extend the method to the large strain case. We proposed an extension of Nitsche's method to contact and friction in the large strain framework. The extension is made also for the friction law, since we consider a Coulomb friction in this chapter instead of Tresca friction. We derived an unbiased formulation that can be more

amenable to self-contact and multi-body contact. A generalization parameter θ is considered to cover an entire set of methods with different numerical properties. The method is constructed independently of the mapping function, but its performance depends on the used mapping. Therefore, we gave a brief comparison of two mapping strategies: projection and ray-tracing.

In this work, we used an hyper-elastic material, but, since the behavior law is used, extending the method to inelastic behavior may need some adaptations.
Being an integral formulation, the performance of Nitsche's method depends on the used quadrature rule. We made the choice of using the classic Gauss rules over the original elements without cutting. This choice was briefly argued, but, still, the effect of numerical integration for Nitsche's method is an interesting perspective of study. Therefore, the third part of this thesis will be devoted to the study of the integration rule influence on the approximation and to the estimation of the quadrature error.

Chapter 5

Influence of the integration error for contact problem

Contents

Introduction

Accurately and efficiently computing the integrals prescribed in the contact formulations (3.16) and (4.31) is one of the main challenges of integral contact algorithms. This is due to the fact that evaluating those quantities requires an integration over the slave contact surface with an integrand containing functions defined on both master and slave sides. In fact, in the case of non conforming surfaces and non-matching meshes, the integrand represents a non-smooth function which cannot be evaluated exactly by using standard Gauss rules. This non-smoothness stems the piecewise terms coming from inner products of quantities defined on both surfaces and also the projection operation presenting the change-over between contact/non-contact and stick/slip states. Integrating such functions through classical numerical quadrature rules generates generally numerical oscillations of the solution on the contact interface and prevent the method from passing the Patch tests.

To overpass these difficulties, many strategies have been proposed in the literature: In [FW05, FW06] the authors choose just to use a high number of integration point without changing the quadrature rule. The used rule in this case is the Gauss one of the slave elements.
Conversely, [ZW98, ML00a, PL03, PL04a] used a segmentation technique to create integration segments. These segments are generated by detecting every intersection between any two contacting elements, Thus, the integrand is polynomial on each segment and the numerical integration is accurate. The cost of this technique is expected to be significant for a 3D geometry undergoing large deformations. In fact, in this case, especially for quadratic elements, the operations of projection and segmentation are not straightforward in implementation neither in computation.
This cost prompt the authors of [FPW15] to combine these two strategies by cutting the integration rule only on the border of the contact surface.
Another integration strategy was proposed and tested in [CLM97, MRW02] and then in [BBWW15] for isogeometric analysis. This strategy named "non-symmetric integration" uses a combination betwen the integration rule of the slave and master sides to reduce the quadrature error. Thus, this method seems to be adequate to the unbiased formulation of contact, since, in this case, the two sides are already used in integration.

The aim of this chapter is to provide a numerical study of the influence of the integration error on the accuracy and convergence of Nitsche's type contact method. A main challenge of this study is to test the different rules already proposed, generally for the mortar method, with the Nitsche's method. To cut off the quadrature error, the main tests studied in this section are different varieties of the patch test, for which the exact solution is known and simple.

This chapter will be organized as follows: Section 5.1 will be a study of the patch test performance of Nitsche's method with different integration rules. In section 5.2 we introduce the non-symmetric integration technique and its adaptation to the method of Nitsche. And, before concluding a study of the influence of quadrature error on the convergence will be provided in section 5.3.

5.1 Integration error and patch test performance for Nitsche's method

5.1.1 Highlighting of the quadrature error for contact in the small strain framework

Throughout this section, we use the same notations and quantities defined in Chapters 2 and 3 for small deformations unilateral contact problem of two elastic bodies and Chapter 4 for large strain one. We let two elastic bodies occupying the domains $\Omega^i \in \mathbb{R}^d$, d being 2 or 3. We consider the same equilibrium and limit conditions (2.26) of section 2.2.2 as well

as the contact conditions (2.27). In this section, we use the classical biased formulation of contact to simplify the analysis of quadrature error, but the results could be generalized to the non-biased method since the integrated terms are the same. If we consider the elasticity equation and the boundary conditions described in (2.26), we will obtain the weak problem(2.31) of section 2.2.2.

To study the quadrature error influence on the approximation, we will begin by considering the simplest case of frictionless contact with $\theta = 0$. For the spatial discretization of the problem, standard isoparametric finite elements with first and second-order interpolation are employed. This defines the usual finite dimensional subspace $\mathbf{V}_h$. In the following, the subscript $()_h$ refers to a spatially discretized quantity. In $\mathbf{V}_h$, the discrete problem reads:

$$\left\{\begin{array}{l} \text{Find } \mathbf{u}_h \in \mathbf{V}_h \text{ such that, } \forall \mathbf{v}_h \in \mathbf{V}_h, \\ \\ \mathbf{a}(\mathbf{u}_h, \mathbf{v}_h) - \displaystyle\int_{\Gamma^1_{C,h}} (\mathbf{v}^1_h - \mathbf{v}^2_h \circ \Pi^1) \cdot \tilde{\mathbf{n}}^1 \left[\sigma^1_n(\mathbf{u}^1_h) - \gamma^1 (\mathbf{u}^1_h - \mathbf{u}^2_h \circ \Pi^1) \cdot \tilde{\mathbf{n}}^1\right]_{\mathbb{R}^-} \mathrm{d}\Gamma = L(\mathbf{v}_h). \end{array}\right. \tag{5.1}$$

A first observation is that, in the formulation (5.1), we integrate a function containing the projection operator $[\cdot]_{\mathbb{R}^-}$ over $\Gamma^1_{C,h}$. The non-smoothness of this operator constitutes a first integration challenge. In fact, numerical quadrature formulas are able to exactly integrate only polynomial integrand; while this projection is not even a continuous function when a non smooth switch between contact and detachment states appear (a corner, for example). We could neglect the influence of this singularity inside the contact area when no change-over between contact and non-contact states is present; but when the projection is active, an important numerical oscillation could be generated by the incapability of quadrature rules to integrate such singular function.

We neglect, momentarily, the projection to better analyze the second type of complication about the integration. The displacement and test functions interpolation is given as:

$$\left\{\begin{array}{ll} \mathbf{u}^1_{h|\Gamma^1_{C,h}} = \sum_{A=1}^{n^1} N^1_A \mathbf{d}^1_A, & \mathbf{v}^1_{h|\Gamma^1_{C,h}} = \sum_{a=1}^{n^1} N^1_a \boldsymbol{\delta}_a, \\ \mathbf{u}^2_{h|\Gamma^2_{C,h}} = \sum_{B=1}^{n^2} N^2_B \mathbf{d}^2_B, & \mathbf{v}^2_{h|\Gamma^2_{C,h}} = \sum_{b=1}^{n^2} N^2_b \boldsymbol{\delta}_b, \end{array}\right. \tag{5.2}$$

where $\mathbf{d}^i_k$ is the discrete nodal displacements on $\Gamma^i_{C,h}$ and the total number of nodes on each edge $\Gamma^i_{C,h}$ of Γ^i_C is n^i. N^i_k is the k^{th} shape fonction defined on the element h of the body (i). Substituting (5.2) into (5.1) produces:

$$\begin{aligned} &\mathbf{a}(\mathbf{u}_h, \mathbf{v}_h) - \sum_{a=1}^{n^1} \Big(\sum_{A=1}^{n^1} \big(\int_{\Gamma^1_{C,h}} N^1_a N^1_A \mathrm{d}\Gamma(\sigma^1_n(\mathbf{d}^1_A) - \gamma^1 \mathbf{d}^1_A)\big) - \sum_{B=1}^{n^2} \int_{\Gamma^1_{C,h}} N^1_a N^2_B \circ \Pi^1 \mathrm{d}\Gamma \mathbf{d}^2_B \Big) \\ &+ \sum_{b=1}^{n^2} \Big(\sum_{A=1}^{n^1} \big(\int_{\Gamma^1_{C,h}} N^2_b \circ \Pi^1 N^1_A \mathrm{d}\Gamma(\sigma^1_n(\mathbf{d}^1_A) - \gamma^1 \mathbf{d}^1_A)\big) - \sum_{B=1}^{n^2} \int_{\Gamma^1_{C,h}} N^2_b \circ \Pi^1 N^2_B \circ \Pi^1 \mathrm{d}\Gamma \mathbf{d}^2_B \Big) = L(\mathbf{v}_h). \end{aligned} \tag{5.3}$$

For exact integration, most of numerical quadrature formulas (e.g. Gauss or Lobatto rules) require a polynomial integrand. If the two meshes are not matching the coordinate mapping is piecewise linear and the inner products $N_a^1 N_B^2 \circ \Pi^1$, $N_b^2 \circ \Pi^1 N_A^1$ and $N_b^2 \circ \Pi^1 N_B^2 \circ \Pi^1$ will not be polynomial on the edge $\Gamma_{C,h}$ of the slave surface. This makes the accuracy of the integration rule a critical issue.
In the frictional contact case (Eq.(3.16)), the projection into the closed ball of radius s^i is not regular and the same inner products of shape functions are integrated. We add to this the mapping function that is not smooth in the discrete configuration. Thus, the same difficulties of numeric integration are faced with the frictional contact.

Those observations suggest that an evaluation of the quadrature error generated by integrating those quantities is an important subject of study that will allow us to quantify and control this error and propose numeric strategies to reduce it.

5.1.2 Integration error without segmentation

The main obstacle hindering the exact evaluation of integrals, as in most contact algorithms, is the form of the gap function g. The expression of g is:

$$g = (\mathbf{y} - \mathbf{x}) \cdot \mathbf{n}$$

This function includes quantities defined on both contact surfaces, the normal vector $\mathbf{n}$ which is not necessary smooth in the discrete set; and it includes, as well, the mapping function that is not smooth neither. This makes the gap a piecewise continuous function along Γ_C with possible discontinuities occurring at the nodes of either contact surfaces.
To better display this, we illustrate in Fig. 5.1 the gap's variation for a given linear discretization of the contact interface. The gap, in this case, is a piecewise $\mathscr{C}^0$-continuous function with the derivative discontinuity occurring at the nodes of either surface.
The kinks present on the gap function causes a first type of singularities in the integrand that we will call "weak discontinuities". This singularities are caused be the discretization and present inside the contact surface.
In many previous works, the authors choose just to use a very high number of integration points to overcome the influence of weak discontinuities (see, for example, [FW05,FW06]).
In Fig. 5.2, we report the error generated by numerical integration of such piecewise linear function.

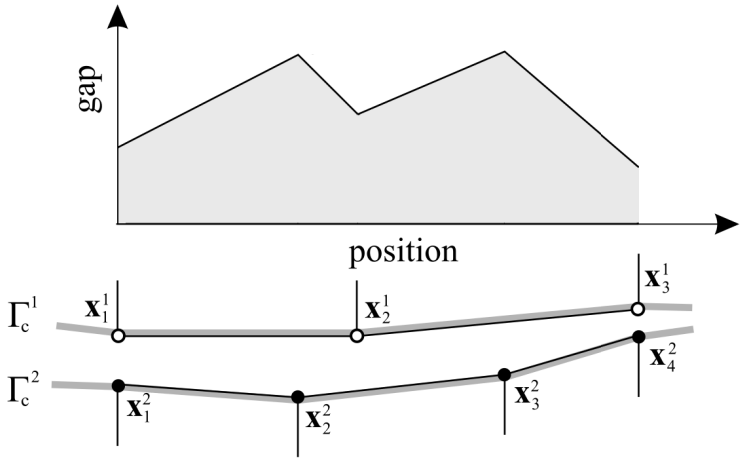

Figure 5.1: Illustration of gap's variation between two surfaces with non-matching mesh.

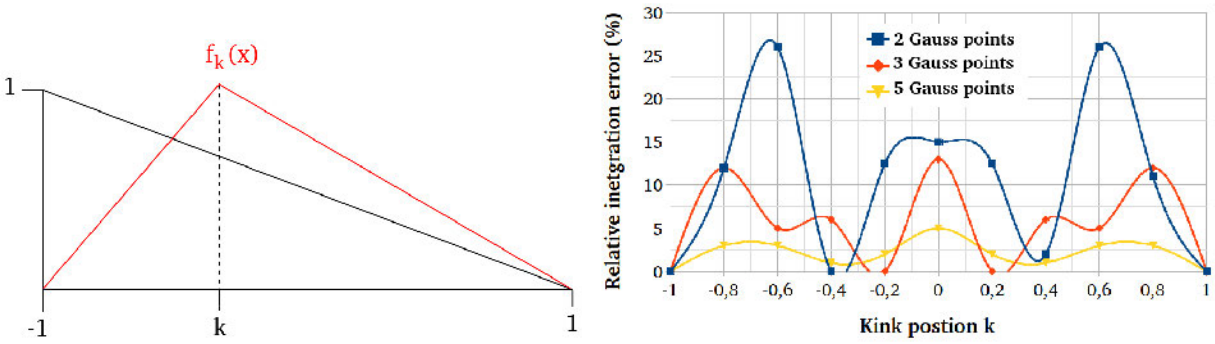

(a) $f_k(x)$ (b) Reported integration error

Figure 5.2: Test case to highlight integration error due to weak discontinuities

We consider a set of functions $f_k(x)$ linear piecewise for $x \in [-1, 1]$ with a kink at $x = k$. We let $f_k(k) = 1$ and $f_k(-1) = f_k(1) = 0$. In this Fig. 5.2-(b) we give the quadrature error of the function $f_k(x)$, ploted in 5.2-(a), when integrating it on $[-1, 1]$ and varying the kink position from -1 to 1 of k. The numerical integration is performed with 2, 3 and 5 Gauss–Legendre points. The reported error decreases, obviously when increasing the integration order, but it depends also on the position of the kink regarding Gauss's points positions. If observing Gauss point positions, one notices that the kink locations with the largest integration errors actually are the integration point positions. This interesting result concluded in [FPW15] for 2D interface problem can be also transferred to the three-dimensional case.

To quantify the integration error generated by this kinks, we call out a classic patch test. The patch test originally proposed in [TP91], investigates the ability of contact formulations to exactly transmit constant normal tractions between two contacting surfaces, regardless of their discretization. The patch tests are typically not passed by NTS

formulation, even though some modifications were introduced to this methods to pass it (see [ZDL09a, ZDL11]). Among available patch tests, we choose the one used several times for the mortar method (see e.g. [PL04a, WB17]).

The test is similar to the patch test introduced in 4.3.1, but it is a 3D one. The configuration of the test is given by Fig. 5.3. On the topmost surface a prescribed displacement $\delta z = -0.5mm$ in z-direction is applied. Both blocks are retained against rigid body motions in the x-y-plane. With the given boundary conditions a uniaxial compression is simulated and thus a constant stress $\hat{\sigma}_z$ can be expected. In this test, we use a linear elastic material with $E = 2 \cdot 10^5 MPa$ and $\nu = 0.3$ and we let Nitsche's parameter $\gamma_0 = 10E$. For the numerical integration, we use a classical Gauss Legendre rule

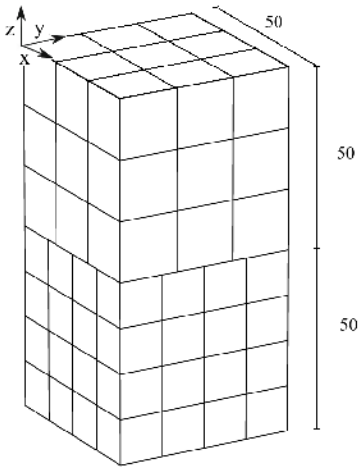

Figure 5.3: 3D Patch test: Geometry and finite element mesh.

on the slave elements without any segmentation. Adopting the nomination of [FPW15], this rule is named "element based integration". When using a conforming mesh, element based integration procedure is able to represent the constant stress exactly (up to machine precision). For the non-matching mesh, the patch test cannot be passed exactly, as expected, because the non-polynomials integrand. The maximum of relative errors in $\hat{\sigma}_{zz}$ for different number of Gauss points is investigated and given in Table 5.1. We inspect as well the maximum of gap error (normal penetration) measured on Gauss's points.

Nbre of Gauss's points/face	7 (conforming mesh)	2	7	20	175
Max pressure relative error	$6.92 \cdot 10^{-15}$	$5.86 \cdot 10^{-2}$	$6.13 \cdot 10^{-3}$	$3.22 \cdot 10^{-3}$	$2.76 \cdot 10^{-4}$
Max gap(mm)	$1.11 \cdot 10^{-16}$	$1.2 \cdot 10^{-3}$	$8.73 \cdot 10^{-5}$	$4.15 \cdot 10^{-5}$	$3.66 \cdot 10^{-6}$

Table 5.1: Maximum of contact pressure relative error and gap.

The first observation is that, even though the integration error generated by weak discontinuities is small, it is significant when compared to the exactly integrated solution.

This error prevent the Nitsche's method from passing this patch test despite it is an integral method.
Obviously, the more integration points are used the better the integral can be approximated and the error is smaller. Still, the error does not decrease significantly even when using a huge number of integration points. This first test shows that adding integration points could improve the method's accuracy for an element-based integration but from a certain order this improvement is no more significant when taking into account the cost of using such number of integration points.

The previous illustration highlights the quadrature error inside the contact surface; but another source of error is the transition in the boundary of a dropping edge. This transition causes the so called "strong discontinuities" (i.e. jumps) . These discontinuities are not caused by the discretization and they are source of large integration errors in general. From a numerical point of view, the strong discontinuities could be detected when the search algorithms used for the mapping operation fails.

For example, with a dropping edge of the master surface the projection operation of some Gauss's points fails. Then a portion of the slave element will have a zero contribution to the integrand and this will affect the exactitude of the quadrature rule. In this case, it could be added to that the singularity of the solution itself, since the dropping age could be a reason of singularity of the contact pressure.

To evaluate the impact of such discontinuities on the accuracy of the approximation, we consider a second patch test similar to the first one but with two non coincident contact surfaces. The lower cube is taken larger than the first one and its upper surface is considered to be the slave one Γ_c^1. This choice will allow us to get strong discontinuities on the borders of the second contact surface. If we impose a vertical displacement on the upper cube, as for the first example, the stress solution will be singular. Thus, to get only the impact of the integration error, we impose a constant pressure on the free upper surface of both cubes. So, a constant vertical stress $\hat{\sigma}_z$ is be expected. The imposed vertical stress is $p = 1346KPa$ which is the obtained pressure in the first test 5.3 with an imposed displacement of $0.5mm$. The configuration of this test is given by Fig.5.4 and we consider the same parameterization of the first example. For this test, we use the biased Nitsche's method and first order Lagrange elements.

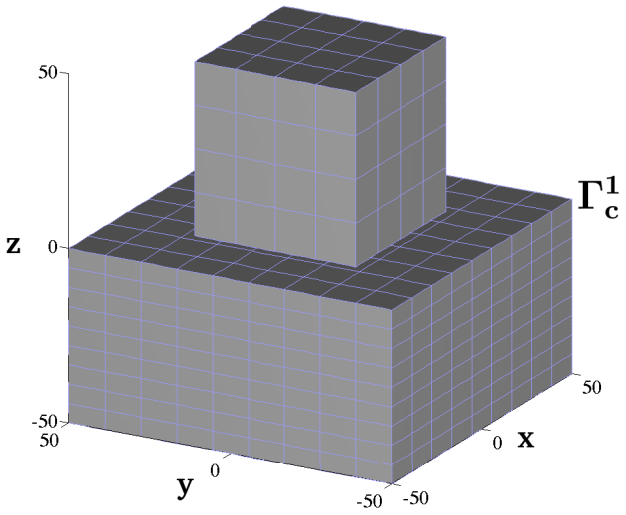

Figure 5.4: 3D Patch test with non-conforming contact surfaces: Geometrie and finite elements mesh.

We measure the relative error of contact pressure and the normal penetration (in mm) on the integration points and we give in Table 5.2 the maximum of these errors with different numbers of quadrature points.

Nbre of Gauss's points/face	7 (conforming mesh)	7	28	80	175
Max pressure relative error	$9.019 \cdot 10^{-10}$	$3.56 \cdot 10^{-2}$	$7.13 \cdot 10^{-3}$	$3.81 \cdot 10^{-3}$	$1.15 \cdot 10^{-2}$
Max gap(mm)	$5.72 \cdot 10^{-13}$	$2.40 \cdot 10^{-3}$	$1.01 \cdot 10^{-4}$	$3.66 \cdot 10^{-5}$	$1.80 \cdot 10^{-3}$

Table 5.2: Maximum of contact pressure relative error and gap.

The magnitude of the error due to the strong discontinuities is not very different from what obtained with weak ones, but the error in this case is about 4 times higher. As for weak discontinuities, enriching the integration rule reduces the error, but even with a lot of integration points we are still far from the exact integration solution. We remark as well that not just the number of the Gauss points influences this error, but also their positions because sometimes, adding integration points does not improve the accuracy of the integration. For example, the obtained error with 175 Gauss points is larger than the obtained with only 28 points. To better locate the error on the contact surface we give in Fig. 5.5 the pressure profile and the gap one on the slave contact surface.

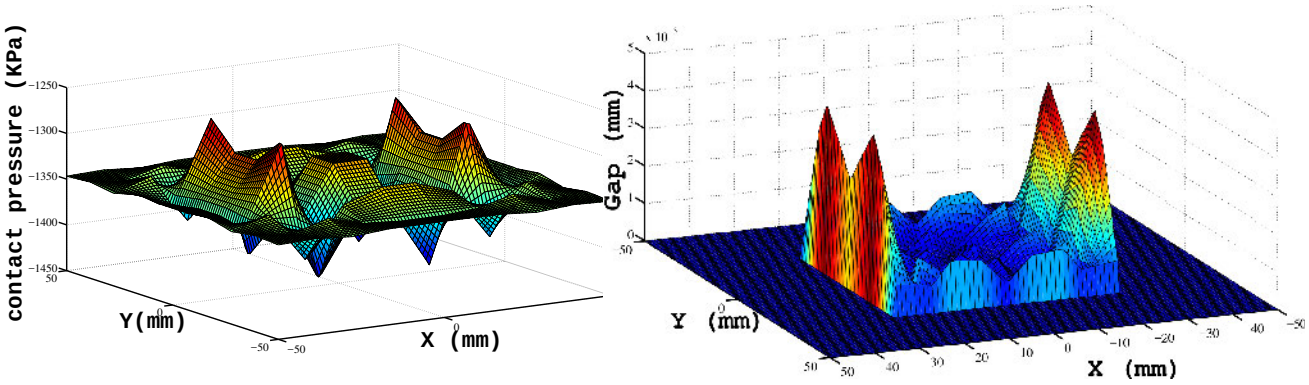

(a) Pressure (b) Gap

Figure 5.5: Pressure and penetration profiles on the contact plane ($z = 0$) of the slave surface

It is clear from the profiles of pressure and gap that the most important error is located near the dropping edges ($x = \pm 25$ and $y = \pm 25$). This irregularity create numeric oscillation around the edges. To avoid this kink of error we could cut the integration method when a dropping age is detected.

Accordingly, any integration rule involving integration points that are dictated by only one of the two surfaces cannot exactly evaluate Eq. (5.4) regardless of the number of integration points used. If however, the integration intervals are cut in any two neighboring nodes regardless of their surface of origin, an exact evaluation is possible. This segmentation of the quadrature rule will generate an additional computation in each Newton iteration. This additional work may be important in the 3D case and a potential difficulty here is that the location of the integration points is not fixed, since the locations of the segment boundaries change due to the relative motion between the two surfaces.

5.1.3 Segment-based integration

As shown in section 5.1, using the element-based integration ignores the occurring discontinuities and accepts integration error that may be significant. To handle this problems, most of the segment-to-segment methods uses an algorithm of segmentation of the integration rule. We will call this technique "segment-based integration". Its general idea was first outlined for the classical segment-to-segment contact methods in [SWT85, ZW98]. Than the technique was applied to the 3D mortar contact formulations in [ML00a, PL03]. Severale adoptions and extensions can for example be found in [PL04a, PL04b, PLS08]. In Fig. 5.6, we illustrate this operation.

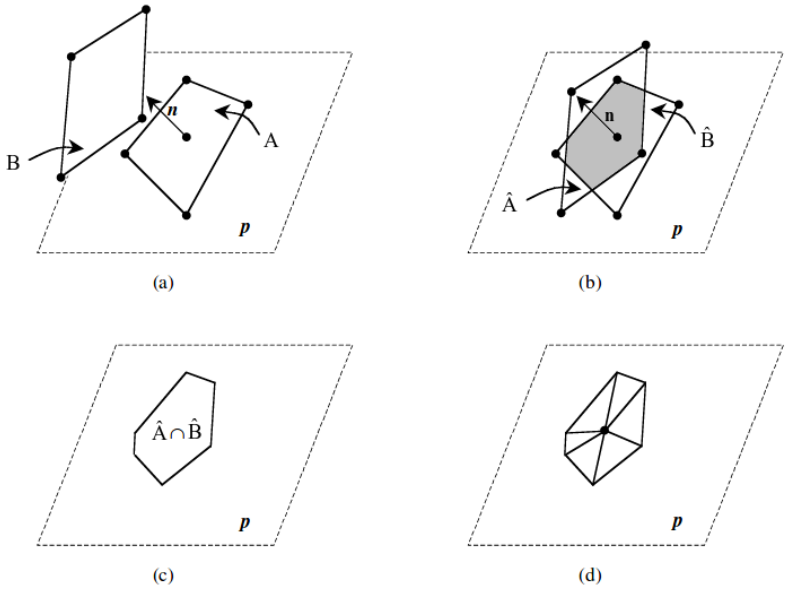

Figure 5.6: Procedure of segmentation of the integration rule (as proposed in [PL03]).

To prevent all possibly occurring discontinuities in the integrand of the method (5.1), the segment based integration propose to cut every slave element according to the corresponding master ones. Then a contact segment (polygon) will be constructed by the overlap of one master and one slave element. The main characteristics of these segments is that the integrand is smooth within each segment. In order to simplify the integration, a piecewise flat approximation of the contact region is used by projecting the two contacting elements into the same plan **p**. Thus we obtain the projected elements $\hat{A}$ and $\hat{B}$. Thus, the determined intersection segment $\hat{A} \cap \hat{B}$ is a flat polygon with up to eight vertices. Then a subdivision of the segment into triangles for example (as in [PL03]) is performed in order to use classical quadrature formulas on each triangle (see Fig. 5.6 (d)). The edges of the triangles connect the center of gravity of the segment with its vertices. This way the number of triangles corresponds to the number of vertices of the segment. The triangles are called integration cells and within each of them a classical Gauss's integration rule is allocated for numerical quadrature.

To evaluate the impact of such segmentation on the accuracy of the integration we consider a bidimentional patch test similar to the test described by 5.4 (see 5.7).

We perform this test for the bi-dimensional case because the implementation of the segmentation algorithm is much simpler in this case, but similar conclusions could be drawn in the 3D case. The first body is discretized to 17×17 quadrangles and the second to 5×5 with linear approximation. We prevent tangential displacements by imposing symmetry conditions on the vertical borders of the two bodies as well as on the lower border of the 1^st body.

We consider always the same material parameters ($E = 2.10^5 MPa$ and $\nu = 0.3$) with an isotropic linear elastic constitutive law. The applied pressure on the top of the upper

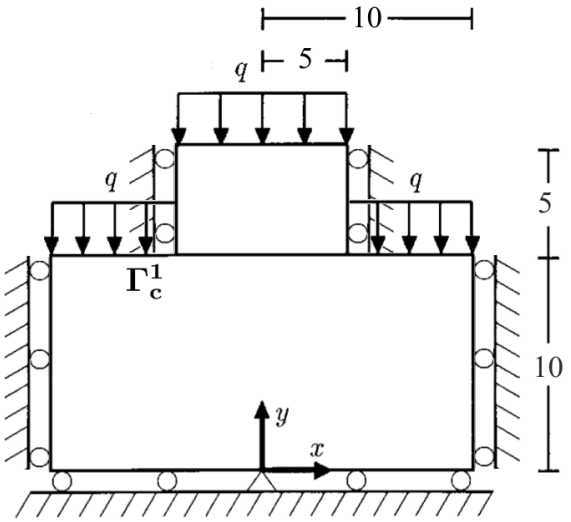

Figure 5.7: 2D Patch test with non conforming contact surfaces

cube is set to $q = 10KPa$ this time.
For the simulation the biased Nitsche's method is used with $\gamma_0 = 10E$. We give in Table 5.3 a comparison between the pressure and penetration errors obtained with and without segmentation. In order to quantify the cost of the segmentation process we give the time of calculation in each case. The approximation with segment-based integration is exact

Nbre of Gauss's points/face (integration method)	3 (conforming mesh)	3 (segment-based)	3 (element-based)	45 (element-based)
Max pressure relative error	$5.48 \cdot 10^{-12}$	$3.87 \cdot 10^{-12}$	$1.11 \cdot 10^{-2}$	$4.51 \cdot 10^{-4}$
Max gap(mm)	$2.61 \cdot 10^{-18}$	$6.02 \cdot 10^{-17}$	$5.68 \cdot 10^{-7}$	$1.20 \cdot 10^{-9}$
Computing time(ms)	86.4	321	89.5	314

Table 5.3: Maximum of contact pressure relative error and gap and computing time with different integration rules.

up to machine precision. So, it is proved from Table 5.3 that the segmentation of the quadrature method allow to compute exactly the contact terms' integrals and to get the same accuracy of using conforming mesh. As for the 3D case, even when using a big number of integration points, the element-based integration do not reach the precision of the segment-based one.
However when observing the time of computing, the segmentation seems to increase considerably the computing cost. Even though the current test is very simple in a 2D assumption the difference of the computation cost is important. Knowing that, in the large strain case, this segmentation has to be performed in every Newton iteration on all the contact surface and that the operation is much more difficult in that case with a 3D

geometry because the location of the integration points is not fixed, we could conclude that using the segment-based integration causes considerable effort for implementation and computation.

5.1.4 Boundary-segmentation

To reduce the computation cost of the segment-based integration, [FPW15] proposed, for the mortar method, a combination of the two integration methods to strike a balance between the simplicity of the first and the accuracy of the second. Noting, in the test described in Fig. 5.4, that the strong discontinuities causes more quadrature error than weak ones, we are going to cut the integration rule only when a strong discontinuity occurs. This technique was named "boundary segmentation".
In other terms, the segment-based integration rule will be employed for problematic slave elements having strong discontinuities in the integrand and for non-critical slave elements within the contact zone the element-based integration will be used. The critical slave elements are the elements containing integration points whose projection misses all of the master elements associated.

For the last test of Fig. 5.7, we give in table 5.4 the reported pressure and gap errors with the three integration rules.

Nbre of Gauss's points/face (integration method)	3 (segment-based)	3 (element-based)	3 (Boundary-segmentation)
Max pressure relative error	$3.87 \cdot 10^{-12}$	$1.11 \cdot 10^{-2}$	$1.9 \cdot 10^{-3}$
Max gap(mm)	$6.02 \cdot 10^{-17}$	$5.68 \cdot 10^{-7}$	$5.37 \cdot 10^{-9}$
Computing time(ms)	321	89.5	112

Table 5.4: Maximum of contact pressure relative error and gap and computing time with different integration rules.

Using boundary-segmentation allows reducing the maximum of pressure relative error by a factor of 10 and the gap's maximum 100 time, with 3 Gauss points per face. The computation time for this boundary segmentation is about 20 ms more than an element-based integration in the same circumstances. Thus the boundary segmentation improve the accuracy of the approximation with a much less computation time; but the error caused by weak discontinuities is still present and we still do not pass the patch test.

For the 3D case we go back to the test of Fig. 5.4. The simulation using the boundary segmentation gives the pressure and gap profiles of Fig. 5.8.

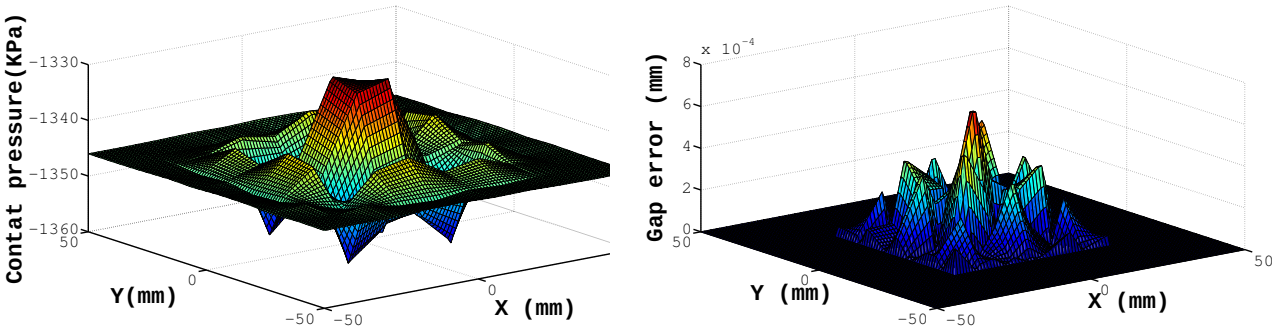

(a) Pressure (b) Gap

Figure 5.8: Pressure and penetration profiles on the contact plane ($z = 0$) of the slave surface (with boundary segmentation)

As expected, the error is no more present close to the limits of contact surfce but within the contact zone. With 7 Gauss points per face, the maximum of pressure error is $1.09 \cdot 10^{-2}$ and of penetration error is to $7.03 \cdot 10^{-4}$ mm. Comparing these results to the ones obtained in Table 5.2, the errors' maximum is reduced especially for the penetration. The simulation in this case took 5.62 s against 2.46 s with element-based integration.

5.1.5 A non-smooth solution patch test

In order to test the ability of the segmentation to improve the approximation with a more realistic configuration, we do over the test of Fig. 5.7 without adding the artificial pressure on the free upper board of the big cube. We eliminate, then, the pressure applied on both cubes and we replace it by an imposed displacement of 0.5 mm on the upper bound of the upper body (See Fig. 5.9). We eliminate as well the spherical conditions dictated on the vertical sides. This case is the mostly encountered one when a dropping edge is present. But in this case the exact solution will be very irregular (especially in pressure; see Fig. 5.9 (b)). To evaluate the error we compute the H^1 norm of the difference between the approximated solution and a reference one obtained with a very fine mesh. The expected pressure profile is obtained in Fig. 5.9(b) with this reference solution.

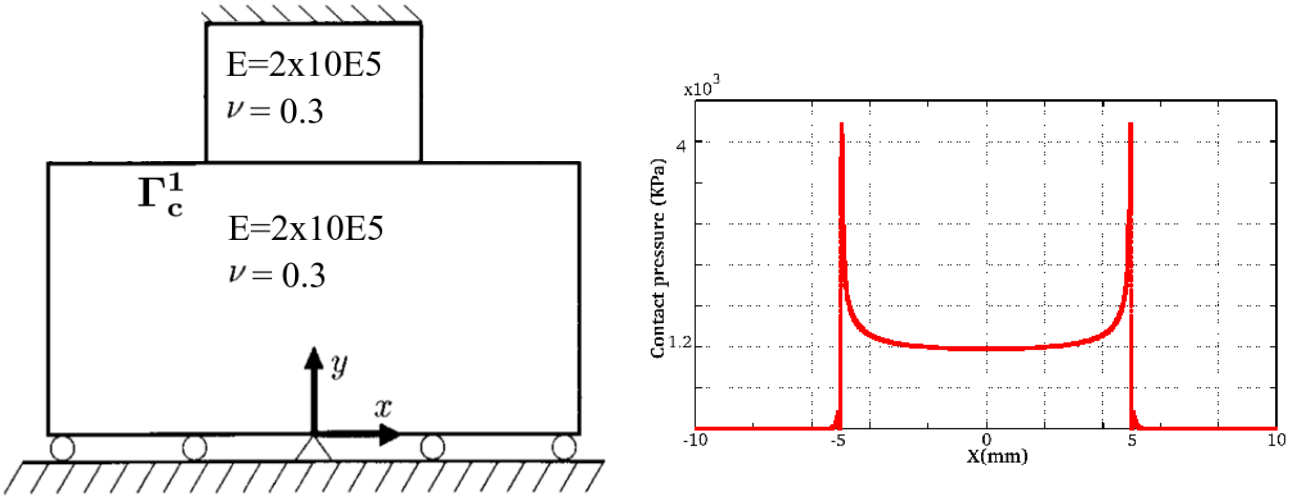

(a) (b)

Figure 5.9: 2D Patch test with imposed vertical displacement (a) and its reference pressure solution (b).

We give in Table 5.5 the obtained H^1 error with the different integration strategies.

Nbre of Gauss's points/face (integration method)	3 (segment-based)	3 (boundary-segmentation)	3 (element-based)	45 (element-based)
H^1 error	$7.82 \cdot 10^{-2}$	$7.93 \cdot 10^{-2}$	$8.07 \cdot 10^{-2}$	$7.94 \cdot 10^{-2}$

Table 5.5: H^1-norm of error of the non-smooth patch test 5.9, with different integration rules.

The error in H^1 norm is not significantly different between the three integration methods. Even adding a big number of Gauss points do not increase the precision. This is due to the fact that the solution itself is very singular. Thus, in some cases, when the solution is very singular, the segmentation could be not efficient.

5.1.6 Integration error for the quadratic interpolation and frictional contact

For element-based integration, no considerable difference in the integration process is present with quadratic since we use classic quadrature rules. However, it has been shown in [EAB01], for a node-to-segment mixed method, and [FPW15], for the mortar method, that the integration error is more important for high order elements and that it affects remarkably the convergence order.
On the other hand, the segmentation process needs to be modified, since the elements are no more straight-lined. A simple adaptation of the segment-based integration was proposed by Puso and Laursen in [PLS08]. The modification consists on dividing the

quadratic elements to linearly interpolated sub-elements and establishing geometric mappings from parent element space so sub-segment space (See Fig. 5.10). Thus, it is possible to evaluate higher-order shape function products in the integrand without any algorithmic changes. However, this operation could influence the optimality of the approximation.

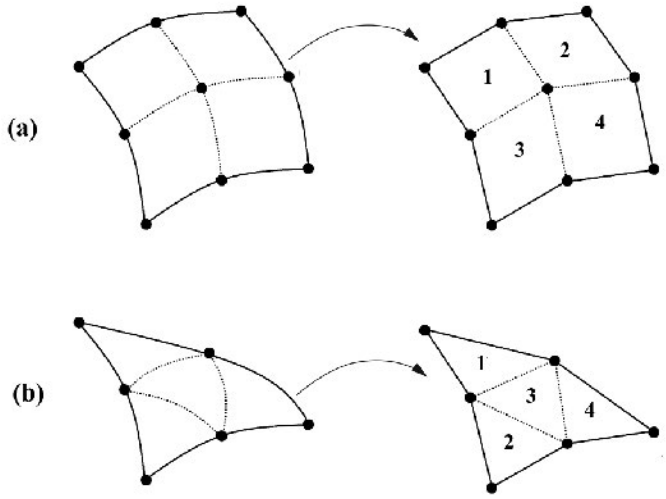

Figure 5.10: Illusration of quadratic elements' division into contact linear sub-segments for quadrangular (a) and triangular elements (b).

To confirm these observations for Nitsche's method, we do over the test of Fig. 5.7 with quadratic elements and then frictional contact. We give in Table 5.6 the maximum of pressure and penetration errors when using $\mathbb{Q}_2$ elements.

Nbre of Gauss's points/face (integration method)	3 (conforming mesh)	3 (segment-based)	3 (element-based)	45 (element-based)
Max pressure relative error	$6.98 \cdot 10^{-7}$	$2.46 \cdot 10^{-6}$	$5.16 \cdot 10^{-2}$	$1.1 \cdot 10^{-3}$
Max gap(mm)	$1.93 \cdot 10^{-11}$	$8.05 \cdot 10^{-12}$	$1.86 \cdot 10^{-7}$	$3.39 \cdot 10^{-8}$

Table 5.6: Maximum of contact pressure relative error and gap with quadratic approximation and without friction

We remark that the use of quadratic element reduce the accuracy of the segment-based integration, but still it is far more precise that the element-based one even with big number of Gauss points. Using a quadratic approximation reduces the penetration error, but the pressure error due to integration increases. The influence of using higher order elements on the convergence is studied in details in section 5.3

For the frictional case, we add to the discontinuities present in the frictionless one the non regularity of the velocity v. This quantity is approximated by difference between tangential gap evaluated at the current time step t_n and the previous time step t_{n-1} , see (2.13). Thus, The integration error in a time step is the accumulation of error at both time steps. Beside this effect, there exist element regions where the element-based integration is not able to detect contributions from master elements because the integration points are generally located within the slave element and not on the edges. According to [FPW15], the resulting loss of precision is important for the velocity v and this affects the decision, whether a node is in stick or slip state; while for frictionless contact, the error is not severe because the evaluated terms within the element dominate the integrals.
For the segment-based integration these differences between frictional and frictionless cases are, in general, not problematic because the integrals for both time steps are calculated with a high precision.

To conclude, the segmentation of all the contact surface is the best solution to get an exact integration of the Nitsche's method but the cost of this operation may be important, especially in the large strain, 3D case. The segmentation of only the elements presenting strong discontinuities is cheaper but it does not eliminate quadrature error inside the contact zone. Although this error is less important than the error generated by strong discontinuities, but it decreases the occupancy of the method and it may influence its convergence order.

5.2 Non symmetric integration

This integration strategy was introduced and theoretically analyzed for mortar method in [CLM97]. Noting that the best approximation error requires a quadrature formula based on the slave side and the consistency error requires one on the master side, the authors propose to use both integration rules. In other words, if we let $(\cdot)^-$ refer to a quantity defined on the slave surface and $(\cdot)^+$ for the master one and $\mathbf{M}_h$ to the space of Lagrange multipliers, instead of choosing between the two space:

$$\mathbf{V}_h^{-+} = \left\{ \mathbf{v}_h \in \mathbf{V}_h : \int_{\Gamma_c^-} v_{nh}^- \mu_h^- \, d\Gamma = \int_{\Gamma_c^+} v_{nh}^+ \mu_h^- \, d\Gamma, \forall \mu_h^- \in \mathbf{M}_h \right\}$$

and

$$\mathbf{V}_h^{--} = \left\{ \mathbf{v}_h \in \mathbf{V}_h : \int_{\Gamma_c^-} v_{nh}^- \mu_h^-, \, d\Gamma = \int_{\Gamma_c^-} v_{nh}^+ \mu_h^- \, d\Gamma, \forall \mu_h^- \in \mathbf{M}_h \right\}$$

to impose the contact condition

$$\int_{\Gamma_c^-} (v_{nh}^+ - v_{nh}^-) \lambda_h^- \, d\Gamma = 0,$$

we use the first space as a test space and the second as a trial one. Then problem reads:

$$\begin{cases} \text{Find } \mathbf{u}_h \in \mathbf{V}_h^{--} \text{ such that, } \forall \mathbf{v}_h \in \mathbf{V}_h^{-+}, \\ \\ \mathbf{a}(\mathbf{u}_h, \mathbf{v}_h) = L(\mathbf{v}_h), \end{cases} \tag{5.4}$$

This approach results in a non-symmetric saddle point problem since we work with different test and trial spaces, resulting in a Petrov-Galerkin approach and a loss of symmetry.

Remark 5.2.1. *The choice of the test and trial spaces can be interpreted as follow: In the mortar approach, The contact condition could be seen as coupled Dirichlet-Neumann problem. On the slave side, a Dirichlet problem has to be considered where the boundary condition is obtained from the trace on the master side. We impose the boundary condition in a weak integral form based on quadrature formulas on the mesh which is the mesh on the slave side. Thus the natural choice for the trial space is* $\mathbf{V}_h^{--}$*. On the other hand, on the master side, we solve a Neumann problem where the boundary conditions are obtained from the residual on the slave side. In this case, a quadrature formula on the master side is the natural choice. Since Neumann boundary conditions enter in a weak form on the right-hand side (they are seen by the test space),* $\mathbf{V}_h^{-+}$ *is the natural choice for the test space.*

Numerical examples in [MRW02] and [BBWW15] show an accuracy close to the case of exact integration, but we note that from the theoretical point of view the well-posedness of this non-symmetric saddle point problem remains unproved.

To adapt this strategy to the Nitsche's method, we need to consider an integration rule on both of the contacting surfaces. Thus it is more natural to consider the non-biased version of the method. The contact integrand in (4.31) is divided into two terms:

$$\begin{aligned} &\frac{1}{2}\int_{\Gamma_c} \frac{1}{\gamma}\boldsymbol{\mathcal{C}}_{\gamma,\mathscr{F}}(\hat{\boldsymbol{\sigma}}_{\boldsymbol{N}}{}^h, g, \mathbf{v}^h, \mathbf{n}_x) \cdot \mathcal{D}\Big(\theta\hat{\boldsymbol{\sigma}}_{\boldsymbol{N}}{}^h + \gamma(\mathbf{u}^h(\mathbf{Y}) - \mathbf{u}^h(\mathbf{X}))\Big)[\delta\mathbf{u}^h]\ d\Gamma \\ &= \frac{1}{2}\int_{\Gamma_c} \frac{1}{\gamma}\boldsymbol{\mathcal{C}}_{\gamma,\mathscr{F}}(\hat{\boldsymbol{\sigma}}_{\boldsymbol{N}}{}^h, g, \mathbf{v}^h, \mathbf{n}_x) \cdot \mathcal{D}\Big(\theta\hat{\boldsymbol{\sigma}}_{\boldsymbol{N}}{}^h - \gamma(\mathbf{u}^h(\mathbf{X}))\Big)[\delta\mathbf{u}^h]\ d\Gamma \\ &+\frac{1}{2}\int_{\Gamma_c} \boldsymbol{\mathcal{C}}_{\gamma,\mathscr{F}}(\hat{\boldsymbol{\sigma}}_{\boldsymbol{N}}{}^h, g, \mathbf{v}^h, \mathbf{n}_x) \cdot \delta\mathbf{u}^h(\mathbf{Y})\ d\Gamma, \end{aligned} \tag{5.5}$$

and every term is integrated on the corresponding surface. To be able to integrate the method on both surfaces we have to project the operator $\boldsymbol{\mathcal{C}}_{\gamma,\mathscr{F}}(\mathbf{X})$ on the corresponding master point $\mathbf{Y}$. Since Γ_c present, here, the union of the two surfaces we could keep the integration domain unchanged and express the changing of the interation side by replacing:

$$\int_{\Gamma_c} \boldsymbol{\mathcal{C}}_{\gamma,\mathscr{F}}(\hat{\boldsymbol{\sigma}}_{\boldsymbol{N}}{}^h, g, \mathbf{v}^h, \mathbf{n}_x) \cdot \delta\mathbf{u}^h(\mathbf{Y})\ d\Gamma$$

by :

$$\int_{\Gamma_c} \boldsymbol{\mathcal{C}}_{\gamma,\mathscr{F}}(\hat{\boldsymbol{\sigma}}_{\boldsymbol{N}}{}^h(\mathbf{Y}), g(\mathbf{Y}), \mathbf{v}^h(\mathbf{Y}), \mathbf{n}_y) \cdot \delta\mathbf{u}^h(\mathbf{X})\ d\Gamma$$

Thus, the obtained method reads:

$$\begin{cases} \mathcal{D}\mathcal{J}(\mathbf{u}^h)[\delta\mathbf{u}^h] - \dfrac{1}{2}\displaystyle\int_{\Gamma_c} \frac{\theta}{\gamma}\hat{\boldsymbol{\sigma}}_{\boldsymbol{N}}{}^h \cdot \mathcal{D}\hat{\boldsymbol{\sigma}}_{\boldsymbol{N}}{}^h[\delta\mathbf{u}^h]\; d\Gamma + \dfrac{1}{2}\displaystyle\int_{\Gamma_c} \frac{\theta}{\gamma}\boldsymbol{\mathcal{C}}_{\gamma,\mathscr{F}}(\hat{\boldsymbol{\sigma}}_{\boldsymbol{N}}{}^h, g, \mathbf{v}^h, \mathbf{n}_x) \cdot \mathcal{D}\hat{\boldsymbol{\sigma}}_{\boldsymbol{N}}{}^h[\delta\mathbf{u}^h] \\ + \dfrac{1}{2}\displaystyle\int_{\Gamma_c} \Big(\boldsymbol{\mathcal{C}}_{\gamma,\mathscr{F}}(\hat{\boldsymbol{\sigma}}_{\boldsymbol{N}}{}^h, g, \mathbf{v}^h, \mathbf{n}_x) - \boldsymbol{\mathcal{C}}_{\gamma,\mathscr{F}}(\hat{\boldsymbol{\sigma}}_{\boldsymbol{N}}{}^h(\mathbf{Y}), g(\mathbf{Y}), \mathbf{v}^h(\mathbf{Y}), \mathbf{n}_y)\Big) \cdot [\delta\mathbf{u}^h(\mathbf{X})]\; d\Gamma = 0 \\ \qquad\qquad \forall\, \delta\mathbf{u}^h \in \mathbf{V}_h. \end{cases} \tag{5.6}$$

To test the ability of the non symmetric integration method to better approximate the contact integrals, we perform a first test of (5.6) with the patch test described in Fig. 5.3. This will allow us to evaluate the ability of non symmetric integration to overcome the weak discontinuities. The maximum of gap and pressure errors are given by Table 5.7 with and without non symmetric integration, using the unbiased version of Nitsche's method with $\theta = 0$.

Nbre of Gauss's points/face (integration method)	7 (conforming mesh)	7 (element-based)	7 (non symmetric)
Max pressure relative error	$1.43 \cdot 10^{-12}$	$6 \cdot 10^{-3}$	$7.26 \cdot 10^{-12}$
Max gap(mm)	$7.68 \cdot 10^{-17}$	$3.85 \cdot 10^{-3}$	$1.21 \cdot 10^{-16}$
Computing time(s)	0.60	0.63	0.60

Table 5.7: Maximum of contact pressure and gap error and Computing time for the test configuration 5.3.

It is obvious from Table 5.7 that the non symmetric integration is able to compute preciously the contact integrals for this patch test. Thus, the non symmetric seems to be a very efficient solution to overcome the weak discontinuities. However, for the strong discontinuities, the obtained error is bigger when using non-symmetric integration: For the 3D patch test with non conforming contact surfaces, described in Fig. 5.4, the maximum of error is : 0.1 for the pressure and $6.46 \cdot 10^{-7}$ for the penetration which is higher than the error got with direct element-based integration, especially for the pressure (see Table 5.2).
The cost of the non-symmetric integration is almost the same as for the element-based one since they use the same integration rules. The only additional cost is the mapping's one that is low for this test.

The non symmetric integration is a good solution to reduce the integration error within the contact surface, but on the boundary of the surface it is needed to cut the integration rule and in that case the boundary segmentation is the adapted strategy.

5.3 Influence of the quadrature error on the convergence order

For the mortar method, early results in [CLM97, MRW02] and [FPW15] showed that the element-based integration does not yield optimal convergence, especially for quadratic elements. More precisely, when the integration rule is chosen on the slave mesh the consistency error is affected. Numerical results confirmed the lack of optimality especially in terms of pressure norm although reasonable results were obtained with linear approximation.

In order to observe the effects of inexact quadrature rules on the convergence we consider the same test case used in [BBWW15] with a Poisson problem:

$$\Delta u^i = -f^i,$$

solved on the domain $\Omega = \Omega^1 \cup \Omega^2$, with $\Omega^1 = [0,1] \times [-1,0]$ and $\Omega^2 = [0,1] \times [0,1]$. We impose $u^i = 0$ on the Dirichlet boundaries: $\Gamma_D^1 = \left\{\mathbf{x} = (x_1, x_2) \in \Omega^1, x_2 = -1\right\}$ and $\Gamma_D^2 = \left\{\mathbf{x} = (x_1, x_2) \in \Omega^2, x_2 = 1\right\}$. A scalar Signorini problem is considered on the contact surfaces: $\Gamma_c^1 = \left\{\mathbf{x} = (x_1, x_2) \in \Omega^1, x_2 = 0\right\}$ and $\Gamma_c^2 = \left\{\mathbf{x} = (x_1, x_2) \in \Omega^2, x_2 = 0\right\}$. We use the unbiased Nitsche method with $\theta = 0$ to model the contact between the two domains. In this case the weak problem with a Nitsche's treatment of contact can be written as:

$$\begin{cases} \text{Find } u_h \in V_h \text{ such that, } \forall v_h \in V_h, \\ \displaystyle\sum_{i=1}^{2} \Big(\int_{\Omega^i} \nabla u_h^i \cdot \nabla v_h^i \, \mathrm{d}\Omega \Big) - \frac{1}{2} \int_{\Gamma_{c,h}^1} \frac{1}{\gamma^1} (v_h^1 - v_h^2) \left[\sigma_n^1(u_h^1) - \gamma^1 (u_h^1 - u_h^2) \right]_{\mathbb{R}^-} \mathrm{d}\Gamma \\ \displaystyle -\frac{1}{2} \int_{\Gamma_{c,h}^2} \frac{1}{\gamma^2} (v_h^2 - v_h^1)) \left[\sigma_n^2(u_h^2) - \gamma^2 (u_h^2 - u_h^1) \right]_{\mathbb{R}^-} \mathrm{d}\Gamma = \sum_{i=1}^{2} \Big(\int_{\Omega} f^i v_h^i \, \mathrm{d}\Omega \Big), \end{cases} \tag{5.7}$$

where $\sigma_n^i(u_h^i) = \nabla u_h^i \cdot \mathbf{n}^i$ and V_h is the discretized Hilbert space such that:

$$V_h = \Big\{ (v_h^1, v_h^2) \in (H^1(\Omega^1) \times H^1(\Omega^2)) : v_{h|T}^i \in \mathbb{P}_k(T)), \forall T \in \mathcal{T}_h^i, v_h^i = 0 \text{ on } \Gamma_D^i \Big\},$$

The internal load is manufactured to have the analytical solution:

$$u(\mathbf{x}) = \cos(\pi x_1) \big(\cos(\frac{\pi}{2} x_2) + \sin(2\pi x_2) \big).$$

Thus, the normal derivative on the interface Γ_c^i is given by $\dfrac{\partial u}{\partial n}(\mathbf{x}) = 2\pi \cos(\pi x_1)$.

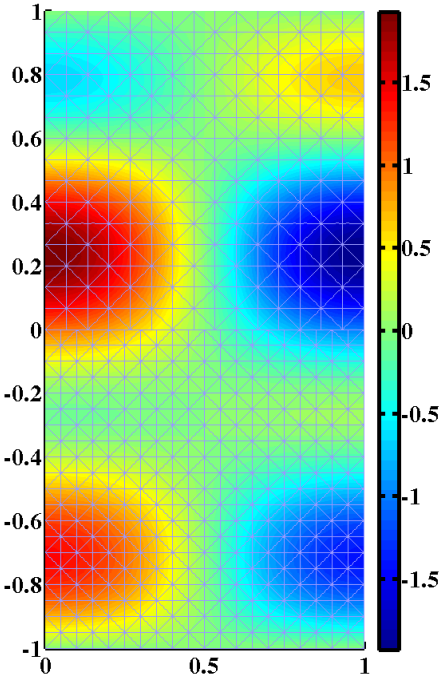

Figure 5.11: Obtained solution u for the scalar Signorini problem with a non-conforming mesh

The obtained solution of (5.7) with Nitsche's method is given in Fig. 5.11. In the following, we provide different numerical error studies. In all cases, the relative H^1 primal error $\frac{\|u-u_h^1\|_{H^1,\Omega^1}}{\|u\|_{H^1,\Omega^1}}$ and the gradient one on the bord: $\frac{\|\frac{\partial u}{\partial n}-\sigma_n^1(u_h^1)\|_{0,\Gamma_c^1}}{\|\frac{\partial u}{\partial n}\|_{0,\Gamma_c^1}}$ are computed by a comparison with the analytical solution stated above. The convergence curves of the two errors are given in Fig. 5.12 for P_1 Lagrange elements and in Fig. 5.13 for P_2 Lagrange element for segment-based integration and element based one with different orders of Gauss-Legendre quadrature rule.

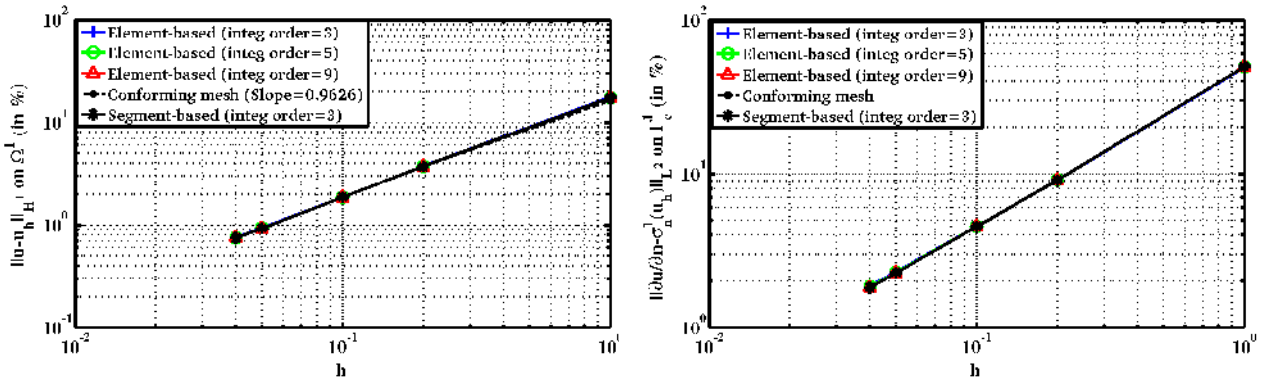

(a) (b)

Figure 5.12: Convergence curves with P_1 elements for different integration rules

The convergence orders of the errors $\|u - u_h^1\|_{H^1,\Omega^1}$ and $\|\frac{\partial u}{\partial n} - \sigma_n^1(u_h^1)\|_{0,\Gamma_c^1}$ are not

affected by integration, for linear approximation, which is the same finding for mortar method in [FPW15, BBWW15].

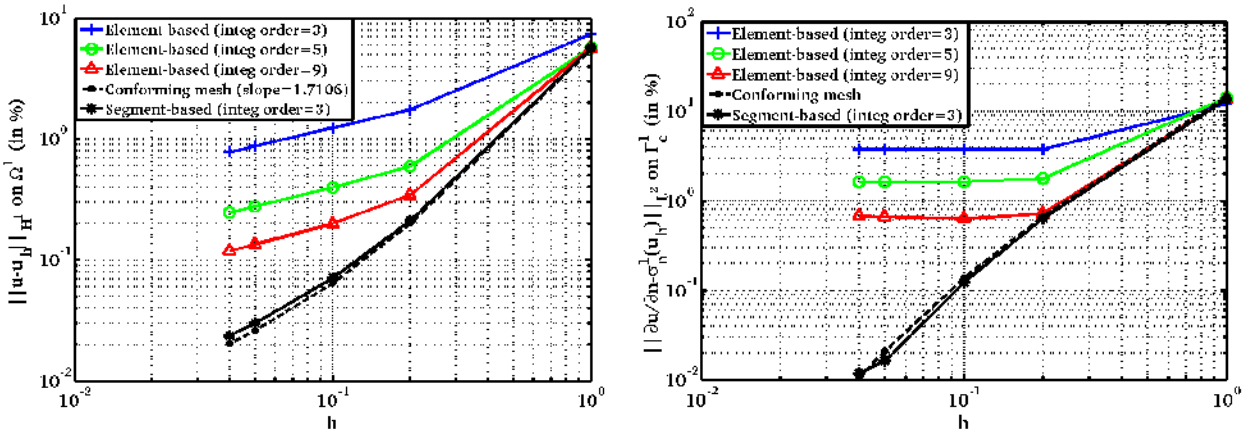

(a) (b)

Figure 5.13: Convergence curves with P_2 elements for different integration rules

For the second order approximation, the results with element-based quadrature rules coincide with the ones with segment-based rule, up to a certain refinement level. Then, the convergence order of the two computed errors is reduced at a certain refinement level and the error is significantly larger than the exact integration one. The starting disturbance threshold is different for different quadrature orders. We note that the gradient error on the interface (equivalent, here to pressure error) is more affected than the primal one by the integration error. Using a higher integration order permits to emprove the convergence but the difference with exact and segment-based integrations remains important.
We get optimal convergence with segment-based integration rule for both linearly and quadratically interpolated elements, as shown by the black solid lines. It is very expected that this behavior would also occur for linear elements, however only for a very small element sizes, which are irrelevant from a practical point of view.

The non symmetric integration proposed in Section 5.2 was an adapted method to avoid weak discontinuities. To confirm that, and since this test involves only weak discontinuities, we plot the convergence curves for P_1 elements, in Fig 5.14, and P_2 elements, in Fig. 5.15, with different integration orders when using non-symmetric integration. The convergence curves got with conforming meshes is plotted in black dashed line to enable comparison.

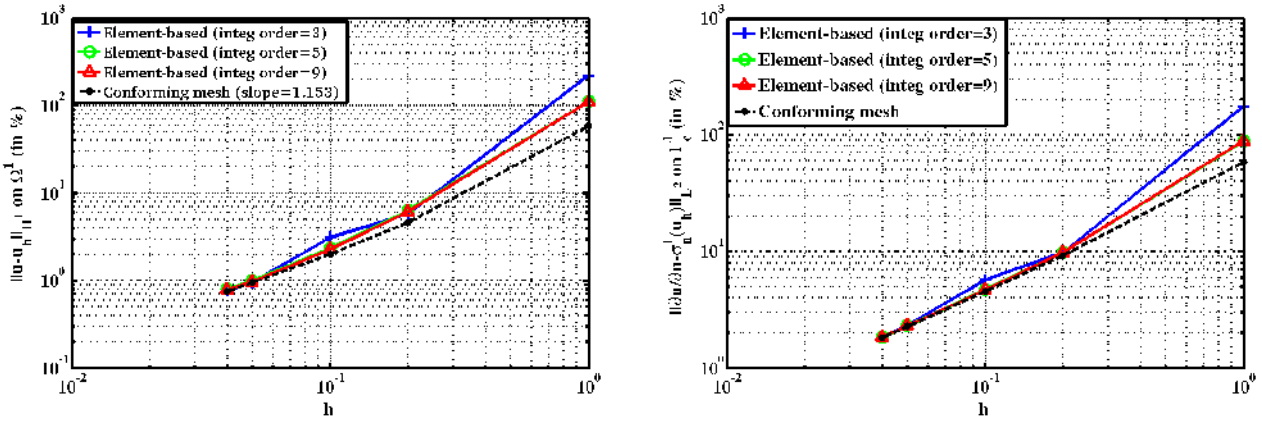

(a) (b)

Figure 5.14: Convergence curves with P_1 elements and non-symetric integration for different integration orders

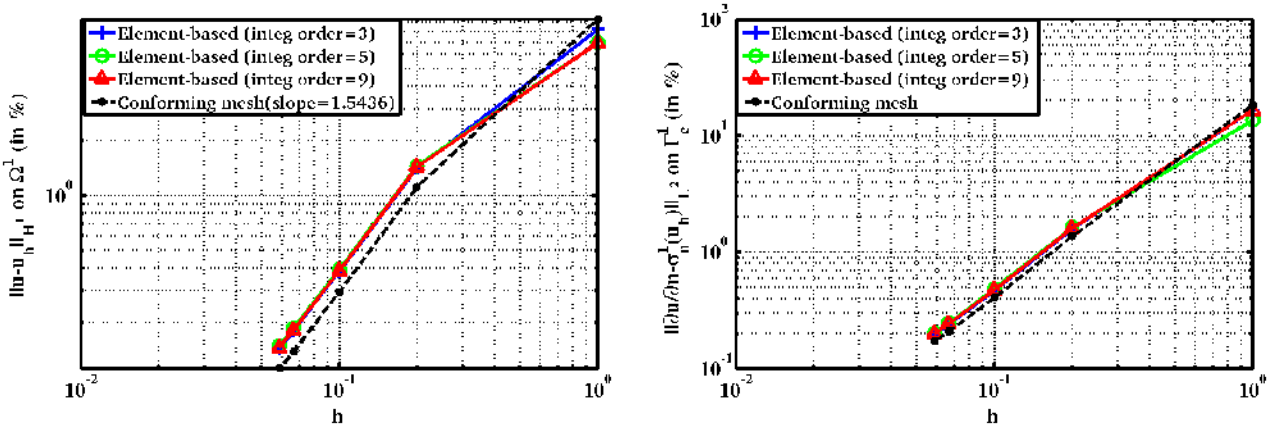

(a) (b)

Figure 5.15: Convergence curves with P_2 elements and non-symmetric integration for different integration orders

In the linear case, results of the non-symmetric approach are comparable to the results of the classic integration case. An additional error appears regarding exact integration, but the error of the two norms keeps decreasing optimally even for small mesh sizes.

The difference between classic and non-symmetric integration is, especially, observable for quadratic approximation. In Fig. 5.15, the optimality is preserved for the two norms even with only an integration order equal to 3.

In some test cases, the influence of quadrature error on the convergence may be limited. As an example, in 3.3, we noted that, for the Hertz problem, the convergence order is not affected by the quadrature error and the optimal convergence is obtained even if using an element-based integration. To confirm that we reconsider Hertz problem, as described in Section 4.3.2 (see Fig. 4.15) with a linear elastic material. A frictionless

contact is considered with only one step charging of 0.1 mm. We plot the convergence curves regarding a reference solution calculated with a very fine mesh. The plots include a segment based integration with a 3^d order Gauss-Legendre integration and an element based one with an integration order equal to 3 and 5. We give the convergence curves of the H^1 error of displacement on the master body Ω^2: $\frac{\|\mathbf{u}_{ref}-\mathbf{u}_h^2\|_{H^1,\Omega^2}}{\|\mathbf{u}_{ref}\|_{H^1,\Omega^2}}$ and L^2 error of contact pressure on the master surface Γ_c^2: $\frac{\|\underline{\underline{\boldsymbol{\sigma}}}(\mathbf{u}_{ref})\mathbf{n}-\underline{\underline{\boldsymbol{\sigma}}}(\mathbf{u}_h)\mathbf{n}\|_{0,\Gamma_c^2}}{\|\underline{\underline{\boldsymbol{\sigma}}}(\mathbf{u}_{ref})\mathbf{n}\|_{0,\Gamma_c^2}}$ for P_1 elements in Fig. 5.16 and for P_2 elements in Fig. 5.17.

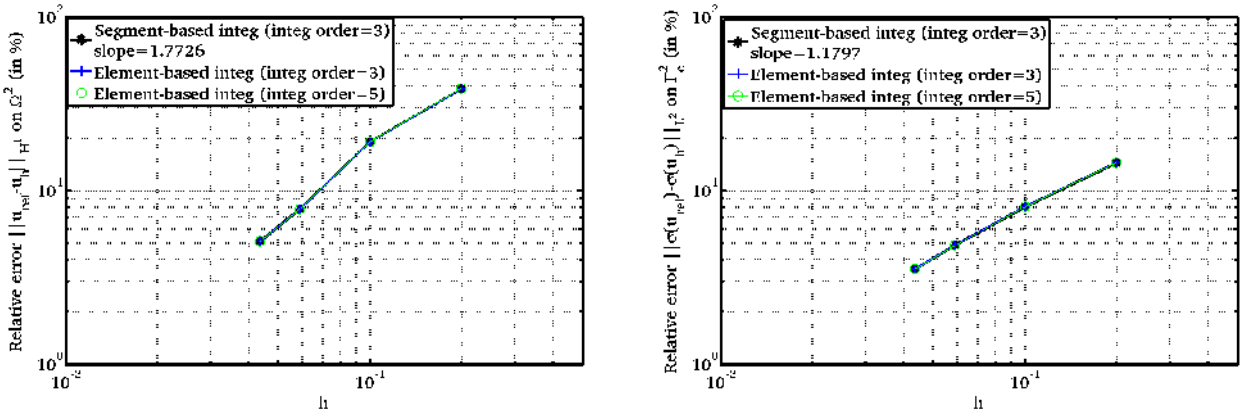

(a) (b)

Figure 5.16: Convergence curves with P_1 elements and different integration rules for Hertz problem

As expected, the convergence order is not influenced by quadrature error for linear approximation. The optimality is conserved for the displacement error as wel as for the contact pressure one. Even when using only a third order integration rule, we obtain the same results as with segmentation.

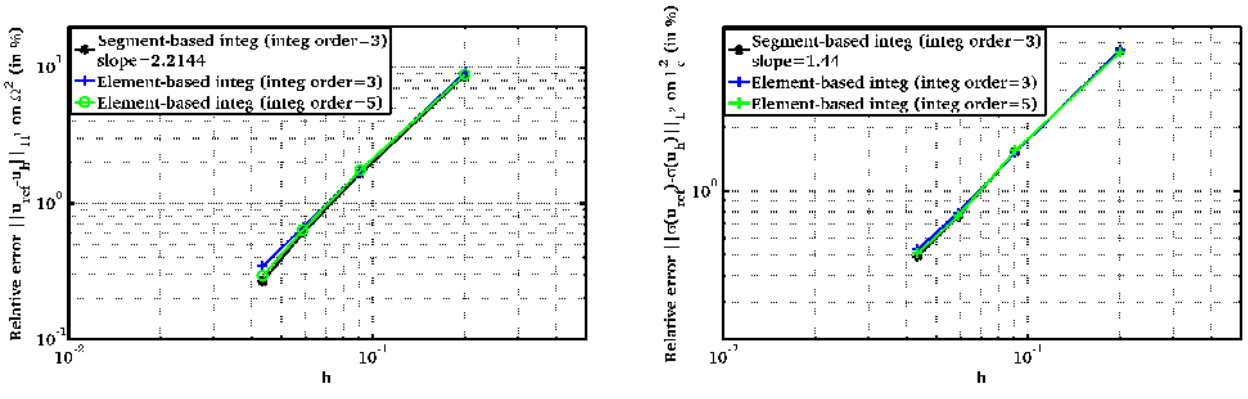

(a) (b)

Figure 5.17: Convergence curves with P_2 elements and different integration rules for Hertz problem

For the quadratic approximation, Fig. 5.17 shows a small difference of convergence

order for small mesh sizes, but it not as significant as for the previous test. In addition, the displacement error is affected by the integration error this time, while the pressure error $\|\underline{\underline{\boldsymbol{\sigma}}}(\mathbf{u}_{ref})\mathbf{n} - \underline{\underline{\boldsymbol{\sigma}}}(\mathbf{u}_h)\mathbf{n}\|_{0,\Gamma_c^2}$ is not influenced. Hertz test is a relatively smooth one, where the active contact zone is limited and the state changing of contact-detachment is continuous. This, could explain the limited influence of quadrature error.

The previous examples proves that segmenting the integration does not increase, necessarily, the convergence order, especially for linear approximation.

Conclusion

The accuracy and the efficiency of integrals computing is an important issue of contact approximation. For Nitsche's method the approximation accuracy is directly influenced by the choice of quadrature rule. In this chapter we provided a numerical study of the patch test performance and the convergence order for different integration strategies. The adapted integration rule depends on the irregularities faced. In the general case, segment-based integration is the more accurate one, but, its high cost motivates the use of other strategies. In addition, in some highly irregular cases the gain of segmentation is not significant. This may be the case, as well when the contact occurs only in a limited surface (as for Hertz problem). The use of the non-symmetric integration is a a good solution to reduce the integration error within the contact surface, but on the boundary of the surface it is needed to cut the integration scheme and in that case the boundary segmentation is the adapted strategy. In general, Nitsche's method seems to be influenced in a similar way by the quadrature error as the mortar method; but a more elaborated comparison of the two methods in this aspect is an interesting continuation of this work. The considered study was limited to the 2D case for the segment-based integration. One could investigate the influence of segmentation in the 3D case. An other important perspective of this study is the test of different integration strategies, especially non-symmetric integration, with a more complex and realistic configuration.

Conclusions and Outlook

This thesis provided a detailed mathematical and numerical study of Nitsche's finite element method for contact and friction. The method was presented for Signorini's problem and generalized to the two elastic bodies contact problem and then presented in a generic formalism appropriate for different type of boundary conditions. The main advantage of the method is the consistent treatment of boundary conditions without adding Lagrange multipliers. It is, as well, intrinsically integral permitting a better handling of non-conforming descritization of the interface.

For the frictional contact, we proposed a classic and then an unbiased formulation that could be seen as a first step to apply Nitsche's method to multi-body contact and self-contact in the generic framework of large strain. A generalization parameter θ is considered to cover an entire set of methods with different numerical and theoretical properties. For a conservative system, we succeed to derive the method from an energy potential. The method was analyzed and we proved its consistency, well-posedness and optimal convergence and the particular case of $\theta = -1$ was proved to be more robust regarding the Nitsche's parameter γ. The theoretical results are, generally, confirmed by numerical tests, especially the optimal convergence and the influence of the parameter γ. Since the analysis in the small strain case was promising, the next step was to extend the method to the large strain case. The extension was made also for the friction law, since we consider a Coulomb friction in this chapter instead of Tresca friction. We derived an unbiased formulation that can be directly amenable to self-contact and multi-body contact. The method is constructed independently of the mapping function, but its performance depends on the used mapping. Therefore, we gave a brief comparison of two mapping strategies: projection and ray-tracing and we noted that ray-tracing is the exceeding choice from the modeling and simulation point of view. The study of Nitsche's method in the large strain framework proved that it is a very competitive contact formulation directly relevant to an unbiased description of the phenomena. The method is as accurate as classic mortar type methods remaining primal. In term of robustness, the method's performance depends on the considered variant θ, but, generally the method succeeds to converge without any additional considerations, even with extreme deformations, and self-contact configurations, and heterogeneous materials.
Being an integral formulation, the performance of Nitsche's method depends on the scheme used to approximate the contact integrals. In the performed tests, we made the choice of using the classic Gauss scheme over the original elements without cutting. This choice was argued in details in Chapter 5. The influence of numerical integration on the accuracy and convergence of Nitsche's type contact method was then studied for different types of quadrature scheme and we concluded that segmenting the contact interface is not always efficient and other integration techniques may be as accurate with a cheaper cost.

The study of quadrature scheme may be supported by a more elaborated test pallet. The tests performed with different integration methods were considered for non-frictional

contact; but a study of the influence of quadrature on the friction approximation is, as well, an important perspective.

For the analytical part, An estimation of error in the L^2-norm and the development of a criterion for adaptative mesh refinement could be envisaged in future work.

In this work, we used an hyper-elastic material, but, since the constitutive law is used in the contact model for Nitsche's method, extending the method to inelastic behavior may need some adaptations, since state variables are typically calculated and stored at quadrature points on the interior of the elements. In a Nitsche approach, such fields will also need to be computed and stored on the surface. Therefore an extension to inelastic materials could be considered in forthcoming studies. The method was analyzed only for two types of mapping: "projection" and "ray-tracing". The comparison between this two methods may be further analyzed. One can use other definitions of the gap such us the construction of an intermediate geometry, as done in [Dur12].

All the current study concerns the implicit model, but in several applications the explicit time scheme are used and an application of Nitsche's method for contact to this framework may be interesting. In that case, the main disadvantage of Nitsche's method, which is its use of the constitutive law, could be overcome since the contact pressure is calculated explicitly. The use of thin-shell structures may be problematic for Nitsche's type formulations because of the use of pressure; but it remains an important development subject.

APPENDICES

Appendix A

Directional derivative of the stress tensor

To make explicit each term in formulation (4.25), we need first the following results on the directional derivatives of deformation tensors, that are obtained after simple computations (see, e.g. [FG11, Chapter 14]):

Proposition A.0.1. *The directional derivatives of* $\underline{\underline{\mathbf{F}}}$ *and* $\underline{\underline{\mathbf{E}}}$ *are:*

$$\begin{aligned} \mathcal{D}\underline{\underline{\mathbf{F}}}(\mathbf{u})[\delta\mathbf{u}] &= \underline{\underline{\boldsymbol{\nabla}}}_X(\delta\mathbf{u}), \\ \mathcal{D}\underline{\underline{\mathbf{E}}}(\mathbf{u})[\delta\mathbf{u}] &= \mathrm{sym}\,(\underline{\underline{\mathbf{F}}}^T(\mathbf{u})\nabla_X(\delta\mathbf{u})) = \underline{\underline{\mathbf{F}}}^T(\mathbf{u})\,\boldsymbol{\epsilon}(\delta\mathbf{u})\,\underline{\underline{\mathbf{F}}}(\mathbf{u}), \end{aligned}$$

where $\mathrm{sym}\,(\cdot)$ *denotes the symmetric part of a second order tensor.*

The computation of the directional derivatives of stress tensors $\underline{\underline{\hat{\boldsymbol{\sigma}}}}$ and $\underline{\underline{\mathbf{S}}}$ is more involved and we recall their expression below (see as well [FG11, Chapter 14]):

Proposition A.0.2. *The directional derivatives of* $\underline{\underline{\mathbf{S}}}$*, resp.* $\underline{\underline{\hat{\boldsymbol{\sigma}}}}$*, are:*

$$\mathcal{D}\underline{\underline{\mathbf{S}}}(\mathbf{u})[\delta\mathbf{u}] = \underline{\underline{\boldsymbol{\mathcal{C}}}}(\mathbf{u}) : \underline{\underline{\mathbf{F}}}^T(\mathbf{u})\underline{\underline{\boldsymbol{\nabla}}}_X(\delta\mathbf{u}) = \underline{\underline{\boldsymbol{\mathcal{C}}}}(\mathbf{u}) : \underline{\underline{\mathbf{F}}}^T(\mathbf{u})\,\boldsymbol{\epsilon}(\delta\mathbf{u})\,\underline{\underline{\mathbf{F}}}(\mathbf{u}). \tag{A.1}$$

$$\mathcal{D}\underline{\underline{\hat{\boldsymbol{\sigma}}}}(\mathbf{u})[\delta u] = \underline{\underline{\boldsymbol{\nabla}}}_X(\delta\mathbf{u})\,\underline{\underline{\mathbf{S}}}(\mathbf{u}) + \underline{\underline{\mathbf{F}}}(\mathbf{u})(\underline{\underline{\boldsymbol{\mathcal{C}}}}(u) : \underline{\underline{\mathbf{F}}}^T(\mathbf{u})\underline{\underline{\boldsymbol{\nabla}}}_X(\delta\mathbf{u})). \tag{A.2}$$

Proof: First, for an hyperelastic law, there holds in fact $\underline{\underline{\mathbf{S}}}(\mathbf{u}) = \underline{\underline{\mathbf{S}}}(\underline{\underline{\mathbf{E}}}(\mathbf{u}))$ and we apply the chain rule:

$$\mathcal{D}\underline{\underline{\mathbf{S}}}(\mathbf{u})[\delta\mathbf{u}] = \mathcal{D}\underline{\underline{\mathbf{S}}}(\underline{\underline{\mathbf{E}}}(\mathbf{u}))[\mathcal{D}\underline{\underline{\mathbf{E}}}(\mathbf{u})[\delta\mathbf{u}]] = \frac{\partial\underline{\underline{\mathbf{S}}}}{\partial\underline{\underline{\mathbf{E}}}}(\mathbf{u}) : \mathcal{D}\underline{\underline{\mathbf{E}}}(\mathbf{u})[\delta\mathbf{u}].$$

Since $\underline{\underline{\boldsymbol{\mathcal{C}}}} = \dfrac{\partial\underline{\underline{\mathbf{S}}}}{\partial\underline{\underline{\mathbf{E}}}}$ and using Proposition A.0.1 we get:

$$\mathcal{D}\underline{\underline{\mathbf{S}}}(u)[\delta\mathbf{u}] = \underline{\underline{\boldsymbol{\mathcal{C}}}}(\mathbf{u}) : \mathrm{sym}\,(\underline{\underline{\mathbf{F}}}^T(\mathbf{u})\underline{\underline{\boldsymbol{\nabla}}}_X(\delta\mathbf{u})).$$

Then (A.1) is obtained with the above formula and the symmetry properties of $\underline{\underline{\boldsymbol{\mathcal{C}}}}$.

Using the relationship $\underline{\underline{\hat{\boldsymbol{\sigma}}}} = \underline{\underline{\mathbf{F}}}\,\underline{\underline{\mathbf{S}}}$ and applying the product rule yield, for $\mathcal{D}\underline{\underline{\hat{\boldsymbol{\sigma}}}}(\mathbf{u})[\delta\mathbf{u}]$:

$$\mathcal{D}\underline{\underline{\hat{\boldsymbol{\sigma}}}}(\mathbf{u})[\delta\mathbf{u}] = \mathcal{D}\underline{\underline{\mathbf{F}}}(\mathbf{u})[\delta\mathbf{u}]\underline{\underline{\mathbf{S}}}(\mathbf{u}) + \underline{\underline{\mathbf{F}}}(\mathbf{u})\mathcal{D}\underline{\underline{\mathbf{S}}}(\mathbf{u})[\delta\mathbf{u}].$$

We use (A.1) and once again Proposition A.0.1 to obtain (A.2). □

As an example, suppose that the constitutive law is those of a Saint-Venant-Kirchhoff material, i.e., that:

$$W(\underline{\underline{\mathbf{E}}}) = \frac{\lambda}{2}(\mathrm{tr}\,(\underline{\underline{\mathbf{E}}}))^2 + \mu\,\mathrm{tr}\,(\underline{\underline{\mathbf{E}}}^2),$$

where λ and μ are material parameters, see, e.g., [BW08, Chapter 5]. The associated second Piola-Kirchhoff stress tensor and elasticity tensor are:

$$\underline{\underline{\mathbf{S}}} = \lambda \mathrm{tr}\,(\underline{\underline{\mathbf{E}}})\underline{\underline{\mathbf{I}}} + 2\mu\underline{\underline{\mathbf{E}}}, \qquad \underline{\underline{\underline{\underline{\boldsymbol{\mathcal{C}}}}}} = \lambda\,\underline{\underline{\mathbf{I}}} \otimes \underline{\underline{\mathbf{I}}} + 2\mu\,\underline{\underline{\underline{\underline{\boldsymbol{\mathcal{I}}}}}}.$$

Let us detail the expression

$$\begin{aligned}\mathcal{D}\underline{\underline{\hat{\boldsymbol{\sigma}}}}(\mathbf{u})[\delta\mathbf{u}] &= \underline{\underline{\boldsymbol{\nabla}}}_X(\delta\mathbf{u})\,\underline{\underline{\mathbf{S}}}(u) + \underline{\underline{\mathbf{F}}}(\mathbf{u})(\underline{\underline{\underline{\underline{\boldsymbol{\mathcal{C}}}}}}(\mathbf{u}) : \underline{\underline{\mathbf{F}}}^T(\mathbf{u})\underline{\underline{\boldsymbol{\nabla}}}_X(\delta\mathbf{u})) \\ &= \underline{\underline{\boldsymbol{\nabla}}}_X(\delta\mathbf{u})\ (\lambda \mathrm{tr}\,(\underline{\underline{\mathbf{E}}}(\mathbf{u}))\underline{\underline{\mathbf{I}}} + 2\mu\underline{\underline{\mathbf{E}}}(\mathbf{u})) + \underline{\underline{\mathbf{F}}}(\mathbf{u})((\lambda\,\underline{\underline{\mathbf{I}}} \otimes \underline{\underline{\mathbf{I}}} + 2\mu\,\underline{\underline{\underline{\underline{\boldsymbol{\mathcal{I}}}}}}) : \underline{\underline{\mathbf{F}}}^T(\mathbf{u})\underline{\underline{\boldsymbol{\nabla}}}_X(\delta\mathbf{u})).\end{aligned}$$

We compute separately

$$\underline{\underline{\mathbf{I}}} \otimes \underline{\underline{\mathbf{I}}} : \underline{\underline{\mathbf{F}}}^T(\mathbf{u})\underline{\underline{\boldsymbol{\nabla}}}_X(\delta\mathbf{u}) = (\underline{\underline{\mathbf{I}}} : \underline{\underline{\mathbf{F}}}^T(\mathbf{u})\underline{\underline{\boldsymbol{\nabla}}}_X(\delta\mathbf{u}))\underline{\underline{\mathbf{I}}} = \mathrm{tr}\,(\underline{\underline{\mathbf{F}}}^T(\mathbf{u})\underline{\underline{\boldsymbol{\nabla}}}_X(\delta\mathbf{u}))\underline{\underline{\mathbf{I}}},$$

and

$$\underline{\underline{\underline{\underline{\boldsymbol{\mathcal{I}}}}}} : \underline{\underline{\mathbf{F}}}^T(\mathbf{u})\underline{\underline{\boldsymbol{\nabla}}}_X(\delta\mathbf{u}) = \mathrm{sym}\,(\underline{\underline{\mathbf{F}}}^T(\mathbf{u})\underline{\underline{\boldsymbol{\nabla}}}_X(\delta\mathbf{u})).$$

This yields

$$\begin{aligned}\mathcal{D}\underline{\underline{\hat{\boldsymbol{\sigma}}}}(\mathbf{u})[\delta\mathbf{u}] &= \underline{\underline{\boldsymbol{\nabla}}}_X(\delta\mathbf{u})\ (\lambda \mathrm{tr}\,(\underline{\underline{\mathbf{E}}}(\mathbf{u}))\underline{\underline{\mathbf{I}}} + 2\mu\underline{\underline{\mathbf{E}}}(\mathbf{u})) \\ &\quad + \underline{\underline{\mathbf{F}}}(\mathbf{u})(\lambda\,\mathrm{tr}\,(\underline{\underline{\mathbf{F}}}^T(\mathbf{u})\underline{\underline{\boldsymbol{\nabla}}}_X(\delta\mathbf{u}))\underline{\underline{\mathbf{I}}} + 2\mu\,\mathrm{sym}\,(\underline{\underline{\mathbf{F}}}^T(\mathbf{u})\underline{\underline{\boldsymbol{\nabla}}}_X(\delta\mathbf{u}))) \\ &= \lambda\left(\mathrm{tr}\,(\underline{\underline{\mathbf{E}}}(\mathbf{u}))\underline{\underline{\boldsymbol{\nabla}}}_X(\delta\mathbf{u}) + \mathrm{tr}\,(\underline{\underline{\mathbf{F}}}^T(\mathbf{u})\underline{\underline{\boldsymbol{\nabla}}}_X(\delta\mathbf{u}))\underline{\underline{\mathbf{F}}}(\mathbf{u})\right) \\ &\quad + 2\mu\left(\underline{\underline{\boldsymbol{\nabla}}}_X(\delta\mathbf{u})\underline{\underline{\mathbf{E}}}(\mathbf{u}) + \underline{\underline{\mathbf{F}}}(\mathbf{u})\,\mathrm{sym}\,(\underline{\underline{\mathbf{F}}}^T(\mathbf{u})\underline{\underline{\boldsymbol{\nabla}}}_X(\delta\mathbf{u}))\right).\end{aligned}$$

We finally obtain $\mathcal{D}\hat{\boldsymbol{\sigma}}_{\boldsymbol{N}}(\mathbf{u})[\delta\mathbf{u}]$ using relationship:

$$\mathcal{D}\hat{\boldsymbol{\sigma}}_{\boldsymbol{N}}(\mathbf{u})[\delta\mathbf{u}] = \mathcal{D}\underline{\underline{\hat{\boldsymbol{\sigma}}}}(\mathbf{u})[\delta\mathbf{u}]\boldsymbol{N},$$

since $\hat{\boldsymbol{\sigma}}_{\boldsymbol{N}} = \underline{\underline{\hat{\boldsymbol{\sigma}}}}\boldsymbol{N}$. The same process can be applied for various constitutive laws.

Appendix B

Partial derivatives of $\boldsymbol{\mathcal{C}}(\boldsymbol{\lambda}, g, \mathbf{v}, \mathbf{n})$

Making use of the Heaviside function, defined as:

$$H(x) = \begin{cases} 0, \text{ for } x < 0 \\ 1, \text{ for } x \geq 0 \end{cases},$$

partial derivatives of the quantity $\tau = \mathscr{F}\,[\boldsymbol{\lambda}\cdot\mathbf{n} + r\,g]_{\mathbb{R}^-}$, with $[.]_{\mathbb{R}^-}$ is the projection into $\mathbb{R}^-$, can be expressed as:

$$\begin{aligned} \partial_{\boldsymbol{\lambda}}\tau &= H(-\boldsymbol{\lambda}\cdot\mathbf{n} - r\,g)\ \mathscr{F}\ \mathbf{n}\,, \\ \partial_{g}\tau &= H(-\boldsymbol{\lambda}\cdot\mathbf{n} - r\,g)\ \mathscr{F}\ r\,, \\ \partial_{\mathbf{n}}\tau &= H(-\boldsymbol{\lambda}\cdot\mathbf{n} - r\,g)\ \mathscr{F}\ \underline{\underline{\mathbf{T}_n}}\ \boldsymbol{\lambda}\,. \end{aligned}$$

Moreover, writing $\mathbf{q}_T = \underline{\underline{\mathbf{T}_n}}\,\mathbf{q}$, partial derivatives of projection $\boldsymbol{\mathcal{P}}_{B(\mathbf{n},\tau)}(\mathbf{q})$ can be expressed as:

$$\partial_{\mathbf{q}}\boldsymbol{\mathcal{P}}_{B(\mathbf{n},\tau)}(\mathbf{q}) = \begin{cases} 0 & \text{for } \tau \leq 0 \\ \underline{\underline{\mathbf{T}_n}} & \text{for } \|\mathbf{q}_T\| \leq \tau \\ \dfrac{\tau}{\|\mathbf{q}_T\|}\left(\underline{\underline{\mathbf{T}_n}} - \dfrac{\mathbf{q}_T}{\|\mathbf{q}_T\|}\otimes\dfrac{\mathbf{q}_T}{\|\mathbf{q}_T\|}\right) & \text{otherwise} \end{cases}$$

$$\partial_{\tau}\boldsymbol{\mathcal{P}}_{B(\mathbf{n},\tau)}(\mathbf{q}) = \begin{cases} 0 & \text{for } \tau \leq 0 \text{ or } \|\mathbf{q}_T\| \leq \tau \\ \dfrac{\mathbf{q}_T}{\|\mathbf{q}_T\|} & \text{otherwise} \end{cases}$$

$$\partial_{\mathbf{n}}\boldsymbol{\mathcal{P}}_{B(\mathbf{n},\tau)}(\mathbf{q}) = \begin{cases} 0 & \text{for } \tau \leq 0 \\ -\mathbf{q}\cdot\mathbf{n}\ \underline{\underline{\mathbf{T}_n}} - \mathbf{n}\otimes\mathbf{q}_T & \text{for } \|\mathbf{q}_T\| \leq \tau \\ -\dfrac{\tau}{\|\mathbf{q}_T\|}\left(\mathbf{q}\cdot\mathbf{n}\left(\underline{\underline{\mathbf{T}_n}} - \dfrac{\mathbf{q}_T}{\|\mathbf{q}_T\|}\otimes\dfrac{\mathbf{q}_T}{\|\mathbf{q}_T\|}\right) + \mathbf{n}\otimes\mathbf{q}_T\right) & \text{otherwise.} \end{cases}$$

Finally, the partial derivatives of function $\boldsymbol{\mathcal{C}}$ can be calculated as:

$$\begin{aligned} \partial_{\boldsymbol{\lambda}}\boldsymbol{\mathcal{C}}(\boldsymbol{\lambda}, g, \mathbf{v}, \mathbf{n}) &= \partial_{q}\boldsymbol{\mathcal{P}}_{B(\mathbf{n},\tau)} + \partial_{\tau}\boldsymbol{\mathcal{P}}_{B(\mathbf{n},\tau)}\otimes\partial_{\boldsymbol{\lambda}}\tau + H(-\boldsymbol{\lambda}\cdot\mathbf{n} - r\,g)\ \mathbf{n}\otimes\mathbf{n}\,, \\ \partial_{g}\boldsymbol{\mathcal{C}}(\boldsymbol{\lambda}, g, \mathbf{v}, \mathbf{n}) &= \partial_{\tau}\boldsymbol{\mathcal{P}}_{B(\mathbf{n},\tau)}\ \partial_{g}\tau + H(-\lambda\cdot\mathbf{n} - r\,g)\ r\ \mathbf{n}\,, \\ \partial_{\mathbf{n}}\boldsymbol{\mathcal{C}}(\boldsymbol{\lambda}, g, \mathbf{v}, \mathbf{n}) &= \partial_{\mathbf{n}}\boldsymbol{\mathcal{P}}_{B(\mathbf{n},\tau)}\partial_{\tau}\boldsymbol{\mathcal{P}}_{B(\mathbf{n},\tau)}\otimes\partial_{\mathbf{n}}\tau \\ &\quad + H(-\boldsymbol{\lambda}\cdot\mathbf{n} - r\,g)\ \left(\mathbf{n}\otimes\boldsymbol{\lambda} - (2\ \boldsymbol{\lambda}\cdot\mathbf{n} + r\,g)\ \mathbf{n}\otimes\mathbf{n} + (\boldsymbol{\lambda}\cdot\mathbf{n} + r\,g)\ \underline{\underline{\mathbf{I}}}\right)\,, \\ \partial_{\mathbf{v}}\boldsymbol{\mathcal{C}}(\lambda, g, \mathbf{v}, \mathbf{n}) &= -r\ \partial_{\mathbf{q}}\boldsymbol{\mathcal{P}}_{B(\mathbf{n},\tau)}\,, \end{aligned}$$

where $\boldsymbol{\mathcal{P}}_{B(\mathbf{n},\tau)} = \boldsymbol{\mathcal{P}}_{B(\mathbf{n},\tau)}(\mathbf{q}) = \boldsymbol{\mathcal{P}}_{B(\mathbf{n},\tau)}(\boldsymbol{\lambda} - r\,\mathbf{v})$ in the presentation of the partial derivatives of $\boldsymbol{\mathcal{C}}$.

Bibliography

[AC88] P. Alart and A. Curnier. A generalized Newton method for contact problems with friction. *Journal of Theoretical and Applied Mechanics*, 7(1):67–82, 1988.

[AC91] P. Alart and A. Curnier. A mixed formulation for frictional contact problems prone to newton like solution methods. *Computer Methods in Applied Mechanics and Engineering*, 92(3):353 – 375, 1991.

[AHD14] C. Annavarapu, M. Hautefeuille, and J. E. Dolbow. A Nitsche stabilized finite element method for frictional sliding on embedded interfaces. Part I: Single interface. *Computer Methods in Applied Mechanics and Engineering*, 268:417–436, 2014.

[Ala88] P. Alart. *Multiplicateurs "augmentés" et méthode de Newton généralisée pour contact avec frottement*. Technical report, Document LMA-DME-EPFL, Lausanne, 1988.

[AM83] V. Alexandrov and S. Mhitaryan. *Contact problems for bodies with thin coatings and interlayers*. Nauka, Moscow, 1983.

[Amd13] S. Amdouni. *Numerical analysis of some saddle point formulation with X-FEM type approximation on cracked or fictitious domains*. PhD thesis, Institut National des Sciences Appliquées de Lyon and École Nationale d'Ingénieurs de Tunis, 2013.

[AP98] F. Armero and E. Petőcz. Formulation and analysis of conserving algorithms for frictionless dynamic contact/impact problems. *Computer Methods in Applied Mechanics and Engineering*, 158(3):269 – 300, 1998.

[AS58] K. Arrow and R. Solow. Gradient methods for constrained maxima, with weakened assumptions. In K. Arrow, L. Hurwicz, and H. Uzawa, editors, *Studies in Linear and Nonlinear Programming*, page 166–176. Stanford University Press, 1958.

[AS98] A. Amassad and M. Sofonea. Analysis of a quasistatic viscoplastic problem involving Tresca friction law. *Discrete and Continuous Dynamical Systems*, 4(1):55–72, 1998.

[ASJ+15] C. Annavarapu, R. Settgast, S. M. Johnson, P. Fu, and E. B. Herbold. A weighted Nitsche stabilized method for small-sliding contact on frictional surfaces. *Computer Methods in Applied Mechanics and Engineering*, 283:763–781, 2015.

[ASWB14] A. Apostolatos, R. Schmidt, R. Wüchner, and K.-U. Bletzinger. A nitsche-type formulation and comparison of the most common domain decomposition methods in isogeometric analysis. *International Journal for Numerical Methods in Engineering*, 97(7):473–504, 2014.

[Bat96] K.-J. Bathe. *Finite element procedures*. Prentice Hall, 1996.

[BAV01] M. Barboteu, P. Alart, and M. Vidrascu. A domain decomposition strategy for nonclassical frictional multi-contact problems. *Computer Methods in Applied Mechanics and Engineering*, 190(37):4785 – 4803, 2001.

[BB99] F. Ben Belgacem. The mortar finite element method with lagrange multipliers. *Numerische Mathematik*, 84(2):173–197, 1999.

[BB00] F. Ben Belgacem. Numerical simulation of some variational inequalities arisen from unilateral contact problems by the finite element methods. *SIAM Journal on Numerical Analysis*, 37(4):1198–1216, 2000.

[BB16] T. Boiveau and E. Burman. A penalty-free Nitsche method for the weak imposition of boundary conditions in compressible and incompressible elasticity. *IMA Journal of Numerical Analysis*, 36(2):770–795, 2016.

[BBHL98] F. Ben Belgacem, P. Hild, and P. Laborde. The mortar finite element method for contact problems. *Mathematical and Computer Modelling*, 28(4):263 – 271, 1998.

[BBHL99] F. Ben Belgacem, P. Hild, and P. Laborde. Extension of the mortar finite element method to a variational inequality modeling unilateral contact. *M Mathematical Models and Methods in Applied Sciences*, 09(02):287–303, 1999.

[BBR03] F. Ben Belgacem and Y. Renard. Hybrid finite element methods for the Signorini problem. *Mathematics of Computation*, 72(243):1117–1145, 2003.

[BBWW15] E. Brivadis, A. Buffa, B. Wohlmuth, and L. Wunderlich. The influence of quadrature errors on isogeometric mortar methods. In B. Jüttler and B. Simeon, editors, *Isogeometric Analysis and Applications*, pages 33–50. Springer International Publishing, 2015.

[BC85] K.-J. Bathe and A. Chaudhary. A solution method for planar and axisymmetric contact problems. *International Journal for Numerical Methods in Engineering*, 21(1):65–88, 1985.

[Ber84] D. P. Bertsekas. *Constrained optimization and Lagrange multiplier methods*. Academic Press, 1984.

[BH90] D. J. Benson and J. O. Hallquist. A single surface contact algorithm for the post-buckling analysis of shell structures. *Computer Methods in Applied Mechanics and Engineering*, 78(2):141 – 163, 1990.

[BH12] E. Burman and P. Hansbo. Fictitious domain finite element methods using cut elements: II. A stabilized Nitsche's method. *Computer Methods in Applied Mechanics and Engineering*, 2(4):328–341, 2012.

[BH17] E. Burman and P. Hansbo. Deriving robust unfitted finite element methods from augmented lagrangian formulations. *arXiv preprint arXiv:1702.08340*, 2017.

[BHL16a] E. Burman, P. Hansbo, and M. Larson. Augmented Lagrangian finite element methods for contact problems. *arXiv preprint arXiv:1609.03326*, 2016.

[BHL16b] E. Burman, P. Hansbo, and M. G. Larson. The Penalty Free Nitsche Method and Nonconforming Finite Elements for the Signorini Problem. *arXiv preprint arXiv:1609.03745*, 2016.

[BHLS17] E. Burman, P. Hansbo, M. G. Larson, and R. Stenberg. Galerkin least squares finite element method for the obstacle problem. *Computer Methods in Applied Mechanics and Engineering*, 313:362–374, 2017.

[BHS03] R. Becker, P. Hansbo, and R. Stenberg. A finite element method for domain decomposition with non-matching grids. *Mathematical Modelling and Numerical Analysis*, 37:209–225, 2003.

[BLM00] T. Belytschko, W. K. Liu, and B. Moran. *Nonlinear finite elements for continua and structures*. Wiley, 2000.

[BMP94] C. Bernardi, Y. Maday, and A. T. Patera. A new nonconforming approach to domain decomposition : the mortar element method. *Nonlinear partial equations and their applications*, page 13–51, 1994.

[Bre68] H. Brezis. équations et inéquations non linéaires dans les espaces vectoriels en dualité. *Annales Institut Fourier(Grenoble)*, 18:115–175, 1968.

[BS05] L. Baillet and T. Sassi. Mixed finite element formulation in large deformation frictional contact problem. *Rev. Européenne Élém. Finis*, 14(2-3):287–304, 2005.

[BS07] S.-C. Brenner and L.-R. Scott. *The mathematical theory of finite element methods*, volume 15 of *Texts in Applied Mathematics*. Springer-Verlag, New York, 2007.

[Bur12] E. Burman. A penalty-free nonsymmetric Nitsche-type method for the weak imposition of boundary conditions. *SIAM Journal on Numerical Analysis*, 50(4):1959–1981, 2012.

[BW08] J. Bonet and R. D. Wood. *Nonlinear continuum mechanics for finite element analysis*. Cambridge University Press, Cambridge (UK), New York, 2008.

[CFH+2] F. Chouly, M. Fabre, P. Hild, J. Pousin, and Y. Renard. Residual-based a posteriori error estimation for contact problems approximated by Nitsche's method. *IMA Journal of Numerical Analysis*, 2. To appear.

[CFH+17] F. Chouly, M. Fabre, P. Hild, R. Mlika, J. Pousin, and Y. Renard. An overview of recent results on nitsche's method for contact problems. In *To appear in Lecture Notes in Computational Science and Engineering*. springer, 2017.

[CH13] F. Chouly and P. Hild. Nitsche-based method for unilateral contact problems: numerical analysis. *SIAM Journal on Numerical Analysis*, 51:1295–1307, 2013.

[CHK95] A. Curnier, Q. He, and A. Klarbring. Continuum mechanics modelling of large deformation contact with friction. *Contact Mechanics*, pages 145–158, 1995.

[Cho14] F. Chouly. An adaptation of Nitsche's method to the tresca friction problem. *Journal of Mathematical Analysis and Applications*, 411:329–339, 2014.

[CHR15a] F. Chouly, P. Hild, and Y. Renard. A Nitsche finite element method for dynamic contact: 1. Space semi-discretization and time-marching schemes. *ESAIM Mathematical Modelling and Numerical Analysis*, 49(2):481–502, 2015.

[CHR15b] F. Chouly, P. Hild, and Y. Renard. A Nitsche finite element method for dynamic contact: 2. Stability of the schemes and numerical experiments. *ESAIM Mathematical Modelling and Numerical Analysis*, 49(2):503–528, 2015.

[CHR15c] F. Chouly, P. Hild, and Y. Renard. Symmetric and non-symmetric variants of Nitsche's method for contact problems in elasticity: theory and numerical experiments. *Mathematics of Computation*, 84:1089–1112, 2015.

[Cia91] P.-G. Ciarlet. *The finite element method for elliptic problems*, volume II of *Handbook of Numerical Analysis (eds. P.G. Ciarlet and J.L. Lions)*. North-Holland Publishing Co., Amsterdam, 1991.

[CLM97] L. Cazabeau, C. Lacour, and Y. Maday. Numerical quadratures and mortar methods. In *Computational Science for the 21st Century*, pages 119–128. John Wiley and Sons, 1997.

[CMR16] F. Chouly, R. Mlika, and Y. Renard. An unbiased Nitsche's approximation of the frictional contact between two elastic structures. *To appear in Numerische Mathematik , Available on HAL as hal-01240068*, 2016.

[Cri00] M. A. Crisfield. Re-visiting the contact patch test. *International Journal for Numerical Methods in Engineering*, 48:435–449, 2000.

[CS07] M. Chernov, A. Maischak and E. Stephan. A priori error estimates for hp penalty BEM for contact problems in elasticity. *Computer Methods in Applied Mechanics and Engineering*, 196:3871–3880, 2007.

[DEP11] D. Doyen, A. Ern, and S. Piperno. Time-integration schemes for the finite element dynamic signorini problem. *SIAM Journal on Scientific Computing*, 33(1):223–249, 2011.

[DH15] G. Drouet and P. Hild. Optimal convergence for discrete variational inequalities modelling Signorini contact in 2D and 3D without additional assumptions on the unknown contact set. *SIAM Journal on Numerical Analysis*, 53(3):1488–1507, 2015.

[DLS+14] R. Dimitri, L. D. Lorenzis, M. Scott, P. Wriggers, R. Taylor, and G. Zavarise. Isogeometric large deformation frictionless contact using t-splines. *Computer Methods in Applied Mechanics and Engineering*, 269(Supplement C):394 – 414, 2014.

[DLWH14] L. De Lorenzis, P. Wriggers, and T. J. Hughes. Isogeometric contact: a review. *GAMM-Mitteilungen*, 37(1):85–123, 2014.

[DLWZ12] L. De Lorenzis, P. Wriggers, and G. Zavarise. A mortar formulation for 3d large deformation contact using nurbs-based isogeometric analysis and the augmented lagrangian method. *Computational Mechanics*, 49(1):1–20, 2012.

[DMB01] J. Dolbow, N. Moës, and T. Belytschko. An extended finite element method for modeling crack growth with frictional contact. *Computer Methods in Applied Mechanics and Engineering*, 190(51):6825 – 6846, 2001.

[DS80] T. Dupont and R. Scott. Polynomial approximation of functions in sobolev spaces. *Mathematics of Computation*, 34:441–463, 1980.

[Dur12] D. Durville. Contact-friction modeling within elastic beam assemblies: an application to knot tightening. *Computational Mechanics*, 49(6):687–707, 2012.

[DVK15] W. Dornisch, G. Vitucci, and S. Klinkel. The weak substitution method – an application of the mortar method for patch coupling in nurbs-based isogeometric analysis. *International Journal for Numerical Methods in Engineering*, 103(3):205–234, 2015.

[EAB01] N. El-Abbasi and K.-J. Bathe. Stability and patch test performance of contact discretizations and a new solution algorithm. *Computers & Structures*, 79(16):1473 – 1486, 2001.

[EG04] A. Ern and J.-L. Guermond. *Theory and practice of finite elements.* vol. 159 of Applied Mathematical Sciences, Springer-Verlag, New York, 2004.

[FG11] A. Fortin and A. Garon. *Les éléments finis: de la théorie à la pratique.* Université Laval, 2011.

[FHW04] A. Fritz, S. Hüeber, and B. Wohlmuth. A comparison of mortar and Nitsche techniques for linear elasticity. *Calcolo*, 41(3):115–137, 2004.

[Fic64] G. Fichera. Problemi elastostatici con vincoli unilaterali : Il problema di signorini con ambigue condizioni al contorno. *Computer Methods in Applied Mechanics and Engineering*, 7:91–140, 1963/1964.

[Fic72] G. Fichera. Boundary value problems of elasticity with unilateral constraints. In C. Truesdell, editor, *Mechanics of Solids, vol. 2,*, page 391–424. Springer-Verlag, 1972.

[FPR16] M. Fabre, J. Pousin, and Y. Renard. A fictitious domain method for frictionless contact problems in elasticity using Nitsche's method. *SMAI Journal of Computational Mathematics*, 2:19–50, 2016.

[FPW15] P. Farah, A. Popp, and W. A. Wall. Segment-based vs. element-based integration for mortar methods in computational contact mechanics. *Computational Mechanics*, 55(1):209–228, 2015.

[FW05] K. A. Fischer and P. Wriggers. Frictionless 2D contact formulations for finite deformations based on the mortar method. *Computational Mechanics*, 36(3):226–244, 2005.

[FW06] K. A. Fischer and P. Wriggers. Mortar based frictional contact formulation for higher order interpolations using the moving friction cone. *Computer Methods in Applied Mechanics and Engineering*, 195:5020–5036, 2006.

[FZ75] A. Francavilla and O. C. Zienkiewicz. A note on numerical computation of elastic contact problems. *International Journal for Numerical Methods in Engineering*, 9(4):913–924, 1975.

[Glo80] R. Glowinski. *Lectures on numerical methods for non-linear variational problems*, volume 65 of *Lectures on Mathematics and Physics, Tata Institute of Fundamental Research.* Springer-Verlag, Bombay, 1980.

[Glo84] R. Glowinski. *Numerical methods for nonlinear variational problems*. Springer Series in Computational Physics. Springer-Verlag, New York, 1984.

[GLT89] R. Glowinski and P. Le Tallec. *Augmented Lagrangian and Operator-Splitting Methods in Nonlinear Mechanics*. Society for Industrial and Applied Mathematics, 1989.

[Han05] P. Hansbo. Nitsche's method for interface problems in computational mechanics. *GAMM-Mitteilungen*, 28(2):183–206, 2005.

[Has77] J. Haslinger. Finite element analysis for unilateral problems with obstacles on the boundary. v*Ceskoslovenská Akademie V*v*ed. Aplikace Matematiky*, 22(3):180–188, 1977.

[HB11] C. Hesch and P. Betsch. Transient three-dimensional contact problems: mortar method. mixed methods and conserving integration. *Computational Mechanics*, 48(4):461–475, 2011.

[HB12] C. Hesch and P. Betsch. Isogeometric analysis and domain decomposition methods. *Computer Methods in Applied Mechanics and Engineering*, 213(Supplement C):104 – 112, 2012.

[HCB05] T. Hughes, J. Cottrell, and Y. Bazilevs. Isogeometric analysis: Cad, finite elements, nurbs, exact geometry and mesh refinement. *Computer Methods in Applied Mechanics and Engineering*, 194(39):4135–4195, 2005.

[HCCB17] Q. Hu, F. Chouly, G. Cheng, and S. P. Bordas. Skew-symmetric nitsche's formulation in isogeometric analysis: Dirichlet and symmetry conditions, patch coupling and frictionless contact. 2017. In preparation.

[Her82] H. Hertz. Über die Berührung fester elastischer Körper. *Journal für die reine und angewandte Mathematik*, 92:156–171, 1882.

[HGB85] J. Hallquist, G. Goudreau, and D. Benson. Sliding interfaces with contact-impact in large-scale lagrangian computations. *Computer Methods in Applied Mechanics and Engineering*, 51(1):107 – 137, 1985.

[HH04a] A. Hansbo and P. Hansbo. A finite element method for the simulation of strong and weak discontinuities in solid mechanics. *Computer Methods in Applied Mechanics and Engineering*, 193:3523–3540, 2004.

[HH04b] A. Hansbo and P. Hansbo. A finite element method for the simulation of strong and weak discontinuities in solid mechanics. *Computer Methods in Applied Mechanics and Engineering*, 193(33-35):3523–3540, 2004.

[HH06] P. Heintz and P. Hansbo. Stabilized lagrange multiplier methods for bilateral elastic contact with friction. *Computer Methods in Applied Mechanics and Engineering*, 195:4323–4333, 2006.

[HH07] G. Haikal and K. Hjelmstad. A finite element formulation of non-smooth contact based on oriented volumes for quadrilateral and hexahedral elements. *Computer Methods in Applied Mechanics and Engineering*, 196:4690 – 4711, 2007.

[HHLTIW12] C. Hager, P. Hauret, P. Le Tallec, and B. I. Wohlmuth. Solving dynamic contact problems with local refinement in space and time. *Atti della Accademia Nazionale dei Lincei*, 201-204(Supplement C):25 – 41, 2012.

[HHN96] J. Haslinger, I. Hlaváĉek, and J. Neĉas. *Numerical methods for unilateral problems in solid mechanics*. Handbook of Numerical Analysis (eds. P.G.Ciarlet and J.L. Lions), 1996.

[Hil00] P. Hild. Numerical implementation of two nonconforming finite element methods for unilateral contact. *Computer Methods in Applied Mechanics and Engineering*, 184:99–123, 2000.

[HLT06] P. Hauret and P. Le Tallec. Energy-controlling time integration methods for nonlinear elastodynamics and low-velocity impact. *Computer Methods in Applied Mechanics and Engineering*, 195(37):4890 – 4916, 2006. John H. Argyris Memorial Issue. Part I.

[HOW+09] S. Hartmann, J. Oliver, R. Weyler, J. Cante, and J. Hernández. A contact domain method for large deformation frictional contact problems. part 2: Numerical aspects. *Computer Methods in Applied Mechanics and Engineering*, 198(33):2607 – 2631, 2009.

[HR09] J. Haslinger and Y. Renard. A new fictitious domain approach inspired by the extended finite element method. *SIAM Journal on Numerical Analysis*, 47(2):1474–1499, 2009.

[HR10] P. Hild and Y. Renard. A stabilized lagrange multiplier method for the finite element approximation of contact problems in elastostatics. *Numerische Mathematik*, 115:101–129, 2010.

[HR12] P. Hild and Y. Renard. An improved a priori error analysis for finite element approximations of Signorini's problem. *SIAM Journal on Numerical Analysis*, 50(5):2400–2419, 2012.

[HRS16] P. Hansbo, A. Rashid, and K. Salomonsson. Least-squares stabilized augmented Lagrangian multiplier method for elastic contact. *Finite Elements in Analysis and Design*, 116:32–37, 2016.

[HTS+76] T. J. Hughes, R. L. Taylor, J. L. Sackman, A. Curnier, and W. Kanoknukulchai. A finite element method for a class of contact-impact problems. *Computer Methods in Applied Mechanics and Engineering*, 8(3):249 – 276, 1976.

[Hug00] T. J. R. Hughes. *The finite element method: linear static and dynamic finite element analysis*. Dover Publications, 2000.

[HW05] S. Hüeber and B. I. Wohlmuth. An optimal a priori error estimate for nonlinear multibody contact problems. *SIAM Journal on Numerical Analysis*, 43(1):156–173, 2005.

[JE99] J. Jarusek and C. Eck. Dynamic contact problems with small coulomb friction for viscoelastic bodies: existence of solutions. *Mathematical Models and Methods in Applied Sciences*, 09(01):11–34, 1999.

[Joh85] K. L. Johnson. *Contact Mechanics*. Cambridge University Press, 1985.

[JP01] R. E. Jones and P. Papadopoulos. A novel three-dimensional contact finite element based on smooth pressure interpolations. *International Journal for Numerical Methods in Engineering*, 51(7):791–811, 2001.

[Kla88] A. Klarbring. On discrete and discretized non-linear elastic structures in unilateral contact (stability, uniqueness and variational principles). *International Journal of Solids and Structures*, 24(5):459 – 479, 1988.

[KO88] N. Kikuchi and J. T. Oden. *Contact problems in elasticity: a study of variational inequalities and finite element methods*. Society for Industrial and Applied Mathematics (SIAM), 1988.

[KROM99] C. Kane, E. Repetto, M. Ortiz, and J. Marsden. Finite element analysis of nonsmooth contact. *Computer Methods in Applied Mechanics and Engineering*, 180(1):1 – 26, 1999.

[KS81] N. Kikuchi and Y. J. Song. Penalty-finite-element approximation of a class of unilateral problems in linear elasticity. *Quarterly of Applied Mathematics*, 39:1–22, 1981.

[KS13] A. Konyukhov and K. Schweizerhof. *Computational Contact Mechanics*. Lecture Notes in Applied and Computational Mechanics. Springer, Berlin, 2013.

[Lau92] T. A. Laursen. *Formulation and treatment of frictional contact problems using finite elements*. PhD thesis, Stanford Univ., CA., 1992.

[Lau02] T. A. Laursen. *Computational contact and impact mechanics*. Springer, Berlin, 2002.

[Liu13] G. Liu. Meshfree method for contact simulation. In Q. J. Wang and Y.-W. Chung, editors, *Encyclopedia of Tribology*, pages 2225–2230. Springer US, Boston, MA, 2013.

[LK03] A. Lotfi and B. Kiss. A domain decomposition method for frictional contact problem. *PAMM*, 2(1):242–243, 2003.

[LR08] P. Laborde and Y. Renard. Fixed point strategies for elastostatic frictional contact problems. *Mathematical Methods in the Applied Sciences*, 31(4):415–441, 2008.

[LS93a] T. Laursen and J. Simo. A continuum-based finite element formulation for the implicit solution of multibody, large deformation frictional contact problems. *International Journal for Numerical Methods in Engineering*, 36:3451–3485, 1993.

[LS93b] T. A. Laursen and J. Simo. A continuum-based finite element formulation for the implicit solution of multibody, large deformation frictional contact problems. *International Journal for Numerical Methods in Engineering*, 36:451–3485, 1993.

[LT94] P. Le Tallec. Domain decomposition method in computational mechanics. In J. T. Oden, editor, *Computational Mechanics Advance*. North-Holland, Amsterdam, 1994.

[LTS95] P. Le Tallec and T. Sassi. Domain decomposition with nonmatching grids: Augmented lagrangian approach. *Mathematics of Computation*, 64(212):1367–1396, 1995.

[Lue03] D. Luenberger. *Linear and nonlinear programming*. Kluwer Academic Publishers, 2003.

[Lur70] A. Lurie. *Theory of elasticity*. Nauka, Moscow, 1970.

[MDB99] N. Moës, J. Dolbow, and T. Belytschko. A finite element method for crack growth without remeshing. *International Journal for Numerical Methods in Engineering*, 46(1):131–150, 1999.

[MK92] M. Moussaoui and K. Khodja. Régularité des solutions d'un problème mêlé dirichlet-signorini dans un domaine polygonal plan. *Comm. Partial Differential Equations*, 17(5-6):805–826, 1992.

[ML00a] T. W. McDevitt and T. A. Laursen. A mortar-finite element formulation for frictional contact problems. *International Journal for Numerical Methods in Engineering*, 48:1525–1547, 2000.

[ML00b] T. W. McDevitt and T. A. Laursen. A mortar-finite element formulation for frictional contact problems. *International Journal for Numerical Methods in Engineering*, 48:1525–1547, 2000.

[MMG94] J. Martins, M. M. Monteiro, and F. Gastaldi. On an example of non-existence of solution to a quasistatic frictional contact problem. *European journal of mechanics Aand Solids*, 13(1):113–133, 1994.

[MO87] J. Martins and J. Oden. Existence and uniqueness results for dynamic contact problems with nonlinear normal and friction interface laws. *Nonlinear Analysis: Theory, Methods & Applications*, 11(3):407 – 428, 1987.

[MP85] J. Middleton and G. Pande. *Penalty and augmented lagrangian formulation for contact problems*. Elsevier, 1985.

[MRC17] R. Mlika, Y. Renard, and F. Chouly. An unbiased nitsche's formulation of large deformation frictional contact and self-contact. *Computer Methods in Applied Mechanics and Engineering*, 325(Supplement C):265 – 288, 2017.

[MRW02] Y. Maday, F. Rapetti, and B. I. Wohlmuth. The influence of quadrature formulas in 2d and 3d mortar element methods. In L. F. Pavarino and A. Toselli, editors, *Recent Developments in Domain Decomposition Methods*, pages 203–221. Springer Berlin Heidelberg, Berlin, Heidelberg, 2002.

[Nit71] J. Nitsche. Über ein Variationsprinzip zur Lösung von Dirichlet-Problemen bei Verwendung von Teilräumen, die keinen Randbedingungen unterworfen sind. *Abhandlungen aus dem Mathematischen Seminar der Universität Hamburg*, 36:9–15, 1971.

[OHC+09] J. Oliver, S. Hartmann, J. Cante, R. Weyler, and J. A. Hernández. A contact domain method for large deformation frictional contact problems. Part 1: Theoretical basis. *Computer Methods in Applied Mechanics and Engineering*, 198:2591–2606, 2009.

[OK82a] J. T. Oden and N. Kikuchi. Finite element methods for constrained problems in elasticity. *International Journal for Numerical Methods in Engineering*, 18:701–725, 1982.

[OK82b] J. T. Oden and S. J. Kim. Interior penalty methods for finite element approximations of the Signorini problem in elastostatics. *Computers & Mathematics with Applications*, 8(1):35–56, 1982.

[PA08] S. Pagano and P. Alart. Self-contact and fictitious domain using a difference convex approach. *International Journal for Numerical Methods in Engineering*, 75(1):29–42, 2008.

[Pan08] O. Pantz. The modeling of deformable bodies with frictionless (self-)contacts. *Archive for Rational Mechanics and Analysis*, 188(2):183–212, 2008.

[PJS95] P. Papadopoulos, R. E. Jones, and J. M. Solberg. A novel finite element formulation for frictionless contact problems. *International Journal for Numerical Methods in Engineering*, 38(15):2603–2617, 1995.

[PL02] M. A. Puso and T. A. Laursen. A 3D contact smoothing method using Gregory patches. *International Journal for Numerical Methods in Engineering*, 54:1161–1194, 2002.

[PL03] M. A. Puso and T. A. Laursen. Mesh tying on curved interfaces in 3d. *Engineering Computation*, 20(3):305–319, 2003.

[PL04a] M. A. Puso and T. A. Laursen. A mortar segment-to-segment contact method for large deformation solid mechanics. *Computer Methods in Applied Mechanics and Engineering*, 193:601–629, 2004.

[PL04b] M. A. Puso and T. A. Laursen. A mortar segment-to-segment frictional contact method for large deformations. *Computer Methods in Applied Mechanics and Engineering*, 193(45):4891–4913, 2004.

[PLS08] M. A. Puso, T. Laursen, and J. Solberg. A segment-to-segment mortar contact method for quadratic elements and large deformations. *Computer Methods in Applied Mechanics and Engineering*, 197(6):555–566, 2008.

[Pow69] M. Powell. A method for nonlinear constraints in minimization problems. In R. Fletcher, editor, *Optimization*, page 283–298. Academic Press,, London, 1969.

[PR15] K. Poulios and Y. Renard. An unconstrained integral approximation of large sliding frictional contact between deformable solids. *Computers & Structures*, 153:75–90, 2015.

[PS98] P. Papadopoulos and J. Solberg. A lagrange multiplier method for the finite element solution of frictionless contact problems. *Mathematical and Computer Modelling*, 28(4):373 – 384, 1998.

[PT92] P. Papadopoulos and R. L. Taylor. A mixed formulation for the finite element solution of contact problems. *Computer Methods in Applied Mechanics and Engineering*, 94(3):373 – 389, 1992.

[PWGW12] A. Popp, B. Wohlmuth, M. Gee, and W. Wall. Dual quadratic mortar finite element methods for 3D finite deformation contact. *SIAM Journal on Scientific Computing*, 34(4):B421–B446, 2012.

[Red04] J. N. Reddy. *An introduction to nonlinear finite element analysis*. Oxford University Press, 2004.

[Ren06] Y. Renard. A uniqueness criterion for the signorini problem with coulomb friction. In P. Wriggers and U. Nackenhorst, editors, *Analysis and Simulation of Contact Problems*, pages 161–169. Springer Berlin Heidelberg, Berlin, Heidelberg, 2006.

[Ren10] Y. Renard. The singular dynamic method for constrained second order hyperbolic equations: Application to dynamic contact problems. *Journal of Computational and Applied Mathematics*, 234(3):906 – 923, 2010.

[Ren13] Y. Renard. Generalized Newton's methods for the approximation and resolution of frictional contact problems in elasticity. *Computer Methods in Applied Mechanics and Engineering*, 256:38–55, 2013.

[Roc70] R. Rockafellar. *Convex analysis*. Princeton University, 1970.

[Roc73] R. T. Rockafellar. The multiplier method of hestenes and powell applied to convex programming. *Journal of Optimization Theory and Applications*, 12(6):555–562, 1973.

[SD15] R. A. Sauer and L. DeLorenzis. An unbiased computational contact formulation for 3D friction. *International Journal for Numerical Methods in Engineering*, 101(4):251–280, 2015.

[Sig33] A. Signorini. Sopra alcune questioni di elastostatica. *Atti della Societa Italiana per Il Progresso delle Scienze*, 1933.

[Sig59] A. Signorini. Questioni di elasticità non linearizzata esemilinearizzata. *Rendiconti di Mathematica e dell sue Apllicazioni*, 18:95–139, 1959.

[SL92] J. Simo and T. A. Laursen. An augmented lagrangian treatment of contact problems involving friction. *Computers & Structures*, 42:97–116, 1992.

[SL13] R. A. Sauer and L. D. Lorenzis. A computational contact formulation based on surface potentials. *Computer Methods in Applied Mechanics and Engineering*, 253(Supplement C):369 – 395, 2013.

[SP05] J. M. Solberg and P. Papadopoulos. An analysis of dual formulations for the finite element solution of two-body contact problems. *Computer Methods in Applied Mechanics and Engineering*, 194(25):2734 – 2780, 2005.

[SS00] P. Seshaiyer and M. Suri. hp submeshing via non-conforming finite element methods. *Computer Methods in Applied Mechanics and Engineering*, 189(3):1011 – 1030, 2000.

[Ste95] R. Stenberg. On some techniques for approximating boundary conditions in the finite element method. *Journal of Computational and Applied Mathematics*, 63:139–148, 1995.

[SV77] F. Scarpini and M.-A. Vivaldi. Error estimates for the approximation of some unilateral problems. *RAIRO Analyse Numérique*, 11(2):197–208, 1977.

[SWT85] J. C. Simo, P. Wriggers, and R. L. Taylor. A perturbed lagrangian formulation for the finite element solution of contact problems. *Computer Methods in Applied Mechanics and Engineering*, 50(2):163–180, 1985.

[TFW09] M. Tur, F. Fuenmayor, and P. Wriggers. A mortar-based frictional contact formulation for large deformations using lagrange multipliers. *Computer Methods in Applied Mechanics and Engineering*, 198:2860–2873, 2009.

[TG70] S. P. Timoshenko and J. N. Goodier. *Theory of elasticity*. McGraw-Hill, 1970.

[TP91] R. L. Taylor and P. Papadopoulios. On a patch test for contact problems in two dimensions. *Nonlinear Computational Mechanics*, pages 690–702, 1991.

[TWH11] I. Temizer, P. Wriggers, and T. Hughes. Contact treatment in isogeometric analysis with nurbs. *Computer Methods in Applied Mechanics and Engineering*, 200(9):1100–1112, 2011.

[WB17] C. Wilking and M. Bischoff. Alternative integration algorithms for three-dimensional mortar contact. *Comp Mech*, 59(2), 2017.

[WK03] B. I. Wohlmuth and R. H. Krause. Monotone multigrid methods on nonmatching grids for nonlinear multibody contact problems. *SIAM Journal on Scientific Computing*, 25(1):324–347, 2003.

[Woh11] B. Wohlmuth. Variationally consistent discretization schemes and numerical algorithms for contact problems. *Acta Numerica*, 20:569–734, 2011.

[Wri95] P. Wriggers. Finite element algorithms for contact problems. *Archives of Computational Methods in Engineering*, 2:4:1–49, 1995.

[Wri06] P. Wriggers. *Computational Contact Mechanics (2nd edn)*. Springer, Berlin, 2006.

[WSS13] P. Wriggers, J. Schröder, and A. Schwarz. A finite element method for contact using a third medium. *Computational Mechanics*, 52(4):837–847, 2013.

[WVS90] P. Wriggers, T. V. Van, and E. Stein. Finite element formulation of large deformation impact-contact problems with friction. *Computers & Structures*, 37(3):319 – 331, 1990.

[WZ08] P. Wriggers and G. Zavarise. A formulation for frictionless contact problems using a weak form introduced by Nitsche. *Computational Mechanics*, 41, 2008.

[Yas11] V. A. Yasterbov. *Computational contact mechanics:geometry, detection and numerical techniques*. PhD thesis, École nationale supérieure des mines de Paris, 2011.

[Yvo04] J. Yvonnet. *Nouvelles approches sans maillage basées sur la méthode des éléments naturels pour la simulation numérique des procédés de mise en forme*. PhD thesis, École Nationale Supérieure d'Arts et Métiers de Paris, 2004.

[ZDL09a] G. Zavarise and L. De Lorenzis. A modified node-to-segment algorithm passing the contact patch test. *International Journal for Numerical Methods in Engineering*, 79(4):379–416, 2009.

[ZDL09b] G. Zavarise and L. De Lorenzis. The node-to-segment algorithm for 2d frictionless contact: Classical formulation and special cases. *Computer Methods in Applied Mechanics and Engineering*, 198(41):3428 – 3451, 2009.

[ZDL11] G. Zavarise and L. De Lorenzis. The contact patch test for linear contact pressure distributions in 2d frictionless contact. In G. Zavarise and P. Wriggers, editors, *Trends in Computational Contact Mechanics*, pages 79–100. Springer Berlin Heidelberg, Berlin, Heidelberg, 2011.

[ZDL12] G. Zavarise and L. De Lorenzis. An augmented lagrangian algorithm for contact mechanics based on linear regression. *International Journal for Numerical Methods in Engineering*, 91(8):825–842, 2012.

[ZT05] O. C. Zienkiewicz and R. L. Taylor. *The finite element method for solid and structural mechanics*. Elsevier Butterworth-Heinemann, 2005.

[ZW98] G. Zavarise and P. Wriggers. A segment-to-segment contact strategy. *Mathematical and Computer Modelling*, 28(4):497 – 515, 1998.

FOLIO ADMINISTRATIF

THESE DE L'UNIVERSITE DE LYON OPEREE AU SEIN DE L'INSA LYON

NOM : MLIKA DATE de SOUTENANCE : 24/01/2018

Prénoms :Rabii

TITRE :**Nitsche method for frictional contact and self-contact: mathematical and numerical study**

NATURE : Doctorat Numéro d'ordre : 2018LYSEI002
Ecole doctorale :MEGA
Spécialité : Génie Mécanique

RESUME :
Dans cette thèse, nous présentons et étudions une nouvelle formulation du problème de contact frottant entre deux corps élastiques se basant sur la méthode de Nitsche. Dans cette méthode les conditions de contact sont imposées faiblement, grâce à un terme de pénalité consistant et stabilisé. En premier lieu, nous introduisons, l'étude effectuée en petites déformations pour une version non biaisée de la méthode. La non-distinction entre une surface maître et une surface esclave permettra à la méthode d'être plus générique et applicable directement au problème d'auto-contact. Le cadre restrictif des petites déformations nous permet d'obtenir des résultats théoriques sur la stabilité et la convergence de la méthode. Ces résultats sont complétés par une validation numérique. Ensuite, nous introduisons l'extension de la méthode de Nitsche au cadre des grandes déformations qui est d'avantage pertinent pour les applications industrielles et les situations d'auto-contact. La méthode de Nitsche est formulée pour un matériau hyper-élastique avec frottement de Coulomb et se décline en deux versions : biaisée ou non. La formulation est généralisée à travers un paramètre réel pour couvrir toute une famille de méthodes et chaque variante particulière a des propriétés différentes du point de vue théorique et numérique, en termes de précision et de robustesse.
La méthode est testée et validée à travers plusieurs cas tests académiques et industriels. Nous effectuons aussi une étude de l'influence de l'intégration numérique sur la précision et la convergence de la méthode. Cette étude couvre une comparaison entre plusieurs schémas d'intégration proposés dans la littérature pour d'autres méthodes intégrales.

MOTS-CLÉS : Contact frottant en petites et grandes déformations, méthode de Nitsche, formulation non biaisée, intégration numérique.

Laboratoire (s) de recherche : LAMCoS

Directeur de thèse: Yves Renard ; Franz Chouly

Président de jury :

Composition du jury : Patrick Letallec ; Laura De Lorenzis ; Miguel Angel Frenandez ; Patrice Hauret.

Abstract

In this thesis, we present and study a new formulation of frictional contact between two elastic bodies based on Nitsche's method. This method aims to treat the interface conditions in a weak sense, thanks to a consistent additional term stabilized with the parameter γ. At first, we introduce the study carried out in the small strain framwork for an unbiased version of the method. The non-distinction between a master surface and a slave one will allow the method to be more generic and directly applicable to the self-contact problem. The restrictive framework of small strain allowed us to obtain theoretical results on the consistency and convergence of the method. Then, we present the extension of the Nitsche method to the large strain case more relevant for industrial applications and situations of self-contact. This Nitsche's method is formulated for an hyper-elastic material and declines in the two versions: biased and unbiased. We describe a class of methods through a generalisation parameter θ . Particular variants have different properties from a numerical point of view, in terms of accuracy and robustness. To prove the accuracy of the method for large deformations, we provide several academic and industrial tests. We also study the influence of numerical quadrature on the accuarcy and convergence of the method. This study covers a comparison of several integration rules proposed in the literature for other integral methods.

Key words — frictional contact for small and large strain, Nitsche's method, unbiased methods, numerical quadrature for contact.

Résumé

Dans cette thèse, nous présentons et étudions une nouvelle formulation du problème de contact frottant entre deux corps élastiques se basant sur la méthode de Nitsche. Dans cette méthode les conditions de contact sont imposées faiblement, grâce à un terme additionnel consistant et stabilisé par un paramètre γ. En premier lieu, nous introduisons, l'étude effectuée en petites déformations pour une version non biaisée de la méthode. La non-distinction entre une surface maître et une surface esclave permettera à la méthode d'être plus générique et applicable directement au problème d'auto-contact. Le cadre restrictif des petites déformations nous permet d'obtenir des résultats théoriques sur la stabilité et la convergence de la méthode. Ces résultats sont complétés par une validation numérique. Ensuite, nous introduisons l'extension de la méthode de Nitsche au cadre des grandes déformations qui est d'avantage pertinent pour les applications industrielles et les situations d'auto-contact. La méthode de Nitsche est formulée pour un matériau hyperélastique avec frottement de Coulomb et se décline en deux versions : biaisée ou non. La formulation est généralisée à travers un paramètre θ pour couvrir toute une famille de méthodes. Chaque variante particulière a des propriétés différentes du point de vue théorique et numérique, en termes de précision et de robustesse. La méthode est testée et validée à travers plusieurs cas tests académiques et industriels. Nous effectuons aussi une étude de l'influence de l'intégration numérique sur la précision et la convergence de la méthode. Cette étude couvre une comparaison entre plusieurs schémas d'integration proposés dans la littérature pour d'autres méthodes intégrales.

Mots clés — contact frottant en petites et grandes déformations, méthode de Nitsche, formulation non biaisée, intégration numérique.